Electrospun Nanofiber Composite Membranes for Hydrogen/Air Fuel Cells

By

Devon J. Powers

Dissertation
Submitted to the Faculty of the
Graduate School of Vanderbilt University
in partial fulfillment of the requirements
For the degree of

DOCTOR OF PHILOSOPHY
in
Chemical Engineering

May 10 2019
Nashville, Tennessee

Approved:

Peter N. Pintauro, Ph.D.

Scott Guelcher, Ph.D.

Paul E. Laibinis, Ph.D.

Shihong Lin, Ph.D.

“This is for the times I’m reminded my mind isn’t mine alone”

-G. Watsky

Acknowledgements

First and foremost, I owe a huge thanks to God. The past few years have been fraught with ups and downs and bumps along the way, but things have come together in a manner that I never could have imagined.

Much of this dissertation is a product of the vision that was passed to me from my research advisor, who trusted in my abilities to carry it out. So, Professor Peter Pintauro, I appreciate all that you've done. Thanks for allowing me to work alongside you in this environment and aiding in my growth as a scholar and researcher. The work that I've been able to do under your direction is quite the stepping-stone toward what I hope is a great career. I am also thankful for the critique and feedback that I received from my committee members, Professors Scott Guelcher, Paul E. Laibinis, and Shihong Lin.

Vanderbilt has been an enriching place to spend the past few years, primarily because of the fantastic people who make up its community. The members of the department staff were vital in helping me wade through paperwork and ordering items, as well as providing an external sounding board to help put my setbacks in perspective. Mark Holmes has been instrumental in troubleshooting and repairing equipment in a timely manner. The staff of VINSE, notably Dr. Tony Hmelo, has worked intently to ensure that the equipment is always ready to be used.

This goals achieved in this project were aided by contributions from external collaborators. Thanks to Dr. Michael Yandrasits at 3M Company for providing several batches the 825, 725, and 660 EW perfluorosulfonic and 660 EW perfluoroimide acid ionomers. In addition, the staff at 3M confirmed some of the results found over the

course of this work. Dr. Mendil-Jakani made contributions to the studies regarding PFIA and PVDF in performing small-angle x-ray scattering measurements on various samples. I appreciate the work that they have done in making this dissertation possible.

My fellow lab mates have made contributions to this work, whether directly or indirectly. Many thanks are due to Dr. Ryszard Wycisk, who has been a constant source of knowledge, critique, and inspiration over the years. Thanks to Jun Woo Park, who provided training and valuable insight as to the type of researcher and student I would want to become. I am speechless when I consider the contributions of Dr. Leslie Dos Santos, one of our former post-doctoral scholars. Her experience and knowledge during her time with us has been instrumental to the things I've been able to do, and her positive attitude and academic acuity were valuable to the work we performed, as well as our approach to understanding the results. I also owe gratitude to John and Krysta, who showed me how to make MEAs, as well as how to be a good academic and informed critic.

Finally, I'm thankful to my family and friends who have been a constant source of strength and positivity during my time at Vanderbilt. Thank you for believing that I was able to succeed, for equipping me to chase such a ridiculous goal, and for being present when I needed to remember why I started this program. And to my family – thanks for understanding why I wasn't always able to be in Texas for holidays. I can't promise that that will change.

This work was funded by a DOE grant through the EERE program in collaboration with 3M Company.

TABLE OF CONTENTS

LIST OF TABLES

Table Page

LIST OF FIGURES

Figure Page

Chapter 1

Introduction

An increasing demand for sustainable energy, along with the limited supply of the fossil fuels that have been a crutch for civilization for years and the rapid environmental changes that are linked to the burning thereof, has led to a growing interest in devices powered by renewable fuels. Fuel cells have become major contenders as an alternative energy device due to their high fuel efficiencies and ability to generate energy from a carbon-free fuel (such as hydrogen gas) and oxygen from air. Proton-exchange membrane fuel cells (PEMFCs), in particular, have received interest due to their potential use for stationary, portable, and automotive power applications. While conventional technologies burn fossil fuels to generate energy, part of the appeal of hydrogen/air PEMFCs lies in their ability to cleanly and directly convert the chemical potential of hydrogen to electrical energy [1,2].

In recent years, various products, most notably vehicles, utilizing fuel cells have emerged on the market, such as the Toyota Mirai, the Honda Clarity, or the Mercedes-Benz F-Cell. However, there are various factors that limit the widespread use of fuel cells such as the development of infrastructure for hydrogen supply, determination of reliable and cost-effective sources for hydrogen, and the durability and cost of the components. The membrane-electrode assembly (MEA), in particular, is important as it contains the materials necessary for conversion of hydrogen and oxygen (from air) to electricity and water. The MEA consists of two electrochemically active electrodes and a proton-

exchange membrane (PEM). This membrane must separate the electrodes, prevent fuel crossover, and allow proton conduction (which is highly dependent on the presence of water) under the various operating conditions of the fuel cell. The membrane is also expected to be resistant to mechanical failure (such as tears or holes) and chemical degradation (polymer degradation by peroxide radicals).

Ionic conductivity is provided to the PEM through the use of an ionomer (i.e. an ion-containing polymer). Ionomers are typically highly conductive when fully hydrated at mild temperatures, but under hot (90-120°C) and dry (below 50% RH) conditions, they exhibit low proton conductivity/high ionic resistance [3–6]. This shortcoming creates the need for built-in humidification equipment in a fuel cell unit (to keep the ionomer hydrated), which can complicate system design. In addition, many ionomers undergo undesirable swelling and shrinking as the fuel cell is turned on/off (going from hot and wet when on to cold and dry when off). Such dimensional changes can lead to the mechanical degradation of the PEM (the generation of cracks or pinholes, or delamination between the membrane and electrode) [7–9], thus shortening the lifetime of the MEA [10–13].

Nafion is a perfluorosulfonic acid (PFSA) ionomer that was developed by DuPont® in the mid-1960's [14]. It is a copolymer, with a poly(tetrafluoroethylene) (PTFE) backbone and pendant perfluoroalkyl ether chains that contain a terminal sulfonic acid group. This terminal acid site allows the polymer to conduct protons when sufficiently hydrated [15]. Due to its high conductivity of ~0.09 S/cm in room-temperature water [16], as well as its good chemical and mechanical durability, it has remained one of the most widely used and studied ionomers for PEMFCs. However, the

conductivity- and durability-related shortcomings of Nafion (loss of conductivity under dry conditions, loss of mechanical integrity when hydrated, susceptibility to chemical degradation), along with its high cost, have inspired work to synthesize an ionomer or fabricate a composite membrane (where an ionomer is blended with a hydrophobic polymer to improve strength and limit water swelling at the cost of proton conductivity) with properties superior to those of Nafion.

The preparation of an ionomer with high conductivity requires a high concentration of ion-exchange sites along the polymer backbone. However, this also increases the water swelling of the ionomer, leading to degradation of the mechanical properties upon hydration. Attempts that have been made in the academic community to fabricate a membrane that is both highly conductive and highly durable (both chemically and mechanically) are described in Chapter 2 of this dissertation. In short, hydrocarbon and fluorocarbon ionomers with high ion-exchange capacities (IECs) have been fabricated, and in some cases, combined with a wide array of components to: (i) improve their conductivity [4,17–19], (ii) improve their mechanical stability [11,17,20], and/or (iii) improve their chemical durability [21–23]. However, no single membrane has exhibited the necessary combination of properties for long-term fuel cell operation. Oftentimes, high conductivity is achieved at the cost of excessive water swelling.

Dual fiber electrospun membranes have been reported to display excellent conductivity and durability properties that are ideal for fuel cell operation. In such a membrane, a nanofiber web of one polymer is embedded in a matrix of a second polymer. While a fiber-reinforced membrane can be fabricated by impregnating a polymer solution into a fiber web of the secondary polymer [20,24], a dual fiber

electrospinning technique has recently been shown to simplify the fabrication method, which circumvents the shortcomings associated with an impregnation technique (multiple impregnation steps, potential for incompletely-filled pores). Pintauro and coworkers have demonstrated that two polymers (an ionomer, such as Nafion, and a reinforcing polymer) can be simultaneously electrospun onto a common collector, and under proper post-processing conditions, the mixed fiber mat can be converted to a dense membrane [16,25,26]. The work of Ballengee and Pintauro showed this process could lead to two distinct structures: an ionomer matrix with embedded hydrophobic polymer fibers (such as poly(phenyl sulfone)), or a hydrophobic matrix with embedded ionomer fibers [16]. In addition, A. Park *et al.* [25] described methods electrospin polymers in order to make a nanofiber composite anion-exchange membrane, and JW. Park *et al.* discussed the use of dual fiber electrospun membranes in a regenerative H_2/Br_2 fuel cell [26]. This dissertation builds on the groundwork laid by Ballengee, A. Park, J. Park, and Pintauro, where electrospinning is used to fabricate a series of composite membranes with properties suitable for H_2/air fuel cell applications. In particular, mechanically strong membranes with an area-specific resistance (ASR) and swelling properties that approach the targets defined by The U.S. Department of Energy (an ASR of 0.02 Ω-cm^2 or less at 80 °C and 40-100 % relative humidity, and an in-plane swelling of 5% or less after equilibration in water) are desired. While chemical durability is important, the focus of this dissertation is to improve the mechanical durability of the membranes while maintaining an acceptable ASR at operational conditions. In addition to the fabrication of PEMs with low ASR and low in-plane swelling, electrospinning is also utilized to combine a cation-exchange polymer and anion-exchange polymer within a single membrane (i.e. a bipolar

membrane), which can be useful for water splitting and electrodialysis salt separations. Chapter 3 – Chapter 6 are stand-alone discussions of how aspects of electrospinning can improve the properties of a composite PEM. Taken as a whole, this dissertation provides several avenues that can lead to PEMs that merge high performance and long-term durability.

Dual fiber electrospinning offers various advantages over impregnation into a pre-formed fiber mat as a technique to prepare dual fiber membranes. For example, the composition of the mixed fiber mat can be varied during electrospinning, leading to a multi-layered structure. Chapter 3 discusses the effect of structure on the in-plane swelling of membranes utilizing 3M's 825 equivalent weight (EW) perfluorosulfonic acid (PFSA) and poly (amide imide) (PAI). One membrane structure utilizes a uniform composition through the membrane. The second structure utilizes a multi-layer membrane design, where the ionomer content is abruptly increased/decreased during electrospinning, leading to three or more distinct layers, each with a uniform composition. The third membrane type utilizes a tri-layer structure with a gradient inner layer (i.e. a symmetric gradient composition). The dependence of proton conductivity and mechanical strength on layer composition and overall membrane structure are reported for NCMs in which an 825 EW PFSA matrix is reinforced with PAI nanofibers.

Efforts to improve the conductivity of composite PEMs often involve increasing the IEC of the ionomer, which necessitates the addition of sufficient reinforcing material to restrict swelling (whether through polymer blending or electrospinning). It was of interest to determine whether a high-IEC ionomer that was reinforced by a high loading of uncharged material would exhibit lower water in-plane swelling as compared to a

lower-IEC ionomer that utilized less reinforcing material without a loss in proton conductivity. To this end, Chapter 4 discusses a series of composite membranes utilizing 3M's 825, 725, or 660 EW PFSA and poly(vinylidene fluoride) (PVDF) that were fabricated via dual fiber and single fiber electrospinning. In a single fiber electrospun mat, PFSA and PVDF were blended and electrospun from a single needle; the resultant mat was hot pressed, leading to a dense membrane[27,28]. The influence of ionomer IEC on the properties of composite membranes was determined in both electrospun blended single fiber and dual fiber membranes.

3M Company recently began synthesizing a novel perfluorinated ionomer that allows for high IECs without sacrificing ionomer crystallinity and stability in water. By introducing an additional acid group in the side chain of the ionomer (thus making a Multi-Acid Side Chain, or MASC, ionomer), the IEC can be increased without reducing the number of (CF_2) units between side chains. The resultant perfluoroimide acid (PFIA) ionomer exhibits high conductivity and lower water uptake [29], as compared to 3M's low-equivalent weight PFSA ionomers. Dual fiber and single fiber membranes utilizing 3M's PFIA were fabricated, and their properties are reported in Chapter 5. The relationship between fabrication technique and the resultant membrane microstructure and physical/electrochemical properties was determined. Their performance in an operational fuel cell is also reported at high and low levels of humidity.

Electrospinning offers the ability to fabricate composite membranes in which the diameter of the reinforcing fibers can be varied. Choi fabricated a series of pore-filled membranes, where an uncharged polymer was impregnated into a pre-fabricated porous nanofiber mat of electrospun PFSA with various average fiber diameters [30]. The

diameter of electrospun PFSA fiber played little role in dictating the properties of the final composite membrane. However, there is interest in fabricating mixed fiber mats where an ionomer matrix is reinforced by an uncharged fiber mat, and where the average diameter of the reinforcing polymer fiber is varied due to the potential for increased fiber strength [31]. In Chapter 6, electrospinning conditions were established to achieve a range of diameters for PVDF reinforcing fibers. These fibers were used to make a series of dual fiber membranes with 825 EW PFSA or 700 EW PFIA, and the effect of fiber diameter on the properties of the membrane is discussed. In addition, Chapter 6 discusses the dependence of fiber diameter on the strength of a reinforcing polymer mat.

1.1 References

[1] K. Dutta, S. Das, P. Kumar, P.P. Kundu, Polymer electrolyte membrane with high selectivity ratio for direct methanol fuel cells: A preliminary study based on blends of partially sulfonated polymers polyaniline and PVdF-co-HFP, Appl. Energy. 118 (2014) 183–191. doi:10.1016/j.apenergy.2013.12.029.

[2] S.J. Peighambardoust, S. Rowshanzamir, M. Amjadi, Review of the proton exchange membranes for fuel cell applications, Int. J. Hydrogen Energy. 35 (2010) 9349–9384. doi:10.1016/j.ijhydene.2010.05.017.

[3] J.B. Ballengee, G.M. Haugen, S.J. Hamrock, P.N. Pintauro, Properties and Fuel Cell Performance of a Nanofiber Composite Membrane with 660 Equivalent Weight Perfluorosulfonic Acid, J. Electrochem. Soc. 160 (2013) F429–F435. doi:10.1149/2.088304jes.

[4] C. Yang, P. Costamagna, S. Srinivasan, J. Benziger, A.B. Bocarsly, Approaches and technical challenges to high temperature operation of proton exchange membrane fuel cells, 103 (2001) 1–9.

[5] M. Maalouf, B. Pyle, C.-N. Sun, D. Wu, S.J. Paddison, M. Schaberg, M. Emery, K.H. Lochhaas, S.J. Hamrock, H. Ghassemi, T.A. Zawodzinski Jr., Proton exchange membranes for high temperature fuel cells: equivalent weight and end group effects on conductivity., ECS Trans. 25 (2009) 1473–1481. doi:10.1149/1.3210704.

[6] F. Wang, M. Hickner, Y. Seung, T.A. Zawodzinski, J.E. Mcgrath, Direct polymerization of sulfonated poly (arylene ether sulfone) random (statistical) copolymers : candidates for new proton exchange membranes, 197 (2002) 231–

242.

[7] J. Wu, X.Z. Yuan, J.J. Martin, H. Wang, J. Zhang, J. Shen, S. Wu, W. Merida, A review of PEM fuel cell durability: Degradation mechanisms and mitigation strategies, J. Power Sources. 184 (2008) 104–119. doi:10.1016/j.jpowsour.2008.06.006.

[8] F.A. De Bruijn, V.A.T. Dam, G.J.M. Janssen, Review : Durability and Degradation Issues of PEM Fuel Cell Components, (2008) 3–22. doi:10.1002/fuce.200700053.

[9] R. Banan, J. Zu, A. Bazylak, Humidity and Temperature Cycling Effects on Cracks and Delaminations in PEMFCs, (2015) 327–336. doi:10.1002/fuce.201400118.

[10] T. Ous, C. Arcoumanis, Degradation aspects of water formation and transport in Proton Exchange Membrane Fuel Cell : A review, J. Power Sources. 240 (2013) 558–582. doi:10.1016/j.jpowsour.2013.04.044.

[11] R. Borup, J. Meyers, B. Pivovar, Y.S. Kim, R. Mukundan, N. Garland, D. Myers, M. Wilson, F. Garzon, D. Wood, P. Zelenay, K. More, K. Stroh, T. Zawodzinski, X.J. Boncella, J.E. Mcgrath, O.M. Inaba, K. Miyatake, M. Hori, K. Ota, Z. Ogumi, S. Miyata, A. Nishikata, Z. Siroma, Y. Uchimoto, K. Yasuda, K. Kimijima, N. Iwashita, Scientific Aspects of Polymer Electrolyte Fuel Cell Durability and Degradation, (2007) 3904–3951.

[12] A. Kusoglu, A.M. Karlsson, M.H. Santare, S. Cleghorn, W.B. Johnson, Mechanical behavior of fuel cell membranes under humidity cycles and effect of swelling anisotropy on the fatigue stresses, J. Power Sources. 170 (2007) 345–358.

doi:10.1016/j.jpowsour.2007.03.063.

[13] M.P. Rodgers, L.J. Bonville, H.R. Kunz, D.K. Slattery, J.M. Fenton, Fuel Cell Perfluorinated Sulfonic Acid Membrane Degradation Correlating Accelerated Stress Testing and Lifetime, (2012).

[14] D.S. Kim, M. D.Guiver, Polymer membranes for fuel cells, Springer, 2009. doi:1010079780387735320.

[15] K.A. Mauritz, R.B. Moore, State of Understanding of Nafion, (2004).

[16] J.B. Ballengee, P.N. Pintauro, Composite fuel cell membranes from dual-nanofiber electrospun mats, Macromolecules. 44 (2011) 7307–7314. doi:10.1021/ma201684j.

[17] Y.S. Kim, F. Wang, M. Hickner, T.A. Zawodzinski, J.E. McGrath, Fabrication and characterization of heteropolyacid (H3PW12O40)/directly polymerized sulfonated poly(arylene ether sulfone) copolymer composite membranes for higher temperature fuel cell applications, J. Memb. Sci. 212 (2003) 263–282. doi:10.1016/S0376-7388(02)00507-0.

[18] Y. Liu, B. Yi, Z. Shao, L. Wang, Pt / CNTs-Nafion reinforced and self-humidifying composite membrane for PEMFC applications, 163 (2007) 807–813. doi:10.1016/j.jpowsour.2006.09.065.

[19] R. Wang, W. Zhang, G. He, P. Gao, Controlling fuel crossover and hydration in ultra-thin proton exchange membrane-based fuel cells using Pt-nanosheet catalysts, J. Mater. Chem. A. 2 (2014) 16416–16423. doi:10.1039/C4TA03799E.

[20] J.A. Kolde, B. Bahar, M.S. Wilson, T.A. Zawodzinski, G. Shimson, Advanced Composite Polymer Electrolyte Fuel Cell Membranes, Prot. Conduct. Membr. Fuel

Cells I Proc. First Int. Symp. Prot. Conduct. Membr. Fuel Cells. 95 (1995) 193–201.

[21] T.R. Ralph, D.E. Barnwell, P.J. Bouwman, A.J. Hodgkinson, M.I. Petch, M. Pollington, Reinforced Membrane Durability in Proton Exchange Membrane Fuel Cell Stacks for Automotive Applications, J. Electrochem. Soc. 155 (2008) B411–B422. doi:10.1149/1.2838163.

[22] M. Zaton, J. Roziere, D.J. Jones, Mitigation of PFSA membrane chemical degradation using composite cerium oxide – PFSA nano fibres, (2017) 5390–5401. doi:10.1039/C6TA10977B.

[23] B.P. Pearman, N. Mohajeri, R.P. Brooker, M.P. Rodgers, D.K. Slattery, M.D. Hampton, D.A. Cullen, S. Seal, The degradation mitigation effect of cerium oxide in polymer electrolyte membranes in extended fuel cell durability tests, J. Power Sources. 225 (2013) 75–83. doi:10.1016/j.jpowsour.2012.10.015.

[24] J. Park, L. Wang, S.G. Advani, A.K. Prasad, Durability Analysis of Nafion/Hydrophilic Pretreated PTFE Membranes for PEMFCs, J. Electrochem. Soc. 159 (2012) F864–F870. doi:Doi 10.1149/2.016301jes.

[25] A.M. Park, F.E. Turley, R.J. Wycisk, P.N. Pintauro, Electrospun and Cross-Linked Nano fiber Composite Anion Exchange Membranes, Macromolecules. 47 (2014) 227–235. doi:10.1021/ma401932h.

[26] J.W. Park, R. Wycisk, P.N. Pintauro, Nafion/PVDF nanofiber composite membranes for regenerative hydrogen/bromine fuel cells, J. Memb. Sci. 490 (2015) 103–112. doi:10.1016/j.memsci.2015.04.044.

[27] G. Lin, P.Y. Chong, V. Yarlagadda, T. V Nguyen, R.J. Wycisk, P.N. Pintauro, M.

Bates, S. Mukerjee, M.C. Tucker, A.Z. Weber, Advanced Hydrogen-Bromine Flow Batteries with Improved Efficiency, Durability and Cost, J. Electrochem. Soc. 163 (2016) A5049–A5056. doi:10.1149/2.0071601jes.

[28] R.J. Wycisk, J.W. Park, D. Powers, P.N. Pintauro, Electrospinning PFSA +PVDF Nanofibers for Fuel CellMembrane Fabrication, in: Meet. Abstr., The Electrochemical Society, 2014: pp. 1199–1199.

[29] M.S. Schaberg, J.E. Abulu, G.M. Haugen, M.A. Emery, S.J. O'Conner, P.N. Xiong, S.J. Hamrock, New Multi Acid Side-Chain Ionomers for Proton Exchange Membrane Fuel Cells, ECS Trans. 33 (2010) 627–633.

[30] J. Choi, K.M. Lee, R. Wycisk, P.N. Pintauro, P.T. Mather, Nanofiber composite membranes with low equivalent weight perfluorosulfonic acid polymers, J. Mater. Chem. 20 (2010) 6282–6290. doi:10.1039/c0jm00441c.

[31] U. Stachewicz, R.J. Bailey, W. Wang, A.H. Barber, Size dependent mechanical properties of electrospun polymer fibers from a composite structure, Polymer (Guildf). 53 (2012) 5132–5137. doi:10.1016/j.polymer.2012.08.064.

[32] C. Shen, R.J. Wycisk, P.N. Pintauro, High performance electrospun bipolar membrane with a 3D junction, Energy Environ. Sci. 10 (2017) 1435–1442. doi:10.1039/C7EE00345E.

Chapter 2

Background

2.1 Fundamentals of H_2/Air Fuel Cells

Fuel cells are a class of electrochemical devices that directly convert the chemical potential of a fuel to electrical energy. In a hydrogen/air fuel cell, hydrogen and oxygen are consumed, resulting in the direct and clean generation of electricity and water. The heart of the fuel cell is the membrane-electrode assembly, which is comprised of an anode, a cathode, and an ion-exchange membrane. The electrodes are made of a mixture of catalyst (typically Platinum [1–3], a Platinum alloy such as PtNi or PtCo [3,4], or a non-Platinum Group Metal [5]) dispersed on carbon particles and an ion-conducting polymer (i.e. an ionomer) that adhere to the ion-exchange membrane. The ion-exchange membrane, which is made primarily of an ionomer, physically separates the electrodes and prevents gas crossover. A schematic of a hydrogen/air fuel cell is shown in Figure 2.1.

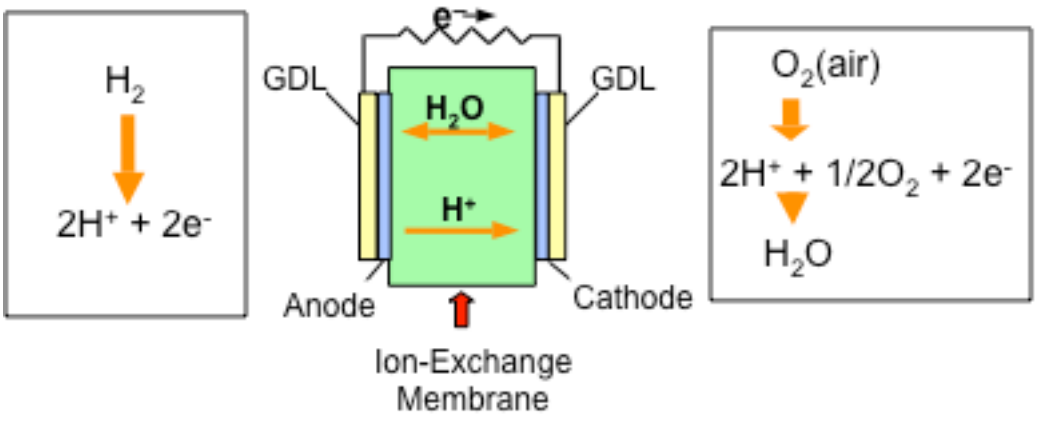

Figure 2.1: Schematic of a Hydrogen/air Fuel Cell using a proton-exchange membrane [6].

In a hydrogen/air fuel cell, hydrogen gas is fed to the anode, where it is oxidized to form protons and electrons. The electrons travel through the external load of the fuel cell, while the protons travel through the membrane to the cathode. At the cathode, electrons and protons recombine with oxygen (from air) to form water. While this pair of electrochemical half-cell reactions (shown in Equation 2.1) has a theoretical potential of 1.23 V (vs. SHE), the fuel cell typically experiences crossover, kinetic, ohmic, and mass transport limitations [7–11] that cause voltage losses during operation. An example of a polarization curve is shown in Figure 2.2. The permeability of the ion-exchange membrane toward hydrogen and oxygen leads to crossover and subsequent mixing of the feed gases, which reduces the working voltage of the fuel cell. At low current densities, voltage losses are caused by the sluggish kinetics of the oxygen reduction reaction at the cathode. At greater current densities, ohmic resistance, which includes electronic resistance in the electrodes and ionic resistance in the membrane [12], dominates the losses. At high current densities, excessive water formation (i.e. “flooding”) at the

cathode or limited access to the catalysts sites of oxygen lead to mass transport limitations and associated voltage losses [10,11].

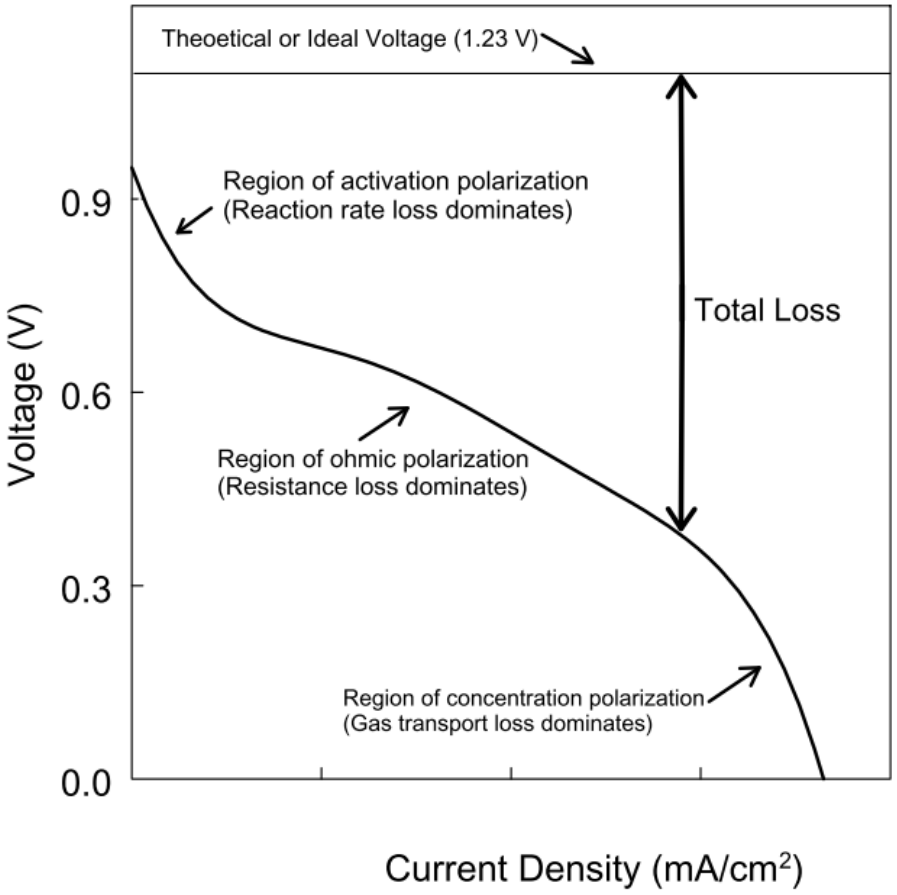

Figure 2.2: Example of fuel cell polarization curve, highlighting limitations due to kinetic (activation), ohmic, and mass transport (concentration) overpotential. Image taken from Reference [13].

Equation 2.1: a) Hydrogen oxidation reaction and b) Oxygen reduction reaction with electrochemical half-cell potential vs. standard hydrogen electrode at 25 °C.

$$H^+ + 2e^- \leftrightarrow H_2 \quad E_0 = 0\ \text{V (vs. SHE)} \qquad \text{a)}$$

$$4H^+ + 4e^- + O_2 \leftrightarrow 2H_2O \quad E_0 = 1.23\ \text{V (vs. SHE)} \qquad \text{b)}$$

The electrodes and membrane are designed to improve the performance of an MEA by achieving better kinetics and reducing ionic, electronic, and mass transport losses. Platinum is added to the electrodes present to improve the kinetics of the hydrogen oxidation reaction (HOR) and oxygen reduction reaction (ORR). The ionomer provides proton pathways from the catalyst sites to the membrane, and the carbon provides electronic pathways to the external load. Finally, the membrane prevents gas crossover, keeping hydrogen and oxygen at their respective electrodes.

2.2 Requirements of PEMs

The proton-exchange membrane (PEM) must exhibit several key characteristics that relate to its performance, durability, and cost. The PEM is expected to be a) highly conductive and/or thin, minimizing resistive losses during proton transport, b) impermeable to H_2 and O_2, c) resistive to electron flow, d) dimensionally stable as it is exposed to high and low humidity conditions, e) chemically and mechanically stable during MEA fabrication and fuel cell operation, and f) inexpensive.

Ideally, a membrane will have a low area-specific resistance (ASR, which is defined as membrane thickness divided by conductivity), which can be achieved by minimizing its thickness or maximizing conductivity. This reduces ohmic overpotential during fuel cell operation. While the ASR of a membrane decreases as the membrane thickness is reduced, the crossover of feed gases (which is associated with the permeability of the membrane) increases, which negatively affects fuel cell performance. The conductivity and hydrophilicity of a membrane are dependent on its ion-exchange capacity (IEC), defined as the concentration of fixed charge groups in the polymer. As the IEC is increased, both the proton conductivity and the water swelling of the

membrane increase. However, at ultra-high IECs, the membrane can tend toward water solubility.

During fuel cell operation, the membrane is exposed to various factors that make it more susceptible to failure. As the fuel cell is turned off/on, the membrane goes from cold and dry to hot and wet, and will expand or contract in response to the increase or decrease in water content. Gas crossover in a fuel cell can result in the generation of peroxide and hydroxyl radicals, which chemically degrade the ionomer. Additionally, the high fuel cell operating temperature can soften the PEM, compromising its mechanical integrity.

Nafion®, formerly developed by du Pont de Nemours and Company (commonly referred to as DuPont) in the 1960's [14] and now manufactured and sold by The Chemours Company, is regarded as the "gold standard" of membrane materials in H_2/air fuel cells that operate at low/moderate temperatures. It is a perfluorosulfonic acid (PFSA) ionomer, with a structure shown in Figure 2.3.

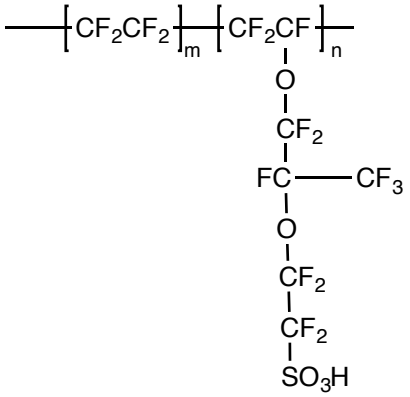

Figure 2.3: Polymer structure of 1100 EW Nafion [15], where m = 7, n = 1.

Nafion boasts a remarkable set of characteristics. First, it has a high proton conductivity in both liquid water (0.09 S/cm at 25 °C) [16] and water vapor (~0.08 S/cm

at 80% RH, 80 °C) [17,18], which arises from its phase-segregated structure and highly acidic fixed charge groups [14]. The perfluorinated vinyl ether chain separating the terminal groups from the polymer backbone allows the sulfonic acid (with a pKa = -6) [19] sites to aggregate and form ionic clusters [19–24]. As Nafion is hydrated, these ionic clusters fill with water and form channels through which protons can move via a vehicle (diffusion of an hydrated proton) and/or Grotthuss (proton "hopping") mechanism [4,10,21,25,26]. Second, the poly(tetrafluoroethylene) (PTFE) backbone is able to crystallize, lending mechanical strength, as well as chemical and dimensional stability, to the resultant film [2,3]. Third, Nafion typically exhibits a low H_2 crossover rate (as low as 1.5 mA/cm^2 for a 50 μm thick film composed of 100 EW Nafion [27]). Despite these attractive characteristics, Nafion degrades when exposed to harsh conditions, such as hydration/dehydration cycles, elevated temperatures, and the highly oxidative environment of a fuel cell. Proton conductivity is heavily dependent on the presence of water, and as Nafion dries, its conductivity dramatically decreases. The resultant increase in ASR leads to a loss in fuel cell performance at low relative humidity. Excessive fuel crossover can lead to the generation of peroxide radicals (which can chemically degrade the ionomer) [2–4,11,28,29], hot spots (which can cause membrane thinning or create a pinhole) [30,31], or a short circuit between the anode and cathode. As Nafion is hydrated and dehydrated when confined in an MEA, its high in-plane swelling (16%, as per reference [16]) leads to the generation of stresses at the membrane/electrode interface. These stresses have been shown to lead to cracks and pinholes in the membrane, as well as delamination between the membrane and the electrodes [3,4,8,11,29,32–35]. Defects

reduce the performance of the fuel cell by allowing hydrogen and oxygen gas to pass freely through the membrane.

While improving every aspect of a PEM is important for the widespread implementation of fuel cell technology, the focus of this particular chapter is to describe the various methods that have been used to improve the durability during humidity cycling (i.e. reduce in-plane swelling) and reduce the ASR of the membrane at both high and low levels of hydration while maintaining low gas crossover.

2.3 Prior Research in PEM Fabrication

Researchers have utilized a variety of PEM materials and fabrication techniques in an attempt to make a membrane that simultaneously meets the conductivity and stability targets described in Chapter 1. High IECs are achieved by adding ion-conducting moieties to the ionomer [36–38]. A hydrophobic component is sometimes added as a reinforcing material to provide mechanical and dimensional stability to the composite film [39,40]. The exception to this is the case of block copolymers [14,41], which are comprised of hydrophilic and hydrophobic segments to provide ionic conductivity and mechanical stability. Cross-linked polymers are also used [42–44], where the chemical cross-links reduce IEC and swelling, and improve polymer strength.

2.3.1 High IEC Ionomers

Increasing the IEC of an ionomer typically involves adding fixed charge sites to its backbone. For sulfonated hydrocarbons, this involves proper control of the degree of sulfonation (which is the number of $-SO_3H$ groups per repeat unit of polymer). As the degree of sulfonation is increased, so does the IEC of the polymer. Similarly, block copolymers achieve increased IECs through control of their hydrophilic:hydrophobic

block ratio. The hydrophobic block is responsible for adding mechanical strength and swelling resistance to the ionomer, and the hydrophilic block, which contains acidic fixed-charge groups, imparts proton conductivity. In perfluoro-type ionomers, like Nafion (Figure 2.3), the length of the side chain and the number of tetrafluoroethylene (TFE) units between side chains influence the IEC of the ionomer. In general, water uptake increases with IEC for each type of membrane. In the sections that follow, more details regarding the benefits and detriments of typical fuel cell membrane ionomers will be discussed.

Sulfonated Hydrocarbons

Various types of hydrocarbons (such as poly(ether ether ketone) (PEEK), poly(arylene ether sulfone), polyimide, polyphenylene, and poly(ether ketone) [14,31,45]) can be used to prepare a sulfonated ionomer membrane. Sulfonated PEEK (SPEEK) serves as a good example for these types of materials. PEEK is high-performance thermoplastic that is sulfonated by dissolution in concentrated H_2SO_4 [46–51]. As a result, sulfonic acid sites are attached to the phenyl rings *ortho* to the ether linkage in the backbone of the polymer. An example of the backbone structure of PEEK and SPEEK are shown in Figure 2.4a and Figure 2.4b, respectively.

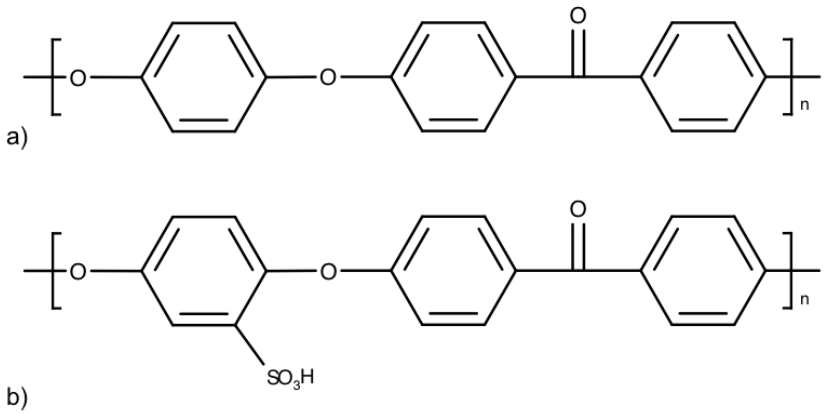

Figure 2.4: Repeat unit of a) poly(ether ether ketone) and b) sulfonated poly(ether ether ketone). Structures adapted from Reference [31].

With increased degrees of sulfonation, the conductivity and water uptake of SPEEK increase (due to the additional acid sites along the backbone), and its solubility in various organic solvents increases (due to a reduction in crystallinity) [46,50,52,53]. SPEEK and similarly sulfonated hydrocarbons exhibit characteristics that can compromise their performance as fuel cell PEMs. At extreme levels of sulfonation (where the IEC exceeds 2.6 mmol/g and proton conductivity at 80°C and 100% RH exceeds 0.2 S/cm, respectively), SPEEK can become soluble in liquid water and brittle when dry [43,53]. In addition, the mechanical properties of SPEEK (tensile modulus and strength) are reduced by over 50% upon complete sulfonation [54,55]. In spite of this reduction in strength, SPEEK with an IEC of 2.4 mmol/g has a tensile modulus of 800 MPa, which is significantly greater than that of Nafion, with a tensile modulus of ~300 MPa [27,55]. While the conductivity of sulfonated hydrocarbons increases with the degree of sulfonation, it is relatively low when compared to Nafion [2,52,56,57]. For example, Zhang & Mukerjee report a SPEEK membrane with an IEC of 1.31 mmol/g and a proton conductivity of 0.065 S/cm at 30 °C. This can be compared to Nafion, with an

IEC of 0.91 mmol/g and a conductivity of 0.091 S/cm at the same conditions [2]. The low SPEEK conductivity has been connected with the lower acidity of the aryl sulfonic acid sites (pKa = -1) compared to the pendant sulfonic acid of Nafion (pKa = -6) [2,19,58]. In addition, the lack of nanoseparation between the rigid backbone and the proton-conducting sites [52,59] contributes to the formation of very narrow water channels upon hydration, which further limits conductivity. The degree of sulfonation of a hydrocarbon ionomer must be increased to achieve a conductivity comparable to or better than that of Nafion [2,53,58]. This also results in greater water uptake, which leads to increased dimensional water swelling and polymer plasticization, both of which are detrimental to performance during PEM fuel cell operation and on/off humidity cycling. In addition, extensive sulfonation has been shown to lead to a loss in crystallinity [14,60].

Block Copolymers

The synthesis of polymers with hydrophilic and hydrophobic blocks (i.e. block copolymers) offers increased control of the degree of sulfonation [61] and segregation of the sulfonic acid sites [14,37,61,62]. The hydrophobic blocks offer mechanical stability, while the hydrophilic blocks increase the IEC and conductivity of the resultant ionomer. Furthermore, the block sequence can be controlled, leading to a well-defined pattern of hydrophilic and hydrophobic regions. Block copolymers have also been shown to exhibit nanophase segregation similar to Nafion, forming ion-rich and ion-poor domains [14,45]. This is advantageous due to the formation of large ionic domains in the polymer [52], which aids in conductivity [63,64]. In addition, the type of sidechain linkage to the main polymer chain can be varied, leading to increased separation between the sulfonic acid sidechain clusters and the polymer backbone [63,64]. As a result, larger water channels

can be formed in the polymer, which can further enhance proton conductivity. The work of Xie *et al.* is a good example of these factors. Several highly branched block copolymers were synthesized and compared to the properties of a statistical random copolymer. The ionomer structure of their branched star-shaped block poly(arylene ether sulfone) with sulfonalkyl pendant groups is shown in Figure 2.5. Their work showed that both block structures – where the hydrophilic chains surrounded a hydrophobic core (6f) or where the hydrophilic core was surrounded by the hydrophobic chains (6s) – exhibited greater proton conductivity than the random copolymer. Further, Xie *et al.* demonstrated that their polymers exhibited nano-scale separation, as evidenced by atomic force microscopy (AFM) in tapping mode.

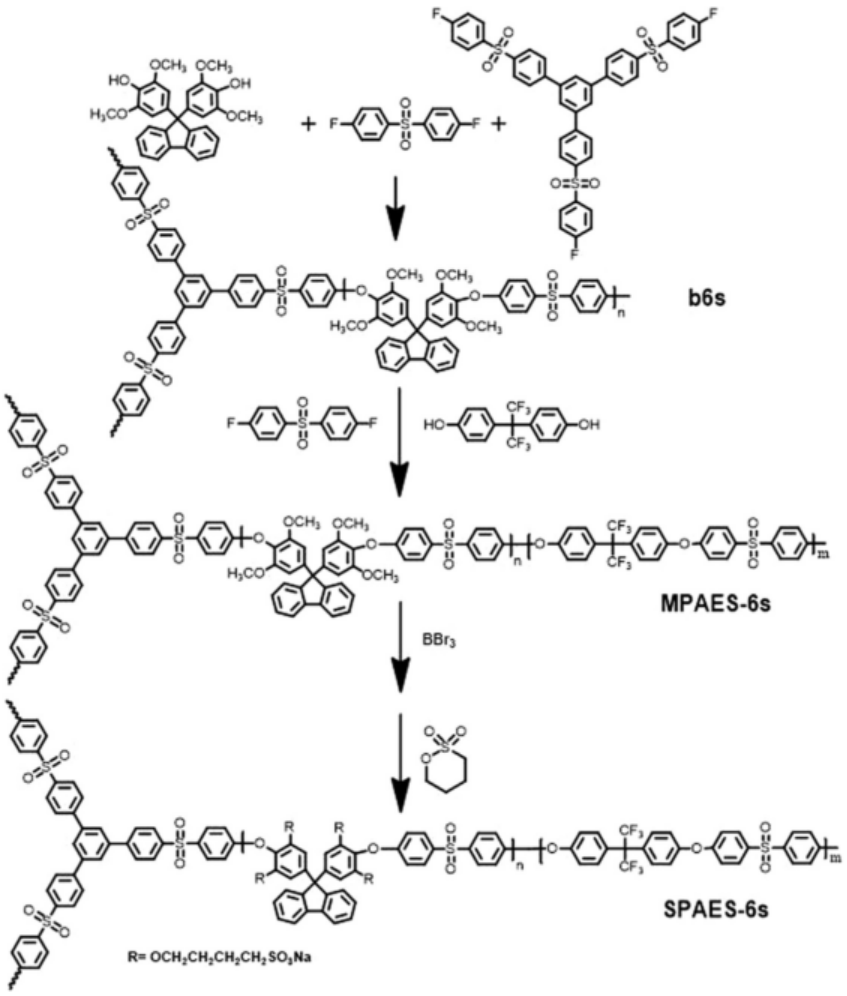

Figure 2.5: Ionomer structure of branched star-shaped block poly(arylene ether sulfone) with sulfonalkyl pendant groups with hydrophilic core surrounded by hydrophobic matrix. Adapted with permission from H. Xie, D. Tao, J. Ni, X. Xiang, C. Gao, L. Wang, *J. Memb. Sci.* 497 (2016) 55-66 [63]. Copyright Elsevier 2016.

While block copolymers have shown numerous advantages, they are susceptible to similar performance and durability limitations. As is common in proton-conducting ionomers, a loss in hydration leads to losses in conductivity and embrittlement of the polymer [53,64]. Similar to sulfonated hydrocarbons, block copolymers require a greater IEC to achieve a conductivity similar to Nafion [61,64], which results in increased water

uptake that can compromise the mechanical integrity of the ionomer during fuel cell operation. Excessive sulfonation can also lead to polymer dissolution, which necessitates modification to ensure stability in a fuel cell environment.

Perfluoro-type ionomers

The most widely studied type of PEM material is Nafion, which was originally manufactured by du Pont de Nemours and Company in the 1960s for usage as permselective membrane separators [20]. Nafion, the structure of which is shown in Figure 2.3, has garnered increased attention due to its high conductivity and good chemical and hydrothermal durability characteristics. In addition, various other perfluoro-type ionomers with high IEC have been synthesized in order to achieve a proton conductivity at low humidity/high temperature superior to that of Nafion while maintaining long-term mechanical stability (due to improved main-chain crystallinity) [65,66]. Typically, increasing the IEC of a PFSA ionomer involves adding more side chains to the backbone or by altering the side chain structure. In either case, the equivalent weight (gram polymer/mole equivalent sulfonic acid) is reduced. Some notable examples of this are Solvay's Aquivion®, which is a short-side chain PFSA (shown in Figure 2.6a), 3M's low equivalent weight PFSA (Figure 2.6b) or perfluoroimide acid ionomer (PFIA), shown in Figure 2.6c.

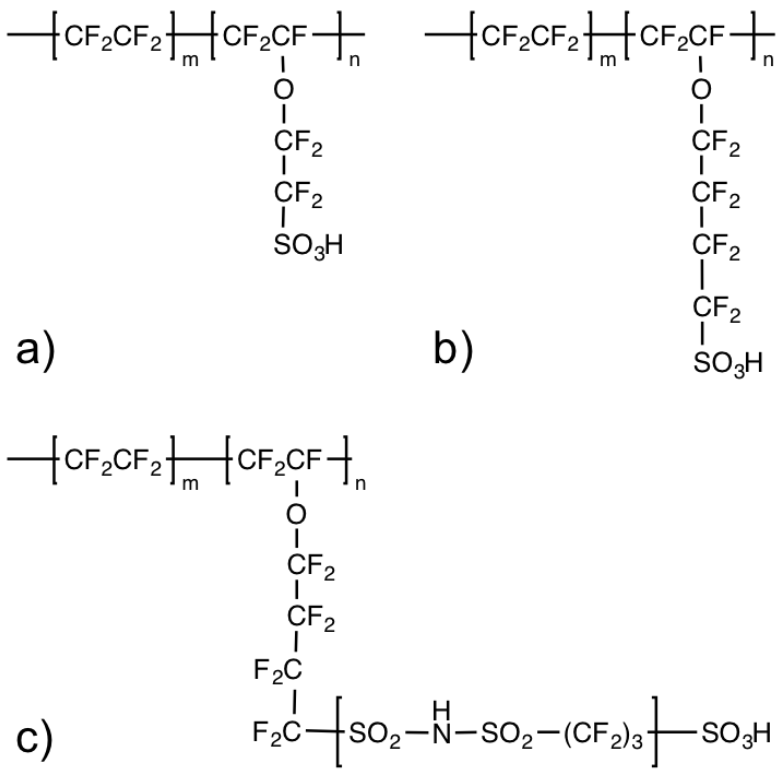

Figure 2.6: Molecular structure of a) short-side chain 830 EW PFSA[67] Aquivion®, where m = 5.5, n = 1; b) 3M PFSA[15], where m = 5, n = 1 for an 825 EW ionomer; c) 3M 660 EW PFIA[35,68,69], where m = 6.5, n = 1.

Table 2.1: Proton conductivity comparison of various perfluoro-type ionomers after treatment in 1.0 M H_2SO_4 and water.

Perfluorinated Ionomer	Proton Conductivity at 25 °C in water [S/cm]	Water Uptake at 25 °C [wt.%]	Equivalent Weight [mmol/g]
Nafion [2,15]	0.091[a]	38	1100
3M PFSA [15]	0.12[b]	68	825
3M PFSA [18]	0.132[c]	71	660
Aquivion [67,70]	0.11[b]	49	830

[a]Membrane was treated in 1.0 M H_2SO_4 for 1 hour at 80 °C, then in H_2O for 1 hour at 80 °C.
[b]Membrane was boiled for 1 hour in 1.0 M acid, then in H_2O for 1 hour.
[c]Membrane was allowed to soak at room temperature for 16 hours in acid, then for 6 hours at room temperature in H_2O.

Variations in the ionomer structure (such as increasing the frequency of the side chains along the PTFE backbone, or reducing the length of the side chain) have been shown to increase IEC and conductivity of PFSAs (see Table 2.1), but can reduce the durability or long-term performance of the ionomer as well. As additional sulfonic acid terminated side chains are added to PFSA, there is an increase in its water uptake due to a loss in backbone crystallinity [18,68,71] and an increase in the concentration of acid conducting sites. As an example, Ballengee *et al.* reported the properties of a low-equivalent weight 3M ionomer, 660 EW PFSA (Figure 2.6b, with m = 2.8, n = 1) [18]. Despite its high conductivity (0.132 S/cm in 25°C water), the ionomer was observed to be soluble in hot water, losing ~40% of its dry weight after immersion in boiling water. The 825 EW PFSA (m = 5, n = 1), as reported by Zhang *et al.* [71], exhibited a lower conductivity than the 660 EW PFSA (0.12 S/cm vs. 0.132 S/cm in 25°C water), but no loss in mass after boiling in water. Similarly, the length of the side chain can be reduced to increase the conductivity of the ionomer [72,73]. This approach has the advantage of maintaining crystallinity in the PTFE backbone. Wide-angle X-ray diffraction was used to show that 830 EW Aquivion, a short-side chain PFSA, has a crystallinity (after annealing at 190°C for 1 hour) of 23% [67], which compares favorably with that of 1100 EW Nafion (which has a crystallinity of 17.7% according to reference [71]). A crystallinity of 0% was observed for 3M's 825 EW PFSA (although the 3M ionomer was annealed at 150°C, rather than 190°C) [71]. The improved crystallinity and greater IEC of short-side chain PFSAs such as Aquivion allow for greater ionic conductivity and water uptake, along with improved stability compared to long-side chain ionomers [67,70,74]. The reduced length of the side chain also restricts the ability of the sulfonic

acid groups to segregate. As a result, the ionic groups in short-side chain ionomers tend to form channels that are less developed than those in long-side chain ionomers (such as Nafion) [70,74], allowing for lower gas crossover.

As an alternative to shortening the side chain of a PFSA, it is also possible to insert additional proton dissociating sites on the side chains [35,68,69,75]. 3M Company has recently developed a series of multi-acid side chain (MASC) ionomers that contain both an imide acid as well as a terminal sulfonic acid. The structure of 3M's 660 EW perfluoroimide acid (PFIA) is shown in Figure 2.6c. Similar to reducing the length of the side chain, this approach has the advantage of maintaining the number of CF_2 units between side chains in the backbone of the ionomer. Thus, the fabrication of MASC ionomers potentially serves as an avenue to attain a low equivalent weight while having a high crystallinity with water-insolubility [68].

2.3.2 Composite Membranes

In order to circumvent the limitations associated with high-IEC ionomers, researchers often mix an uncharged polymer with the ionomer. While this reduces the effective proton conductivity of the resultant composite membrane, the swelling of the membrane decreases the mechanical properties are improved. Furthermore, the utilization of a composite membrane lowers membrane cost, as the relative percent of the membrane composed of expensive ionomer is reduced.

While the IEC of an ionomer can be increased to obtain a membrane with high conductivity, the hydrophilicity of the protogenic groups also causes it to swell excessively in water. In extreme cases, the ionomer can become water soluble, which is particularly problematic in applications where liquid water may be present. Furthermore,

excessive swelling of the membrane leads to degradation of its mechanical properties when fully hydrated, which compromises its durability in a fuel cell when confined in an MEA. When restricted by electrodes and fuel cell hardware, such swelling can lead to the formation of cracks/pinholes, or delamination between the membrane and the electrodes [8]. In addition, there is the potential for membrane thinning, which can reduce its electrical resistivity [3,4,8,11,29,32]. To circumvent these potential shortcomings, high IEC ionomers are utilized in PEMs by combining with hydrophobic polymers, which both reinforce and reduce the overall water uptake of the membrane.

Solution-cast Blends

Polymer blends are a simple method of fabricating a composite membrane with moderate conductivity and dimensional stability. After mixing in a common solvent, the blend is cast onto a surface. After evaporation of the solvent, the resultant dense composite membrane can be used as a PEM. Despite the ease of fabrication, polymer blends have various shortcomings that limit their practical application. Blended films at intermediate compositions have been shown to exhibit proton conductivities lower than what would be expected based on a linear mixing rule, which has been connected to percolation limitation [38,58,76]. These limitations arise primarily due to poor interactions between the components, which can lead to large isolated domains of the ionomer or reinforcing polymer [76,77]. For example, blends of sulfonated poly(ether ketone ketone) (sPEKK) and poly(ether imide) (PEI) were fabricated over a range of ionomer contents by Swier *et al.* for use as a PEM [78]. While the addition of PEI, which formed micron-scale domains in the final membrane, led to a reduction in membrane water uptake, the conductivity decreased dramatically from 0.04 S/cm for neat SPEKK at

25°C and 98% RH to ~0.01 S/cm for the 50/50 SPEKK/PEI blended membrane at the same conditions [78]. The authors showed that control of the casting temperature and IEC of sPEKK could aid in reducing the PEI domain size, but there was no reported effect on conductivity. Furthermore, the composite membranes failed prematurely during MEA testing in a fuel cell due to excessive membrane swelling [78], suggesting that the reductions achieved by blending sPEKK with PEI were insufficient to improve long-term durability.

Zhang *et al.* [41] reported an effort to fabricate miscible polymer blends that exhibited high conductivity. Miscibility was achieved by utilizing the tetraethylamine salt form of the sulfonated poly(phenylene arylene) (SPA) and sulfonated polyimide (SPI) block copolymer (synthesis and structures shown in Figure 2.7), with the polymers mixed in an appropriate solvent (the authors indicated that m-cresol was best) [41]. The homogeneity of the films suggested miscibility of the components, as well as the potential for high performance. In addition, the reported conductivities of membrane samples suggested good control of the blend morphology of the membranes. For example, a 50:50 blend of SPA:SPI exhibited a proton conductivity and water uptake of 0.211 S/cm and 67% in 60 °C water, which can be compared to 0.243 S/cm and 70% for the SPA and 0.127 S/cm and 64% for the SPI at the same conditions [41].

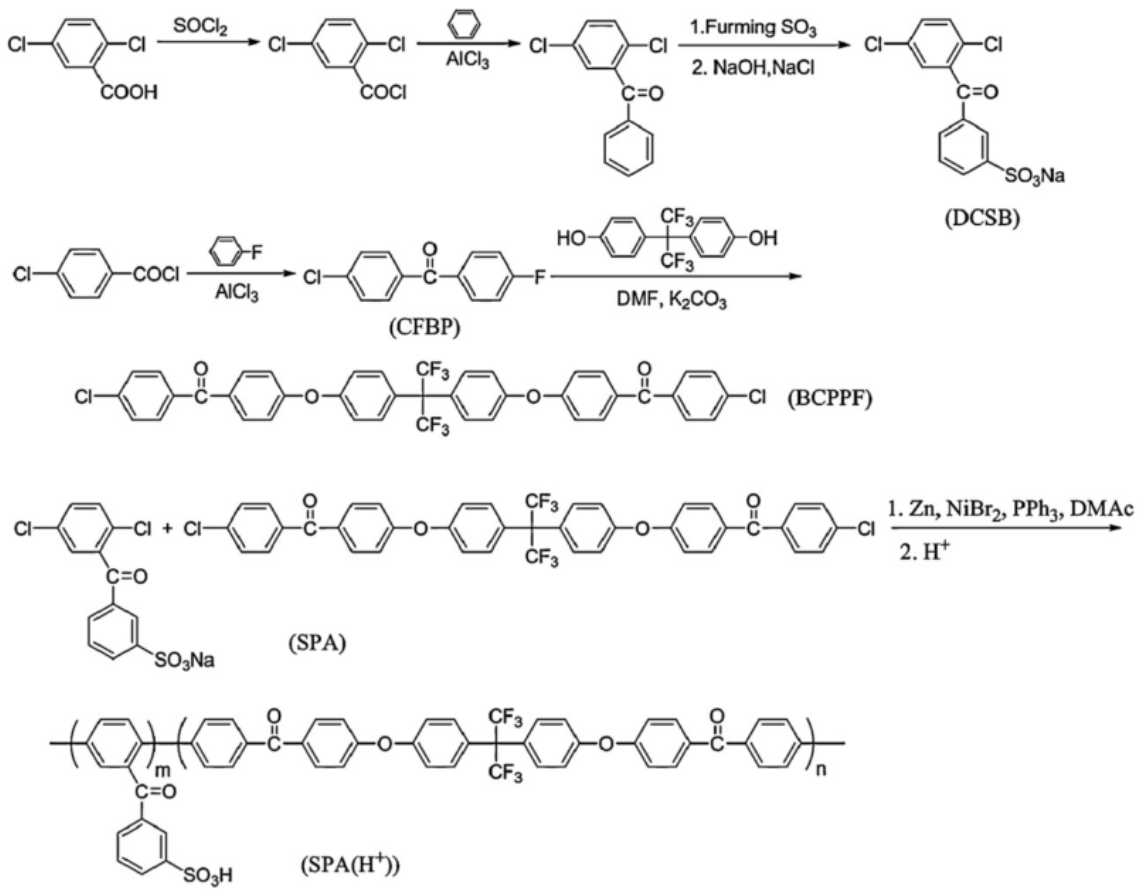

Figure 2.7: Synthesis of sulfonated poly(phenylene phenyl ketone-co-arylene ether ketone) copolymer [41]. Adapted with permission from X. Zhang, S. Chen, J. Liu, Z. Hu, S. Chen, L. Wang, *J. Memb. Sci.* 371 (2011) 276-285. Copyright Elsevier 2011.

Composite Membranes via Impregnation into a Porous Support

Composite membranes consisting of an ionomer impregnated into a porous support have been reported to exhibit low dimensional swelling in water. An example of a pore-filled membrane is the GORE-Select membrane. The GORE membranes were first reported by W.L. Gore and Associates in 1995, and utilize a PTFE web that has been impregnated with PFSA, leading to high strength and conductivity [79,80]. While many of the characteristics of this type of pore-filled membrane are classified, it has been

shown that a GORE-Select membrane using a 900 EW ionomer exhibits low in-plane swelling [80] (~3% vs. ~11% for Nafion 117) and extended lifetime in an on/off humidity cycling test [81,82] while matching the fuel cell performance of Nafion [82]. The GORE-Select membrane described in reference [81] exhibits a lifetime of up to 600 hours in an accelerated fuel cell RH cycling stress test; by comparison, the lifetime of the unreinforced membrane was less than 24 hours. A GORE-Select membrane maintained a H_2 crossover less than 5 mA/cm^2 for 1200 hours[2], while Nafion lasted no more than 500 hour s[82]. The presence of the reinforcing web adds dimensional stability and strength to the membrane, allowing it to be thinner than conventional Nafion, leading to improved lifetime and a reduced ASR [80].

Composite Membranes via Electrospinning

While conventional blend membranes often suffer losses in conductivity at intermediate compositions, nanofiber composite membranes have been shown to exhibit proton conductivities that are linearly dependent on ionomer content. Similar to a solution cast blend, a nanofiber composite membrane is one in which an uncharged polymer and an ionomer are combined to simultaneously meet conductivity and dimensional stability targets. Unlike a blend, however, a nanofiber composite membrane is a bi-continuous system, where one of the components (the ionomer or the uncharged reinforcing polymer) comprises the matrix, and the other exists as fibers. Neither component forms isolated domains, which allows the conductivity to be dictated by the ionomer content [18,27,83–85].

Choi *et al.* utilized electrospinning to make a nanofiber composite membrane in which PFSA fibers were reinforced by a polyurethane matrix [17]. Nanofibers of 825 or

725 EW PFSA were electrospun with a small amount of poly(ethylene oxide) as a carrier, and after annealing, the mats were impregnated with the UV-crosslinkable liquid urethane pre-polymer (Norland Optical Adhesive 63) to form dense and defect-free membranes. Dual fiber electrospinning was introduced in 2011 by Ballengee and Pintauro [27] as an alternative to impregnation of an electrospun mat or a macroporous support. In their work, Ballengee and Pintauro utilized PFSA nanofibers (in this case, Nafion from du Pont de Nemours and Company), which were co-electrospun with poly(phenyl sulfone) (PPSU) fibers for reinforcement. The resultant mixed fiber mats could be converted into membranes in which: a) PPSU fibers reinforced a Nafion matrix or b) Nafion fibers were embedded in a PPSU matrix [27]. In both cases, the resultant nanofiber composite membranes exhibited lower in-plane swelling and gravimetric water uptake as compared to the neat ionomer, while the conductivity was described by a Nafion volume fraction mixing rule [27], which was also observed by Choi *et al.* [86]. A schematic of a dual fiber electrospinning apparatus is shown in Figure 2.8.

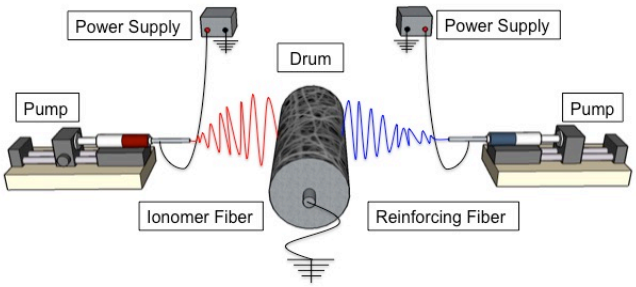

Figure 2.8: Illustration of dual fiber electrospinning apparatus.

2.3.3 Thin Membranes

The fabrication of thin membranes is also a subject of interest due to the desire for a low ASR and for back-diffusion of water in an operating H_2/air fuel cell. During fuel cell operation, water is generated at the cathode, creating a concentration gradient through the MEA. With a sufficiently thin membrane, water is expected to diffuse to the anode, providing additional hydration even at low levels of humidity [7,87–89]. In addition, lower proton conductivity can be tolerated as membrane thickness is reduced. Because of these benefits (which can also include reduced overall membrane cost, as less ionomer and reinforcing material would be used in ultra-thin membranes), reports of fabrication and utilization of ultra thin membranes have become increasingly common. Such thin membranes are inherently weaker, making them more prone to failure during MEA fabrication or under fuel cell operating conditions [65,80,90,91]. In addition, the reduced thickness will increase gas crossover [91], further reducing the performance of the fuel cell. Attempts to fabricate thin membranes have focused on methods to mitigate some of these issues.

Brietweiser *et al.* reported on the fabrication of a 12 μm thick composite membrane by directly depositing the components on to gas diffusion electrodes (GDEs). Reinforcing poly(vinylidene fluoride-*co*-hexafluoropropylene) (PVDF-HFP) fibers were electrospun onto a GDE, and a Nafion dispersion was subsequently inkjet-printed onto the porous web [90]. A membrane-electrode assembly was prepared by stacking the GDEs with the membrane sides facing each other. The resultant MEA, which contained the 12 μm thick unannealed Nafion/PVDF-HFP composite membrane, was loaded into a fuel cell and compared to a commercial MEA containing a 20 μm reinforced Nafion membrane. In a

fuel cell operating at 80°C, 95% RH with a H_2/air flow rate of 1.5/2.5 L/min at atmospheric pressure, the 12 μm membrane achieved a maximum power density of 0.58 W/cm^2, which is greater than the power density achieved by the 20 μm Nafion membrane (0.48 W/cm^2). Similar improvements in power density were observed when the fuel cell was operated at 100 °C and 120 °C. The authors attributed the increased power density to reduced ASR and improved back-diffusion of water through the thin membrane.

Inorganic additives have been used in PEMs in order to enhance proton conductivity at low humidity [9,22,45,56] or to reinforce the composite membrane [8,45]. Some of these particles, such as CeO_x or Pt-SiO_2, have exhibited beneficial properties in preventing fuel crossover [91,92] or peroxide generation [11,93] in a PEM fuel cell. Wang *et al.* fabricated a 9 μm composite membrane that utilized platinum on layered double hydrides (Pt-LDH) to control fuel crossover and improve fuel cell performance [91]. Pt catalysts are typically present in the electrodes to drive the HOR and ORR; in this case, they were embedded into a Nafion membrane (which would reduce its electronic resistance) via solution casting to convert any H_2 and O_2 that penetrated the membrane into water. Thus, the membrane possessed several benefits: the Pt-LDH additives reduced fuel crossover (from ~5 mA/cm^2 for a 9 μm Nafion film to ~1 mA/cm^2 for the composite), promoted membrane self-humidification, and improved mechanical strength and back-diffusion of water. In addition, the thin Nafion membrane with Pt-LDH additives exhibited an increase in maximum power density compared to a pure Nafion film of the same thickness (1174 mW/cm^2 for a 9-μm thick Nafion/Pt-LDH film vs. 873 for a 9-μm thick Nafion film) when operating in a fuel cell at 60 °C with no humidification, H_2/O_2 flow rates of 100 sccm, and 100 kPa backpressure.

2.4 Electrospinning Background

Electrospinning is a technique that allows for the fabrication of polymer fibers with nano-scale diameters [17,109,110]. The technique was patented in the early 1900's by Formhals [111,112], but has recently experienced increased popularity due, in part, to the beneficial properties that arise from sub-micron fibers, such as short transport lengths [113], intrafiber porosity [114], high fiber aspect ratios, and high fiber mechanical strength [115,116]. During electrospinning, a polymer solution or melt is pumped through a needle that is set to a high voltage relative to a grounded target. The strong electrostatic field induces a surface potential on the polymer solution/melt, which overcome surface tension forces, causing a "necking" down of the filament at the spinneret tip and drawing it into a Taylor cone [117,118]. As the polymer jet emerges from the Taylor cone and travels to a grounded collector surface, whipping instabilities cause fiber elongation and a narrowing of its diameter. Solvent evaporates from the polymer jet as it travels to the collector, and under the proper conditions, dry fibers are deposited on the collector surface as a non-woven mat. Successful electrospinning requires proper control of the voltage, flow rate, relative humidity, and solution parameters (i.e. solvent/dispersant type and polymer concentration).

The electrospinning technique can be used for a variety of applications through intelligent selection of the components for the resultant mat. A wide range of polymers, including poly(phenyl sulfone) [18,27,85,119,120], poly(vinylidene fluoride) [83], chloromethylated poly(phenyl sulfone) [85], poly(phenylene oxide) [121], and poly(ether ketone) [84], have been utilized to fabricate nanofiber composite mats for anion exchange

membranes, H_2/Br_2 fuel cells [83], or bipolar membranes [97]. The addition of Pt/C catalyst particles to an ionomer/carrier electrospinning solution can result in a nanofiber mat that is suitable as an electrode in an MEA [114,122]. The addition of carbon and silicon to poly(acrylic acid) has been shown to lead to fiber mats that can be used as Li-ion battery anodes [113,123]. Electrospun nanofibers have also found use in biomedical applications as artificial blood vessels or wound dressings [124–126]. The high surface area and porosity of an electrospun mat make it attractive as a scaffold for tissue growth [125,127]. The electrospinning process can also be tuned to make layered structures that mimic the function of a prototypical blood vessel [128]. Furthermore, biocompatible and biodegradable polymers can be incorporated into an electrospun mat [124], which will aid in the repair of damaged tissue.

2.5 References

[1] W. Zhang, P.N. Pintauro, High-Performance Nanofiber Fuel Cell Electrodes, ChemSusChem. 4 (2011) 1753–1757. doi:10.1002/cssc.201100245.

[2] L. Zhang, S. Mukerjee, Investigation of Durability Issues of Selected Nonfluorinated Proton Exchange Membranes for Fuel Cell Application, J. Electrochem. Soc. 153 (2006) A1062. doi:10.1149/1.2180715.

[3] J. Wu, X.Z. Yuan, J.J. Martin, H. Wang, J. Zhang, J. Shen, S. Wu, W. Merida, A review of PEM fuel cell durability: Degradation mechanisms and mitigation strategies, J. Power Sources. 184 (2008) 104–119. doi:10.1016/j.jpowsour.2008.06.006.

[4] F.A. De Bruijn, V.A.T. Dam, G.J.M. Janssen, Review : Durability and Degradation Issues of PEM Fuel Cell Components, (2008) 3–22. doi:10.1002/fuce.200700053.

[5] E. Proietti, F. Jaouen, M. Lefévre, N. Larouche, J. Tian, J. Herranz, J. Dodelet, Iron-based cathode catalyst with enchanced power density in polymer electrolyte membrane fuel cells, Nat. Commun. 2 (2011) 1–9. doi:10.1038/ncomms1427.

[6] P.N. Pintauro, Fabrication, Structure, and Properties of Nanofiber Composite Ion-Exchange Membranes, (2012).

[7] F. Liu, G. Lu, C.Y. Wang, Water transport coefficient distribution through the membrane in a polymer electrolyte fuel cell, J. Memb. Sci. 287 (2007) 126–131. doi:10.1016/j.memsci.2006.10.030.

[8] T. Ous, C. Arcoumanis, Degradation aspects of water formation and transport in

Proton Exchange Membrane Fuel Cell : A review, J. Power Sources. 240 (2013) 558–582. doi:10.1016/j.jpowsour.2013.04.044.

[9] C. Yang, P. Costamagna, S. Srinivasan, J. Benziger, A.B. Bocarsly, Approaches and technical challenges to high temperature operation of proton exchange membrane fuel cells, 103 (2001) 1–9.

[10] I.H. Hristov, S.J. Paddison, R. Paul, Molecular modeling of proton transport in the short-side-chain perfluorosulfonic acid ionomer, J. Phys. Chem. B. 112 (2008) 2937–2949. doi:10.1021/jp7108434.

[11] T.R. Ralph, D.E. Barnwell, P.J. Bouwman, A.J. Hodgkinson, M.I. Petch, M. Pollington, Reinforced Membrane Durability in Proton Exchange Membrane Fuel Cell Stacks for Automotive Applications, J. Electrochem. Soc. 155 (2008) B411–B422. doi:10.1149/1.2838163.

[12] K.R. Cooper, V. Ramani, J.M. Fenton, H.R. Kunz, Experimental Methods and Data Analyses for Polymer Electrolyte Fuel Cells, Scribner Associates Inc, 2005.

[13] J.B. Ballengee, Electrospun Nanofiber Composite Proton Exchange Membranes, Sch. Vanderbilt Univ. (2013) 233.

[14] Y. Zhao, M. Yoshida, T. Oshima, S. Koizumi, M. Rikukawa, N. Szekely, A. Radulescu, D. Richter, Elucidation of the morphology of the hydrocarbon multi-block copolymer electrolyte membranes for proton exchange fuel cells, Polymer (Guildf). 86 (2016) 157–167. doi:10.1016/j.polymer.2016.01.061.

[15] W. Zhang, D.L. Kish, P.N. Pintauro, Morphology and Performance of Stretched PFSA for Direct Methanol Fuel Cells, ECS Trans. 33 (2010) 635–645.

[16] K.S. Lee, M.H. Jeong, Y.J. Kim, S. Bin Lee, J.S. Lee, Fluorinated aromatic

polyether ionomers containing perfluorocyclobutyl as cross-link groups for fuel cell applications, Chem. Mater. 24 (2012) 1443–1453. doi:10.1021/cm203539m.

[17] J. Choi, K.M. Lee, R. Wycisk, P.N. Pintauro, P.T. Mather, Nanofiber composite membranes with low equivalent weight perfluorosulfonic acid polymers, J. Mater. Chem. 20 (2010) 6282–6290. doi:10.1039/c0jm00441c.

[18] J.B. Ballengee, G.M. Haugen, S.J. Hamrock, P.N. Pintauro, Properties and Fuel Cell Performance of a Nanofiber Composite Membrane with 660 Equivalent Weight Perfluorosulfonic Acid, J. Electrochem. Soc. 160 (2013) F429–F435. doi:10.1149/2.088304jes.

[19] D.S. Kim, M. D.Guiver, Polymer membranes for fuel cells, Springer, 2009. doi:1010079780387735320.

[20] K.A. Mauritz, R.B. Moore, State of Understanding of Nafion, (2004).

[21] M. Maalouf, C.N. Sun, B. Pyle, M. Emery, G.M. Haugen, S.J. Hamrock, T.A. Zawodzinski, Factors enabling high mobility of protons and water in perfluorosulfonate membranes under low hydration conditions, Int. J. Hydrogen Energy. 39 (2014) 2795–2800. doi:10.1016/j.ijhydene.2013.11.006.

[22] Y. Liu, B. Yi, Z. Shao, L. Wang, Pt / CNTs-Nafion reinforced and self-humidifying composite membrane for PEMFC applications, 163 (2007) 807–813. doi:10.1016/j.jpowsour.2006.09.065.

[23] T.D. Gierke, G.E. Munn, F.C. Wilson, The Morphology in Nafion Perfluorinated Membrane Products, as Determined by Wide- and Small- Angle X-Ray Studies, J. Polym. Sci. Polym. Phys. Ed. 19 (1981) 1687–1704. doi:10.1002/pol.1981.180191103.

[24] S.J. Paddison, Proton Conduction Mechanisms At Low Degrees of Hydration in Sulfonic Acid-Based Polymer Electrolyte Membranes, Annu. Rev. Mater. Res. 33 (2003) 289–319. doi:10.1146/annurev.matsci.33.022702.155102.

[25] N. Agmon, The Grotthuss mechanism, Chem. Phys. Lett. 50 (1995) 456–462.

[26] K. Kreuer, S.J. Paddison, E. Spohr, M. Schuster, K. Kreuer, S.J. Paddison, E. Spohr, M. Schuster, Transport in Proton Conductors for Fuel-Cell Applications : Simulations , Elementary Reactions , and Phenomenology Transport in Proton Conductors for Fuel-Cell Applications : Simulations , Elementary Reactions , and Phenomenology, 104 (2004) 4637–4678. doi:10.1021/cr020715f.

[27] J.B. Ballengee, P.N. Pintauro, Composite fuel cell membranes from dual-nanofiber electrospun mats, Macromolecules. 44 (2011) 7307–7314. doi:10.1021/ma201684j.

[28] S. Hommura, K. Kawahara, T. Shimohira, Development of a Method for Clarifying the Perfluorosulfonated Membrane Degradation Mechanism in a Fuel Cell, (2008) 29–33. doi:10.1149/1.2800171.

[29] M.P. Rodgers, L.J. Bonville, H.R. Kunz, D.K. Slattery, J.M. Fenton, Fuel Cell Perfluorinated Sulfonic Acid Membrane Degradation Correlating Accelerated Stress Testing and Lifetime, (2012).

[30] K. Ramya, G. Velayutham, C.K. Subramaniam, N. Rajalakshmi, K.S. Dhathathreyan, Effect of solvents on the characteristics of Nafion®/PTFE composite membranes for fuel cell applications, J. Power Sources. 160 (2006) 10–17. doi:10.1016/j.jpowsour.2005.12.082.

[31] R. Jiang, H.R. Kunz, J.M. Fenton, Investigation of membrane property and fuel

cell behavior with sulfonated poly (ether ether ketone) electrolyte : Temperature and relative humidity effects, 150 (2005) 120–128. doi:10.1016/j.jpowsour.2005.03.180.

[32] R. Borup, J. Meyers, B. Pivovar, Y.S. Kim, R. Mukundan, N. Garland, D. Myers, M. Wilson, F. Garzon, D. Wood, P. Zelenay, K. More, K. Stroh, T. Zawodzinski, X.J. Boncella, J.E. Mcgrath, O.M. Inaba, K. Miyatake, M. Hori, K. Ota, Z. Ogumi, S. Miyata, A. Nishikata, Z. Siroma, Y. Uchimoto, K. Yasuda, K. Kimijima, N. Iwashita, Scientific Aspects of Polymer Electrolyte Fuel Cell Durability and Degradation, (2007) 3904–3951.

[33] A. Kusoglu, A.M. Karlsson, M.H. Santare, S. Cleghorn, W.B. Johnson, Mechanical behavior of fuel cell membranes under humidity cycles and effect of swelling anisotropy on the fatigue stresses, J. Power Sources. 170 (2007) 345–358. doi:10.1016/j.jpowsour.2007.03.063.

[34] A. Theiler, L. Karpenko-Jereb, Modelling of the mechanical durability of constrained Nafion membrane under humidity cycling, Int. J. Hydrogen Energy. 40 (2015) 9773–9782. doi:10.1016/j.ijhydene.2015.05.110.

[35] R. Wycisk, P.N. Pintauro, J.W. Park, New developments in proton conducting membranes for fuel cells, Curr. Opin. Chem. Eng. 4 (2014) 71–78. doi:10.1016/j.coche.2014.01.012.

[36] Z. Zhu, N.M. Walsby, H.M. Colquhoun, D. Thompsett, E. Petrucco, Microblock ionomers: A new concept in temperature swelling-resistant membranes for PEM fuel cells, in: Fuel Cells, 2009: pp. 305–317. doi:10.1002/fuce.200800140.

[37] M.A. Hickner, H. Ghassemi, Y.S. Kim, B.R. Einsala, J.E. McGrath, Alternative

Polymer Systems for Proton Exchange Membranes, Chem. Rev. 104 (2004) 4587–4612. doi:10.1021/cr020711a.

[38] H.-L. Wu, C.-C.M. Ma, C.-H. Li, T.-M. Lee, C.-Y. Chen, C.-L. Chiang, C. Wu, Sulfonated poly(ether ether ketone)/poly(amide imide) polymer blends for proton conducting membrane, J. Memb. Sci. 280 (2006) 501–508. doi:10.1016/j.memsci.2006.02.005.

[39] N.A. Nazir, N. Kim, W.G. Iglesias, A. Jakli, T. Kyu, Conductive behavior in relation to domain morphology and phase diagram of Nafion/poly(vinylidene-co-trifluoroethylene) blends, Polymer (Guildf). 53 (2012) 196–204. doi:10.1016/j.polymer.2011.11.019.

[40] X. Liu, X. Meng, J. Wu, J. Huo, L. Cui, Q. Zhou, Microstructure and properties of novel SPEEK/PVDF-g-PSSA blends for proton exchange membrane with improved compatibility, RSC Adv. 5 (2015) 69621–69628. doi:10.1039/c5ra11894h.

[41] X. Zhang, S. Chen, J. Liu, Z. Hu, S. Chen, L. Wang, Preparation and properties of sulfonated poly(phenylene arylene)/sulfonated polyimide (SPA/SPI) blend membranes for polymer electrolyte membrane fuel cell applications, J. Memb. Sci. 371 (2011) 276–285. doi:10.1016/j.memsci.2011.01.054.

[42] H. Jiang, X. Guo, G. Zhang, J. Ni, C. Zhao, Z. Liu, L. Zhang, M. Li, S. Xu, H. Na, Cross-linked high conductive membranes based on water soluble ionomer for high performance proton exchange membrane fuel cells, J. Power Sources. 241 (2013) 529–535. doi:10.1016/j.jpowsour.2013.04.151.

[43] S.L.N.H. Rhoden, C.A. Linkous, N. Mohajeri, D.J. Díaz, P. Brooker, D.K.

Slattery, J.M. Fenton, Low equivalent weight Friedel-Crafts cross-linked sulfonated poly(ether ether ketone), J. Memb. Sci. 376 (2011) 290–301. doi:10.1016/j.memsci.2011.04.039.

[44] C. Liu, Z. Wu, Y. Xu, S. Zhang, C. Gong, Y. Tang, D. Sun, H. Wei, C. Shen, Facile one-step fabrication of sulfonated polyhedral oligomeric silsesquioxane cross-linked poly(ether ether ketone) for proton exchange membranes, Polym. Chem. 9 (2018) 3624–3632. doi:10.1039/c8py00650d.

[45] Y.S. Kim, F. Wang, M. Hickner, T.A. Zawodzinski, J.E. McGrath, Fabrication and characterization of heteropolyacid (H3PW12O40)/directly polymerized sulfonated poly(arylene ether sulfone) copolymer composite membranes for higher temperature fuel cell applications, J. Memb. Sci. 212 (2003) 263–282. doi:10.1016/S0376-7388(02)00507-0.

[46] F. Wang, T. Chen, J. Xu, Sodium sulfonate-functionalized poly(ether ether ketone)s, 1426 (1998) 1421–1426.

[47] F. Trotta, E. Drioli, G. Moraglio, E.B. Poma, Sulfonation of Polyetheretherketone by Chlorosulfuric Acid, (1998) 477–482.

[48] B.C. Johnson, I. Yilgor, C. Tran, M. Iqbal, D.R. Lloyd, Synthesis and Characterization of Sulfonated Poly(arylene Ether Sulfones) *, J. Polym. Sci. Part A Polym. Chem. 22 (1984) 721–737.

[49] C. Bailly, D.J. Williams, F.E. Karasz, W.J. Macknight, The sodium salts of sulphonated poly (aryl- ether-ether-ketone) (PEEK): Preparation and characterization, 28 (1986).

[50] X. Jin, M.T. Bishop, T.S. Ellis, F.E. Karaszt, A Sulphonated Poly(aryl Ether

Ketone), Br. Polym. J. 17 (1985) 4–10.

[51] J. Lee, C.S. Marvel, Polyaromatic Ether-Ketone Sulfonamides Prepared from Polydiphenyl Ether-Ketones by Chlorosulfonation and Treatment with Secondary Amines, J. Polym. Sci. Part A Polym. Chem. 22 (1984) 295–301.

[52] J. Roziére, D. Jones, Non-Fluorinated Polymer Materials for Proton Exchange Membrane Fuel Cells, Annu. Rev. Mater. Res. 20 (2003) 503–557. doi:10.1146/annurev.immunol.20.100301.064801.

[53] C.C. de Araujo, K.D. Kreuer, M. Schuster, G. Portale, H. Mendil-Jakani, G. Gebel, J. Maier, Poly(p-phenylene sulfone)s with high ion e exchange capacity: ionomers with unique microstructural and transport features, Phys. Chem. Chem. Phys. 11 (2009) 3305–3312. doi:10.1039/b905911n.

[54] F.J. Medellin-Rodriguez, P.J. Phillips, Crystallization and Structure-Mechanical Property Relations in Poly (Ary1 Ether Ether Ketone) [PEEK], Polym. Eng. Sci. 30 (1990) 860–869.

[55] M. Javad, S. Rowshanzamir, F. Gashoul, Comprehensive investigation of physicochemical and electrochemical properties of sulfonated poly (ether ether ketone) membranes with different degrees of sulfonation for proton exchange membrane fuel cell applications, Energy. 125 (2017) 614–628. doi:10.1016/j.energy.2017.02.143.

[56] J. Choi, K.M. Lee, R. Wycisk, P.N. Pintauro, P.T. Mather, Sulfonated Polysulfone/POSS Nanofiber Composite Membranes for PEM Fuel Cells, J. Electrochem. Soc. 157 (2010) B914. doi:10.1149/1.3392294.

[57] B. Jung, B. Kim, J.M. Yang, Transport of methanol and protons through partially

sulfonated polymer blend membranes for direct methanol fuel cell, J. Memb. Sci. 245 (2004) 61–69. doi:10.1016/j.memsci.2004.07.016.

[58] F. Wang, M. Hickner, Y. Seung, T.A. Zawodzinski, J.E. Mcgrath, Direct polymerization of sulfonated poly (arylene ether sulfone) random (statistical) copolymers : candidates for new proton exchange membranes, 197 (2002) 231–242.

[59] A. Kraytsberg, Y. Ein-Eli, Review of Advanced Materials for Proton Exchange Membrane Fuel Cells, Energy & Fuels. 28 (2014) 7303–7330. doi:10.1021/ef501977k.

[60] V. Di Noto, M. Piga, G.A. Giffin, G. Pace, Broadband electric spectroscopy of proton conducting SPEEK membranes, J. Memb. Sci. 390–391 (2012) 58–67. doi:10.1016/j.memsci.2011.10.049.

[61] W.L. Harrison, M. a Hickner, Y.S. Kim, J.E. McGrath, Poly(arylene ether sulfone) copolymers and related systems from disulfonated monomer building blocks: synthesis, characterization, and performance - a topical review, Fuel Cells. 5 (2005) 201–212. doi:10.1002/fuce.200400084.

[62] Y.A. Elabd, M.A. Hickner, Block Copolymers for Fuel Cells, (2011) 1–11. doi:10.1021/ma101247c.

[63] H. Xie, D. Tao, J. Ni, X. Xiang, C. Gao, L. Wang, Synthesis and properties of highly branched star-shaped sulfonated block polymers with sulfoalkyl pendant groups for use as proton exchange membranes, J. Memb. Sci. 497 (2016) 55–66. doi:10.1016/j.memsci.2015.09.035.

[64] G. Titvinidze, K. Kreuer, M. Schuster, C.C. De Araujo, J.P. Melchior, W.H.

Meyer, Proton Conducting Phase-Separated Multiblock Copolymers with Sulfonated Poly (phenylene sulfone) Blocks for Electrochemical Applications : Preparation , Morphology , Hydration Behavior , and Transport, Adv. Funct. Mater. 22 (2012) 4456–4470. doi:10.1002/adfm.201200811.

[65] A. Kusoglu, A.Z. Weber, New Insights into Perfluorinated Sulfonic-Acid Ionomers, Chem. Rev. 117 (2017) 987–1104. doi:10.1021/acs.chemrev.6b00159.

[66] E. Moukheiber, G. De Moor, L. Flandin, C. Bas, Investigation of ionomer structure through its dependence on ion exchange capacity (IEC), J. Memb. Sci. 389 (2012) 294–304. doi:10.1016/j.memsci.2011.10.041.

[67] R. Fischer, P.N. Pintauro, G.K. Jennings, Properties of Stretched 830 EW Aquivion, Diss. Vanderbilt Univ. (2012).

[68] M.S. Schaberg, J.E. Abulu, G.M. Haugen, M.A. Emery, S.J. O'Conner, P.N. Xiong, S.J. Hamrock, New Multi Acid Side-Chain Ionomers for Proton Exchange Membrane Fuel Cells, ECS Trans. 33 (2010) 627–633.

[69] Y. Bai, M. Maalouf, A. Papandrew, T. a. Zawodzinski Jr., Proton Conductivity and Partial Molar Volume of Different Polymer Electrolyte Membranes, ECS Trans. 41 (2011) 1545–1553. doi:10.1149/1.3635686.

[70] A. Ghielmi, P. Vaccarono, C. Troglia, V. Arcella, Proton exchange membranes based on the short-side-chain perfluorinated ionomer, 145 (2005) 108–115. doi:10.1016/j.jpowsour.2004.12.068.

[71] W. Zhang, R. Wycisk, D.L. Kish, P.N. Pintauro, Pre-Stretched Low Equivalent Weight PFSA Membranes with Improved Fuel Cell Performance, J. Electrochem. Soc. 161 (2014) F770–F777. doi:10.1149/2.085406jes.

[72] K.D. Kreuer, M. Schuster, B. Obliers, O. Diat, U. Traub, A. Fuchs, U. Klock, S.J. Paddison, J. Maier, Short-side-chain proton conducting perfluorosulfonic acid ionomers : Why they perform better in PEM fuel cells ଙ, 178 (2008) 499–509. doi:10.1016/j.jpowsour.2007.11.011.

[73] S. Subianto, S. Cavaliere, D.J. Jones, J. Rozière, Effect of side-chain length on the electrospinning of perfluorosulfonic acid ionomers, J. Polym. Sci. Part A Polym. Chem. 51 (2013) 118–128. doi:10.1002/pola.26286.

[74] J. Li, H. Tang, Understanding short-side-chain perfluorinated sulfonic acid and its application for high temperature polymer electrolyte fuel cells, RSC Adv. (2014) 3944–3965. doi:10.1039/c3ra43735c.

[75] J.K. Clark, S.J. Paddison, Proton dissociation and transfer in proton exchange membrane ionomers with multiple and distinct pendant acid groups: An ab initio study, Electrochim. Acta. 101 (2013) 279–292. doi:10.1016/j.electacta.2012.11.138.

[76] J. V. Gasa, R.A. Weiss, M.T. Shaw, Structured polymer electrolyte blends based on sulfonated polyetherketoneketone (SPEKK) and a poly(ether imide) (PEI), J. Memb. Sci. 320 (2008) 215–223. doi:10.1016/j.memsci.2008.03.075.

[77] C. Manea, M. Mulder, Characterization of polymer blends of polyethersulfone/sulfonated polysulfone and polyethersulfone/sulfonated polyetheretherketone for direct methanol fuel cell applications, J. Memb. Sci. 206 (2002) 443–453. doi:10.1016/S0376-7388(01)00787-6.

[78] S. Swier, M.T. Shaw, R.A. Weiss, Morphology control of sulfonated poly(ether ketone ketone) poly(ether imide) blends and their use in proton-exchange

membranes, J. Memb. Sci. 270 (2006) 22–31. doi:10.1016/j.memsci.2005.06.037.

[79] S. Ahn, Y. Lee, H. Yong, S. Hong, I. Oh, Properties of the reinforced composite membranes formed by melt soluble ion conducting polymer resins for PEMFCs, Electrochim. Acta. 50 (2004) 571–575. doi:10.1016/j.electacta.2004.01.133.

[80] J.A. Kolde, B. Bahar, M.S. Wilson, T.A. Zawodzinski, G. Shimson, Advanced Composite Polymer Electrolyte Fuel Cell Membranes, Prot. Conduct. Membr. Fuel Cells I Proc. First Int. Symp. Prot. Conduct. Membr. Fuel Cells. 95 (1995) 193–201.

[81] M. Crum, W. Liu, Effective Testing Matrix for Studying Membrane Durability in PEM Fuel Cells: Part 2. Mechanical Durability and Combined Mechanical and Chemical Durability, ECS Trans. 3 (2006) 541–550.

[82] W. Liu, K. Ruth, G. Rusch, Membrane Durability in PEM Fuel Cells, J. New Mater. Electrochem. Syst. 231 (2001) 227–231.

[83] J.W. Park, R. Wycisk, P.N. Pintauro, Nafion/PVDF nanofiber composite membranes for regenerative hydrogen/bromine fuel cells, J. Memb. Sci. 490 (2015) 103–112. doi:10.1016/j.memsci.2015.04.044.

[84] M. Oroujzadeh, S. Mehdipour-Ataei, M. Esfandeh, Proton exchange membranes with microphase separated structure from dual electrospun poly(ether ketone) mats: Producing ionic paths in a hydrophobic matrix, Chem. Eng. J. 269 (2015) 212–220. doi:10.1016/j.cej.2015.01.088.

[85] A.M. Park, F.E. Turley, R.J. Wycisk, P.N. Pintauro, Electrospun and Cross-Linked Nano fiber Composite Anion Exchange Membranes, Macromolecules. 47 (2014) 227–235. doi:10.1021/ma401932h.

[86] J. Choi, R. Wycisk, W. Zhang, P.N. Pintauro, K.M. Lee, P.T. Mather, High conductivity perfluorosulfonic acid nanofiber composite fuel-cell membranes, ChemSusChem. 3 (2010) 1245–1248. doi:10.1002/cssc.201000220.

[87] Q. Yan, H. Toghiani, J. Wu, Investigation of water transport through membrane in a PEM fuel cell by water balance experiments, J. Power Sources. 158 (2006) 316–325. doi:10.1016/j.jpowsour.2005.09.013.

[88] S.S. Kocha, J.D. Yang, J.S. Yi, Characterization of Gas Crossover and Its Implications in PEM Fuel Cells, 52 (2006). doi:10.1002/aic.

[89] T. a. Zawodzinski, Water Uptake by and Transport Through Nafion® 117 Membranes, J. Electrochem. Soc. 140 (1993) 1041. doi:10.1149/1.2056194.

[90] M. Breitwieser, C. Klose, M. Klingele, A. Hartmann, J. Erben, H. Cho, J. Kerres, R. Zengerle, S. Thiele, Simple fabrication of 12 μm thin nanocomposite fuel cell membranes by direct electrospinning and printing, J. Power Sources. 337 (2017) 137–144. doi:10.1016/j.jpowsour.2016.10.094.

[91] R. Wang, W. Zhang, G. He, P. Gao, Controlling fuel crossover and hydration in ultra-thin proton exchange membrane-based fuel cells using Pt-nanosheet catalysts, J. Mater. Chem. A. 2 (2014) 16416–16423. doi:10.1039/C4TA03799E.

[92] X. Zhu, H. Zhang, Y. Zhang, Y. Liang, X. Wang, An Ultrathin Self-Humidifying Membrane for PEM Fuel Cell Application : Fabrication , Characterization , and Experimental Analysis, (2006) 14240–14248.

[93] M. Zaton, J. Roziere, D.J. Jones, Mitigation of PFSA membrane chemical degradation using composite cerium oxide – PFSA nano fibres, (2017) 5390–5401. doi:10.1039/C6TA10977B.

[94] M. Manohar, V.K. Shahi, Graphene Oxide-Polyaniline as a Water Dissociation Catalyst in the Interfacial Layer of Bipolar Membrane for Energy-Saving Production of Carboxylic Acids from Carboxylates by Electrodialysis, ACS Sustain. Chem. Eng. 6 (2018) 3463–3471. doi:10.1021/acssuschemeng.7b03734.

[95] K.N. Grew, J.P. McClure, D. Chu, P.A. Kohl, J.M. Ahlfield, Understanding Transport at the Acid-Alkaline Interface of Bipolar Membranes, J. Electrochem. Soc. 163 (2016) F1572–F1587. doi:10.1149/2.0941614jes.

[96] D.A. Vermaas, S. Wiegman, T. Nagaki, W.A. Smith, Ion transport mechanisms in bipolar membranes for (photo)electrochemical water splitting, Sustain. Energy Fuels. (2018). doi:10.1039/c8se00118a.

[97] C. Shen, R.J. Wycisk, P.N. Pintauro, High performance electrospun bipolar membrane with a 3D junction, Energy Environ. Sci. 10 (2017) 1435–1442. doi:10.1039/C7EE00345E.

[98] K. Nagasubramanian, F.P. Chlanda, K.J. Liu, Use of bipolar membranes for generation of acid and base - an engineering and economic analysis, J. Memb. Sci. 2 (1977) 109–124. doi:10.1016/S0376-7388(00)83237-8.

[99] T. Xu, Development of bipolar membrane-based processes, 140 (2001) 247–258.

[100] M.B. Mcdonald, M.S. Freund, Graphene Oxide as a Water Dissociation Catalyst in the Bipolar Membrane Interfacial Layer, (2014). doi:10.1021/am503242v.

[101] Y. Liu, J. Chen, R. Chen, T. Zhou, C. Ke, X. Chen, Effects of multi-walled carbon nanotubes on bipolar membrane properties, Mater. Chem. Phys. 203 (2018) 259–265. doi:10.1016/j.matchemphys.2017.09.068.

[102] M.B. McDonald, S. Ardo, N.S. Lewis, M.S. Freund, Use of bipolar membranes for

maintaining steady-state pH gradients in membrane-supported, solar-driven water splitting, ChemSusChem. 7 (2014) 3021–3027. doi:10.1002/cssc.201402288.

[103] Y. Xue, T. Xu, R. Fu, Y. Cheng, W. Yang, Catalytic water dissociation using hyperbranched aliphatic polyester (Boltorn ® series) as the interface of a bipolar membrane, 316 (2007) 604–611. doi:10.1016/j.jcis.2007.08.052.

[104] M. Manohar, A.K. Das, V.K. Shahi, Efficient Bipolar Membrane with Functionalized Graphene Oxide Interfacial Layer for Water Splitting and Converting Salt into Acid/Base by Electrodialysis, Ind. Eng. Chem. Res. 57 (2018) 1129–1136. doi:10.1021/acs.iecr.7b03885.

[105] R. Simons, Preparation of a high performance bipolar membrane, J. Memb. Sci. 78 (1993) 13–23. doi:10.1016/0376-7388(93)85243-P.

[106] Y. Xue, N. Wang, C. Huang, Y. Cheng, T. Xu, Catalytic water dissociation at the intermediate layer of a bipolar membrane : The role of carboxylated Boltorn ® H30, J. Memb. Sci. 344 (2009) 129–135. doi:10.1016/j.memsci.2009.07.042.

[107] F.G. Wilhelm, Bipolar Membrane Electrodialysis - Membrane Development and Transport Characteristics, 2001. doi:10.1016/S0927-5193(07)12017-9.

[108] M. Ünlü, J. Zhou, I. Anestis-Richard, H. Kim, P.A. Kohl, Improved gas diffusion electrodes for hybrid polymer electrolyte fuel cells, Electrochim. Acta. 56 (2011) 4439–4444. doi:10.1016/j.electacta.2011.02.017.

[109] P.P. Lu, Z.L. Xu, H. Yang, Y.M. Wei, H.T. Xu, Effects of ethanol and isopropanol on the structures and properties of polyethersulfone/perfluorosulfonic acid nanofibers fabricated via electrospinning, J. Polym. Res. 19 (2012). doi:10.1007/s10965-012-9854-0.

[110] J.B. Ballengee, P.N. Pintauro, Morphological Control of Electrospun Nafion Nanofiber Mats, J. Electrochem. Soc. 158 (2011) B568–B572. doi:10.1149/1.3561645.

[111] A. Formhals, Artifical Thread and Method of Producing Same, 156167, 1940.

[112] A. Formhals, Process and Apratus for Preparing Artifical Threads, 500283, 1934.

[113] E.C. Self, R. Wycisk, P.N. Pintauro, Electrospun titania-based fi bers for high areal capacity Li-ion battery anodes, J. Power Sources. 282 (2015) 187–193. doi:10.1016/j.jpowsour.2015.02.036.

[114] M. Brodt, R. Wycisk, P.N. Pintauro, Nanofiber Electrodes with Low Platinum Loading for High Power Hydrogen / Air PEM Fuel Cells, J. Electrochem. Soc. 160 (2013) 744–749. doi:10.1149/2.008308jes.

[115] S.C. Wong, A. Baji, S. Leng, Effect of fiber diameter on tensile properties of electrospun poly(ε-caprolactone), Polymer (Guildf). 49 (2008) 4713–4722. doi:10.1016/j.polymer.2008.08.022.

[116] U. Stachewicz, R.J. Bailey, W. Wang, A.H. Barber, Size dependent mechanical properties of electrospun polymer fibers from a composite structure, Polymer (Guildf). 53 (2012) 5132–5137. doi:10.1016/j.polymer.2012.08.064.

[117] S. Megelski, J.S. Stephens, D.B. Chase, J.F. Rabolt, Micro- and Nanostructured Surface Morphology on Electrospun Polymer Fibers, Macromolecules. 35 (2002) 8456–8466.

[118] T. Subbiah, G.S. Bhat, R.W. Tock, S. Parameswaran, S.S. Ramkumar, Electrospinning of Nanofibers, J. Appl. Polym. Sci. 96 (2004) 557–569. doi:10.1002/app.21481.

[119] A. Park, P. Pintauro, Electrospun Composite Membranes for Alkaline Fuel Cells, ECS Trans. 41 (2011) 1817–1826.

[120] A.M. Park, P.N. Pintauro, Alkaline Fuel Cell Membranes from Electrospun Fiber Mats, Electrochem. Solid-State Lett. 15 (2012) B27. doi:10.1149/2.010203esl.

[121] A.M. Park, R.J. Wycisk, X. Ren, F.E. Turley, P.N. Pintauro, Crosslinked poly(phenylene oxide)-based nanofiber composite membranes for alkaline fuel cells, J. Mater. Chem. A Mater. Energy Sustain. 4 (2015) 132–141. doi:10.1039/C5TA06209H.

[122] W. Zhang, M.W. Brodt, P.N. Pintauro, Nanofiber Cathods for Low and High Humidity Hydrogen Fuel Cell Operation, ECS Trans. 41 (2011) 891–899.

[123] E.C. Self, E.C. Mcren, P.N. Pintauro, High Performance Particle / Polymer Nanofiber Anodes for Li-ion Batteries using Electrospinning, ChemSusChem. 9 (2016) 208–215. doi:10.1002/cssc.201501393.

[124] A. Gholipour-kanani, S.H. Bahrami, Review on Electrospun Nanofibers Scaffold and Biomedical Applications, Trends Biomater Artif Organs. 24 (2010) 93–115.

[125] S. Agarwal, J.H. Wendorff, A. Greiner, Use of electrospinning technique for biomedical applications, Polymer (Guildf). 49 (2008) 5603–5621. doi:10.1016/j.polymer.2008.09.014.

[126] X. Zong, K. Kim, D. Fang, S. Ran, B.S. Hsiao, B. Chu, Structure and process relationship of electrospun bioabsorbable nanofiber membranes, Polymer (Guildf). 43 (2002) 4403–4412.

[127] S. Agarwal, A. Greiner, J.H. Wendorff, Functional materials by electrospinning of polymers, Prog. Polym. Sci. 38 (2013) 963–991.

doi:10.1016/j.progpolymsci.2013.02.001.

[128] C.P. Grey, S.T. Newton, G.L. Bowlin, T.W. Haas, D.G. Simpson, Gradient fiber electrospinning of layered scaffolds using controlled transitions in fiber diameter, Biomaterials. 34 (2013) 4993–5006. doi:10.1016/j.biomaterials.2013.03.033.

Chapter 3

Electrospun Tri-Layer Membranes for H_2/Air Fuel Cells

3.1 Introduction

One focus area for fuel cell R&D has been the synthesis of high ion exchange capacity (IEC) perfluorinated sulfonic acid ionomers and their fabrication into high performance proton-exchange membranes (PEMs). By increasing the concentration of ion-conducting sites in the ionomer [1] or by adding inorganic proton conductors (i.e. heteropolyacids or sulfonated inorganic nanoparticles [2]), the ionic conductivity of a membrane can be increased. Increased proton conductivity is particularly important during fuel cell operation under reduced feed gas humidification conditions. Increasing membrane ion-exchange capacity, however, also leads to greater ionomer swelling by water [3,4]. While proton conductivity is normally viewed as the single most important property of a fuel cell membrane, low in-plane water swelling is also required to maintain the mechanical integrity of the membrane during on/off fuel cell cycling [5,6]. Excessive in-plane expansion and contraction of a membrane under wet/dry (on/off) conditions, when the membrane becomes part of a membrane-electrode-assembly (MEA) in a fuel cell stack, will cause membrane cracks and pinholes to form, leading to the mixing of hydrogen fuel and air and significant power losses [6–10].

A number of methods have been employed to restrict the swelling behavior of fuel cell PEMs. Such methods include the use of: (i) block copolymers [6,11], (ii) polymer blends of an ionomer and uncharged polymer [12–16], and (iii) composite membranes where an ionomer is impregnated into a porous uncharged polymer support

[17–19]. For the latter two approaches, the introduction of an uncharged polymer into the membrane results in a decrease in proton conductivity due to ionomer dilution and percolation effects [13,20–22]. A variant on method (iii) is the use of dual fiber electrospinning [18,22,23] which was introduced by Pintauro and coworkers to simplify the procedure of fabricating polymer-reinforced cation exchange membranes [24]. Membranes were made by simultaneously electrospinning ionomer and uncharged polymer fibers from separate spinnerets, followed by mat hot pressing or exposure to organic vapor, to transform the porous mat into a dense and defect-free membrane. Using such an approach, two nanofiber composite membrane structures were made from the same dual fiber mat: (1) uncharged reinforcing polymer fibers embedded in an ionomer matrix (this structure works well for hydrogen/air fuel cells [18]) or (2) ionomer fibers surrounded by an uncharged polymer (which is the preferred membrane morphology for an alkaline fuel cell [25,26] and a H_2/Br_2 regenerative/redox flow battery [27]). For proton conducting membranes, poly(phenyl sulfone) or poly(vinylidene fluoride) was typically employed as the reinforcing component, and a perfluorosulfonic acid ionomer (Nafion® or a 3M Co. polymer) was used as the cation-exchange material. Nanofiber composite membranes typically exhibited a proton conductivity of 0.02-0.07 S/cm with an in-plane swelling of 4-7% (both were measured for samples equilibrated in room temperature water) [18].

An unexplored extension of the dual fiber electrospinning technique is its use to create multi-layered membranes, where the distribution of reinforcing fibers varies in the membrane thickness direction. Such structures can be easily made during dual fiber electrospinning by changing the flow rates of the ionomer and reinforcing polymer

solutions. Reinforced and layered films cannot be made by conventional ionomer impregnation into a porous support because the uncharged support material is typically of uniform porosity. Nevertheless, some impregnated composite films possess a tri-layer structure due to the presence of charged polymer overlayers, created inadvertently or by design [28–32]. Additionally, there are a limited number of reports in the literature of multi-layer fuel cell membranes which were prepared by sequential solution casting of blended polymer films, e.g., the study by Feng and coworkers [33] who prepared a tri-layer film by spreading a layer of sulfonated carbon nanotubes onto a preformed solution cast film of sulfonated poly(arylene ether nitrile) (SPEN), followed by the casting of a second SPEN layer. The resulting tri-layer film, which contained 1 wt.% sulfonated carbon nanotubes, exhibited less in-plane water swelling as compared to a conventional blend [33] with a homogeneous distribution of nanotubes (8.4% vs. 16.5%), but the conductivity (0.073 S/cm) was too low for commercial fuel cell applications.

In the present paper, we report on the fabrication of single-layer and multi-layer composite membranes that were prepared by dual fiber electrospinning of 825 EW PFSA ionomer and polyamide-imide (PAI). PAI was selected as the reinforcing material because of its excellent chemical stability and superior mechanical properties (in particular, a tensile strength of 117 MPa [34] after sufficient curing above its glass transition temperature, which is greater than 285°C [35]). Two types of composite PFSA-PAI membranes were fabricated: (1) Single-layer membranes with a uniform distribution of PFSA and PAI in the thickness direction, and (2) Multi-layer membranes with a high PFSA content in the surface layers and a low PFSA content in the inner layers.

Three types of multi-layer membrane structures were studied. The first utilized neat PFSA in the outer layers and 70 wt.% PFSA (30 wt.% PAI) in the inner layers, where the total number of layers was 3, 5, 7, or 9. This structure is shown schematically in Figure 3.1a. Such a film with 3 sub-layers simulates the structure of commercially available reinforced fuel cell membranes, e.g., Gore-SELECT, where neat ionomer is impregnated into and overlays a pre-fabricated porous support. The second type of multi-layer membrane utilized a tri-layer structure with outer layers that contained 95 wt.% PFSA (5 wt.% PAI to reduce the swelling of the outer layers), with an inner layer that contained a uniform PFSA content of 75, 60, or 40 wt.% PFSA. This structure is shown schematically in Figure 3.1b. The third membrane type was a tri-layer design with surface layers containing 95 wt.% PFSA and a low PFSA content inner layer with a symmetric gradient in PFSA content. This structure (shown in Figure 3.1c) was chosen to eliminate the step-change in ionomer content between sub-layers, thus reducing the swelling gradient within the membrane. While conventional impregnation methods of a porous mat can lead to fiber-reinforced membranes similar to structure #1 and multiple laminated reinforced sub-layers could, in principle, be used to fabricate a multi-layer membrane (Figure 3.1a and Figure 3.1b), dual fiber electrospinning is the only way to create a tri-layer membrane with a reinforcing layer of variable composition (Figure 3.1c).

Figure 3.1: Schematic visualization of the three new types of electrospun composite membrane structures fabricated and studied in the present work, where the dark colors indicate regions of high PFSA content and the light colors indicate regions of low PFSA content: (a) Multi-layer membrane with uniform layers, where the number of layers is 5, 7, or 9, (b) Tri-layer membrane with the uniform inner layer, and (c) Tri-layer membrane with a gradient inner layer.

A single layer composite membrane had a PFSA content of 80 wt.% and thickness of ~ 20 μm. This composition and thickness were selected to obtain low area-specific resistance (ASR, 0.022 Ωcm^2 in water at 25°C), which would provide good performance (a low IR drop) during fuel cell operation. In order to reduce the membrane's in-plane swelling, the PAI was redistributed in the thickness direction to form alternating multi-layers. A series of such membranes was prepared with 3, 5, 7, and 9 layers, where the PFSA content alternated from neat PFSA at the outer layers to a PFSA-PAI nanofiber mixture. The overall PFSA content in each membrane was kept constant at 80 wt.%. Thus, the effective IEC of the composite membranes (0.97 mmol/g, given that the IEC of 3M's 825 EW ionomer is 1.21 mmol/g) was greater than that of 1100 EW Nafion (0.91 mmol/g). An additional series of tri-layer films were fabricated with ~5 μm surface layers containing 5 wt.% PAI and an inner layer containing 25 wt.%, 40 wt.%, or 60 wt.% PAI. These membranes had thicknesses of 17-23 μm and their inner layer thickness was

adjusted so that the overall membrane composition was held constant at 80 wt.% PFSA and 20 wt.% PAI. All the single-layer, tri-layer, and multi-layer membranes were compared in terms of proton conductivity, gravimetric water uptake, in-plane water swelling, and mechanical properties.

3.2 Experimental

3.2.1 Materials and Solution Preparation

825 EW perfluorosulfonic acid (PFSA) from 3M Co. and Torlon® 4000T (polyamide-imide, PAI) from Solvay Specialty Polymers were both received as dry powders. Dimethylformamide (DMF), dimethylacetamide (DMAc), tetrahydrofuran (THF), and poly(ethylene oxide) (PEO) with a molecular weight of 600 kDa were obtained from Sigma-Aldrich, and used without further purification. N-propanol was obtained from Fisher Scientific and was used without further purification.

Dispersions of 825 EW PFSA and solutions of PEO were prepared separately in 2:1 (wt:wt) n-propanol:water. The two mixtures were combined to obtain a PFSA-PEO solution with a polymer mass ratio of 99:1, and a total polymer content of 20 wt.%. This solution was mixed for 1-3 hours prior to electrospinning. A 15 wt.% PAI electrospinning solution was prepared by dissolving Torlon® in a mixed solvent of 98:2 (wt:wt) DMF:THF.

3.2.2 Electrospinning

Dual fiber mats were prepared by simultaneously electrospinning the PFSA-PEO and PAI solutions from separate syringes, fitted with 22-gauge needles and loaded into automatic syringe pumps. Fibers were electrospun onto a rotating and oscillating aluminum drum in a closed chamber, where the relative humidity was 20-25%. The

PFSA/PAI composition in the thickness direction of a dual-fiber composite mat was controlled by adjusting the relative flow rates of each polymer during electrospinning. An example of the electrospinning conditions used to fabricate a dual fiber mat with a uniform distribution of PAI fibers and an overall composition of 80 wt.% PFSA and 20 wt.% PAI is shown in Table 3.1. For tri-layer mats, the flow rate of the PFSA was held constant at 0.5 mL/hr and the PAI flow rate was varied from 0.04 mL/hr (for a 95/5 weight ratio of PFSA/PAI fibers) to 0.85 mL/hr (for a PFSA/PAI fiber weight ratio of 40/60). For tri-layer mats with a gradient inner layer, a Chemyx Inc. programmable syringe pump (Model: Fusion 100) was used for delivery of the PAI solution. This pump allowed the flow rate of the PAI solution to be automatically and continually varied during the electrospinning process.

Table 3.1: Electrospinning conditions for an 825 EW PFSA/PAI dual fiber composite mat.

Spinning Parameter	99:1 825 EW PFSA:PEO (600 kDa)	PAI
Voltage [kV]	11	14
Solvent	2:1 n-Propanol:H_2O	98:2 DMF:THF
Flow Rate [mL/hr]	0.50	0.15
STC[a] [cm]	8	10.5
Concentration [wt.%]	20	15

[a] – Spinner-to-Collector Distance

3.2.3 Membrane Fabrication

After electrospinning, the composite mat was removed from the collector drum and dried for 6-12 hours at 70°C under vacuum to ensure complete removal of solvents. The fiber mat was then mechanically compacted at 2,500 psi and 143°C for 5 minutes, during which time the entire fiber mat was compressed in thickness and the PFSA-PEO fibers softened and flowed to fill the inter-fiber void space between PAI fibers. As shown

in previous studies by Pintauro and coworkers, hot pressing of a dual fiber electrospun mat led to a dense and defect-free composite membrane as indicated by low hydrogen gas crossover during a fuel cell test [18,27,36]. The resulting dense membrane (a PAI reinforcing fiber mat embedded in a PFSA-PEO matrix) was then annealed at 200°C for 1 hour for proper crystallization of the PFSA ionomer and partial curing of PAI nanofibers (normally, PAI is cured at a temperature greater than 285°C [35]; a lower temperature was used in the present study to minimize PFSA degradation). The membrane was then pretreated by boiling in 1.0 M H_2SO_4 for 1 hour, followed by boiling in water for 1 hour; these soaking steps were performed to remove the water soluble PEO and to insure that all the sulfonic acid sites in the PFSA were in the H^+ counterion form. Films were stored in DI water at room temperature until further testing.

A solution cast film of neat 825 EW PFSA was made using a 20 wt.% ionomer solution with a 2:1 weight ratio n-propanol:water solvent. A blended film containing 80 wt.% PFSA and 20 wt.% PAI was solution cast using DMAc as the solvent, where the total polymer content of the casting solution was 15 wt.%.

3.2.4 Proton Conductivity

In-plane proton conductivity was measured using an AC impedance method with a BekkTech 4-electrode cell, where membranes samples were equilibrated in 25^{o}C water and in 80^{o}C air at 40% and 90% relative humidity. An impedance spectrum was generated on a membrane of known width and thickness using a Gamry Reference 3000 potentiostat. In-plane conductivity ($\sigma_{In\text{-}Plane}$ with units of S/cm) was calculated using the following equation:

$$\sigma_{In-Plane} = {}^{L}/_{t \times w \times R} \quad (3.1)$$

where L (cm) is the distance between the electrodes, t (cm) is the membrane thickness, w (cm) its width, and R (Ω) is the resistance between the electrodes, extracted from a Nyquist plot as the intersection of the impedance curve with the real axis.

The through-plane conductivity, $\sigma_{\text{Through-Plane}}$ (S/cm), measured only for membranes immersed in 25°C water, was calculated using the following equation:

$$\sigma_{Through-Plane} = {}^{t}/_{A \times (R - R_n)} \quad (3.2)$$

where t (cm) is the sample thickness, A is the electrode area of the conductivity cell (0.063794 cm^2) and R and R_n are the measured cell resistance and the non-membrane resistance, respectively (both were obtained from Nyquist plots). In the present study, R and R_n were measured using a custom-built 2-electrode pressure-loaded cell set to 307 psi that was submerged in 25°C water, as described in Reference 27. The measured through-plane impedance of samples typically ranged from 2-20 Ω, and included non-membrane impedances, e.g., a contact resistance between the membrane and electrodes. In order to extract the impedance of the membrane, film samples were stacked to obtain a range of thicknesses and an impedance spectrum for each stack was recorded. As an example, the high frequency portions of Nyquist plots for membrane stacks (3-7 nanofiber composite tri-layer membranes) are shown in Figure **3**.2a and a plot of measured impedance vs. stack thickness is shown in Figure **3**.2b. The measured cell resistance (R in Eq. 3.2) was found from the extrapolated real impedance (x-axis) intercept in Figure **3**.2a and the sum

of all non-membrane impedances (R_n in Eq. 3.2) was estimated from the straight-line y-axis intercept in Figure **3**.2b.

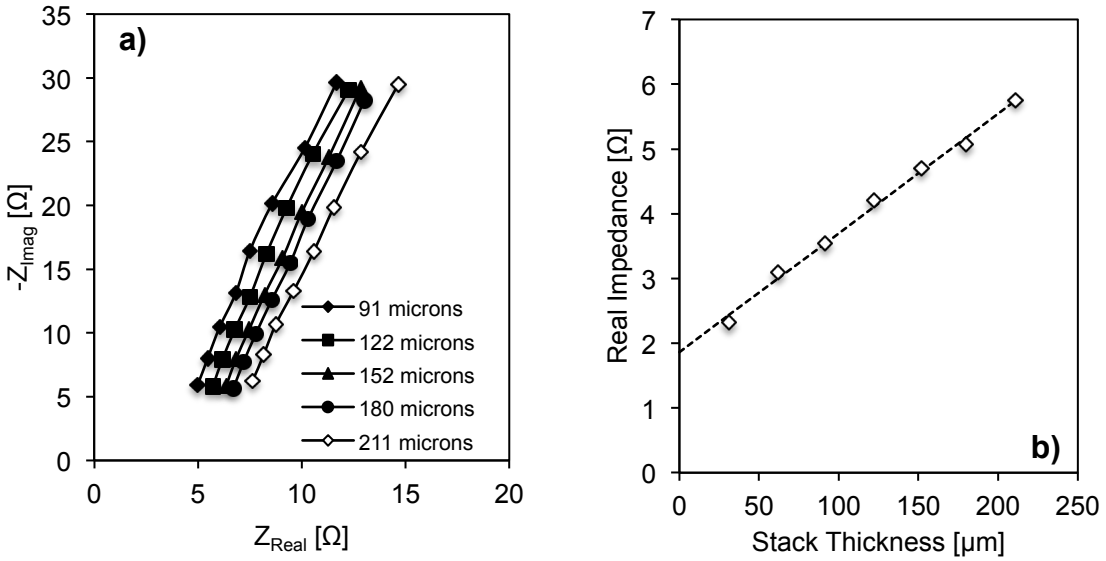

Figure 3.**2**: a) Nyquist plots of an 80 wt.% 825 EW PFSA/20 wt.% PAI electrospun tri-layer membrane in 2-electrode conductivity cell demonstrating the effect of membrane stacking on resultant high frequency sections (1 MHz – 200 kHz) of impedance spectra, and b) extrapolation of thicknesses to find non-membrane impedance. The dotted line is the linear regression curve.

3.2.5 Gravimetric Water Uptake and In-Plane Swelling

Gravimetric water uptake and in-plane swelling of membrane samples were determined after equilibration in room temperature water. After excess water was removed from the surfaces of a membrane sample, the swollen properties of the membrane (mass, length, and width) were recorded. Membranes were dried at 100°C for ca. 1 hour under vacuum (until the weight stabilized) and the mass and sample dimensions were re-measured. Swelling properties (%) were determined using Eq. 3.3,

$$Swelling = \left({X_{wet} - X_{dry}}/{X_{dry}}\right) \times 100 \quad (3.3)$$

where x_{wet} represents the wet mass, length, or width of the membrane, and x_{dry} represents the corresponding dry film quantities.

3.2.6 IEC Determination

Ion-exchange capacity (IEC) was used to determine the average content of PFSA in a nanofiber composite membrane, i.e., the ratio of experimentally measured IEC to that of neat 825 EW PFSA (found to be 1.21 mmol/g from a separate experiment) is the PFSA/PAI weight ratio in a film. IEC was measured by a standard ion-exchange and titration technique. First, a membrane sample of known dry mass was equilibrated in 1.0 M H_2SO_4 and then soaked in numerous volumes of H_2O to remove excess acid. The membrane was then submerged in 50 mL of a 2.0 M NaCl solution for at least 24 hours to exchange Na^+ for H^+ counterions. The soak solution was titrated with 0.01N NaOH to a neutral pH. The IEC of the membrane was calculated using the following equation:

$$IEC = 1000 \times \left({V \times N}/{m_d}\right) \quad (3.4)$$

where V (mL) is the volume of titrant required to bring the soak solution to a neutral pH, N (mol/L) is the normality of the titrant, and m_d (g) is the dry mass of the membrane sample.

3.2.7 Tensile Tests

Tensile stress-strain data of neat polymer films and composite membranes were collected using a TA Q800 Dynamic Mechanical Analyzer operating in tension mode.

Membrane samples were pre-dried in an oven at 70°C for up to 4 hours prior to testing. After equilibration in air at 30-50% relative humidity and 25°C, samples were loaded into the apparatus and elongated at 5%/minute until failure.

3.2.8 SEM Imaging

Scanning electron micrographs of electrospun mats, dense membrane surfaces, and freeze-fractured membrane cross-sections were obtained using a Hitachi S-4200 scanning electron microscope. Samples were sputter-coated with gold (~5 nm in thickness) to inhibit charging and reduce thermal damaging. Freeze fracturing was performed by submerging samples in liquid nitrogen for 2 minutes.

3.2.9 Fuel Cell Performance

Membrane-electrode assemblies (MEAs) were prepared using either a tri-layer membrane or Nafion 211 combined with Pt/C electrodes. A catalyst ink for the anode and cathode was prepared by mixing Pt/C catalyst (TEC10F50E, 47 wt.% Pt on carbon from Tanaka Kikinzoku Kogyo K.K.) with dry Nafion in a 1:1 (wt:wt) mixture of n-propanol:water, as described previously [37]. A sufficient amount of ink was painted onto carbon paper Sigracet 29BC gas diffusion layers from Ion Power Inc. for a Pt loading of 0.10 mg/cm^2. The electrodes were hot pressed onto the membrane at 140°C for 5 minutes at 580 psi.

Fuel cell tests were carried out at 80°C and 200 kPa backpressure using a Scribner 850e fuel cell test station with H_2/air flow rates of 0.125/0.5 L/min. Prior to collection of polarization curves, the MEAs were conditioned by cycling between high (0.6 V) and low (0.2 V) voltages for ~3 hours. Hydrogen crossover was measured via linear sweep voltammetry under H_2/N_2 flow rates of 0.125/0.5 L/min, as described elsewhere [38].

3.3 Results and Discussion

3.3.1 Electrospun Single-Layer and Solution Cast PFSA/PAI Composite Membranes

A top-down SEM image of a dual fiber mat (80 wt.% PFSA and 20 wt.% PAI) is shown in Figure 3.3a. PFSA and PAI fibers are indistinguishable, with an average fiber diameter of 290 nm ± 90 nm. Top-down and freeze-fractured cross-section SEMs of the dense membrane created from the 80/20 PFSA/PAI mat are shown in Figure 3.3b and Figure 3.3c, respectively. The processed membrane surface is featureless (no fibers are present) due to thin layers of neat PFSA at the membrane surfaces; this is a consequence of allowing the PFSA fibers to soften and flow when the mat was hot pressed. These overlayers are clearly visible in the membrane cross-section (Figure 3.3c) and appear to be 1- 2 μm in thickness. The SEM image of the single-layer membrane cross-section also confirms that the mat processing step of compaction and heating effectively closed all interfiber voids via softening and flow of PFSA, while leaving intact the PAI fibers, which are uniformly dispersed in the PFSA matrix.

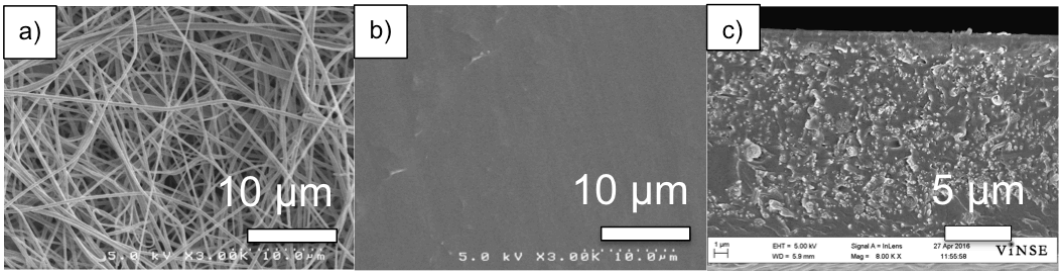

Figure 3.3: SEM image of a) a dual fiber mat (top-down view) composed of 80 wt.% 825 EW PFSA and 20 wt.% PAI nanofibers, b) a top-down view of the fully processed membrane made from the mat in a), and c) a freeze-fractured cross-section of the membrane in b) which was obtained from the mat in a). Membrane SEMs were collected after the acid treatment and water boiling pretreatment steps.

Photographs of neat PFSA and 80 wt.% PFSA/20 wt.% PAI films (solution cast and single layer nanofiber composite) are shown in Figure 3.4(a-c). The neat 825 EW PFSA was transparent whereas both PFSA/PAI films were translucent due to: (1) phase separation between the PFSA and PAI components, (2) a difference in refractive index between PFSA and PAI, and (3) the small size of the PAI light scatterers.

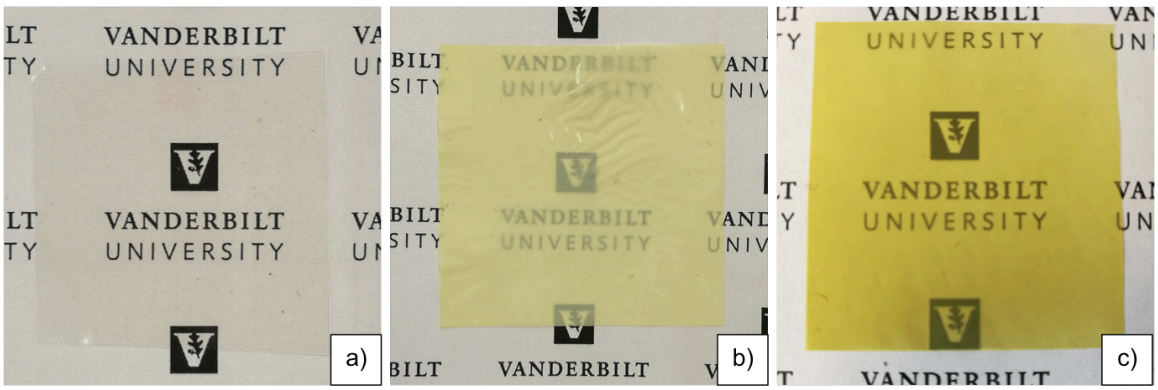

Figure 3.4: Optical membrane photographs for: a) a solution-cast 825 EW PFSA film, b) an 80 wt.% 825 EW PFSA (20 wt.% PAI) nanofiber composite membrane, and c) an 80 wt.% PFSA (20 wt.% PAI) solution-cast blended membrane that was cast from DMAC.

In-plane and through-plane proton conductivities are shown for neat 825 EW PFSA, an 80 wt.% PFSA (20 wt.% PAI) nanofiber composite membrane, and an 80 wt.% PFSA solution-cast blended film in Table 3.2. A solution-cast and thermally annealed film of neat 825 EW PFSA was used to determine the pure ionomer conductivity (100 wt.% PFSA), as opposed to making a dense membrane by hot pressing a mat of PFSA fibers. Isotropic in-plane and through-plane conductivity behavior was observed for the nanofiber composite membrane, due to the random distribution and orientation of PFSA and PAI fibers in the dual fiber mat prior to hot pressing and annealing. In addition, membrane conductivity conforms to a simple rule of mixtures, i.e., the presence of PAI dilutes the PFSA in a linear fashion based on the weight fraction of the uncharged polymer. Such a linear behavior has been observed in prior studies on nanofiber composite membranes with 1100 EW Nafion ionomer and reinforcing fibers of poly(phenyl sulfone) [18].

Gravimetric water uptake and in-plane water swelling of the single-layer films are also shown in Table 3.2. Water uptake for the nanofiber composite membrane is less than that of the neat PFSA or the solution cast blend due to the coupled effect of: (i) PAI sorbing no water (which would lead to a linear mixing behavior) and (ii) PAI fibers constraining/lowering the water swelling behavior of the PFSA ionomer. Restricted water swelling is mostly pronounced in the in-plane direction, with a 2.5X decrease vs. that for the neat ionomer. Such behavior, which is highly desirable for fuel cell membranes, has been observed previously in nanofiber composite membranes with Nafion [18,19,27]. It should be noted that the swelling data in Table 3.2 represent the average of linear length and width changes for a membrane sample when wet and dry, as per Equation 3. In general, dimensional changes were found to be isotropic in the length and width directions, indicating areal uniformity in the distribution of PAI fibers. The blended film exhibited a through-plane proton conductivity of 0.081 S/cm, with a very high in-plane swelling (34%), and gravimetric water uptake (78%); the latter two properties are undesirable for a fuel cell membrane.

Table 3.2: The properties of membranes in water at 25°C: neat 825 EW PFSA, 80/20 PFSA/PAI nanofiber composite membrane, and 80/20 PFSA/PAI solution cast blended membrane.

Membrane	In-plane/Through-plane Conductivity [S/cm][a]	Gravimetric Water Uptake [%][a]	In-Plane Swelling [%][a]	Thickness [μm][b]	ASR [Ω-cm^2][a]
Solution cast Neat 825 EW PFSA film	0.115/0.110	60	28.8	20	0.018
Nanofiber composite PFSA/PAI membrane (80 wt.% PFSA)	0.091/0.087	43.2	11.5	20	0.022
Solution cast PFSA/PAI blended membrane (80 wt.% PFSA)	0.074/0.081	77.8	34	30	0.037

[a] – Measured in room-temperature water

[b] – The standard deviation of the membrane thicknesses was ± 1 μm.

The high ionomer IEC of 1.21 mmol/g for the 825 EW PFSA used in the present study allowed for the fabrication of composite (reinforced) membranes that are comparable to neat 1100 EW Nafion in terms of conductivity, but with reduced in-plane swelling. Thus, the through-plane conductivity of an 80 wt.% 825 EW PFSA (20 wt.% PAI) nanofiber composite membrane in water at 25°C is similar to that of Nafion (0.087 vs. 0.091 S/cm) while displaying a significantly lower in-plane swelling than Nafion (11.5% vs. 16%) [39]. For a hydrogen/air fuel cell membrane, the key performance metrics are low area specific resistance (ASR) and minimal in-plane water swelling. While a 20 μm thick single layer 80/20 PFSA/PAI nanofiber composite membrane has an ASR that is acceptable for fuel cell applications (0.022 Ω-cm^2 in water at 25°C vs. the U.S. DOE [40] target of 0.030 Ω-cm^2 at 30°C and 95% RH), the in-plane swelling of the composite film exceeded the DOE specification of < 5% [41]**.** This was the motivating factor for the present study, where a series of multi-layer membranes was fabricated to

determine how the distribution of reinforcing PAI fibers (at a single overall PAI content of 20 wt.%) affects the properties (in particular the in-plane swelling) of a composite membrane.

3.3.2 Multi-Layer Nanofiber Composite Membranes

In an initial attempt to reduce the in-plane swelling of an 80/20 PFSA/PAI nanofiber composite membrane, a series of multi-layer membranes were fabricated, with 3, 5, 7, or 9 alternating layers of neat PFSA and a mixture of 70 wt.% PFSA and 30 wt.% PAI fibers, as per the structure in Figure 3.1a, where the thickness of the high and low PFSA content layers in a given film were equal and the overall composition of all films was the same. The measured properties of the resultant membranes, which had overall compositions of ~80 wt.% PFSA, are summarized in Table 3.3. As expected, the proton conductivity was dictated by the overall 825 EW PFSA content in the membrane and not by the layering morphology. In addition, the membranes exhibited isotropic in-plane/through-plane proton conductivities (within the estimated experimental accuracy of ± 10%), indicating a lack of significant layer-to-layer interfacial resistance, which would reduce the membrane's conductivity in the thickness direction. While there was a reduction in the in-plane swelling of the multi-layer film when transitioning from a single-layer to a tri-layer film, there was no obvious trend in gravimetric water uptake or in-plane swelling as the number of layers increased. Furthermore, none of the multi-layer films in Table 3.3 met the 5% in-plane swelling target. Thus, increasing the number and reducing the thickness of the reinforcing layers did not introduce any additional benefits to the properties of the composite membrane beyond what was observed for a tri-layer

film. There is an apparent relationship between layer thickness and in-plane swelling that cannot be exploited by adding more layers that are thinner.

Table 3.3: Summary of Multi-Layer Nanofiber Composite Membrane Properties.

Overall Membrane Composition: ~80 wt.% 825 EW PFSA + 20 wt.% PAI						
# Layers	Conductivity In-Plane/Through-Plane [S/cm][a]	Thickness [um]	Area-Specific Resistance [Ω-cm^2][a]	In-Plane Swelling [%][a]	Gravimetric Water Uptake [%][a]	Stress at Break [MPa][b]
3	0.083/0.083	19±1	0.023	8.5	41.8	16.5
5	0.081/0.077	21±1	0.027	8.4	41.0	20.0
7	0.086/0.082	20±1	0.024	8.2	42.6	19.0
9	0.076/0.074	21±1	0.028	7.5	43.2	18.6

[a] – Measured in room-temperature water
[b] – Air-dried samples

3.3.3 Electrospun Tri-layer Composite PFSA/PAI Membranes

To further reduce the in-plane swelling of nanofiber composite membranes, tri-layer membranes were prepared with a small amount of PAI (5 wt.%) in the outer layers. Two types of tri-layer membranes were prepared, with a compositionally uniform inner layer and with a gradient composition inner layer. Membranes of the first type had an inner layer PFSA content of 75 wt.%, 60 wt.%, or 40 wt.%. 75 wt.% PFSA was chosen (slightly more PFSA that the tri-layer film in Table 3.3) to compensate for the added PAI in the outer layers and to insure that the inner layer thickness would be identical to the tri-layer membrane in Table 3.3. 60 wt.% and 40 wt.% PFSA inner layer films were examined to determine the effect of a high PAI content inner layer on membrane properties. For these two inner layer compositions, the thickness of the outer layers was increased to keep the overall membrane composition constant at 80 wt.% PFSA and 20

wt.% PAI. Since the total membrane thickness was held constant, the thickness of the inner layer was reduced as the PAI content of the inner layer was increased, as shown in Table 3.4. These tri-layer films are listed as membranes A-C in Table 3.4. A representative SEM image of freeze-fractured tri-layer membrane cross-section is shown in Figure 3.5a, where well-formed PAI fibers are clearly seen as being uniformly distributed in the inner layer, with complete closure of the interfiber voids throughout the cross-section.

The second type of tri-layer membrane utilized a symmetric compositional gradient inner layer with a continuously changing PFSA content in the layer thickness direction (See Figure 3.1c) and a centerline composition equal to its uniform inner layer counterpart. The surface layers of the membrane contained 95 wt.% PFSA. When electrospinning the inner layer onto the mixed fiber surface layer, the initial fiber deposition rate produced a 95/5 PFSA/PAI mixture. The PAI flow rate was then continuously increased and then decreased to create a smooth and symmetric PFSA/PAI nanofiber mixture profile, where the mid-plane PFSA content was either 75 wt.%, 60 wt.%, or 40 wt.% and the inner layer thickness was adjusted so that the overall membrane composition was 80 wt.% PFSA and 20 wt.% PAI (as verified by membrane IEC measurements). These tri-layer films with a gradient-composition inner layer are listed as membranes D-F in Table 3.4 and a representative SEM freeze-fractured cross-section is shown in Figure 3.5b. It should be noted that there was no evidence of delamination for any tri-layer membrane after pretreatment (acid boiling and water boiling steps) and after numerous physical property tests involving drying and rehydrating the films.

Table 3.4: The structure of tri-layer films with either a uniform or gradient composition inner layer, containing 825 EW PFSA and PAI. The overall/effective PFSA content of the films is 80 wt.%, with surface layers containing 95 wt.% PFSA.

Membrane	Tri-layer Membrane Structure	Inner Layer PFSA Content [wt.%]	Inner Layer Thickness [µm][a]	Total Thickness [µm][b]
A	Uniform Inner Layer	75	8.2	20
B	Uniform Inner Layer	60	6.9	20
C	Uniform Inner Layer	40	4.2	20
D	Gradient Inner Layer	75[c]	12.4	17
E	Gradient Inner Layer	60[c]	10.8	17
F	Gradient Inner Layer	40[c]	10.7	23

[a] – From SEM freeze-fractured cross-sections
[b] – The standard deviation of the membrane thicknesses was ± 1 µm.
[c] – PFSA content at the mid-plane of the gradient composition inner layer

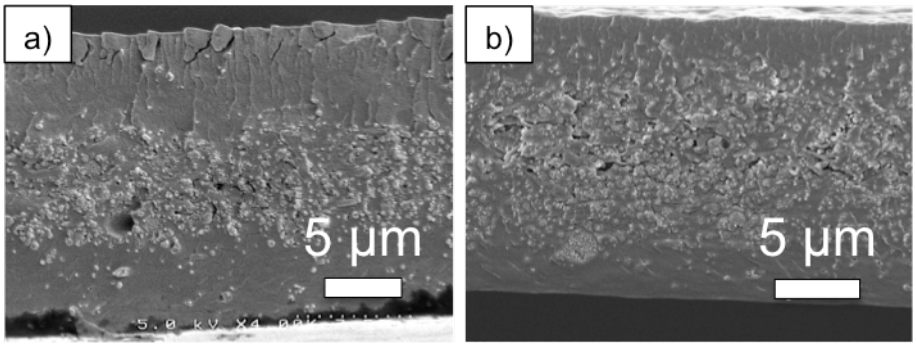

Figure 3.5: Freeze-fractured cross-section SEM images of 80 wt.% PFSA nanofiber composite membranes; a) tri-layer with a uniform inner layer, b) tri-layer with a symmetric gradient inner layer. Membrane SEMs were collected after the acid treatment and water boiling pretreatment steps.

3.3.4 Effect of Inner Layer Composition and Thickness on Tri-Layer Membrane Properties

The proton conductivity (in-plane and through-plane), gravimetric water uptake, in-plane swelling, and stress at break of tri-layer membranes are listed in Table 3.5. All tri-layer membranes exhibited isotropic in-plane/through-plane conductivities with essentially the same conductivity (within ± 5%) as that of the single layer nanofiber composite membrane with a uniform PAI fiber distribution (cf. Table 3.2). Thus, as expected, proton conductivity was solely a function of nanofiber composite membrane composition (i.e., with 20 wt.% PAI, the membrane conductivity is 0.8 x the conductivity of a neat 825 EW PFSA film) and not a function of how the PAI fibers were distributed in the membrane. This linear mixing rule relationship of conductivity vs. composition, which has been observed in prior studies by Pintauro and coworkers [17,18,27], is due to a well-mixed and uniform distribution of PFSA and PAI fibers prior to hot pressing and the relatively low overall PAI content of the membrane, so that the tortuosity for proton conduction is essentially 1.0. Gravimetric water uptake was generally lower in tri-layer films, as compared to a single layer nanofiber composite membrane with a uniform PFSA/PAI distribution, but there was no clear trend among the six different tri-layer membranes, which differed in terms of composition, thickness, and PAI fiber distribution of the inner layer.

Table 3.5: Summary of Tri-Layer membrane properties with a uniform or gradient composition inner layer.

Membrane	Inner Layer Structure	Conductivity In-Plane/Through-Plane [S/cm][a]	Area-Specific Resistance [Ω-cm^2][a]	Gravimetric Water Uptake [%][a]	In-Plane Swelling [%][a]	Stress at Break [MPa][b]
A	Uniform	0.087/0.086	0.023	42.3	5.9	26.1
B	Uniform	0.090/0.096	0.021	37.4	9.3	19.7
C	Uniform	0.088/0.083	0.024	46.1	10.7	17.8
D	Gradient	0.089/0.089	0.019	39.3	5.2	20.2
E	Gradient	0.089/0.092	0.018	40.1	6.2	19.9
F	Gradient	0.087/0.089	0.026	39.8	8.8	13.8

[a] – Measured in room-temperature water
[b] – Air-dried samples

The measured in-plane proton conductivities of a neat 825 EW PFSA film and a tri-layer membrane after equilibration with water vapor at 40% RH and 90% RH, are listed in Table 3.6. As expected, the conductivity of both membranes are lower than that in liquid water and decrease with a reduction in RH (i.e., proton conductivity decreases as the membrane water content drops [5,42-44]). In addition, the conductivity of the tri-layer membrane at the low RH value (40%) was less than expected based on a simple mixing rule.

Table 3.6: Proton conductivity of a neat 825 EW PFSA membrane and a tri-layer nanofiber composite membrane at 90% and 40% relative humidity.

In-Plane Proton Conductivity at 80°C [S/cm]		
Membrane	90% RH	40% RH
825 EW PFSA	0.178	0.026
Tri-Layer Membrane	0.134	0.012

In-plane swelling of tri-layer films showed an unusual, counter-intuitive trend, where swelling was not controlled by the amount of uncharged PAI in the inner layer, but rather by the inner layer thickness (which was inversely proportional to its PAI content, to keep the overall membrane PFSA/PAI weight ratio constant). Thus, the two films with a thick inner layer containing the highest PFSA/PAI weight ratio (75 wt.% PFSA) exhibited the lowest in-plane swelling for both the uniform and gradient composition inner layer (membranes A and D). The three tri-layer membranes with a gradient inner layer (membranes D, E, and F in Table 3.5) have a lower in-plane water swelling as compared to their uniform inner layer composition counterparts (membranes A, B, and C in Table 3.5). Thus, they appear to be preferred for fuel cell applications. The gradient inner layer morphology may provide additional benefits in terms of long-term membrane durability due to a reduction in stresses during on/off (wet/dry) fuel cell operation. Humidity cycling experiments in a fuel cell test fixture are needed to assess these benefits. Such experiments were not performed in the present study, but will be the subject of a future publication. The in-plane swelling of all six tri-layer films was lower than that of a single layer nanofiber composite membrane with a uniform distribution of PFSA and PAI fibers or a neat 825 EW PFSA film. While some variation in total membrane thickness was observed (Membrane D was 17 μm thick while Membrane A

was 20 μm thick), these variations do not affect the resultant membrane properties (proton conductivity and mechanical properties were corrected for membrane thickness and in-plane swelling is independent of membrane thickness).

Stress-strain plots for single-layer and tri-layer membranes are shown in Figure 3.6. The tensile strength results show that: (i) tri-layer films with an inner layer of uniform composition exhibit a higher stress at break than their tri-layer membrane counterparts and (ii) tensile strength increases with increasing inner layer thickness (and decreasing PAI content) for both types of tri-layer membrane. These results suggest that for high membrane strength, it is preferable to have a moderately high concentration of PAI fibers within an inner layer of substantial thickness in a tri-layer film, as opposed to diluting the PAI fibers over the entire membrane thickness (a single-layer membrane) or by having a very narrow band of very high PAI content, as is the case at the mid-plane in the tri-layer films with a gradient inner layer. All nanofiber composite membranes with PAI fibers exhibited a greater tensile strength, as compared to the neat 825 EW PFSA film with values typically near 20 MPa.

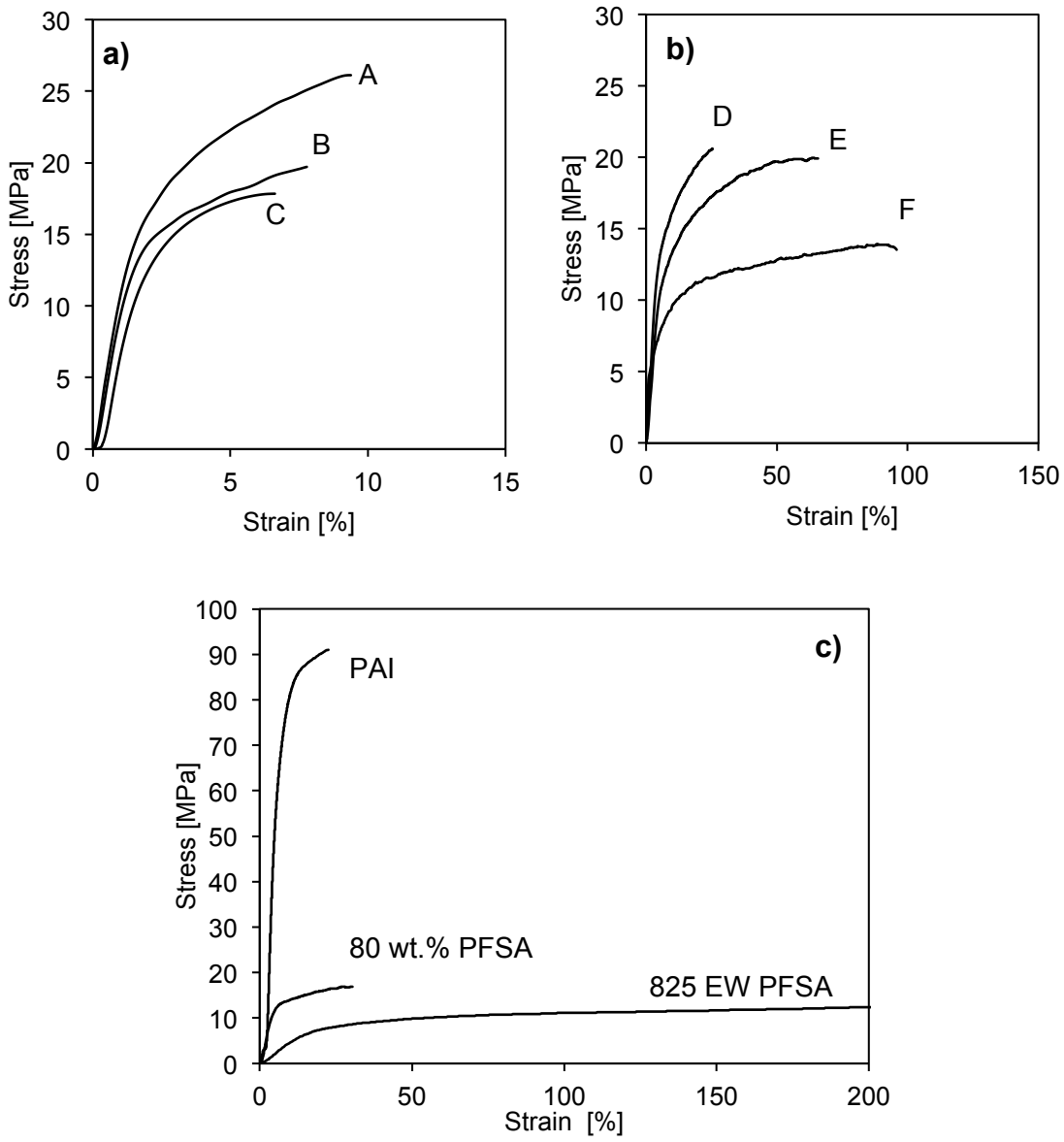

Figure 3.6: Stress-strain plots for: a) tri-layer films with a uniform inner layer composition (membranes A-C in **Table 3.5**), b) tri-layer films with a gradient inner layer composition (membranes D-F in **Table 3.5**), and c) experimental data for solution-cast 825 EW PFSA, solution-cast PAI, and a single-layer 80 wt.% PFSA/20 wt.% PAI film. All membranes were equilibrated in room temperature air at 40% RH before taking measurements.

The overall benefits of PAI fiber reinforcement of an 825 EW PFSA film can be summarized as follows: for a 20% drop in proton conductivity due to dilution of the PFSA with 20 wt.% PAI, the in-plane swelling is reduced by over 50% and the membrane tensile strength is increased by about 25% in a single-layer film. The results also suggest that: (i) discontinuous compositional interfaces within a laminated film are to be avoided, to minimize in-plane swelling and (ii) low-swelling/high-strength sub-layers in a multi-layer film must have sufficient thickness to impart desirable properties to the membrane. Therefore, an ideal tri-layer membrane would have a hybrid inner layer structure that captures the features of both a constant composition and gradient composition morphology, i.e., (i) an inner layer of uniform PFSA/PAI content with sufficient thickness to control in-plane swelling and (ii) a zone of transitioning PFSA/PAI composition between the inner and surface layers of high-PFSA content. This structure is shown schematically in Figure 3.7.

Figure 3.7: Schematic representation of an ideal tri-layer nanofiber composite membrane where the inner layer is of constant PFSA/PAI composition with a gradient composition between the inner and surface layers.

3.3.5 Fuel Cell Performance of an Electrospun Tri-layer Membrane

The fuel cell performance of membrane-electrode-assemblies (MEAs) with either an electrospun tri-layer membrane (membrane A from Table 3.5) or Nafion 211 are compared in Figure 3.8 (H_2/air fuel cell polarization curves) and Table 3.7 (measured H_2 crossover data). The performance of the tri-layer membrane-based MEA matches that of the Nafion 211 MEA (both films have similar area specific resistances). Hydrogen crossover was low for the 20-μm electrospun tri-layer membrane (measured as a current density of 4.9 mA/cm^2) and compares well with that for Nafion 211 (25 μm in thickness, with a hydrogen crossover of 4.1 mA/cm^2) thus providing additional evidence that the hot pressing step during dual fiber membrane fabrication is removing pinholes and defect pores. The combination of low in-plane swelling, high proton conductivity, and good fuel cell performance, warrants further study of the tri-layer composite films.

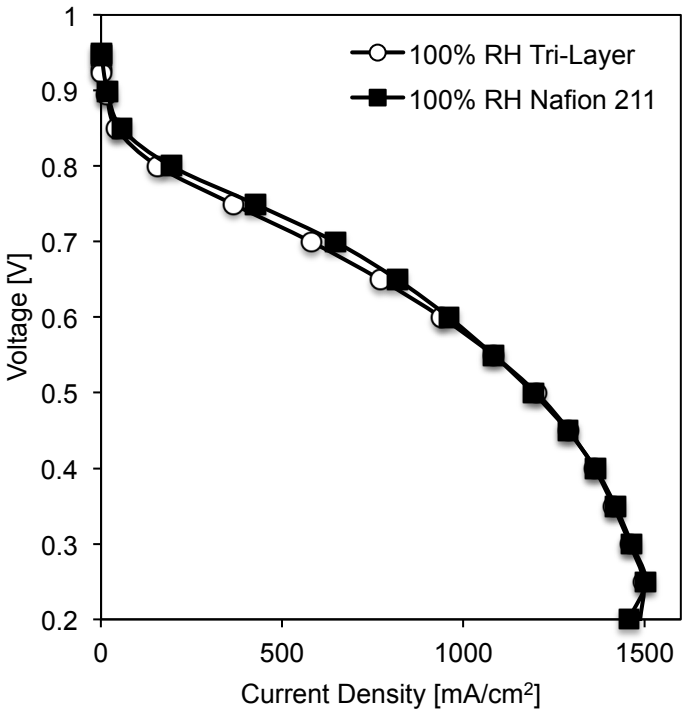

Figure 3.8: Polarization data for tri-layer membrane A (○) and Nafion 211 (■) at 100% RH, pressure of 200 kPa, H_2/air flow rates of 0.125/0.5 L/min, 80°C.

Table 3.7: Hydrogen crossover for Nafion 211 and electrospun tri-layer membrane A at 80°C, 200 kPa backpressure, and 100% RH.

Membrane	Dry Thickness [μm]	H_2 Crossover [mA/cm^2]
Nafion 211	25	4.1
Tri-Layer Membrane A from **Table 3.5**	20	4.9

3.4 Conclusions

A series of single and multi-layer nanofiber composite membranes, for possible use in a proton exchange membrane fuel cell, was fabricated where a low equivalent weight 3M ionomer (825 EW perfluorosulfonic acid, PFSA) was reinforced by Torlon®

polyamide-imide (PAI) nanofibers. Three different types of composite membranes were prepared by dual fiber electrospinning: (1) a single-layer membrane (80 wt.% PFSA), where PAI fibers were homogeneously distributed throughout the membrane in the thickness direction, (2) multi-layer membranes with 3, 5, 7, or 9 layers of alternating neat PFSA layers and 70/30 weight ratio PFSA/PAI layers, where the overall membrane composition was 80 wt.% PFSA (20 wt.% PAI), and (3) tri-layer membranes (80 wt.% PFSA), with 5 wt.% PAI in the surface layers and an inner layer that contained 25-60 wt.% PAI, either as a uniform distribution of PAI fibers or a symmetric gradient variation in PAI fiber content. Each membrane was characterized in terms of through-plane and in-plane conductivity in water, gravimetric water uptake, in-plane (lateral) water swelling, and tensile strength.

A number of general observations emerged from the experimental work: (1) proton conductivity was a linear function of overall membrane PFSA content (a simple weight fraction rule of mixtures) and was not dependent on the way reinforcing PAI fibers were distributed in the layers, (2) all membranes exhibited isotropic in-plane and through-plane conductivity, (3) gravimetric water uptake and in-plane water swelling were smaller than predicted based on a rule of mixtures using PFSA weight fraction, (4) the overall properties of a multi-layer membrane did not improve when the number of high/low PFSA content sub-layers was increased from 3 to 9, and (5) for membranes of constant overall PFSA/PAI composition, tri-layer membranes with a thick inner layer (of low PAI content) exhibited less in-plane swelling and a higher stress at break, as compared to those with a thin inner layer (of higher PAI content).

The best membrane for fuel cell applications, identified in this study, had a tri-layer morphology with surface layers containing 95 wt.% PFSA (with 5 wt.% PAI fibers) and a uniform PAI fiber composition inner layer (where the mid-plane composition of the inner layer contained 75 wt.% PFSA). This 20 μm thick membrane exhibited an area specific resistance of 0.023 Ω-cm^2, an in-plane water swelling of 5%, a tensile strength of 26 MPa, and a H_2/air fuel cell performance comparable to Nafion 211.

3.5 Acknowledgements

The authors would like to thank the US DOE (EERE Cooperative Agreement No. DE-EE0006362) for funding this work, as well as Dr. Michael Yandrasits at 3M for providing the 825 EW PFSA used in this study.

3.6 References

[1] M. Maalouf, C.N. Sun, B. Pyle, M. Emery, G.M. Haugen, S.J. Hamrock, T.A. Zawodzinski, Factors enabling high mobility of protons and water in perfluorosulfonate membranes under low hydration conditions, Int. J. Hydrogen Energy. 39 (2014) 2795–2800. doi:10.1016/j.ijhydene.2013.11.006.

[2] J. Choi, K.M. Lee, R. Wycisk, P.N. Pintauro, P.T. Mather, Sulfonated Polysulfone/POSS Nanofiber Composite Membranes for PEM Fuel Cells, J. Electrochem. Soc. 157 (2010) B914. doi:10.1149/1.3392294.

[3] A. Kusoglu, T.J. Dursch, A.Z. Weber, Nanostructure / Swelling Relationships of Bulk and Thin-Film PFSA Ionomers, (2016) 4961–4975. doi:10.1002/adfm.201600861.

[4] K.D. Kreuer, M. Schuster, B. Obliers, O. Diat, U. Traub, A. Fuchs, U. Klock, S.J. Paddison, J. Maier, Short-side-chain proton conducting perfluorosulfonic acid ionomers: Why they perform better in PEM fuel cells, J. Power Sources. 178 (2008) 499–509. doi:10.1016/j.jpowsour.2007.11.011.

[5] S.J. Peighambardoust, S. Rowshanzamir, M. Amjadi, Review of the proton exchange membranes for fuel cell applications, Int. J. Hydrogen Energy. 35 (2010) 9349–9384. doi:10.1016/j.ijhydene.2010.05.017.

[6] M.A. Hickner, H. Ghassemi, Y.S. Kim, B.R. Einsala, J.E. McGrath, Alternative Polymer Systems for Proton Exchange Membranes, Chem. Rev. 104 (2004) 4587–4612. doi:10.1021/cr020711a.

[7] T.R. Ralph, D.E. Barnwell, P.J. Bouwman, A.J. Hodgkinson, M.I. Petch, M. Pollington, Reinforced Membrane Durability in Proton Exchange Membrane Fuel

Cell Stacks for Automotive Applications, J. Electrochem. Soc. 155 (2008) B411–B422. doi:10.1149/1.2838163.

[8] K. Yadav, R., DiLeo, G., Dale, N., Adjemian, Emperical Correlations to Predict In-situ Durability of Polymer Electrolyte Membranes in Fuel Cells, J. Chem. Inf. Model. 53 (2013) 1689–1699. doi:10.1017/CBO9781107415324.004.

[9] K.-D. Kreuer, Ion Conducting Membranes for Fuel Cells and other Electrochemical Devices, Chem. Mater. 26 (2013) 361–380. doi:10.1021/cm402742u.

[10] J. Wu, X.Z. Yuan, J.J. Martin, H. Wang, J. Zhang, J. Shen, S. Wu, W. Merida, A review of PEM fuel cell durability: Degradation mechanisms and mitigation strategies, J. Power Sources. 184 (2008) 104–119. doi:10.1016/j.jpowsour.2008.06.006.

[11] H. Xie, D. Tao, J. Ni, X. Xiang, C. Gao, L. Wang, Synthesis and properties of highly branched star-shaped sulfonated block polymers with sulfoalkyl pendant groups for use as proton exchange membranes, J. Memb. Sci. 497 (2016) 55–66. doi:10.1016/j.memsci.2015.09.035.

[12] A. Mokrini, M.A. Huneault, Proton exchange membranes based on PVDF/SEBS blends, J. Power Sources. 154 (2006) 51–58. doi:10.1016/j.jpowsour.2005.04.021.

[13] S. Swier, V. Ramani, J.M. Fenton, H.R. Kunz, M.T. Shaw, R.A. Weiss, Polymer blends based on sulfonated poly(ether ketone ketone) and poly(ether sulfone) as proton exchange membranes for fuel cells, J. Memb. Sci. 256 (2005) 122–133. doi:10.1016/j.memsci.2005.02.013.

[14] S. Swier, M.T. Shaw, R.A. Weiss, Morphology control of sulfonated poly(ether

ketone ketone) poly(ether imide) blends and their use in proton-exchange membranes, J. Memb. Sci. 270 (2006) 22–31. doi:10.1016/j.memsci.2005.06.037.

[15] H.-L. Wu, C.-C.M. Ma, C.-H. Li, T.-M. Lee, C.-Y. Chen, C.-L. Chiang, C. Wu, Sulfonated poly(ether ether ketone)/poly(amide imide) polymer blends for proton conducting membrane, J. Memb. Sci. 280 (2006) 501–508. doi:10.1016/j.memsci.2006.02.005.

[16] X. Zhang, S. Chen, J. Liu, Z. Hu, S. Chen, L. Wang, Preparation and properties of sulfonated poly(phenylene arylene)/sulfonated polyimide (SPA/SPI) blend membranes for polymer electrolyte membrane fuel cell applications, J. Memb. Sci. 371 (2011) 276–285. doi:10.1016/j.memsci.2011.01.054.

[17] J. Choi, K.M. Lee, R. Wycisk, P.N. Pintauro, P.T. Mather, Nanofiber composite membranes with low equivalent weight perfluorosulfonic acid polymers, J. Mater. Chem. 20 (2010) 6282–6290. doi:10.1039/c0jm00441c.

[18] J.B. Ballengee, P.N. Pintauro, Composite fuel cell membranes from dual-nanofiber electrospun mats, Macromolecules. 44 (2011) 7307–7314. doi:10.1021/ma201684j.

[19] J. Choi, R. Wycisk, W. Zhang, P.N. Pintauro, K.M. Lee, P.T. Mather, High conductivity perfluorosulfonic acid nanofiber composite fuel-cell membranes, ChemSusChem. 3 (2010) 1245–1248. doi:10.1002/cssc.201000220.

[20] J. V. Gasa, R.A. Weiss, M.T. Shaw, Structured polymer electrolyte blends based on sulfonated polyetherketoneketone (SPEKK) and a poly(ether imide) (PEI), J. Memb. Sci. 320 (2008) 215–223. doi:10.1016/j.memsci.2008.03.075.

[21] L.M. Robeson, H.H. Hwu, J.E. Mcgrath, Upper bound relationship for proton

exchange membranes : Empirical relationship and relevance of phase separated blends, J. Memb. Sci. 302 (2007) 70–77. doi:10.1016/j.memsci.2007.06.029.

[22] M. Oroujzadeh, S. Mehdipour-Ataei, M. Esfandeh, Proton exchange membranes with microphase separated structure from dual electrospun poly(ether ketone) mats: Producing ionic paths in a hydrophobic matrix, Chem. Eng. J. 269 (2015) 212–220. doi:10.1016/j.cej.2015.01.088.

[23] J.B. Ballengee, P.N. Pintauro, Preparation of nanofiber composite proton-exchange membranes from dual fiber electrospun mats, J. Memb. Sci. 442 (2013) 187–195. doi:10.1016/j.memsci.2013.04.023.

[24] J.B. Ballengee, P.N. Pintauro, Morphological Control of Electrospun Nafion Nanofiber Mats, J. Electrochem. Soc. 158 (2011) B568–B572. doi:10.1149/1.3561645.

[25] A.M. Park, F.E. Turley, R.J. Wycisk, P.N. Pintauro, Electrospun and Cross-Linked Nano fiber Composite Anion Exchange Membranes, Macromolecules. 47 (2014) 227–235. doi:10.1021/ma401932h.

[26] A.M. Park, R.J. Wycisk, X. Ren, F.E. Turley, P.N. Pintauro, Crosslinked poly(phenylene oxide)-based nanofiber composite membranes for alkaline fuel cells, J. Mater. Chem. A Mater. Energy Sustain. 4 (2015) 132–141. doi:10.1039/C5TA06209H.

[27] J.W. Park, R. Wycisk, P.N. Pintauro, Nafion/PVDF nanofiber composite membranes for regenerative hydrogen/bromine fuel cells, J. Memb. Sci. 490 (2015) 103–112. doi:10.1016/j.memsci.2015.04.044.

[28] T.L. Yu, H. Lin, K. Shen, L. Huang, Y. Chang, G. Jung, J.C. Huang, Nafion /

PTFE Composite Membranes for Fuel Cell Applications, J. Polym. Res. 11 (2004) 217–224.

[29] E. Moukheiber, G. De Moor, L. Flandin, C. Bas, Investigation of ionomer structure through its dependence on ion exchange capacity (IEC), J. Memb. Sci. 389 (2012) 294–304. doi:10.1016/j.memsci.2011.10.041.

[30] M.M. Hasani-sadrabadi, I. Shabani, M. Soleimani, Novel nanofiber-based triple-layer proton exchange membranes for fuel cell applications, J. Power Sources. 196 (2011) 4599–4603. doi:10.1016/j.jpowsour.2011.01.002.

[31] S. Moll, V. Compa, Polyvinyl alcohol nanofiber reinforced Nafion membranes for fuel cell applications, J. Memb. Sci. 372 (2011) 191–200. doi:10.1016/j.memsci.2011.02.001.

[32] S. Ahn, Y. Lee, H. Yong, S. Hong, I. Oh, Properties of the reinforced composite membranes formed by melt soluble ion conducting polymer resins for PEMFCs, Electrochim. Acta. 50 (2004) 571–575. doi:10.1016/j.electacta.2004.01.133.

[33] M. Feng, Y. You, P. Zheng, J. Liu, K. Jia, Low-swelling proton conducting multi-laye rcomposite membranes containing polyarylene ether nitrile and sulfonated carbon nanotubes for fuel cells, Int. J. Hydrogen Energy. 41 (2016) 1–10. doi:10.1016/j.ijhydene.2016.01.085.

[34] T.J. Murray, Poly (amide-imides): Wire Enamels with Excellent Thermal and Chemical Properties, Macromol. Mater. Eng. 293 (2008) 350–360. doi:10.1002/mame.200700365.

[35] S.H. Lee, S.Y. Kim, J.R. Youn, D.G. Seong, S.Y. Jee, J. Il Choi, J.R. Lee, Processing of continuous poly(amide-imide) nanofibers by electrospinning, Polym.

Int. 59 (2010) 212–217. doi:10.1002/pi.2710.

[36] J.B. Ballengee, G.M. Haugen, S.J. Hamrock, P.N. Pintauro, Properties and Fuel Cell Performance of a Nanofiber Composite Membrane with 660 Equivalent Weight Perfluorosulfonic Acid, J. Electrochem. Soc. 160 (2013) F429–F435. doi:10.1149/2.088304jes.

[37] M. Brodt, R. Wycisk, N. Dale, P. Pintauro, Power Output and Durability of Electrospun Fuel Cell Fiber Cathodes with PVDF and Nafion / PVDF Binders, J. Electrochem. Soc. 163 (2016) 401–410. doi:10.1149/2.0711605jes.

[38] W. Zhang, R. Wycisk, D.L. Kish, P.N. Pintauro, Pre-Stretched Low Equivalent Weight PFSA Membranes with Improved Fuel Cell Performance, J. Electrochem. Soc. 161 (2014) F770–F777. doi:10.1149/2.085406jes.

[39] K.S. Lee, M.H. Jeong, Y.J. Kim, S. Bin Lee, J.S. Lee, Fluorinated aromatic polyether ionomers containing perfluorocyclobutyl as cross-link groups for fuel cell applications, Chem. Mater. 24 (2012) 1443–1453. doi:10.1021/cm203539m.

[40] T. Abdel-Baset, T. Benjamin, R. Borup, K.E. Martin, N. Garland, S. Hirano, J. Kopasz, B. Lakshmanmn, D. Masten, M. Mehall, D. Myers, D. Papageorgopoulos, W. Podolski, T. Trabold, B. Vermeersch, J. Waldecker, DOE Fuel Cell Technical Team Roadmap, 2017. doi:10.2172/1220127.

[41] M. Yandrasits, New Fuel Cell Membranes with Improved Durability and Performance, in: DOE Annu. Merit Rev., 2017.

[42] R. Wycisk, P.N. Pintauro, J.W. Park, New developments in proton conducting membranes for fuel cells, Curr. Opin. Chem. Eng. 4 (2014) 71–78. doi:10.1016/j.coche.2014.01.012.

Chapter 4

Dependence of Electrospun Composite Membrane Properties on Ionomer Equivalent Weight

4.1 Introduction

The desire for high-performance H_2/air fuel cells has driven interest in producing proton-exchange membranes (PEMs) with high conductivity and good chemical/mechanical durability. The membrane, which must simultaneously act as a gas separator and a solid electrolyte, is expected to exhibit high conductivity at high and low levels of humidity, as well as resistance to mechanical and chemical degradation. Perfluorosulfonic acid (PFSA) ionomers, like Nafion® from The Chemours Company, are attractive as PEM materials due to their good chemical stability and high proton conductivity when fully hydrated. However, such materials lose a significant portion of their conductivity under dry conditions. For example, the conductivity of 1100 equivalent weight (EW) Nafion equilibrated in 80°C water vapor is reduced from 0.09 S/cm to 0.03 S/cm when the humidity is decreased from 80% to 50% [1]. Increases in proton conductivity are achieved primarily by increasing the ion-exchange capacity (IEC, defined as the mmol/g of ion-exchange sites in a dry ionomer, where IEC = 1000/EW) of the ionomer. This is generally accomplished by adding ion-conducting sites directly to the polymer backbone [2–8] or by employing additional or shorter side chains for the case of perfluoro-type ionomers [9–11]. A third approach is by blending the ionomer with inorganic additives that contain ion-exchange groups [12,13]. However, increases in IEC

have an associated increase in membrane water swelling that compromises the mechanical integrity of the PEM [2].

PFSAs typically exhibit significant swelling/shrinking when they are hydrated/dehydrated due to the presence of hydrophilic fixed charge sites [14]. Increases in the IEC of a PFSA exacerbate the severity of these gravimetric and dimensional changes [14,15]. Excessive swelling of the ionomer, particularly in the in-plane direction, leads to short membrane lifetimes under continuous on/off humidity cycling in a fuel cell, which is one of the factors limiting wide-spread usage of low equivalent weight (EW) ionomers. The stresses that are generated during water swelling/shrinking lead to cracks and pinholes in the membrane [16–19]. In addition, there is the potential for delamination between the membrane and electrodes, further reducing MEA performance [19–21].

At ultra-low EWs (below ~700 g/mol), the increased hydrophilicity and loss of backbone crystallinity in PFSAs [1,22] leads to such excessive swelling that the ionomer becomes soluble in boiling water. Attempts to restrict the swelling of a low EW PFSA have involved adding a hydrophobic component to form a composite membrane [23–27]. The goal of this work is to determine how ionomer equivalent weight (ionomer IEC) dictates the amount of uncharged polymer needed to effectively restrict in-plane water swelling of an electrospun composite membrane while maintaining low area specific resistance (defined as membrane thickness divided by proton conductivity).

An initial set of 825 EW PFSA/PVDF composite membranes was fabricated via dual fiber and single fiber electrospinning in order to demonstrate the effect of PVDF content on the resultant membrane properties. A second set of composite membranes utilizing various low EW ionomers was fabricated with a constant overall IEC via single

fiber and dual fiber electrospinning with PVDF in order to determine how the effective membrane IEC affected transport and mechanical properties. The structure of 3M's low equivalent weight PFSA ionomers (825, 725, and 660 EW) is shown in Figure 4.1. The behavior of dual fiber membranes (made through dual fiber electrospinning) with PFSA and poly (phenyl sulfone) has been documented by researchers in the Pintauro group [1,24,28], who showed that the proton conductivity is dependent on ionomer content while the in-plane swelling is less than what would be expected based on a simple ionomer volume fraction mixing rule [23,24,29]. Recently, Park and Pintauro [30] reported on the novel fabrication of a membrane in which the ionomer and uncharged polymer were blended into a single electrospun fiber.

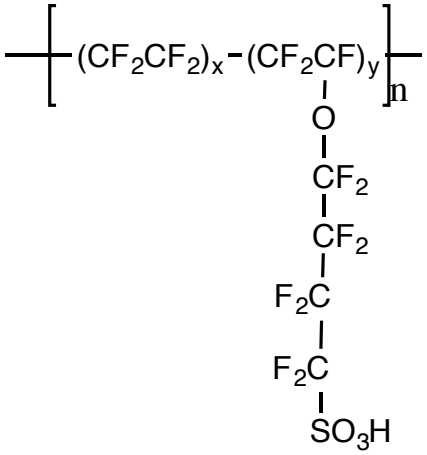

Figure 4.1: Chemical structure of 3M PFSA, with x = 4.5 (for 825 EW), 3.5 (for 725 EW), or 2.8 (for 660 EW), y = 1.

For dual fiber electrospinning, post-electrospinning steps lead to a PFSA matrix that is reinforced by PVDF fibers, which has been shown to exhibit low in-plane swelling, a critical parameter for H_2/air fuel cells. Single fiber electrospinning leads to a dense membrane. The proton conductivity, swelling, and mechanical strength of single

fiber and dual fiber membranes were evaluated to determine their dependence on effective membrane IEC (reinforcing polymer content) and membrane structure.

4.2 Experimental

4.2.1 Materials

Several perfluorosulfonic acid (PFSA) ionomers (with equivalent weights of 825, 725, and 660 g/mol) were obtained from 3M Company. The 825 EW and 725 EW PFSA were received as a dry powder, and the 660 EW PFSA was dispersed in a mixture of alcohol and water. For the latter, the liquid was evaporated at room temperature to obtain dry polymer. Poly (vinylidene fluoride) (Solef ®, PVDF) was received from Solvay Specialty Polymers as a dry powder and was used without further treatment. Acetone, N,N-Dimethylacetamide (DMAc), and n-propanol were obtained from Fischer Scientific and used as received. Poly (ethylene oxide) (PEO) with a molecular weight of 600 kDa was obtained from Millipore Sigma as a dry powder.

4.2.2 Membrane Fabrication

a) Dual fiber membranes

Dual fiber electrospun mats were fabricated through a dual fiber electrospinning technique as described by Ballengee and Pintauro [24,31]. PFSA and PEO (which is a carrier polymer) were separately dispersed/dissolved into a 2:1 (wt:wt) ratio of n-propanol:water solvent. PFSA forms a micellar dispersion instead of a true polymer solution [25], and requires a high-molecular weight carrier to enable electrospinning. In the present study, PEO was used as the carrier. PEO was added to the ionomer dispersion to achieve a 99:1 wt:wt PFSA:PEO ratio, with a total polymer content in solution of 20 wt.%. A 12.5 wt.% PVDF electrospinning solution was prepared by dissolving dry

polymer into a 7:3 (wt:wt) mixture of DMAc:acetone. The two solutions were simultaneously electrospun from separate spinnerets onto a common collector. The composition of the dual fiber mat was controlled through the relative flow rates and concentrations of the two solutions. A summary of the electrospinning conditions is given in Table 4.1.

Table 4.1: Electrospinning conditions for 70 wt.% 825 EW PFSA dual fiber and single fiber membranes.

Parameter	**Mat Structure**		
	Dual Fiber		Single Fiber
	PFSA/PEO (600 kDa)	PVDF	PFSA/PVDF
Solution Composition (wt./wt.)	99/1	100	70/30
Polymer Concentration (wt.%)	20	12.5	19.2
Voltage (kV)	11	10	10
Solution flow rate (mL/h)	0.5	0.24	0.25
Spinneret to collector distance (cm)	20	10.5	8
Relative Humidity (%)	25		30

After electrospinning, the mixed nanofiber mat was dried at 60°C overnight, then pressed at 143°C for 5 minutes at 2500 psi to selectively soften the PFSA, allowing it to flow and fill the inter-fiber void spaces between PVDF fibers. After hot-pressing, the dense film was annealed at 200°C for 30 minutes [32]. A summary of the dual fiber membranes prepared in this study is given in Table 4.2.

Table 4.2: Summary of dual fiber membranes prepared in this study.

PFSA EW [g/mol]	PFSA content [wt.%]	PVDF content [wt.%]	Thickness [µm]
825	80	20	25
825	60	40	28
825	30	70	27
725	72	28	22
660	66	34	27

b) Single fiber membranes

PVDF and PFSA were pre-dissolved separately in a 7:3 (wt:wt) DMAc:acetone solution. The PFSA and PVDF were then mixed to make a blended polymer solution. As mentioned earlier, electrospinning of PFSA typically requires a carrier. In these experiments, PVDF acted as both a carrier and reinforcing (hydrophobic) polymer. A series of single fiber electrospinning solutions were prepared, as shown in Table 4.3. As the PVDF content was increased, the overall solution concentration decreased. After electrospinning, the mats were dried at 70°C overnight, hot pressed at 188°C for 2.5 min at 7000 psi, and finally annealed at 200°C for 15 min. The electrospinning conditions for the single fiber mats are shown in Table 4.1.

Table 4.3: Electrospinning solution compositions for single fiber mats using 3M PFSA and PVDF.

PFSA EW	PFSA Content [wt.%]	Solution Concentration [wt.%]	Membrane Thickness [µm]
825	80	31.3	28
825	60	22.7	26
825	40	17.9	21
725	72	24.8	20
660	66	27.2	26

A series of dual fiber and single fiber membranes were fabricated with a PFSA content ranging from 30 wt.% - 80 wt.% as shown in Table 4.2 and Table 4.3. Dual fiber and single fiber membranes fabricated from 825 EW PFSA/PVDF or 725 EW PFSA/PVDF were treated for 1 hour at 80°C in 1.0 M H_2SO_4, followed by 1 hour at 80°C in H_2O. Membranes utilizing 660 EW PFSA were allowed to soak at room temperature for 16 hours in 1.0 M H_2SO_4, followed by 6 hours in room temperature H_2O [1]. The acid treatment was performed in order to remove PEO (which has been shown to reduce conductivity [25]) and ensure the sulfonic acid sites were in the proton counter-ion form. The 660 EW PFSA is partially water-soluble at elevated temperatures; treatment at room temperature was adequate for removing PEO without causing dissolution of the PFSA (as determined from a separate set of experiments).

c) Solution cast PFSA and PFSA/PVDF blends

Neat PFSA films were prepared through a conventional solution casting technique. The ionomer was dispersed in a 2:1 (wt:wt) mixture of n-propanol:water. The dispersion concentration was 20 wt.%. PFSA/PVDF solution cast blended films were also prepared through a conventional solution casting technique. Blends of PFSA and PVDF were prepared as described in Table 4.3. Each solution was cast onto a glass surface, and after solvent evaporation at 60°C, the films were annealed for 30 minutes at 200°C. Neat ionomer films and solution cast blended membranes containing 825 or 725 EW PFSA were treated for 1 hour at 80°C in 1.0 M H_2SO_4, followed by 1 hour at 80°C in H_2O. Films containing 660 EW PFSA were allowed to soak at room temperature in 1.0 M H_2SO_4 for 16 hours, followed by 6 hours at room temperature in H_2O, as described previously [1].

4.2.3 Proton Conductivity

Proton conductivities were measured using an ac impedance method. Membrane samples (~0.5 cm in width) were loaded into a BekkTech 4-probe conductivity cell and equilibrated in water. In-plane conductivity was calculated using Eq. 4.1,

$$\sigma_{IP} = {}^{L}/_{wtR} \qquad [4.1]$$

where L (cm) is the distance between the electrodes, *w* (cm) is the water-swollen width of the membrane sample, *t* (cm) is its thickness, and R (Ω) is the measured resistance between the electrodes.

The proton conductivity of vapor-equilibrated membrane samples was measured at 80°C in an ESPEC temperature- and humidity-controlled oven. Air-dried samples were loaded into the BekkTech cell, and then allowed to equilibrate at each set point prior to impedance measurements. For these measurements, the air-dried thickness and width of the membrane were used to calculate conductivity.

4.2.4 Water Swelling

Gravimetric water uptake, in-plane water swelling, and thickness water swelling were measured for samples equilibrated in liquid water. After equilibration, excess water was removed from the sample surfaces, and its water swollen mass (m_w) or length (l_w) was measured. The sample was then dried at 99°C under vacuum until the mass stabilized (typically 1 hour). The sample's dry mass (m_d) or length (l_d) was then re-measured. Swelling was calculated using Eq. 4.2, where X represents the mass (for gravimetric water uptake), length (for in-plane swelling), or thickness (for thickness swelling) of the membrane sample in the dry (d) or wet (w) state.

$$Swelling = 100\times\left(\frac{(X_w - X_d)}{X_d}\right) \qquad [4.2]$$

4.2.5 IEC Determination

PFSA/PVDF membrane composition was verified through ion-exchange capacity (IEC) measurements. Membrane samples in the H^+ form were converted to the Na^+ form by soaking for 48 hours with periodic agitation in 50 mL of 2.0 M NaCl. After ion-exchange, the soak solution was titrated with dilute NaOH to a neutral pH, as detected via indicator solution. The membrane IEC was determined using Eq. 4.3,

$$IEC = \frac{VN}{m_d} \quad [4.3]$$

where V [L] is the volume of titrant needed to neutralize the ion-exchange soak solution, N [mol/L] is the normality of the titrant, and m_d [g] is the dry mass of the membrane sample. The precise PFSA/PVDF content of a membrane was found from the IEC of a neat ionomer film and that of a composite membrane. This analysis assumes fully accessible ion exchange sites in a composite membrane. In general, the IEC found from the analysis of composite membranes matched that anticipated from the experimental membrane PFSA and PVDF contents.

4.2.6 Mechanical Properties

Mechanical properties of the membranes were measured using a TA Q800 Dynamic Mechanical Analyzer (DMA) operating in tension mode. Samples were dried at 60°C for several hours prior to testing. Measurements were performed at room temperature and ~40% humidity. Samples were elongated at a constant rate of 5%/minute until fracture.

4.2.7 Dynamic Scanning Calorimetry

Thermal characteristics of the films were obtained using a TA Q200 Differential Scanning Calorimeter (DSC). The temperature was increased from -80°C to 200°C at a

heating rate of 5°C/minute. The melting enthalpy and melting temperature of PVDF in the membrane samples were quantified by integrating the DSC curve from 100°C to 180°C (this range was used to capture the onset of the melting point of PVDF). This range overlaps the α-transition temperature (T_α) of PFSA. However, T_α is not typically observed in DSC, so this analysis assumes that only the thermal transitions of PVDF were detected. The crystallinity of PVDF in the membrane was determined using Eq. 4.4, where X_c is the crystallinity of the composite, ΔH_c and ΔH_0 are the enthalpy of the membrane sample and pure PVDF (105 J/g [33]) and X_m is the weight fraction of PVDF in the composite membrane.

$$X_c = 100\times\left[{}^{\Delta H_c}/_{\Delta H_0}\right]/X_m \qquad [4.4]$$

4.2.8 Scanning Electron Microscopy

Fiber and membrane cross-sections morphologies were characterized using a Zeiss Merlin Scanning Electron Microscope. Samples were sputter-coated with ~5 nm of gold prior to imaging to improve electron conductivity. Freeze-fractured cross-section samples were prepared by submersion in liquid nitrogen for 2 minutes. The average fiber diameters were measured using ImageJ.

4.3 Results and Discussion

4.3.1 Fiber Structure and Membrane Morphology

Single Fiber Mats

Proper electrospinning conditions allowed for the fabrication of well-formed nanofibers of neat PFSA, neat PVDF, and blends of PFSA/PVDF, as confirmed by SEM images of electrospun nanofiber mats, which are shown in Figure 4.2. The average fiber diameter of the PFSA/PVDF blended nanofibers was strongly affected by the PVDF

content in the electrospinning solution. As shown in Figure 4.2(a-c) and measured using ImageJ, the PFSA/PVDF blended fibers have diameters ranging from 280 ± 60 nm for the 80 wt.% 825 EW PFSA fibers up to 1000 ± 250 nm for the 40 wt.% 825 EW PFSA fibers. The increase in fiber diameter corresponds to an increase in electrospinning solution viscosity. It is widely understood that increasing the viscosity of an electrospinning solution results in fibers with larger diameters [34]. As viscosity increases, the electrospun jet undergoes less bending instabilities, leading to a shorter travel distance and time during which the jet would be elongated [35].

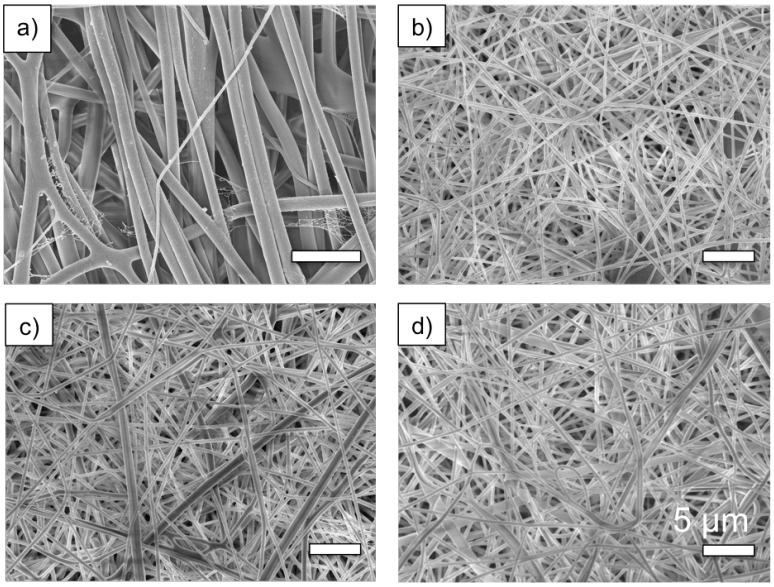

Figure 4.2: SEM images of electrospun nanofiber mats with 5 µm scale bars. a) 40 wt.% 825 EW PFSA (60 wt.% PVDF) Single Fiber; b) 80 wt.% 825 EW PFSA (20 wt.% PVDF) Single Fiber; c) 66 wt.% 660 EW PFSA (34 wt.% PVDF) Single Fiber; d) 80 wt.% 825 EW PFSA (20 wt.% PVDF) Dual Fiber.

Dual Fiber Mats

Well-formed nanofibers of PFSA and PVDF were obtained from the dual fiber electrospinning process. The two fibers were practically indistinguishable in the SEM

images. The PFSA and PVDF solutions were pumped from separate needles, so the PFSA content in the composite mat was controlled through its flow rate relative to the PVDF solution flow rate, and concentration. The average diameter of the dual fiber mat (PFSA and PVDF could not be distinguished under SEM) was practically unchanged, going from 380 ± 70 nm to 400 ± 70 nm as the PFSA content was reduced from 80 wt.% to 40 wt.%.

Membrane Cross-Section Images

SEM cross-section images of the dense membranes from single fiber and dual fiber electrospun mats are shown in Figure 4.3, where the void-free cross-sections indicate complete pore closure for both structures. As shown in a previous study [30], traces of the original fibers can be seen in the single fiber membrane cross-section (Figure 4.3a). Follow-on processing of a dual fiber mat allowed for the PFSA to be selectively softened by pressing above its α-transition temperature of 100-105°C [36,37], but below the melting temperature of PVDF. As a result, the PVDF fibers were retained in the membrane, as has been shown in previous studies [23,24]. This membrane structure is shown in Figure 4.3b.

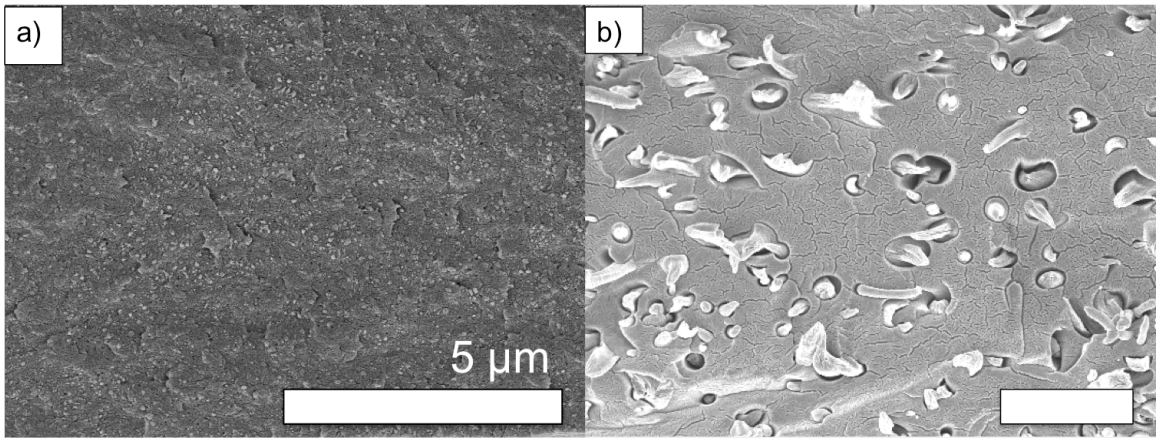

Figure 4.3: Cross-section SEM images of a dense a) single fiber membrane and b) dual fiber membrane using 70 wt.% 825 EW PFSA. The scale bar for both cross-section images is 5 µm.

4.3.2 Composition Effects in 825 EW PFSA/PVDF Composite Membranes

The in-plane conductivity of water-equilibrated single fiber and dual fiber membranes at 25°C containing 825 EW PFSA and PVDF with PFSA contents ranging from 20 – 60 wt.% are shown in Figure 4.4. Each data point is an average from 3 samples. As shown in previous studies [23–25,38], the conductivity of an dual fiber membrane is linearly dependent on the ionomer content via a simple weight fraction mixing rule. Regardless of composition, the dual fiber electrospinning technique allows for a continuous percolating network of PFSA. The conductivity of the single fiber membranes deviated from the mixing rule prediction at PFSA contents of 60 wt.% or less.

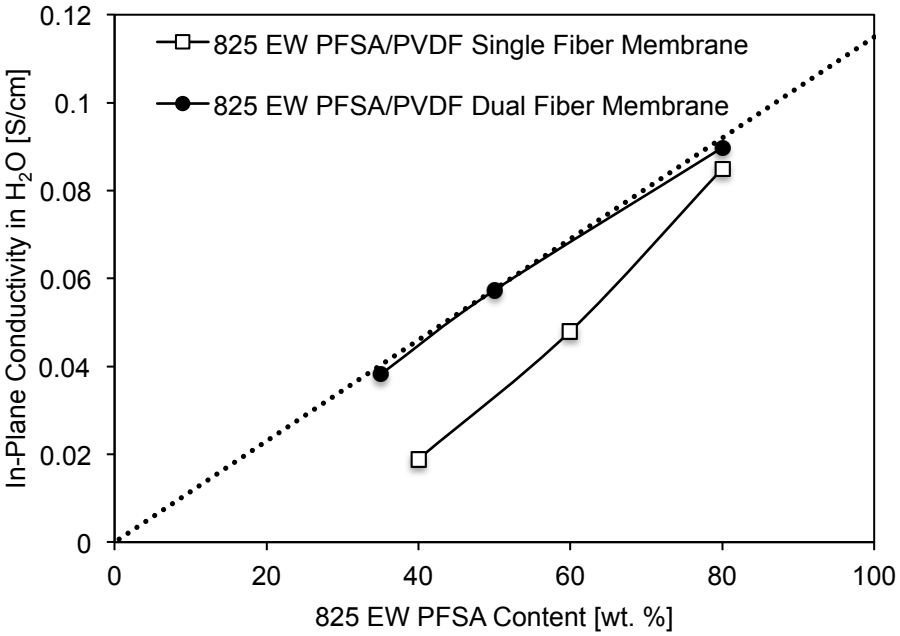

Figure 4.4: In-plane conductivity in liquid H_2O at 25°C of 825 EW PFSA/PVDF dual fiber membranes (□) and single fiber membranes (●). Dotted line represents conductivity based on a simple weight fraction mixing rule (where the conductivity at 100% PFSA was measured in a solution cast film).

The in-plane swelling and gravimetric water uptake for 825 EW PFSA/PVDF membranes made from dual fiber and single fiber mats are shown in Figure 4.5a and Figure 4.5b, respectively. Both membrane structures displayed lower in-plane swelling than predicted by a PFSA weight fraction mixing rule, which has been observed in dual fiber electrospun membranes by Ballengee and Pintauro [24]. The in-plane swelling of the dual fiber membranes was lower than the single fiber membranes. Membrane structure has been observed to control the in-plane swelling of an electrospun composite membrane. Park *et al.* [23] showed that a dual fiber Nafion membrane with embedded PVDF fibers exhibited more pronounced anisotropy in swelling than a PVDF membrane

with embedded Nafion fibers; Ballengee and Pintauro [24] made a similar observation for Nafion/poly (phenyl sulfone) electrospun composite membranes. The greater gravimetric water uptake observed for the 825 EW PFSA/PVDF dual fiber membrane is indicative of better interconnectivity of the ionic domains of PFSA, as compared to the single fiber membrane, which was previously observed by Park *et al.* for Nafion/PVDF electrospun composite membranes [30].

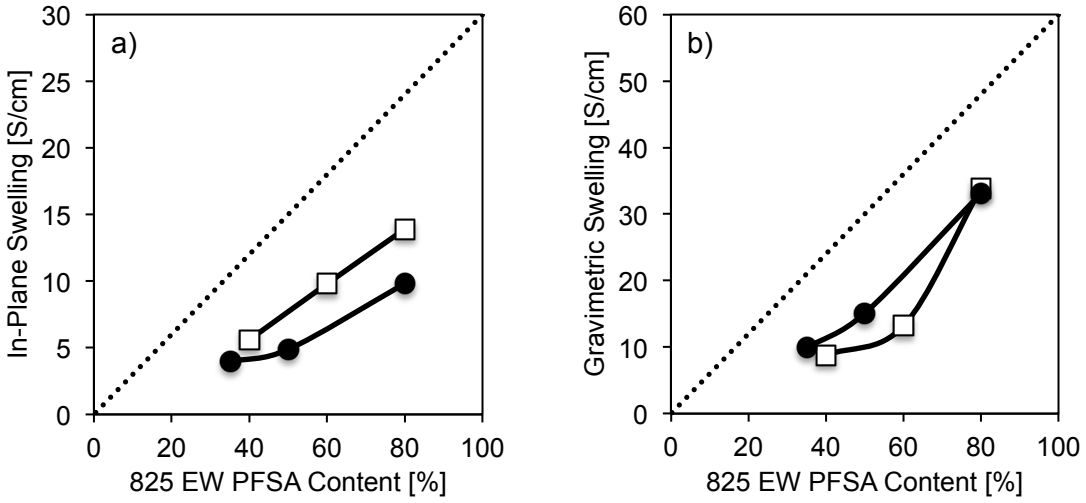

Figure 4.5: In-plane water swelling (a) and gravimetric water uptake (b) of 825 EW PFSA/PVDF (□) single fiber membranes and (●) dual fiber membranes at 25°C. Dotted line represents swelling based on simple weight fraction mixing rule (where the swelling at 100% PFSA was measured for a solution cast film).

4.3.3 Ionomer Equivalent Weight Effects in PFSA/PVDF Composite Membranes

The average in-plane conductivity of solution-cast PFSA and PFSA/PVDF composite membranes with different equivalent weight (EW) ionomers is shown in Figure 4.6. All of the membranes were fabricated to have an effective IEC of ~1.0 mmol/g. This was done in order to determine how the ionomer EW affects membrane

swelling at a fixed IEC. Membranes with lower EW ionomers required a greater PVDF content to maintain the target IEC. The in-plane conductivity of neat PFSA increased with IEC due to the increased concentration of fixed charge groups in the polymer. The single fiber, dual fiber, and solution cast blended membranes exhibited reductions in conductivity when PVDF was added. This is due to the dilution effect of adding PVDF. No significant changes in conductivity were observed for the dual fiber membranes as the ionomer EW was reduced. Continuous proton conduction pathways were maintained over the entire PFSA/PVDF compositional range, allowing the conductivity to be controlled by the ionomer content, as previously discussed. The conductivity of the single fiber, dual fiber, and solution cast blended membranes using 825 and 725 EW PFSA were practically identical. The single fiber and solution cast blended membranes with 660 EW PFSA show a lower conductivity than the dual fiber membrane, which is consistent with the findings of Park *et al*. These results are also consistent with the data in Figure 4.4, where the higher conductivity of the dual fiber membranes corresponds with their higher gravimetric water uptake as compared to the single fiber membranes.

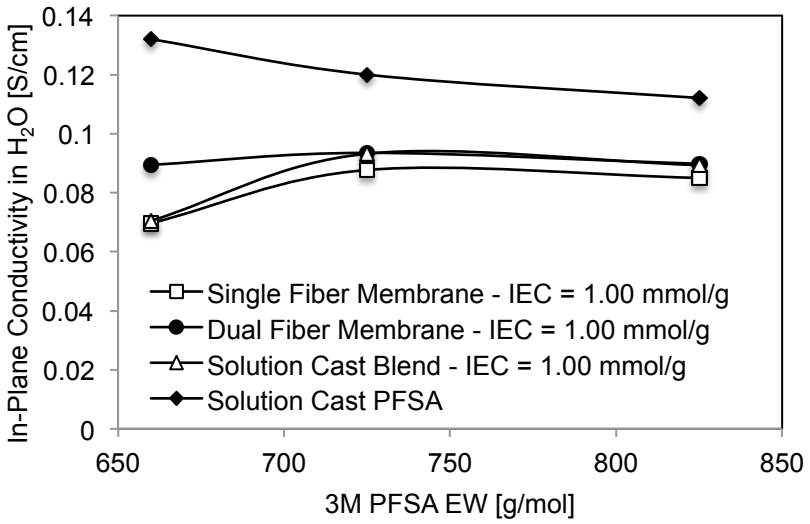

Figure 4.6: In-plane conductivity in liquid H_2O at 25°C of 825 EW, 725 EW, 660 EW PFSA/PVDF single fiber membranes (□), dual fiber membranes (●), solution cast blended membranes (△), and solution-cast 3M PFSA films (◆). The IEC of the composite films is ~1.0 mmol/g.

In-plane conductivities for pristine solution-cast PFSA films, dual fiber membranes, single fiber membranes, and solution cast blended membranes using PFSA ionomers with different EWs were also measured after equilibration in water vapor at 80°C at 90% and 40% relative humidity, and the results are shown in Figure 4.7(a-b). As expected, solution cast films of pristine PFSA are the best in terms of proton conductivity. The composite membranes have the same effective IEC (1.0 mmol/g), and exhibit the same relative humidity dependence, where proton conductivity is significantly reduced as relative humidity goes from 90% to 40%. Surprisingly, the conductivity of the 660 EW PFSA/PVDF composite membranes was similar among the samples at both high and low relative humidity, which is in contrast with the data in Figure 4.6.

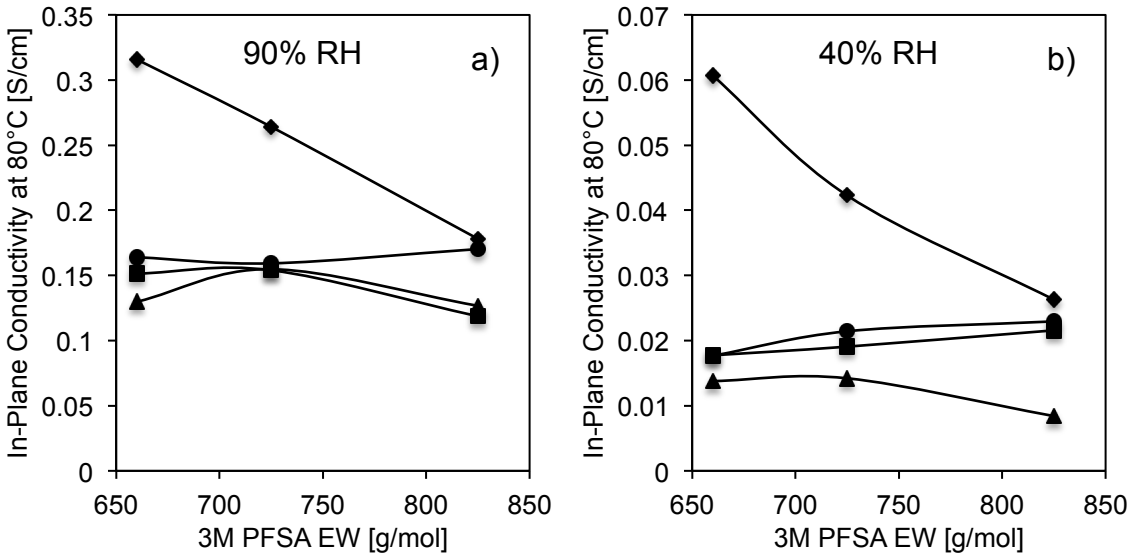

Figure 4.7: In-plane conductivity in H_2O vapor at 80°C (a) at 90% RH, and (b) at 40% RH for dual fiber membranes (●), single fiber membranes (■), solution cast blended membranes (▲), and pristine solution cast PFSA (◆) as a function of ionomer EW.

In contrast to conductivity, the average gravimetric water uptake and in-plane water swelling of dual fiber membranes, single fiber membranes, and solution cast blended membranes are strongly affected by variations in the ionomer EW used to prepare the films, as shown in Figure 4.8(a-c). For comparison, the in-plane swelling and gravimetric water uptake for the neat PFSAs are shown in Figure 4.8d. As seen in the literature, the gravimetric water uptake and in-plane swelling of the neat solution cast PFSA films increased as ionomer EW decreased due to the greater concentration of fixed charge sites [14]. Surprisingly, the gravimetric water uptake of a solution cast blended membrane was greatest when the 725 EW PFSA was used, which highlights the competing effects between the hydrophobicity of PVDF and the hydrophilicity of PFSA. The gravimetric water uptake of the dual fiber membranes was greater than that for the single fiber membranes, which corresponds to previous studies [23]. There was an

unusual minimum in gravimetric water uptake and in-plane swelling for the dual fiber membrane when the 725 EW PFSA was used. The single fiber membrane utilizing 725 EW PFSA only exhibited a minimum in gravimetric water uptake. This is attributed to the backbone crystallinity of this PFSA. As the EW of PFSA decreases below ~700 g/mmol, the backbone begins to become amorphous (which also leads to high water swelling and eventual dissolution in water) [9,39]. The 825 EW PFSA is more crystalline than the 725 EW PFSA, but the lower PVDF content used to achieve the target IEC led to greater water uptake in the electrospun membranes.

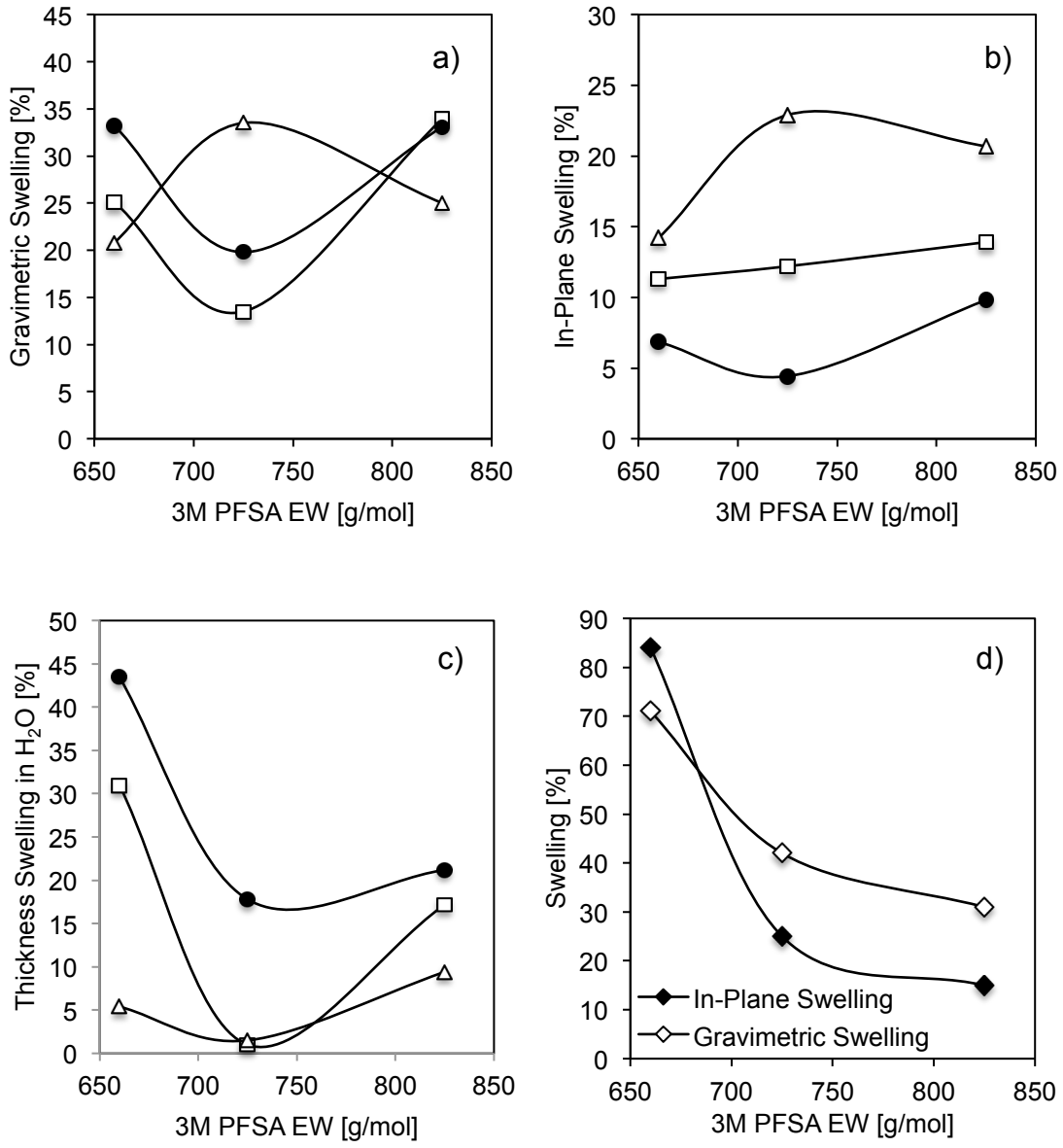

Figure 4.8: In-plane water swelling (a), gravimetric water uptake (b), thickness swelling (c) of 825 EW, 725 EW, and 660 EW PFSA/PVDF dual fiber membrane (□), single fiber membrane (●), and solution cast blended membrane (△), and c) in-plane water swelling and gravimetric water uptake of pure solution-cast PFSA membranes.

The in-plane swelling of the dual fiber membranes was lower than that of the single fiber or solution cast blended membranes, which is in agreement with the data

shown in Figure 4.5. The PVDF fibers in the dual fiber membranes restricted expansion in the lateral direction while allowing swelling in the thickness direction (Figure 4.8c). The unusual minimum in the in-plane swelling was not observed in the single fiber membranes; instead, an approximately linear reduction in the swelling with decreasing ionomer EW was observed. A non-linear relationship was expected based on Figure 4.5a; however, the increase in ionomer hydrophilicity appears to balance the hydrophobicity of PVDF for this compositional range (20 – 34 wt.% PVDF). The swelling behavior of the single fiber membranes more closely mimics that of a polymer blend with more isotropic swelling (Figure 4.8c).

These results reveal a relationship between PFSA ionomer EW and PVDF content for electrospun membranes. High swelling was observed for composite electrospun membranes utilizing 660 EW PFSA (which is 0% crystalline [37]). The low crystallinity of the ionomer overwhelms the high amount of PVDF added to maintain the target IEC. Thus, crystallinity controls swelling. The membranes containing 825 EW PFSA (which is 8.5% crystalline [37]) also exhibited high swelling, which is due to the lower amount of PVDF used to meet the target IEC. The membranes utilizing 725 EW PFSA balanced these effects. There was an adequate amount of PVDF to control swelling, and the ionomer had sufficient crystallinity (2% crystalline [37]) to not swell excessively. These results suggest that proper control of PEM swelling requires both hydrophobic reinforcing material and some degree of PFSA crystallinity.

4.3.4 Crystallinity of PVDF in Composite Membranes

In addition to PFSA, the crystallinity of PVDF is expected to influence the swelling and mechanical properties of composite membranes. The DSC thermograms of

an 80 wt.% 825 EW PFSA (20 wt.% PVDF) dual fiber and single fiber membrane are shown in Figure 4.9, and the melting temperature, heat of fusion, and crystallinity of the electrospun membranes are summarized in Table 4.4. The melting temperature above 160°C observed for the two membranes in Figure 4.9 was attributed to the PVDF. As PFSA and PVDF were electrospun separately in the fabrication of the dual fiber membrane, the ionomer did not affect the thermal behavior of PVDF. As a result, the crystallinity of the dual fiber membranes was essentially unaffected by membrane composition, and minor variations in the melting temperature of PVDF were observed. Larger deviations in the melting temperature of PVDF were observed in the single fiber membrane samples. These were attributed to the interactions between PFSA and PVDF, and are in agreement with literature trends for similar PFSA/PVDF blends [40]. The single fiber membranes exhibited a reduction in the crystallinity of PVDF as the PFSA content increased. The greater crystallinity of PVDF in the dual fiber membranes may be influential for the lower in-plane swelling of such films, as shown in Figure 4.5a and Figure 4.8a.

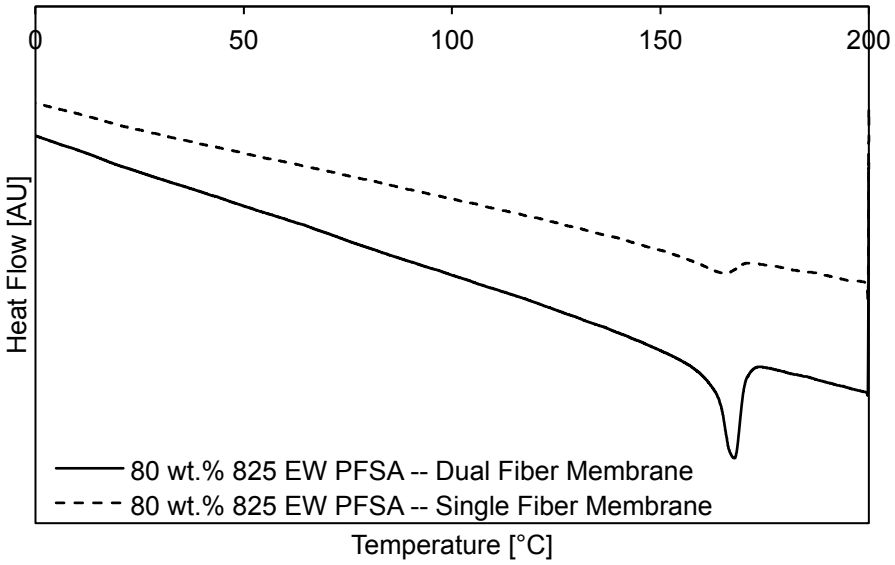

Figure 4.9: DSC curves of an 80 wt.% 825 EW PFSA (20 wt.% PVDF) dual fiber membrane (solid line) and a single fiber membrane (dotted line).

Table 4.4: Melting temperature and crystallinity of PVDF in composite membranes via DSC measurements.

PVDF Content [wt.%]	PFSA EW [g/mol]	Melting Temperature [°C]	Heat of Fusion [J/g]	PVDF Crystallinity [%]
Dual Fiber Membrane				
70	825	167.2	26.49	36.0
50	825	167.0	17.35	33.0
20	825	167.6	9.85	46.9
28	725	167.5	10.71	36.4
34	660	168.0	13.82	38.7
Single Fiber Membrane				
60	825	165.9	22.67	36.0
40	825	166.9	11.18	26.6
20	825	164.7	4.53	21.6
28	725	166.0	5.68	19.3
34	660	167.0	10.42	29.2

4.3.5 Mechanical Properties

In addition to restricting swelling, the presence of PVDF improved the strength of composite membranes. Increased strength has been associated with improved PEM durability [19,41], so a gain in proportional limit stress (PLS) and stress at break are likely to result in improved membrane lifetimes in a fuel cell. Representative stress-strain curves of dual fiber and single fiber membranes utilizing 660 EW and 825 EW PFSA are shown in Figure 4.10, and the mechanical properties (PLS and stress at break) of all membranes are summarized in Table 4.5. As expected (Figure 4.10), composite membrane strength increased with PVDF content for both the dual fiber and single fiber membranes, and was greater than the properties of the solution-cast ionomer. The dual fiber membranes exhibited greater mechanical strength than the single fiber membranes when utilizing 825 or 725 EW PFSA. This is attributed to the greater crystallinity of PVDF in the dual fiber membrane, which overcomes the reduction in PFSA crystallinity as compared to the single fiber membranes (825 EW and 725 EW PFSA have a reported crystallinity of 8.5% and 2%, respectively [37]). Surprisingly, the single fiber membrane exhibited greater PLS than the dual fiber membrane when 660 EW PFSA was used, potentially due to some degree of hydration (tensile measurements were performed at ambient conditions of ~40% relative humidity).

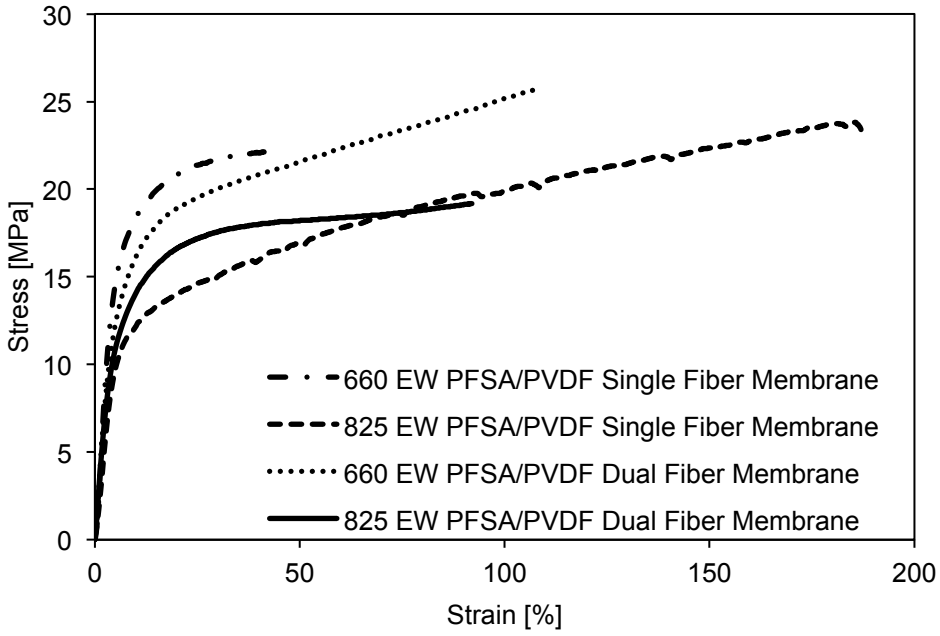

Figure 4.10: Tensile curves of dry PFSA/PVDF dual fiber and single fiber membranes using 825 EW PFSA and 660 EW PFSA.

Table 4.5: Summary of mechanical properties of PFSA/PVDF dual fiber and single fiber membranes. All composite membranes have effective IEC of ~1.0 mmol/g.

PFSA Content [wt.%]	PFSA EW [g/mol]	PLS [MPa]	Stress at Break [MPa]
100	825	10.5	15.2
100	725	8.1	15.5
100	660	7.7	10.2
Dual Fiber Membranes			
30	825	24.6	50.7
50	825	19.2	37.5
80	825	17.1	19.2
72	725	16.9	24.8
66	660	18.3	25.6
Single Fiber Membranes			
40	825	28.5	33.2
60	825	22.0	27.5
80	825	13.9	23.8
72	725	14.2	25.7
66	660	19.7	22.1

4.4 Conclusion

The dependence of membrane properties on ionomer EW was evaluated in membranes with the same overall IEC. Electrospinning of 825, 725, and 660 EW PFSA and PVDF was used to fabricate a series of composite membranes with two distinct structures: (1) membranes made from single fiber PFSA/PVDF blends (followed by softening of the fibers to produce a dense membrane), and (2) membranes made from dual fiber mats, where separate PFSA and PVDF solutions were electrospun, followed by selective softening of the PFSA ionomer, leading membranes where PVDF fibers were embedded in an ionomer matrix. The quantity and equivalent weight of PFSA was varied in the final membranes so that the effective IEC was fixed at 1.0 mmol/g, and the resultant properties of the composite membranes were characterized.

In general, the dual fiber membranes exhibited greater proton conductivities in liquid water and water vapor at 80°C as compared to the single fiber or solution cast blended membranes. The conductivity of both fiber-based membranes was consistent with a simple PFSA/PVDF simple weight fraction mixing rule for 725 and 825 EW ionomers, but the single fiber membrane utilizing 660 EW PFSA displayed an unusual drop in conductivity when immersed in water, due to the reduced water uptake as compared to the dual fiber membrane. Lower in-plane swelling in liquid water was observed for the dual fiber membranes, as compared to the single fiber and solution cast blended membranes, which is consistent with literature data. The dual fiber membranes were also found to be mechanically stronger due to the higher crystallinity of the PVDF reinforcing fibers and the PFSA matrix.

The gravimetric water uptake and in-plane swelling exhibited an unusual minimum when the 725 EW PFSA was used in dual fiber and single fiber membranes. This was attributed to the higher crystallinity of 725 EW PFSA, as compared to that of 660 EW PFSA and the higher PVDF content, as compared to a membrane made with 825 EW PFSA. This suggests that the preservation of ionomer backbone crystallinity is also important to effectively controlling composite membrane swelling.

4.5 References

[1] J.B. Ballengee, G.M. Haugen, S.J. Hamrock, P.N. Pintauro, Properties and Fuel Cell Performance of a Nanofiber Composite Membrane with 660 Equivalent Weight Perfluorosulfonic Acid, J. Electrochem. Soc. 160 (2013) F429–F435. doi:10.1149/2.088304jes.

[2] T. Tamura, H. Kawakami, Membranes for Fuel Cell Electrolytes, (2010) 1324–1328. doi:10.1021/nl1007079.

[3] S. Swier, M.T. Shaw, R.A. Weiss, Morphology control of sulfonated poly(ether ketone ketone) poly(ether imide) blends and their use in proton-exchange membranes, J. Memb. Sci. 270 (2006) 22–31. doi:10.1016/j.memsci.2005.06.037.

[4] M.A. Hickner, H. Ghassemi, Y.S. Kim, B.R. Einsala, J.E. McGrath, Alternative Polymer Systems for Proton Exchange Membranes, Chem. Rev. 104 (2004) 4587–4612. doi:10.1021/cr020711a.

[5] J. V. Gasa, R.A. Weiss, M.T. Shaw, Structured polymer electrolyte blends based on sulfonated polyetherketoneketone (SPEKK) and a poly(ether imide) (PEI), J. Memb. Sci. 320 (2008) 215–223. doi:10.1016/j.memsci.2008.03.075.

[6] Y. Zhao, M. Yoshida, T. Oshima, S. Koizumi, M. Rikukawa, N. Szekely, A. Radulescu, D. Richter, Elucidation of the morphology of the hydrocarbon multi-block copolymer electrolyte membranes for proton exchange fuel cells, Polymer (Guildf). 86 (2016) 157–167. doi:10.1016/j.polymer.2016.01.061.

[7] Y.A. Elabd, M.A. Hickner, Block Copolymers for Fuel Cells, (2011) 1–11. doi:10.1021/ma101247c.

[8] H. Xie, D. Tao, J. Ni, X. Xiang, C. Gao, L. Wang, Synthesis and properties of

highly branched star-shaped sulfonated block polymers with sulfoalkyl pendant groups for use as proton exchange membranes, J. Memb. Sci. 497 (2016) 55–66. doi:10.1016/j.memsci.2015.09.035.

[9] G.A. Gi, G.M. Haugen, S.J. Hamrock, V. Di Noto, Interplay between Structure and Relaxations in Per fl uorosulfonic Acid Proton Conducting Membranes, (2013).

[10] K.D. Kreuer, M. Schuster, B. Obliers, O. Diat, U. Traub, A. Fuchs, U. Klock, S.J. Paddison, J. Maier, Short-side-chain proton conducting perfluorosulfonic acid ionomers: Why they perform better in PEM fuel cells, J. Power Sources. 178 (2008) 499–509. doi:10.1016/j.jpowsour.2007.11.011.

[11] M.G.A.G.L.M.M.C. V. Arcella, AQUIVION -- The short-side-chain and low-EW PFSA for next-generation PEFCs expands production and utilization, ECS Trans. 26 (2010) 279–283.

[12] L. Zhao, Y. Li, H. Zhang, W. Wu, J. Liu, J. Wang, Constructing proton-conductive highways within an ionomer membrane by embedding sulfonated polymer brush modi fi ed graphene oxide, J. Power Sources. 286 (2015) 445–457. doi:10.1016/j.jpowsour.2015.04.005.

[13] G.J. Schlichting, Y. Yang, Advanced Hybrid Super Acidic Inorganic-Organic PEMs for Hotter and Drier Operation. Andrew M. Herring, 50 (2012) 1193–1198. doi:10.1149/05002.1193ecst.

[14] J. Li, H. Tang, Understanding short-side-chain perfluorinated sulfonic acid and its application for high temperature polymer electrolyte fuel cells, RSC Adv. (2014) 3944–3965. doi:10.1039/c3ra43735c.

[15] A. Kusoglu, T.J. Dursch, A.Z. Weber, Nanostructure / Swelling Relationships of Bulk and Thin-Film PFSA Ionomers, (2016) 4961–4975. doi:10.1002/adfm.201600861.

[16] J. Wu, X.Z. Yuan, J.J. Martin, H. Wang, J. Zhang, J. Shen, S. Wu, W. Merida, A review of PEM fuel cell durability: Degradation mechanisms and mitigation strategies, J. Power Sources. 184 (2008) 104–119. doi:10.1016/j.jpowsour.2008.06.006.

[17] F.A. De Bruijn, V.A.T. Dam, G.J.M. Janssen, Review : Durability and Degradation Issues of PEM Fuel Cell Components, (2008) 3–22. doi:10.1002/fuce.200700053.

[18] R. Borup, J. Meyers, B. Pivovar, Y.S. Kim, R. Mukundan, N. Garland, D. Myers, M. Wilson, F. Garzon, D. Wood, P. Zelenay, K. More, K. Stroh, T. Zawodzinski, X.J. Boncella, J.E. Mcgrath, O.M. Inaba, K. Miyatake, M. Hori, K. Ota, Z. Ogumi, S. Miyata, A. Nishikata, Z. Siroma, Y. Uchimoto, K. Yasuda, K. Kimijima, N. Iwashita, Scientific Aspects of Polymer Electrolyte Fuel Cell Durability and Degradation, (2007) 3904–3951.

[19] M.P. Rodgers, L.J. Bonville, H.R. Kunz, D.K. Slattery, J.M. Fenton, Fuel Cell Perfluorinated Sulfonic Acid Membrane Degradation Correlating Accelerated Stress Testing and Lifetime, (2012).

[20] T. Ous, C. Arcoumanis, Degradation aspects of water formation and transport in Proton Exchange Membrane Fuel Cell : A review, J. Power Sources. 240 (2013) 558–582. doi:10.1016/j.jpowsour.2013.04.044.

[21] A. Kusoglu, A.M. Karlsson, M.H. Santare, S. Cleghorn, W.B. Johnson,

Mechanical behavior of fuel cell membranes under humidity cycles and effect of swelling anisotropy on the fatigue stresses, J. Power Sources. 170 (2007) 345–358. doi:10.1016/j.jpowsour.2007.03.063.

[22] R. Wycisk, P.N. Pintauro, J.W. Park, New developments in proton conducting membranes for fuel cells, Curr. Opin. Chem. Eng. 4 (2014) 71–78. doi:10.1016/j.coche.2014.01.012.

[23] J.W. Park, R. Wycisk, P.N. Pintauro, Nafion/PVDF nanofiber composite membranes for regenerative hydrogen/bromine fuel cells, J. Memb. Sci. 490 (2015) 103–112. doi:10.1016/j.memsci.2015.04.044.

[24] J.B. Ballengee, P.N. Pintauro, Composite fuel cell membranes from dual-nanofiber electrospun mats, Macromolecules. 44 (2011) 7307–7314. doi:10.1021/ma201684j.

[25] J. Choi, K.M. Lee, R. Wycisk, P.N. Pintauro, P.T. Mather, Nanofiber composite membranes with low equivalent weight perfluorosulfonic acid polymers, J. Mater. Chem. 20 (2010) 6282–6290. doi:10.1039/c0jm00441c.

[26] K.-D. Kreuer, Ion Conducting Membranes for Fuel Cells and other Electrochemical Devices, Chem. Mater. 26 (2013) 361–380. doi:10.1021/cm402742u.

[27] J.A. Kolde, B. Bahar, M.S. Wilson, T.A. Zawodzinski, G. Shimson, Advanced Composite Polymer Electrolyte Fuel Cell Membranes, Prot. Conduct. Membr. Fuel Cells I Proc. First Int. Symp. Prot. Conduct. Membr. Fuel Cells. 95 (1995) 193–201.

[28] J.B. Ballengee, P.N. Pintauro, Preparation of nanofiber composite proton-exchange

membranes from dual fiber electrospun mats, J. Memb. Sci. 442 (2013) 187–195. doi:10.1016/j.memsci.2013.04.023.

[29] J. Choi, R. Wycisk, W. Zhang, P.N. Pintauro, K.M. Lee, P.T. Mather, High conductivity perfluorosulfonic acid nanofiber composite fuel-cell membranes, ChemSusChem. 3 (2010) 1245–1248. doi:10.1002/cssc.201000220.

[30] J.W. Park, R. Wycisk, G. Lin, P.Y. Chong, D. Powers, T. Van Nguyen, R.P. Dowd Jr., P.N. Pintauro, Electrospun Nafion/PVDF single-fiber blended membranes for regenerative H2/Br2 fuel cells, J. Memb. Sci. 541 (2017) 85–92. doi:10.1016/j.memsci.2017.06.086.

[31] M. Oroujzadeh, S. Mehdipour-Ataei, M. Esfandeh, Proton exchange membranes with microphase separated structure from dual electrospun poly(ether ketone) mats: Producing ionic paths in a hydrophobic matrix, Chem. Eng. J. 269 (2015) 212–220. doi:10.1016/j.cej.2015.01.088.

[32] A.P. Saab, F.H. Garzon, T.A. Zawodzinski, Determination of Ionic and Electronic Resistivities in Carbon/Polyelectrolyte Fuel-Cell Composite Electrodes, J. Electrochem. Soc. 149 (2002) A1541. doi:10.1149/1.1516771.

[33] S. Vidhate, A. Shaito, J. Chung, N.A.D. Souza, Crystallization , Mechanical , and Rheological Behavior of Polyvinylidene Fluoride / Carbon Nanofiber Composites, (2008). doi:10.1002/app.

[34] C.J. Thompson, G.G. Chase, A.L. Yarin, D.H. Reneker, Effects of parameters on nanofiber diameter determined from electrospinning model, Polymer (Guildf). 48 (2007) 6913–6922. doi:10.1016/j.polymer.2007.09.017.

[35] C. Mit-uppatham, M. Nithitanakul, P. Supaphol, Ultrafine Electrospun Polyamide-

6 Fibers : Effect of Solution Conditions on Morphology and Average Fiber Diameter, 6 (2004) 2327–2338. doi:10.1002/macp.200400225.

[36] M.S. Schaberg, J.E. Abulu, G.M. Haugen, M.A. Emery, S.J. O'Conner, P.N. Xiong, S.J. Hamrock, New Multi Acid Side-Chain Ionomers for Proton Exchange Membrane Fuel Cells, ECS Trans. 33 (2010) 627–633.

[37] A. Kusoglu, A.Z. Weber, New Insights into Perfluorinated Sulfonic-Acid Ionomers, Chem. Rev. 117 (2017) 987–1104. doi:10.1021/acs.chemrev.6b00159.

[38] J. Choi, K.M. Lee, R. Wycisk, P.N. Pintauro, P.T. Mather, Nanofiber network ion-exchange membranes, Macromolecules. 41 (2008) 4569–4572. doi:10.1021/ma800551w.

[39] W. Zhang, R. Wycisk, D.L. Kish, P.N. Pintauro, Pre-Stretched Low Equivalent Weight PFSA Membranes with Improved Fuel Cell Performance, J. Electrochem. Soc. 161 (2014) F770–F777. doi:10.1149/2.085406jes.

[40] T. Kyu, J. Yang, Miscibility Studies of Perfluorinated Nafion Ionomer and Poly(viny1idene fluoride) Blends, Macromolecules. 23 (1990) 176–182.

[41] Y. Tang, A. Kusoglu, A.M. Karlsson, M.H. Santare, S. Cleghorn, W.B. Johnson, Mechanical properties of a reinforced composite polymer electrolyte membrane and its simulated performance in PEM fuel cells, J. Power Sources. 175 (2008) 817–825. doi:10.1016/j.jpowsour.2007.09.093.

Chapter 5

Properties of Single Fiber and Dual Fiber Membranes Using 700 EW PFIA and PVDF

5.1 Introduction

The properties of a proton-conducting ionomer can often limit the performance of a H_2/air fuel cell. In proton-exchange membrane fuel cells (PEMFCs), which have been shown to be useful for automotive applications, the membrane must serve as both a separator of feed gases and a solid electrolyte for proton transport. The membrane must survive the highly oxidative conditions and fluctuating levels of humidity in an operating fuel cell. Therefore, high proton conductivity, dimensional stability (i.e. low in-plane swelling), and good chemical and mechanical stability are critical to short- and long-term performance of PEMFCs. One of the most widely used ionomers is the perfluorosulfonic acid (PFSA) from the Chemours Company, Nafion. Its high proton conductivity, chemical/thermal stability (which arise from its Teflon backbone), and highly nanophase segregated morphology in the hydrated state [1] make it an attractive choice for PEMs. However, Nafion (and similar PFSAs like Aquivion or 3M's low equivalent weight PFSA ionomers) undergoes undesirable gravimetric water uptake and in-plane water swelling/shrinking as the membrane cycles between low and high hydration levels. Excessive swelling and shrinking, particularly in the in-plane direction, can lead to the development of cracks in the membrane that cause excessive gas crossover and subsequent failure of the membrane-electrode assembly. In addition, membrane conductivity is heavily dependent on water content, decreasing from 0.08 S/cm to 0.02 S/cm when going from 80% to 40% relative humidity at 80°C [2].

While improvements in conductivity can be achieved by increasing the ion-exchange capacity (IEC, the concentration of fixed charge sites per gram of polymer) of the ionomer, direct modifications – such as increasing the degree of sulfonation in a sulfonated hydrocarbon [3–5], increasing the hydrophilic block ratio in block copolymers [6–8], or adding more sulfonic acid-terminated side chains to the PTFE backbone of a PFSA [9–11] – all result in increased water swelling and, in extreme cases, ionomer dissolution in water [12]. 3M Co. has recently developed a low equivalent weight (EW, defined as 1000/IEC) ionomer, which has 2 proton-conducting groups on its side chains; the molecular structure of this 700 EW perfluoroimide acid (PFIA) is contrasted with that of Nafion in Figure 5.1. 700 EW PFIA is advantageous for fuel cell operation due to the longer backbone (-CF_2-) segment length between the side chains, as compared to a PFSA of the same equivalent weight, which allows for greater polymer crystallinity [13]. This results in a low equivalent weight ionomer that is more resistant to excessive swelling and water dissolution.

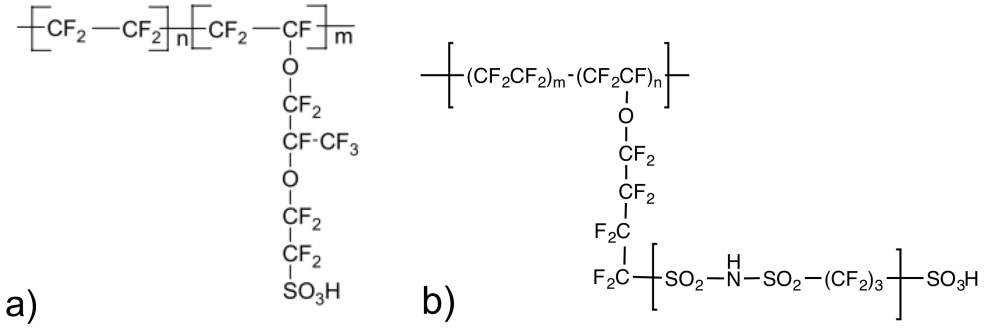

Figure 5.1: Molecular Structure of a) 1100 EW Nafion, with a m:n ratio of 6.5:1, and b) 700 EW PFIA, with an m:n ratio of 7.3:1.

The crystallinity of the backbone in PFSA-type ionomers is related to the mechanical strength and swelling of the ionomer, and is consequently critical for its

durability [13]. High EW ionomers (such as 1100 EW Nafion) have a sufficient number of tetrafluoroethylene units between side chains to impart a high degree of crystallinity (up to 20%) [14,15] and mechanical stability. As more side chains are added to the ionomer backbone, its degree of crystallinity decreases, leading to excessive swelling or water dissolution [16,17]. For example, Ballengee *et al.* observed a 40% loss in mass of 660 EW PFSA after boiling in 1 M H_2SO_4 and water [2]. Thus, more tetrafluoroethylene units between side chains are ideal to ensure sufficient backbone crystallinity. While crystallinity of the backbone is important for stability of the ionomer, the size of the ionic clusters is important for its conductivity. Upon hydration, the acid-conducting groups on the side chains aggregate to form proton conducting channels [18]. Hydrocarbons with sulfonic acid functionalities directly on the backbone form narrow channels and have lower conductivities than a PFSA of similar EW. Tan and coworkers used 3,4-dimethylbenzaldehyde to artificially broaden the ionic channels of Nafion, thus increasing its conductivity by up to 34% [14]. 3M's PFIA is potentially advantageous because it allows for improved backbone crystallinity while maintaining ionic cluster connectivity.

Enhanced ionomer stability in water can be obtained through crosslinks. The addition of physical crosslinks (through polymer blends or dual-fiber electrospinning) is known to reduce the in-plane swelling of a PEM at the cost of conductivity. For example, Ballengee *et al.* used a dual-fiber electrospinning technique to fabricate composite membranes in which a Nafion matrix was reinforced by uncharged poly(phenyl sulfone) (PPSU) nanofibers [19]. A Nafion/PPSU dual fiber membrane with 61% Nafion exhibited 3% in-plane swelling (vs. 16% for pure Nafion) and an in-plane conductivity of

0.050 S/cm (vs. 0.09 S/cm for pure Nafion) in room temperature water [20]. A PFSA/PVDF blend could also be electrospun, as shown by Park *et al.* using Nafion and PVDF [21]. In this case, PVDF acts as both the carrier and the reinforcing polymer in the fiber mat. These PFSA/PVDF single fiber mats were then completely densified to produce an electrospun blended single fiber membrane which can be useful for regenerative H_2/Br_2 fuel cells [22]. This membrane structure mimics a solution-cast blend (that is, there are no remaining fibers in the resultant film) while displaying greater proton conductivity and limited thermodynamic phase separation of the components. While the single fiber electrospinning technique allowed for a membrane with a high PVDF domain aspect ratio (which helps reduce bromine permeability, a key parameter for H_2/Br_2 flow batteries), the properties relevant to a H_2/air fuel cell (specifically gas crossover) have yet to be compared to a dual fiber membrane. It is also of interest to determine if and how the addition of uncharged PVDF enhances the stability of PFIA.

The present study aims to correlate nanofiber-based proton exchange membrane structure and composition with its macroscopic properties. Composite membranes were fabricated using 700 EW PFIA as the ionomer and PVDF as the reinforcing component through single fiber and dual fiber electrospinning. The two techniques lead to a membrane structure where: a) both components are softened into a nano-dispersed film, or b) the uncharged polymer fibers are preserved and embedded in an ionomer matrix. Small-angle X-ray scattering (SAXS), differential scanning calorimetry (DSC), and X-ray diffraction (XRD) data were collected to understand how the fabrication technique affects the resultant structure of the ionic domains of 700 EW PFIA and the crystallinity of PVDF. Relevant membrane properties, such as proton conductivity in liquid water and

water vapor, water uptake, dimensional swelling, and mechanical strength, were determined for the composite membranes, and their relationship to membrane microstructure is discussed. Finally, the performance of a membrane as part of a fuel cell membrane-electrode assembly (MEA) was examined, where hydrogen crossover and power density at 80°C were measured. Both single fiber and dual fiber membranes were used in the MEAs.

5.2 Experimental Section

5.2.1 Material

700 EW perfluoroimide acid (PFIA) and 825 EW perfluorosulfonic acid (PFSA) were supplied by 3M Company, and poly(vinylidene fluoride) (Solef 6020-1001, PVDF) was provided by Solvay Specialty Polymers. N,N-dimethylacetamide 99.8% (DMAc), tetrahydrofuran 99.9% (THF), n-propanol, acetone, and poly(ethylene oxide) (Mw= 1 MDa) (PEO) were purchased from Millipore Sigma and used as received.

5.2.2 Membrane fabrication

Dual fiber membrane

Dual fiber membranes of 700 EW PFIA and PVDF were fabricated by simultaneously electrospinning the polymers from separate syringes onto a common collector. 700 EW PFIA and PEO (Mw= 1 MDa) were separately dispersed in a mixture of n-propanol/water at a 2:1 mass ratio. As with PFSAs, 700 EW PFIA does not form a true polymer solution [23], instead forming a micellar dispersion. A high molecular weight carrier (PEO) was added in order to induce chain entanglements and enable the electrospinning of PFIA nanofibers [9,24–28]. The PEO solution was added to the ionomer dispersion, leading to a mixture that was 20 wt.% polymer with a 99:1 (wt:wt)

ratio of 700 EW PFIA:PEO. PVDF was dissolved into a mixture of 7:3 (wt:wt) DMAc:acetone at a polymer content of 12.5 wt.%. The 700 EW PFIA and PVDF were electrospun from 7.5 kV and 10 kV respectively, with the electrospinning chamber held at a relative humidity of 25%, and the composition of the electrospun mat was adjusted by varying the PVDF flow rate. The electrospinning conditions for a dual fiber mat are summarized in Table 5.1.

Table 5.1: Electrospinning conditions for 80 wt.% 700 EW PFIA/20 wt.% PVDF dual fiber and single fiber mat (voltage, spinneret to collector distance (SCD), flow rates, relative humidity (RH)).

Mat Structure	**Dual Fiber**		**Single Fiber**
	99:1 700 EW PFIA:PEO Fibers	PVDF Fibers	80:20 700 EW PFIA:PVDF Fibers
Voltage [kV]	7.5	10	14
Flow Rate [mL/h]	0.50	0.17	0.25
STC [cm]	8	10.5	8
RH [%]	25	25	20
Solvents	2:1 n-Propanol:H_2O	7:3 DMAc:Acetone	7:3 DMAc:Acetone
Concentration [%]	20	12.5	26

The electrospun mat was dried at 60°C overnight prior to conversion into a dense membrane. Densification of the dual fiber mat was performed by hot pressing at 143°C for 5 minutes at a pressure of 2500 psi. During this step, the 700 EW PFIA fibers soften and flow to fill the void space between the PVDF fibers. The resultant membrane was then thermally annealed for 30 minutes at 200°C to ensure crystallization of the 700 EW PFIA matrix. The membrane was prepared for testing by immersion into room temperature 1.0 M H_2SO_4 for 16 hours, followed by an additional 16 hours of soaking in H_2O at room temperature.

Single fiber membrane

Single fiber electrospun mats were fabricated by electrospinning a blend of PFIA and PVDF. 700 EW PFIA and PVDF were separately dispersed/dissolved in DMAc (50 wt.%) and in DMAc:acetone 7:3 (wt:wt) (12.5 wt. %) respectively. The PVDF solution was then added to the PFIA dispersion and the solution was mixed at least 4 hours before electrospinning. Because PVDF can act as both the reinforcing and the carrier polymer, the addition of PEO was not required. The total polymer concentration of the mixture was 26 wt.%. The electrospinning parameters were: 20% relative humidity, flow rate of 0.25 mL/hr, voltage of 10 - 15 kV, spinneret to collector (STC) distance of 8 cm, and deposited volume of 3.5 mL. Table 5.1 summarizes the solution composition and electrospinning conditions for an 80 wt.% 700 EW PFIA/20 wt.% PVDF single fiber mat. After drying at 60°C under vacuum for 24 hours to evaporate the residual solvent, the electrospun mat was compressed to 2500 psi at 188°C for 2.5 min. This allowed the fibers to soften and fill the void spaces in the mat, leading to a dense blended fiber membrane. The film was then annealed in vacuum at 200°C for 15 min. The resultant single fiber membrane was immersed in 1.0 M H_2SO_4 for 24 hours at room temperature, followed by immersion in deionized water for 24 hours to protonate all ion-exchange sites and hydrate the film.

Solution Cast Blend

Neat 700 EW PFIA and conventional blended films were prepared by solution casting. A 20 wt.% dispersion of neat PFIA was prepared in a 2:1 (wt:wt) mixture of n-propanol:water. Solution cast blended membranes were prepared by mixing pre-dissolved PVDF with 700 EW PFIA (same solvents as the electrospinning solutions, where the

PFIA/PVDF mass ratio was 70/30). The PFIA dispersion and the PFIA/PVDF blend were cast onto glass plates, and the films were dried at 70°C overnight. The films were then annealed at 200°C for 30 minutes, and preconditioned by immersion in 1.0 M H_2SO_4 for 16 hours at room temperature, then in H_2O for another 16 hours.

5.2.3 Membrane Characterization

Scanning Electron Microscopy

Images of electrospun mats and membranes were collected with a Hitachi S-4200 scanning electron microscope. Samples were sputter-coated with a layer of gold (~5 nm) to provide electrical conductivity. Freeze-fractured membrane cross sections were prepared by immersing samples in liquid nitrogen for up to 2 minutes.

Ion-Exchange Capacity Determination

The PFIA content in composite membranes was verified via ion-exchange capacity (IEC) measurements. After acid treatment, a membrane with a known dry mass (m_{dry}) was submerged into 2.0 M NaCl for 48 hours. After ion exchange, where the protons in the membrane were replaced with Na^+ ions, the soak solution was titrated to a neutral pH with 0.01 N NaOH. The IEC was determined using Eq. 5.1, where N (mmol/L) is the normality of the titrant, V (L) is the volume of titrant required to neutralize the soak solution, and IEC_{sample} (mmol/g) is the IEC of the film. The IEC of the neat ionomer film and that of a composite membrane were used to determine the effective PFIA/PVDF composition, as described in Chapter 4 of this dissertation.

$$IEC_{sample} = \frac{V \times N}{m_d} \tag{5.1}$$

Water Uptake and Swelling

Gravimetric water uptake and in-plane swelling were measured after membrane equilibration in room temperature water using Eq. 5.2.

$$Water\ Swelling\ (\%) = \frac{x_{wet} - x_{dry}}{x_{dry}} \times 100 \quad (5.2)$$

In Eq. 5.2, x represents the membrane's mass (g) or length (cm) in the wet (w) or dry (d) state corresponding to gravimetric water uptake or in-plane swelling, respectively. The wet mass (m_{wet}) and length (l_{wet}) of a membrane sample were measured after equilibration in room temperature water. The membrane's dry mass (m_{dry}) and length (l_{dry}) were measured after drying at 70°C overnight, followed by 1 hour drying at 100°C under vacuum.

Gravimetric water uptake after equilibration in room temperature liquid water is also reported as λ, the number of water molecules per sulfonic acid site, which is calculated using Eq. 5.3, where m_{wet} and m_{dry} represent the wet and dry mass (g) of a membrane sample, and MW_{water} is the molecular weight of water (18 g/mol).

$$\lambda = \left(\frac{m_{wet} - m_{dry}}{m_{dry}}\right) \times \left(\frac{1}{1000 \times IEC \times MW_{water}}\right) \quad (5.3)$$

Conductivity

In-plane proton conductivity was measured using an *ac*-impedance method in room temperature liquid water and 80°C water vapor. Water-equilibrated membrane samples were loaded into a BekkTech four-electrode cell and immersed in water. Vapor-state conductivity was measured for humidity levels ranging from 20 – 90% where the BekkTech cell was placed inside an ESPEC Corp. temperature/humidity controlled

environmental chamber (Model: SH-241). Conductivity was calculated using the following Eq. 5.4:

$$\sigma = \frac{L}{Rw\delta} \quad (5.4)$$

where σ (S/cm) is proton conductivity, R (Ω) is the measured resistance between the electrodes, L (cm) is the distance between the electrodes, w (cm) is the membrane sample width (usually 0.5 cm), and δ (cm) is the sample thickness (typically between 0.0015 and 0.0040 cm). For conductivities measured in water vapor, the dry dimensions of the membrane were used in Eq. 5.4. For conductivities measured in liquid water, the water-swollen dimensions were used.

Dynamic mechanical analysis

Mechanical properties were measured with a TA Q800 dynamic mechanical analyzer (DMA). Stress-strain curves were obtained for dry membranes at ambient conditions of 25°C and ~40% RH (all membranes were pre-dried in vacuum at 60°C for 12 hours before being testing). The DMA was operated in tension mode, and the samples were deformed at a strain rate of 10%/minute until fracture.

Small Angle X-ray Scattering

Small-angle X-ray scattering (SAXS) spectra were recorded with a homemade apparatus at CEA-Grenoble/INAC, using a CuK_{α} radiation (λ=1.5418 Å) source generated by a rotating anode. A sample to detector distance of 0.80 m with an off-centred configuration was chosen and allowed to cover an angular "q" range from 0.01 $Å^{-1}$ to 0.3 $Å^{-1}$. Two pieces of water swollen membrane were superimposed and were placed in a SAXS cell between two Kapton® foils. Usual corrections were applied to the data for background subtraction and normalization [29].

X-Ray Diffraction

XRD measurements were performed using a Scintag XGEN-4000 X-ray diffractometer with a CuKα (λ = 0.154 nm) radiation source delivering a linear beam. Axial divergence was limited by Y rad Soller slits. The measurements were performed in reflection geometry.

Differential Scanning Calorimetry

The melting temperature of PVDF in composite membrane samples was determined via differential scanning calorimetry (DSC). Measurements were performed using a TA Q200 DSC equipped with a cooling apparatus under a nitrogen atmosphere. Samples were heated at a rate of 10°C/minute from -60°C to 250°C.

Freezable water content for select membranes was also determined via DSC according to previously published procedures [22,30,31]. Circular samples (~5 mg) of a water-equilibrated membrane were quickly wiped to remove excess water, and were then loaded into a DSC hermetically sealed pan and cooled to 220 K. The pan was then heated from 220 K to 320 K at a heating rate of 10 K/minute. The freezable water content, λ_f (water that was loosely bound to the sulfonic acid sites), was determined by comparing the enthalpy of fusion for water in the sample (determined by integrating the melting endotherm using TA analysis software) to that of bulk water, which was taken to be 334 J/g [22,32]. Non-freezable water, λ_{nf} (water tightly bound to the sulfonic acid sites), was determined by subtracting λ_f from the total water content of the membrane, found from the gravimetric water uptake experiments described previously.

Fuel cell Polarization

Fuel cell polarization curves were obtained for PFIA/PVDF membranes in a 5 cm^2 MEA (membrane-electrode assembly) at a cell temperature of 80°C and a backpressure of 100 kPa. The dry thickness of the membrane was 25 μm. Catalyst inks were prepared using a 40 wt.% Pt/C catalyst (Alfa Aesar) and 825 EW PFSA dispersed in a 2:1 (wt:wt) n-propanol:water mixture. For all experiments, the Pt/C electrode catalyst loading was 0.25 mg/cm^2, with 35 wt. % 825 EW PFSA as the binder. Electrodes were painted onto Sigracet BC29 carbon paper gas-diffusion layers (GDLs) from Ion Power, and MEAs were fabricated by hot-pressing the electrodes onto the membrane for 10 min at 143°C and 580 psi. Prior to fuel cell testing, the MEA was preconditioned for several hours at 80°C by repeatedly cycling the cell for 2 min at a low voltage (0.2 V) and 2 min at a high voltage (0.6 V). Hydrogen crossover was determined using linear sweep voltammetry, where the cell was operated under H_2/N_2. In a fuel cell experiment, feed gases were supplied at 125 mL/min (hydrogen) and 500 mL/min (air) for the anode and cathode, respectively. Polarization curves were obtained by measuring the current at specified voltages after 60 seconds of equilibration.

5.3 Results and discussion

5.3.1 Membrane Structure

Fiber And Membrane Morphology

In a single fiber membrane, 700 EW PFIA and PVDF were mixed in a common solvent and then electrospun to produce a blended single fiber mat. As shown in Figure 5.2A, well-formed fibers (i.e. no beads or droplets) of a 700 EW PFIA/PVDF blend (70 wt.% PFIA and 30 wt.% PVDF) were obtained after electrospinning. After hot pressing

and annealing, the blended fibers were completely softened leading to a dense membrane cross-section, as shown in Figure 5.2B. The absence of voids confirms complete densification of the membrane and melting of the components.

In a dual fiber membrane, 700 EW PFIA and PVDF were simultaneously electrospun from separate syringes to fabricate a mixed fiber mat. Because the ionomer was selectively softened, the resultant film had PVDF fibers embedded in a PFIA matrix. An SEM image of a 70 wt.% 700 EW PFIA/30 wt.% PVDF dual fiber mat is shown in Figure 5.2C. The PVDF and 700 EW PFIA fibers are indistinguishable, with fiber diameters ranging from 600 – 800 nm. The processed membrane cross-section, shown in Figure 5.2D, reveals a dense matrix of 3M 700 EW PFIA with embedded PVDF fibers. Retention of the PVDF fiber structure was achieved after the hot pressing and annealing steps of the dual fiber membrane, and complete pore closure was obtained for both types of fiber mats. As expected, the cross-section of a PFIA/PVDF solution cast blended membrane (Figure 5.2E) was featureless.

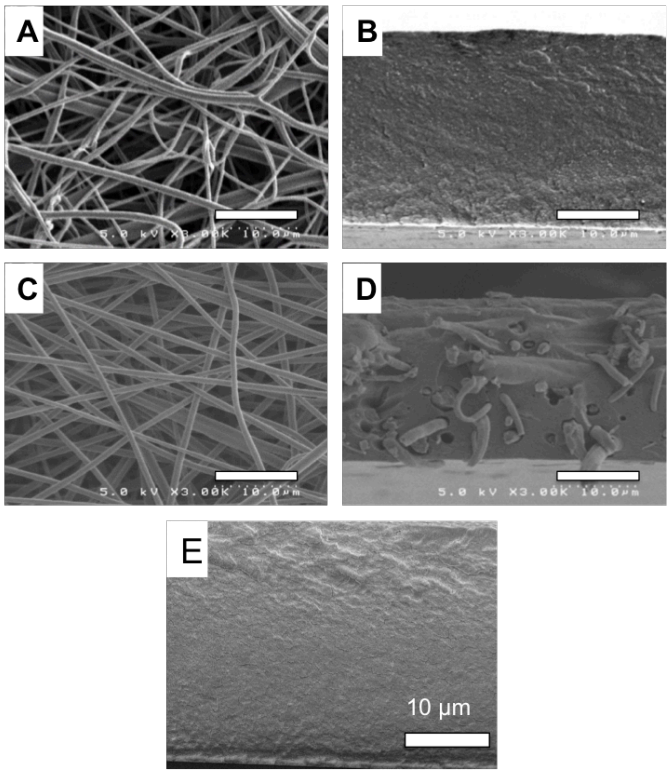

Figure 5.2: Scanning electron microscopy images of single fiber (A) and dual fiber (C) 70 wt.% 700 EW PFIA/30 wt.% PVDF mats. Freeze fracture cross-section of a single fiber membrane (B) and a dual fiber membrane (D) 70/30 wt.% 700 EW PFIA/PVDF made from the mats in (A) and (C), respectively. Freeze fracture cross-section of solution cast blended membrane containing 70 wt.% 700 EW PFIA/30 wt.% PVDF (E). 10 µm scale bar.

Membrane Crystallinity

Differential scanning calorimetry (DSC) and X-ray diffraction (XRD) were used to observe the effect of membrane structure on the PVDF and PFIA crystallinity. Membranes with 70 wt.% 700 EW PFIA/30 wt.% PVDF were analyzed to highlight the impact of the fabrication technique (single fiber vs. dual fiber electrospinning) on the crystallinity of PVDF in the final membrane. Figure 5.3 shows the DSC thermograms of

a neat PFIA, single fiber membrane, a dual fiber membrane, and a solution cast blended membrane at a heating rate of 10°C/min under nitrogen.

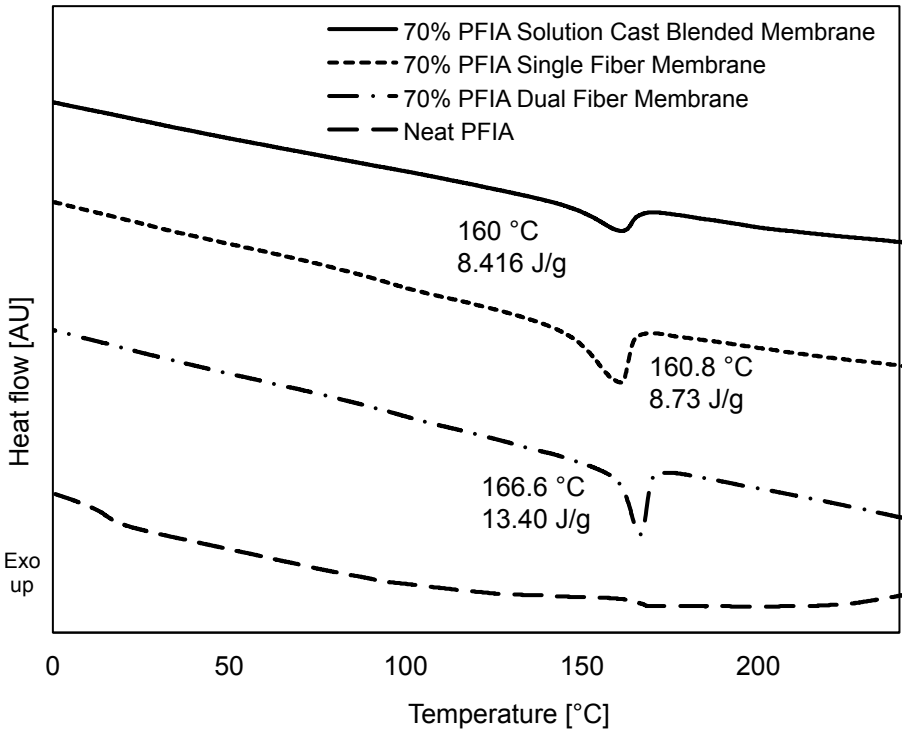

Figure 5.3: DSC thermograms of 70 wt.% 700 EW PFIA/30 wt.% PVDF solution cast blended, single fiber, and dual fiber membranes at 10°C/min.

The crystallinity of the PVDF in the three membranes was determined by integrating the DSC thermograms. The results of the thermal analysis (melting temperature and crystallinity) are summarized in Table 5.2. No melting was observed in neat PFIA. Perfluoro-type ionomers have an α-transition temperature between 100°C and 150°C, but such transitions are typically not observed in DSC. The DSC thermograms show a similar melting behavior for all films with a peak between 160°C and 167°C, typical of the semi-crystalline PVDF polymer [33–35]. The melting temperature (T_m) of PVDF in a single fiber and solution cast blended membrane was approximately 161°C,

and was slightly higher in a dual fiber membrane at 166.6°C. The depression of the melting point of PVDF when blended with PFIA is indicative of the intimate molecular interactions (i.e. miscibility) between the polymers in the single fiber and solution cast blended membranes [36]. The crystallinity of PVDF in the membranes was calculated based on the heat of fusion of an ideal PVDF crystal, ΔH_f^o = 104.7 J/g [37,38]. The degree of crystallinity was determined using the following the formula [39]:

$$\chi_c = \left(\frac{\Delta H_m}{\Delta H_f^0} \Big/ X_m \right) \times 100 \quad (5.5)$$

where ΔH_m (J/g) is the melting enthalpy of the sample and X_m is the weight fraction of PVDF in the membrane. The degree of PVDF crystallinity in single fiber and solution cast blended membranes were similar, 26.8% and 27.8% respectively. The dual fiber membrane showed a higher degree of PVDF crystallinity of 42.7%. As all the membranes were annealed at 200°C, the increased melting temperature and crystallinity of PVDF in the dual fiber membrane is attributed to the purity and continuity of PVDF fibers. In the single fiber and solution cast blended membranes, the 700 EW PFIA and PVDF are intimately mixed, which reduces the crystallinity of the PVDF.

Table 5.2: Melting temperature (T_m), heat of fusion (ΔH_m) and crystallinity (X_m) of 70 wt.% 700 EW PFIA/30 wt.% PVDF dual fiber, single fiber, and solution cast blended membranes.

Membrane Type	Melting Temperature [°C]	Heat of Fusion [J/g]	PVDF Crystallinity [%]
Solution cast blended membrane	160.6	8.42	26.8
Single fiber membrane	160.8	8.73	27.8
Dual fiber membrane	166.6	13.40	42.7
PFIA	---	---	---

Wide-angle X-ray Diffraction (WAXD) was used to determine the crystallinity of solution cast 700 EW PFIA. The X-ray pattern for the ionomer is shown in Figure **5**.4, with a crystalline peak superimposed on an amorphous halo, as described in Reference [40]. The spectrum was deconvoluted using Pearson VII distribution functions to find the crystallinity. The crystallinity of 700 EW PFIA was calculated as the area under the crystalline (cr) curve divided by the area under both the crystalline and amorphous (am) curves [40,41], as shown in Eq. 5.6.

$$W_{cr} = \int I_{cr}(2\theta)d(2\theta) \Big/ [\int I_{cr}(2\theta)d(2\theta) + \int I_{am}(2\theta)d(2\theta)] \quad (5.6)$$

In Eq. 5.6, I(2 θ) is the intensity of the crystalline (cr) and amorphous (am) scattering peaks. Based on this analysis, the crystallinity of 700 EW PFIA was approximately 18.3%. This is significantly greater than the crystallinity of 660 EW PFSA (zero crystallinity [15]) and similar to the crystallinity of a low EW 3M ionomer (~23% [42] for 850 EW PFSA). The similarity in crystallinity to the 850 EW ionomer is reasonable as PFIA is prepared from an ~800 EW precursor [13], i.e. the distance between sidechains is similar to that of 800 EW PFSA.

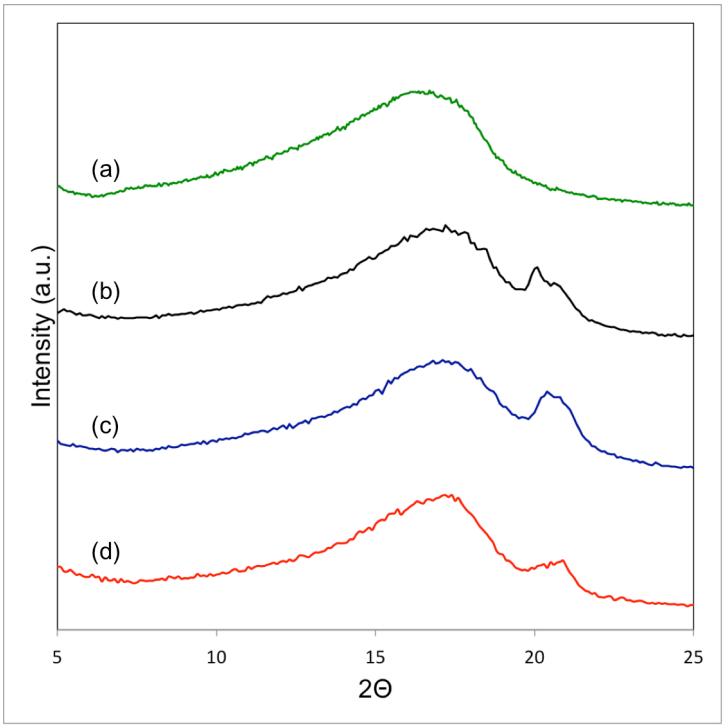

Figure 5**.4:** XRD diffractograms for (a) solution cast 700 EW PFIA, (b) solution cast blended membrane, (c) single fiber membrane and (d) dual fiber membrane 70 wt.% 700 EW PFIA/30 wt.% PVDF membranes.

The X-ray patterns of the 3 composite membrane structures (dual fiber, single fiber, and solution cast blended membranes) are shown in Figure **5**.4. For each membrane, a broad halo was observed, centered at $2\theta = 17.5°$ due to PFIA. This halo overlapped with the PVDF reflections at $2\theta = 17.5°$ (100) and 18.6° (020). Because of this overlap, the crystallinity of PFIA in the composite membranes could not be calculated. Two peaks located at $2\theta = 19.7°$ and 20.6° were superimposed and are characteristic of (110) and (011) reflections of the α-phase and β-phase of PVDF (19.9° and 20.5° according to reference [43]). For the solution cast blended film, a predominance of the reflection at 19.9° versus 20.6° is observed. In the case of the single

fiber membrane, the 2 peaks are present at same magnitude. The reflection at 20.6° dominates in the dual fiber membrane, showing a different organization of the PVDF crystallites in the 3 structures. Thus, the membrane fabrication technique (electrospinning vs. solution casting) influenced the crystalline phase of PVDF in the final membrane, and dual fiber electrospinning appears to have led to a predominance of the β-phase of PVDF.

Nanostructure

The nanophase segregation between the hydrophilic and hydrophobic domains of hydrated PFIA, which is a key property of ionomers, drives the membrane's overall functionalities. Small-Angle X-ray Scattering (SAXS) was used to obtain important information related to the shape of the hydrated domains and the distance between ionic crystallites at the nanoscale in the 700 EW PFIA/PVDF composite films. Figure 5.5 shows the SAXS profiles of a 70 wt.% 700 EW PFIA/30 wt.% PVDF solution cast blended membrane, single fiber membrane, and dual fiber membrane equilibrated in liquid water at room temperature. The shapes of the curves (namely the small angle region and the peak width and position) were influenced by the membrane microstructure, which was dependent on the membrane fabrication process. The three membranes displayed a scattering peak located in the 0.1 $Å^{-1}$ "q" range, which was identified as the "ionomer peak", the fingerprint of the hydrophilic/hydrophobic phase segregation at the nanoscale. The solution casting and single fiber electrospinning methods gave rise to similar ionic domain sizes and organization at the nanoscale. Their ionomer peaks are located at very close positions: q_{iono}~0.110 $Å^{-1}$ for the solution cast blended membrane and ~0.114 $Å^{-1}$ for the single fiber membrane, corresponding to Bragg spacings ($d = 2\pi/q$) of ~55 Å and 57 Å for the ionic domains in the two different films. It

can be noted that the ionomer peak of the single fiber membrane is slightly sharper than that of the cast membrane (see the inset of Figure 5.5 displaying the SAXS data on a linear scale). This observation shows that the polydispersity of the ionic domain size was somewhat higher in the solution cast blended membrane, likely due to the slower evaporation rate of the solvent during membrane fabrication.

Interestingly, the dual fiber membrane exhibited different ionic domain sizes. The ionomer peak is significantly leftward shifted to ~0.100 $Å^{-1}$ (Bragg spacing~63 Å) and is very broad. The dual fiber electrospinning technique gave rise to larger ionic domains with a greater size polydispersity compared to what was observed for the single fiber membrane. This is likely because the polymers are not blended in the dual fiber membrane. In both the single fiber membrane and solution cast blended membrane, the presence of PVDF regulated the size of the ionic domains due to intimate mixing of the two components. The single fiber membrane exhibited a sharper peak in the ionomer region because fast solvent evaporation prevented reorganization of the domains during fiber formation. However, in the dual fiber membrane, PFIA was practically free of contaminants during electrospinning. The hydrophilic environment resulted in fewer size restrictions for the ionic domains, leading to larger ionic clusters with a wider range of ionic domain sizes.

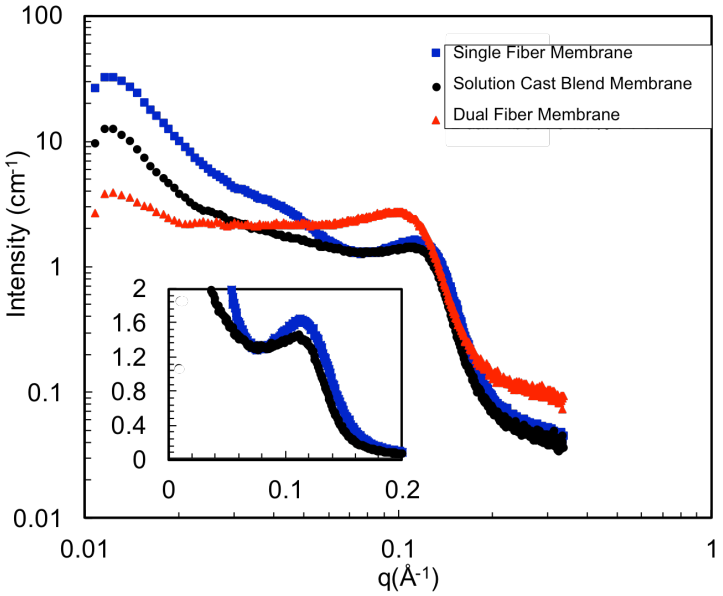

Figure 5.5: Log-log Small-Angle X-Ray Scattering profiles of water swollen solution cast blended membrane (black dot), single fiber membrane (blue square), and dual fiber membrane (red triangle) containing 70 wt.% 700 EW PFIA/30 wt.% PVDF at room temperature. The inset displays the SAXS profile of the single fiber and solution cast blended membrane in linear scale.

The smaller "q"-region also shows distinct scattering features that are dependent on the membrane's fabrication method. A rather intense bump was observed in only the single fiber membrane. This "matrix knee", is usually understood as originating from inter-crystallite interferences [44]. During electrospinning, the 700 EW PFIA/PVDF blend morphology was frozen due to the short solvent evaporation time; proper crystallization of the PFIA backbone was ensured by the hot-pressing and annealing steps. Surprisingly, the solution cast blended membrane exhibits a q^{-1} power law without any obvious bump while its PFIA backbone crystallinity is similar to that of the single

fiber membrane. These findings suggest that the matrix peak's shape and intensity do not depend on just the degree of crystallinity, but also on the membrane fabrication technique that drives their long-range organization, which corresponds well with literature findings [45,46].

The dual fiber membrane showed a flat profile in the low "q"-region. As the dual fiber membrane was also hot-pressed and annealed (which allowed for proper crystallization of the PFIA backbone), it is likely that its broad ionomer peak overlaps with the expected matrix knee.

5.3.2 Membrane Properties

Swelling in Liquid and in Vapor Phase

Membrane properties, including gravimetric water uptake and in-plane swelling in liquid water for a 70 wt.% PFIA solution cast blend, single fiber, and dual fiber membrane are shown in Table 5.3. The dual fiber membrane had greater gravimetric water uptake and lower in-plane swelling as compared to the solution cast blended membrane or single fiber membrane. Water uptake is dependent on diffusion of water into and through the membrane, as well as swelling and reorganization of the hydrophobic domains in the polymer [47,48]. It is likely that this process is impaired when the single fiber membrane and solution cast blended membrane are exposed to liquid because of the close proximity of hydrophobic PVDF and PFIA domains. The dual fiber membrane, which utilized a matrix composed of pure PFIA, would experience no such limitations. These results are consistent with the work reported by Park *et al.* [49], which showed that an electrospun membrane, where PVDF fibers were embedded in a Nafion matrix, exhibited greater gravimetric water uptake than a solution cast blended

membrane. Park *et al.* also recently reported work regarding the fabrication of Nafion/PVDF single-fiber mats [22]. The TEM images of the fibers and the resultant membrane indicated that each fiber is composed of numerous Nafion and PVDF fibrils with diameters of 2-5 nm oriented in the fiber axis direction [22]. The close proximity of PVDF with the ionomer in a blend weakened the hydration forces that cause water to associate with the sulfonic acid sites of the ionomer, which limited the ionomer's ability to take up water. Because the dual fiber membranes in this study utilized an independently electrospun ionomer, broader ionic domains were formed, which had less limitation on water uptake, leading to greater gravimetric water uptake compared to the other structures. The greater intensity of the ionomer peak in the low "q"-region (i.e., the polydispersity of the ionic domains) for the dual fiber membrane compared to the single fiber membrane (see Figure 5.5) corroborates these observations.

Table 5.3: Membrane gravimetric water uptake, in-plane swelling, and in-plane conductivity in liquid water for 70 wt.% 700 EW PFIA (30 wt.% PVDF) composite membranes.

Membrane	Gravimetric Water Uptake [%]	In-Plane Swelling [%]	In-Plane Proton Conductivity [S/cm]	Thickness [μm]	ASR [Ωcm^2]
Dual fiber membrane	59.3	5.4	0.094	25	0.027
Single fiber membrane	19.4	12	0.084	25	0.030
Solution cast blended membrane	21.5	15.1	0.075	45	0.060
Neat PFIA	120	34	0.125	30	0.024

The dual fiber membrane exhibited less in-plane swelling than the single fiber membrane. As shown in previous studies [23,49,50] and in Chapter 4 of this dissertation, the presence of a reinforcing fiber network is beneficial to reducing the in-plane swelling of ionomer membranes. This is attributed to the lack of connectivity of the uncharged fibers in the thickness direction of the dual fiber membrane. The PVDF fibers were not welded, so as the membrane took on water, the fibers preferentially separated in the thickness direction while resisting changes in the lateral direction. In the single fiber membrane, the 700 EW PFIA and PVDF were mixed and melted, improving their distribution in 3-dimensions, leading to more isotropic swelling [19].

In-Plane Conductivity in Liquid Water and in Water Vapor

The in-plane conductivity and area-specific resistance (ASR, defined as membrane thickness divided by proton conductivity) in liquid water at 25°C of a 70 wt.% PFIA composite membrane is shown in Table 5.3 for single fiber, dual fiber, and solution cast blended membranes. The addition of uncharged PVDF led to a reduction in proton conductivity of the composite membranes, as compared to the neat PFIA film; this effect has been previously observed in electrospun composite membranes [2,19,22,49]. The proton conductivity of the dual fiber membrane could be described by a simple PFIA weight fraction mixing rule. In addition, it exhibited greater proton conductivity than the single fiber membrane, which is consistent with the difference in gravimetric water uptake and ionic domain size between the two samples. The solution cast blended membrane exhibited a low conductivity, disproportional to its composition, possibly due to phase-separation and percolation limitations of the ionomer phase [23,51–53]. The single fiber and dual fiber membranes reported in Table 5.3 compare favorably with

Nafion/PVDF and 660 EW PFSA/PPSU electrospun membranes reported in the literature [2,22,49]. Ballengee *et al*. reported a 660 EW PFSA/PPSU dual fiber membrane (thickness of 51 μm) with an ASR of 0.048 Ωcm^2 and an in-plane swelling of 5%; Park *et al.* reported a Nafion/PVDF single fiber membrane (thickness of 18 μm) with an ASR of 0.03 Ωcm^2. The combination of high conductivity/low thickness of the PFIA-based membranes led to a lower ASR, which is favorable for H_2/air fuel cells.

Differences in conductivity were also observed between the 70 wt.% 700 EW PFIA/30 wt.% PVDF solution cast blended membrane, single fiber membrane, and dual fiber membrane in water vapor at 80°C (Figure 5.6). As observed in liquid water, the single fiber and solution cast blended membranes exhibited a lower conductivity than the dual fiber membrane, likely due to percolation effects. Solution cast blended membranes are known to have an ionic conductivity lower than what would be expected based on a linear mixing rule due to thermodynamic isolation of ionic domains, particularly at mid-range compositions [52,54–56] The superior conductivity of a dual fiber membrane compared to a solution cast blended membrane has previously been demonstrated in a Nafion/PVDF system [49] and in Chapter 3 of this dissertation, with 825 EW PFSA/PAI films.

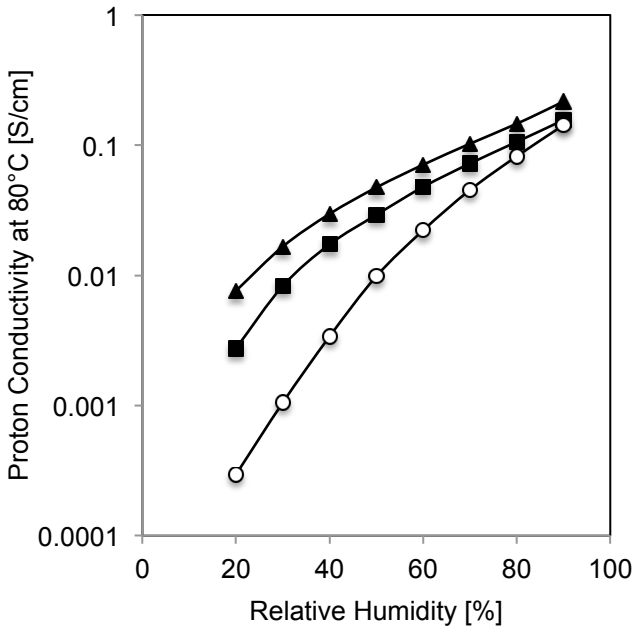

Figure 5.6: Proton conductivity at 80°C versus relative humidity for 70 wt.% 700 EW PFIA/30 wt.% PVDF single fiber membrane (■), dual fiber membrane (▲), and solution cast blended membrane (○).

While the single fiber membrane does not achieve an ionic conductivity greater than a dual fiber membrane, the fast evaporation rate of solvent during fiber formation results in a combination of regularly spaced/sized ionic domains (as shown by SAXS measurements in Figure 5.5) and limited thermodynamic segregation of the ionomer and PVDF (as shown by TEM [22]). The reduced tortuosity allowed the single fiber membrane to achieve a greater conductivity than the solution cast blended membrane. The differences in conductivity are also well correlated with the differences in freezable/non-freezable water in the membranes, as shown in Table 5.4. DSC analysis of absorbed water in electrospun and solution cast Nafion:PVDF blended membranes [22] showed that the single fiber membrane typically has more loosely bound (freezable)

water, as compared to a solution cast blend which led to a greater proton conductivity [22,30]. Similarly, the freezable water content in the dual fiber membrane, as determined by DSC, was greater than that in the single fiber or solution cast blended membrane, also contributing to its higher proton conductivity. Despite their differences, none of the membranes retained water well, with all exhibiting a large drop in conductivity as the humidity was reduced, which is typical of perfluoro-type ionomers.

Table 5.4: Freezable (λ_f), non-freezable (λ_{nf}), and total water content (λ_{total}) (H_2O/SO_3-) in 70 wt.% PFIA/ 30 wt.% PVDF composite membranes after equilibration in room-temperature water.

Membrane	λ_f (H_2O/SO_3^-)	λ_{nf} (H_2O/SO_3^-)	λ_{Total} (H_2O/SO_3^-)
Solution cast blended membrane	10.7	5.5	16.2
Single fiber membrane	11.8	5.2	17.0
Dual fiber membrane	16.3	15.6	31.9

Mechanical Properties

Mechanically robust membranes are ideal for PEMFCs due to the cyclic stresses generated during successive start/stop cycles. These stresses can lead to the generation of pinholes and cracks in the membrane [57–60].

The presence of mechanically robust PVDF improved the strength of the composite membranes. The mechanical properties of a 70 wt.% 700 EW PFIA/30 wt.% PVDF solution cast blend, single fiber, and dual fiber membrane are summarized in Table 5.5, and representative stress-strain curves of the films are shown in Figure 5.7, along with tensile curves for solution cast neat 700 EW PFIA and neat PVDF. It is clear that the addition of PVDF led to an increase in both the modulus and the proportional

limit stress (PLS) of all the composite membranes, as shown in Figure 5.7. An 18% improvement in the modulus and a 24% improvement in the proportional limit stress (PLS) were obtained in the single fiber membrane compared to solution cast PFIA. The dual fiber membrane exhibited greater strength than the single fiber membrane or the pure PFIA, with a PLS and modulus of 12.5 and 155 MPa, respectively. The difference in mechanical properties between the structures is likely due to the greater PVDF crystallinity in the dual fiber membrane. This is a result of the continuous PVDF fibers (instead the smaller and more dispersed PVDF domains as in the case of a single fiber and solution cast blended membrane), as discussed above. Despite these improvements, the electrospun PFIA/PVDF membranes were weaker than Nafion 211 (tensile strength of 18.3 MPa) or 660 EW PFSA (tensile strength of ~16 MPa).

Table 5.5: Summary of mechanical properties for neat PFIA, PVDF, and 70 wt.% 700 EW PFIA/30 wt.% PVDF composite membranes.

Membrane Structure	**Young's Modulus [MPa]**	**PLS [MPa]**
Dual fiber membrane	154.9	12.5
Single fiber membrane	90.4	8.3
Solution cast blended membrane	162.9	11.2
Neat Membrane	**Young's Modulus [MPa]**	**PLS [MPa]**
Solution-Cast 700 EW PFIA	76.7	6.7
Poly(vinylidene fluoride) film	1799.3	42.6

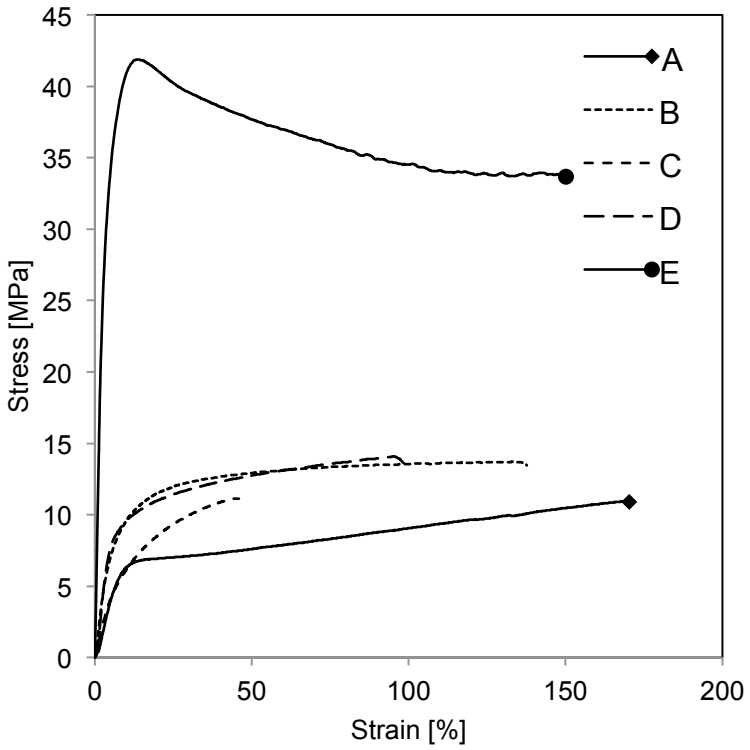

Figure 5.7: Tensile curves for air-dried PFIA, PVDF, and 70 wt. % 700 EW PFIA/30 wt. % PVDF composite membranes. Solution cast PFIA (A), 70 wt.% PFIA/30 wt.% PVDF dual fiber membrane (B), 70 wt.% PFIA/30 wt.% PVDF single fiber membrane (C), 70 wt.% PFIA/30 wt.% PVDF solution cast blended membrane (D), solution cast PVDF (E).

According to Idarraga-Mora *et al.* [61] the modulus of a composite membrane should be bounded by two rules of mixtures. In the first, the matrix component (PFIA) and filler component (PVDF) are both oriented parallel to the direction of the load (i.e. a parallel model described by Eq. 5.7 [62]); this defines the upper bound for the modulus of a composite film. In the second, PFIA and PVDF are oriented perpendicular to the direction of the load (i.e. a series model described by Eq. 5.8), which defines the lower bound for the modulus of a composite film. The model (Eq. 5.7 and 5.8) reported by Friedel *et al.* also includes an efficiency factor that accounts for the aspect ratio (α) of the

filler component. Estimates for the moduli of the dual fiber, single fiber, and solution cast blended membranes using Eq. 5.7 and 5.8 are reported in Table 5.6.

$$E_{composite} = (1 - f)E_{PFIA} + \eta f E_{PVDF} \quad (5.7)$$

$$E_{composite} = \left(\frac{1-f}{E_{PFIA}} + \frac{f}{\eta E_{PVDF}}\right)^{-1} \quad (5.8)$$

$$\eta = 1 - \frac{\tanh \alpha\beta}{\alpha\beta} \quad (5.9)$$

$$\alpha = \frac{length}{diameter} \quad (5.10)$$

$$\beta = \sqrt{\frac{2G_{PFIA}}{E_{PVDF} \ln \delta}} \quad (5.11)$$

$$\delta = \sqrt{\frac{2\pi}{\sqrt{3}f}} \quad (5.12)$$

Table 5.6: Estimated modulus of composite membranes based on Eq. 5.7 and Eq. 5.8

Membrane Structure	**Estimated Modulus based on**	
	Series Model [MPa]	Parallel Model [MPa]
Dual Fiber Membrane	544	100
Single Fiber Membrane	323	99
Solution Cast Blended Membrane	233	97

In Eq. 5.7 through 5.12, f is the volume fraction of PVDF and G_{PFIA} is the shear modulus of PFIA (estimated through the relation E = 2G(1-ν), where Poisson's ratio of PFIA, ν, is 0.4). The aspect ratio of PVDF in the single fiber and solution cast blended membranes were taken from reference [22]. The estimates for the moduli of the dual fiber and solution cast blended PFIA/PVDF membranes are in agreement with the experimental data. The dual fiber membrane is better described with the series model. This indicates that long-range stress transfer is not observed in the film, which is due to the random orientation of the reinforcing PVDF fibers. The modulus of the solution cast

blend is approximately an average of the two models, suggesting some degree of co-continuity in the membrane. Both models of composite membrane strength overestimate the modulus of the single fiber membrane. A number of conclusions can be drawn from this analysis. First, the PVDF fibers in a dual fiber membrane are not strongly oriented in any particular direction, which can be a result of the whipping of the jet during electrospinning or the comparable translation/rotation rates of the electrospinning apparatus. Second, PVDF was found to be co-continuous in the solution cast blend. The single fiber membrane was not well-described by the model, indicating that additional effects may be controlling the strength of the membrane. Finally, this analysis assumes that the mechanical properties of PVDF and PFIA are fully accessible in the composite membrane.

5.3.3 Fuel Cell Performance and Hydrogen Crossover

Hydrogen/air fuel cell performance at 80°C of MEAs containing a 70 wt.% 700 EW PFIA film, with either a dual fiber, single fiber, or solution cast blended membrane morphology, as well as commercial Nafion 211 is shown in Figure 5.8.

High open-circuit voltage (OCV) (>0.9 V) and low fuel crossover (<2.5 mA/cm^2) for the MEAs indicated that the membranes were free of pinholes. The MEA containing the dual fiber membrane outperformed the single fiber membrane, the solution cast blended membrane, and commercial Nafion MEAs, achieving a higher power density at a given voltage for high (100%) and low (40%) levels of humidity. The higher power density for the dual fiber membrane MEA is a consequence of its lower ASR, as shown in Table 5.3.

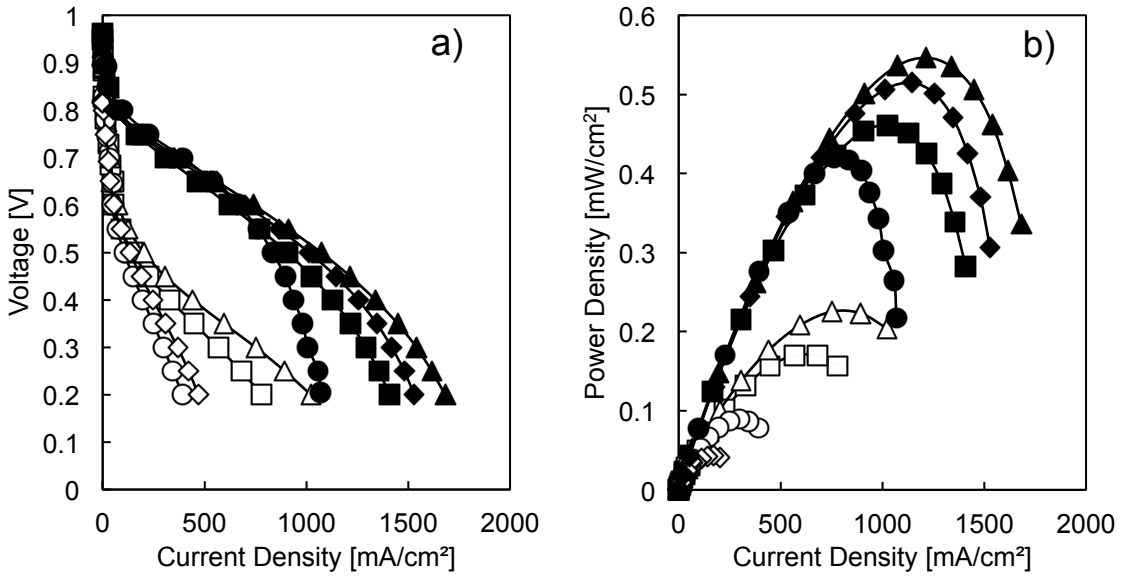

Figure 5.8: Fuel cell performance of composite membranes containing 700 EW PFIA. (A) Fuel cell polarization curves and (B) power density versus current density for a single fiber membrane MEA, a dual fiber membrane MEA, a solution cast blended membrane MEA, and a Nafion 211 MEA. (▲) Dual fiber membrane MEA, 100% RH; (△) dual fiber membrane MEA, 40% RH; (■) single fiber membrane MEA, 100% RH; (□) single fiber membrane MEA, 40% RH; (●) solution cast blended membrane MEA, 100% RH; (○) solution cast blended membrane MEA, 40% RH; (◆) Nafion MEA, 100% RH; (◇) Nafion MEA, 40% RH. The anode/cathode catalyst loading was 0.25 mg/cm^2 Pt and the binder was 3M 825 EW PFSA ionomer. Data was collected using H_2/air flow rates of 0.125/0.5 L/min, backpressure of 100 kPa and 80°C.

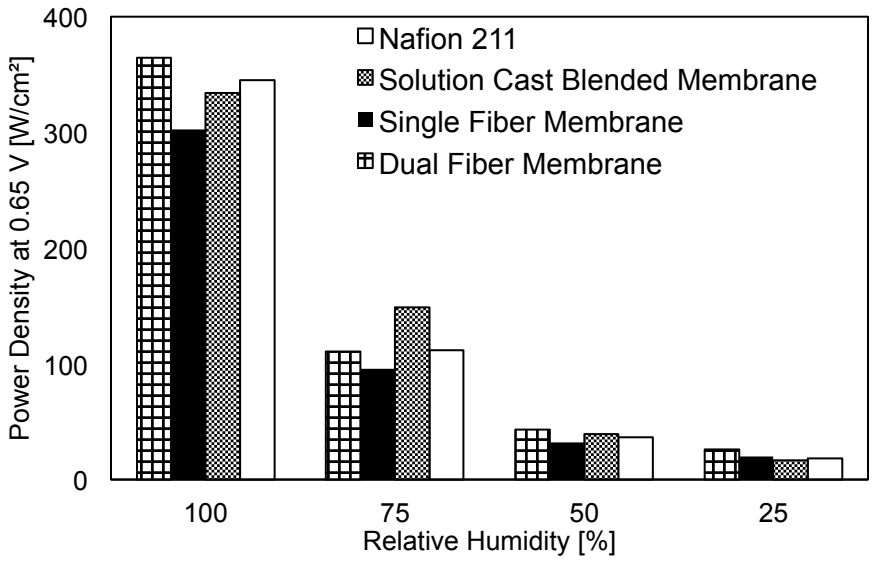

Figure 5.9: Power density output at 0.65 V at 80°C as a function of relative humidity for 700 EW PFIA/PVDF electrospun composite membranes and Nafion 211.

The power density at 0.65 V at four values of relative humidity is presented in Figure 5.9. Similar to the ASR differences observed in Table 5.3, the dual fiber membrane MEA achieved greater power densities than the single fiber membrane and Nafion at 40% and 100% relative humidity. Similarly, the Nafion MEA exhibited greater power densities than the single fiber membrane MEA due to the difference in ASR of the membranes.

Hydrogen crossover was determined via linear sweep voltammetry experiments for MEAs with H_2/N_2 feed gas flow rates of 0.125/0.5 L/min. The dual fiber membrane showed greater fuel crossover, as shown in Table 5.7, which decreased with humidity. This humidity effect has been observed by other researchers [63–65]. For example, Sakai *et al.* found that the permeability of H_2 in PFSA decreases with decreasing relative humidity [66,67]. The low fuel crossover of the single fiber membrane for all values of relative humidity is a result of the lower water uptake of the film (as shown in Table 5.3).

Furthermore, the low fuel crossover of both membranes is indicative of complete pore closure during the fabrication steps (i.e. no residual void spaces are left in the membranes). However, only the single fiber membrane meets the DOE target [68] for hydrogen crossover (<2 mA/cm^2 at 80°C).

Table 5.7: Hydrogen crossover of a 70 wt.% 700 EW PFIA dual fiber and single fiber membranes as a function of relative humidity. Fuel cell was operated using H_2/N_2 flow rates of 0.125/0.5 L/min at 80°C and 100 kPa.

Relative Humidity	**Hydrogen Crossover [mA/cm^2]**	
	Dual fiber membrane	Single fiber membrane
100%	2.32	1.51
70%	1.69	1.35
50%	1.41	1.31

5.4 Conclusion

Composite membranes were fabricated using dual fiber and single fiber electrospinning techniques with 3M's new PFIA ionomer. Single fiber electrospinning was achieved by mixing 700 EW PFIA and PVDF in a common solvent, with PVDF acting as the carrier and reinforcing polymer. After electrospinning, the blended fibers were softened to create a dense film. A dual fiber mat was obtained by simultaneously electrospinning 700 EW PFIA with PEO as a carrier and PVDF onto a common surface. After electrospinning, the 700 EW PFIA fibers were selectively softened to produce a composite membrane where PVDF fibers were embedded in the PFIA ionomer matrix. Both techniques resulted in dense, defect-free membranes, as shown by SEM cross-section images and gas crossover measurements. The various membrane structures displayed differences in the crystallinity of PVDF, as well as differences in the 700 EW

PFIA crystallite sizes, separation distances, and polydispersities. In addition, a solution-cast PFIA film was found to be significantly more crystalline than a PFSA of similar EW.

The different membrane structures also exhibited differing properties in liquid water and water vapor. The addition of PVDF to PFIA led to a reduction in proton conductivity for all composite membranes. The conductivity of a dual fiber membrane was described by a simple PFIA weight fraction mixing rule, while that of the single fiber and solution cast blended membrane was less than predicted. Single fiber and dual fiber membranes achieved improved mechanical strength and reduced swelling as compared to the pure PFIA due to the presence of the hydrophobic PVDF. The dual fiber membrane outperformed the single fiber membrane in many of these areas. The formation of broad ionic domains and the presence of highly crystalline PVDF proved to be ideal for H_2/air fuel cells. Lower hydrogen crossover was observed for the single fiber membrane as compared to the dual fiber membrane. The dual fiber membrane exhibited lower ASR (due to its higher proton conductivity), leading to a higher power density. Fuel cell performance with these films was acceptable, suggesting that these membranes could be good candidates for PEMFCs.

Acknowledgements

The authors would like to thank 3M Company and the US DOE research grant for funding these research efforts.

5.5 References

[1] K.D. Kreuer, On the development of proton conducting polymer membranes for hydrogen and methanol fuel cells, J. Memb. Sci. 185 (2001) 29–39.

[2] J.B. Ballengee, G.M. Haugen, S.J. Hamrock, P.N. Pintauro, Properties and Fuel Cell Performance of a Nanofiber Composite Membrane with 660 Equivalent Weight Perfluorosulfonic Acid, J. Electrochem. Soc. 160 (2013) F429–F435. doi:10.1149/2.088304jes.

[3] J.J. Luo, S.J. Wang, M. Xiao, D.M. Han, Y.Z. Meng, Fluorene-containing block sulfonated poly(ether ether ketone) as proton-exchange membrane for PEM fuel cell application, Eur. Polym. J. 46 (2010) 1736–1744. doi:10.1016/j.eurpolymj.2010.05.005.

[4] W.L. Harrison, M. a Hickner, Y.S. Kim, J.E. McGrath, Poly(arylene ether sulfone) copolymers and related systems from disulfonated monomer building blocks: synthesis, characterization, and performance - a topical review, Fuel Cells. 5 (2005) 201–212. doi:10.1002/fuce.200400084.

[5] M.A. Hickner, H. Ghassemi, Y.S. Kim, B.R. Einsala, J.E. McGrath, Alternative Polymer Systems for Proton Exchange Membranes, Chem. Rev. 104 (2004) 4587–4612. doi:10.1021/cr020711a.

[6] Y. Zhao, M. Yoshida, T. Oshima, S. Koizumi, M. Rikukawa, N. Szekely, A. Radulescu, D. Richter, Elucidation of the morphology of the hydrocarbon multi-block copolymer electrolyte membranes for proton exchange fuel cells, Polymer (Guildf). 86 (2016) 157–167. doi:10.1016/j.polymer.2016.01.061.

[7] Y.A. Elabd, M.A. Hickner, Block Copolymers for Fuel Cells, (2011) 1–11. doi:10.1021/ma101247c.

[8] K.-D. Kreuer, Ion Conducting Membranes for Fuel Cells and other Electrochemical Devices, Chem. Mater. 26 (2013) 361–380. doi:10.1021/cm402742u.

[9] J. Choi, K.M. Lee, R. Wycisk, P.N. Pintauro, P.T. Mather, Nanofiber composite membranes with low equivalent weight perfluorosulfonic acid polymers, J. Mater. Chem. 20 (2010) 6282–6290. doi:10.1039/c0jm00441c.

[10] W. Zhang, R. Wycisk, D.L. Kish, P.N. Pintauro, Pre-Stretched Low Equivalent Weight PFSA Membranes with Improved Fuel Cell Performance, J. Electrochem. Soc. 161 (2014) F770–F777. doi:10.1149/2.085406jes.

[11] R. Wycisk, J. Ballengee, P.N. Pintauro, Polymer Membranes for Fuel Cells, (2012).

[12] R. Wycisk, P.N. Pintauro, J.W. Park, New developments in proton conducting membranes for fuel cells, Curr. Opin. Chem. Eng. 4 (2014) 71–78. doi:10.1016/j.coche.2014.01.012.

[13] M.S. Schaberg, J.E. Abulu, G.M. Haugen, M.A. Emery, S.J. O'Conner, P.N. Xiong, S.J. Hamrock, New Multi Acid Side-Chain Ionomers for Proton Exchange Membrane Fuel Cells, ECS Trans. 33 (2010) 627–633.

[14] R. Wang, X. Yan, X. Wu, G. He, L. Du, Z. Hu, M. Tan, Modification of hydrophilic channels in Nafion membranes by DMBA: Mechanism and effects on proton conductivity, J. Polym. Sci. Part B Polym. Phys. 52 (2014) 1107–1117. doi:10.1002/polb.23540.

[15] A. Kusoglu, A.Z. Weber, New Insights into Perfluorinated Sulfonic-Acid Ionomers, Chem. Rev. 117 (2017) 987–1104. doi:10.1021/acs.chemrev.6b00159.

[16] S. Hamrock, Membranes and MEA's for Dry, Hot Operating Conditions, (2010).

[17] A. Kusoglu, T.J. Dursch, A.Z. Weber, Nanostructure / Swelling Relationships of Bulk and Thin-Film PFSA Ionomers, Adv. Funct. Mater. 26 (2016) 4961–4975. doi:10.1002/adfm.201600861.

[18] K.A. Mauritz, R.B. Moore, State of Understanding of Nafion, (2004).

[19] J.B. Ballengee, P.N. Pintauro, Composite fuel cell membranes from dual-nanofiber electrospun mats, Macromolecules. 44 (2011) 7307–7314. doi:10.1021/ma201684j.

[20] K.S. Lee, M.H. Jeong, Y.J. Kim, S. Bin Lee, J.S. Lee, Fluorinated aromatic polyether ionomers containing perfluorocyclobutyl as cross-link groups for fuel cell applications, Chem. Mater. 24 (2012) 1443–1453. doi:10.1021/cm203539m.

[21] R.J. Wycisk, J.W. Park, D. Powers, P.N. Pintauro, Electrospinning PFSA +PVDF Nanofibers for Fuel CellMembrane Fabrication, in: Meet. Abstr., The Electrochemical Society, 2014: pp. 1199–1199.

[22] J.W. Park, R. Wycisk, G. Lin, P.Y. Chong, D. Powers, T. Van Nguyen, R.P. Dowd Jr., P.N. Pintauro, Electrospun Nafion/PVDF single-fiber blended membranes for regenerative H2/Br2 fuel cells, J. Memb. Sci. 541 (2017) 85–92. doi:10.1016/j.memsci.2017.06.086.

[23] J.B. Ballengee, P.N. Pintauro, Composite Fuel Cell Membranes from Dual-Nanofiber Electrospun Mats, Macromolecules. 44 (2011) 7307–7314. doi:10.1021/ma201684j.

[24] B. Loppinet, G. Gebel, C.E. Williams, Small-angle scattering study of perfluorosulfonated ionomer solutions, J. Phys. Chem. B. 101 (1997) 1884–1892.

[25] J. Choi, R. Wycisk, W. Zhang, P.N. Pintauro, K.M. Lee, P.T. Mather, High conductivity perfluorosulfonic acid nanofiber composite fuel-cell membranes., ChemSusChem. 3 (2010) 1245–8. doi:10.1002/cssc.201000220.

[26] J.B. Ballengee, G.M. Haugen, S.J. Hamrock, P.N. Pintauro, Properties and Fuel Cell Performance of a Nanofiber Composite Membrane with 660 Equivalent Weight Perfluorosulfonic Acid, J. Electrochem. Soc. 160 (2013) F429–F435. doi:10.1149/2.088304jes.

[27] A. Laforgue, L. Robitaille, A. Mokrini, A. Ajji, Fabrication and Characterization of Ionic Conducting Nanofibers, Macromol. Mater. Eng. 292 (2007) 1229–1236. doi:10.1002/mame.200700200.

[28] K.M. Lee, J. Choi, R. Wycisk, P.N. Pintauro, P. Mather, Nafion Nanofiber Membranes, ECS Trans. 25 (2009) 1451–1458. doi:10.1149/1.3210701.

[29] P. Linder, T. Zemb, Neutron, X-Rays and light scattering: Introduction to an investigate tool for colloidal and polymeric systems, North Holl, Amsterdam, 1991.

[30] A. Siu, J. Schmeisser, S. Holdcroft, S. Fraser, V. Uni, B.C. Va, Effect of Water on the Low Temperature Conductivity of Polymer Electrolytes, (2006) 6072–6080. doi:10.1021/jp0531208.

[31] Y.S. Kim, L. Dong, M.A. Hickner, T.E. Glass, V. Webb, J.E. Mcgrath, State of Water in Disulfonated Poly(arylene ether sulfone) Copolymers and a Perfluorosulfonic Acid Copolymer (Nafion) and Its Effect on Physical and

Electrochemical Properties, Macromolecules. 36 (2003) 17–21.

[32] J.R. Rumble, ed., Physical Constant of Organic Compounds, in: CRC Handb. Phys. Chem., 98th (Inte, CRC Press/Taylor & Francis, Boca Raton, FL, n.d.

[33] Z. Cui, N.T. Hassankiadeh, Y. Zhuang, E. Drioli, Y.M. Lee, Crystalline polymorphism in poly(vinylidenefluoride) membranes, Prog. Polym. Sci. 51 (2015) 94–126. doi:10.1016/j.progpolymsci.2015.07.007.

[34] B.-E. El Mohajir, N. Heymans, Changes in structural and mechanical behaviour of PVDF with processing and thermomechanical treatments. 1. Change in structure, Polymer (Guildf). 42 (2001) 5661–5667. doi:10.1016/S0032-3861(01)00064-7.

[35] W.M. Prest, D.J. Luca, The formation of the γ phase from the α and β polymorphs of polyvinylidene fluoride, J. Appl. Phys. 49 (1978) 5042. doi:10.1063/1.324439.

[36] T. Kyu, J. Yang, Miscibility Studies of Perfluorinated Nafion Ionomer and Poly(viny1idene fluoride) Blends, Macromolecules. 23 (1990) 176–182.

[37] C. Marega, A. Marigo, Influence of annealing and chain defects on the melting behaviour of poly(vinylidene fluoride), Eur. Polym. J. 39 (2003) 1713–1720. doi:10.1016/S0014-3057(03)00062-4.

[38] Y.J. Park, Y.S. Kang, C. Park, Micropatterning of semicrystalline poly(vinylidene fluoride) (PVDF) solutions, Eur. Polym. J. 41 (2005) 1002–1012. doi:10.1016/j.eurpolymj.2004.11.022.

[39] S. Vidhate, A. Shaito, J. Chung, N.A. D'Souza, Crystallization, mechanical, and rheological behavior of polyvinylidene fluoride/carbon nanofiber composites, J. Appl. Polym. Sci. 112 (2009) 254–260. doi:10.1002/app.29413.

[40] W. Zhang, D.L. Kish, P.N. Pintauro, Morphology and Performance of Stretched

PFSA for Direct Methanol Fuel Cells, ECS Trans. 33 (2010) 635–645.

[41] S.E. Creager, J.J. Sumner, R.D. Bailey, J.J. Ma, W.T. Pennington, D.D. Desmarteau, Equivalent Weight and Crystallinity Effects on Water Content and Proton Conductivity in Bis [(perfluoroalkyl) sulfonyl] imide-Based Ionomers, Electrochem. Solid-State Lett. 2 (1999) 434–436. doi:10.1149/1.1390862.

[42] N. V. Aieta, J.E. Leisch, M.M. Santos, M.A. Yandrasits, S.J. Hamrock, A.M. Herring, Tracking Crystallinity Changes in PFSA Polymers During Ex-Situ Peroxide Degradation Niccolo V. Aieta, ECS Trans. 11 (2007) 1157–1164.

[43] R. Gregorio, Determination of the α, β, and γ crystalline phases of poly(vinylidene fluoride) films prepared at different conditions, J. Appl. Polym. Sci. 100 (2006) 3272–3279. doi:10.1002/app.23137.

[44] M. Fujimura, T. Hashimoto, H. Kawai, Small-angle x-ray scattering study of perfluorinated ionomer membranes. 1. Origin of two scattering maxima, Macromolecules. 14 (1981) 1309–1315. doi:10.1021/ma50006a032.

[45] R.B. Moore, C. R. Martin, Chemical and Morphological Properties of Solution-Cast Perfluorosulfonate Ionomers, Macromolecules. (1988) 1334–1339.

[46] G. Gebel, P. Aldebert, M. Pineri, Structure and Related Properties of Solution-Cast Perfluorsulfonated Ionomer Films, Macromolecules. 20 (1987) 1425–1428.

[47] Q. Zhao, P. Majsztrik, J. Benziger, Diffusion and Interfacial Transport of Water in Nafion, (2011) 2717–2727. doi:10.1021/jp1112125.

[48] M.B. Satterfield, J.B. Benziger, Non-Fickian Water Vapor Sorption Dynamics by Nafion Membranes, J. Phys. Chem. B. 112 (2008) 3693–3704. doi:10.1021/jp7103243.

[49] J.W. Park, R. Wycisk, P.N. Pintauro, Nafion/PVDF nanofiber composite membranes for regenerative hydrogen/bromine fuel cells, J. Memb. Sci. 490 (2015) 103–112. doi:10.1016/j.memsci.2015.04.044.

[50] M. Oroujzadeh, S. Mehdipour-Ataei, M. Esfandeh, Proton exchange membranes with microphase separated structure from dual electrospun poly(ether ketone) mats: Producing ionic paths in a hydrophobic matrix, Chem. Eng. J. 269 (2015) 212–220. doi:10.1016/j.cej.2015.01.088.

[51] N.W. DeLuca, Y.A. Elabd, Direct methanol fuel cell performance of Nafion/poly(vinyl alcohol) blend membranes, J. Power Sources. 163 (2006) 386–391. doi:10.1016/j.jpowsour.2006.09.009.

[52] J. V. Gasa, R.A. Weiss, M.T. Shaw, Structured polymer electrolyte blends based on sulfonated polyetherketoneketone (SPEKK) and a poly(ether imide) (PEI), J. Memb. Sci. 320 (2008) 215–223. doi:10.1016/j.memsci.2008.03.075.

[53] X. Zhang, S. Chen, J. Liu, Z. Hu, S. Chen, L. Wang, Preparation and properties of sulfonated poly(phenylene arylene)/sulfonated polyimide (SPA/SPI) blend membranes for polymer electrolyte membrane fuel cell applications, J. Memb. Sci. 371 (2011) 276–285. doi:10.1016/j.memsci.2011.01.054.

[54] S. Swier, V. Ramani, J.M. Fenton, H.R. Kunz, M.T. Shaw, R.A. Weiss, Polymer blends based on sulfonated poly(ether ketone ketone) and poly(ether sulfone) as proton exchange membranes for fuel cells, J. Memb. Sci. 256 (2005) 122–133. doi:10.1016/j.memsci.2005.02.013.

[55] M.K. Song, Y.T. Kim, J.M. Fenton, H. Russell Kunz, H.W. Rhee, Chemically-modified Nafion®/poly(vinylidene fluoride) blend ionomers for proton exchange

membrane fuel cells, J. Power Sources. 117 (2003) 14–21. doi:10.1016/S0378-7753(03)00166-6.

[56] J. Lin, J.K. Lee, M. Kellner, R. Wycisk, P.N. Pintauro, Nafion-Flourinated Ethylene-Propylene Resin Membrane Blends for Direct Methanol Fuel Cells, J. Electrochem. Soc. 153 (2006) A1325. doi:10.1149/1.2196687.

[57] T.R. Ralph, D.E. Barnwell, P.J. Bouwman, A.J. Hodgkinson, M.I. Petch, M. Pollington, Reinforced Membrane Durability in Proton Exchange Membrane Fuel Cell Stacks for Automotive Applications, J. Electrochem. Soc. 155 (2008) B411. doi:10.1149/1.2838163.

[58] A. Kusoglu, A.M. Karlsson, M.H. Santare, S. Cleghorn, W.B. Johnson, Mechanical behavior of fuel cell membranes under humidity cycles and effect of swelling anisotropy on the fatigue stresses, J. Power Sources. 170 (2007) 345–358. doi:10.1016/j.jpowsour.2007.03.063.

[59] Y.-H. Lai, C.K. Mittelsteadt, C.S. Gittleman, D.A. Dillard, Viscoelastic Stress Analysis of Constrained Proton Exchange Membranes Under Humidity Cycling, J. Fuel Cell Sci. Technol. 6 (2009) 021002. doi:10.1115/1.2971045.

[60] T.T. Aindow, J. O'Neill, Use of mechanical tests to predict durability of polymer fuel cell membranes under humidity cycling, J. Power Sources. 196 (2011) 3851–3854. doi:10.1016/j.jpowsour.2010.12.031.

[61] J.A. Idarraga-Mora, A.S. Childress, P.S. Friedel, D.A. Ladner, A. Rao, S. Husson, Role of Nanocomposite Support Stiffness on TFC Membrane Water Permeance, Membranes (Basel). 8 (2018) 111. doi:10.3390/membranes8040111.

[62] L.M. Robeson, A. Noshay, M. Matzner, C.N. Merriam, Physical Property

Characteristics, Die Angew. Makromol. Chemie. 30 (1973) 47–62.

[63] R. Jiang, H.R. Kunz, J.M. Fenton, Investigation of membrane property and fuel cell behavior with sulfonated poly (ether ether ketone) electrolyte : Temperature and relative humidity effects, 150 (2005) 120–128. doi:10.1016/j.jpowsour.2005.03.180.

[64] H. Xu, Y. Song, H.R. Kunz, J.M. Fenton, Effect of Elevated Temperature and Reduced Relative Humidity on ORR Kinetics for PEM Fuel Cells, (2005) 1828–1836. doi:10.1149/1.1984351.

[65] K. Don, B. Ki, M. Soo, Effects of operating parameters on hydrogen crossover rate through Nafion(R) membranes in polymer electrolyte membrane fuel cells, Renew. Energy. 57 (2013) 234–239. doi:10.1016/j.renene.2013.01.046.

[66] T. Sakai, H. Takenaka, N. Wakabayashi, Y. Kawami, T. Sakai, H. Takenako, E. Torikai, Gas Permeation Properties of Solid Polymer Electrolyte Gas Permeation Properties of Solid Polymer Electrolyte (SPE) Membranes, J. Electrochem. Soc. 132 (1985) 1328–1332. doi:10.1149/1.2114111.

[67] T. Sakai, H. Takenaka, E. Torikai, Gas Diffusion in the Dried and Hydrated Nations, J. Electrochem. Soc. 133 (1986) 88–92.

[68] M. Yandrasits, New Fuel Cell Membranes with Improved Durability and Performance, in: DOE Annu. Merit Rev., 2017.

Chapter 6

Dual Fiber Membranes with Large-Diameter Reinforcing Fibers

6.1 Introduction

Dual fiber electrospinning was introduced in 2011 as a technique to simplify the fabrication of reinforced composite membranes for H_2/air fuel cells [1]. In this method, an ionomer and an uncharged reinforcing polymer were simultaneously electrospun using separate needle spinnerets onto a common collector. The ionomer component of the dual fiber mat was then selectively softened, leading to a dense and defect free membrane where uncharged polymer fibers were embedded in the ionomer matrix. The method is simple and robust. Incompatible charged and uncharged polymers can be easily electrospun into a well-mixed dual fiber mat, where the relative amount of each fiber type is varied/controlled via the electrospinning flow rate. Additionally, the method circumvents the need for a separate ionomer impregnation step, which can be problematic due to incomplete pore-filling. The resultant membranes exhibited ion conductivities which are linearly dependent on the weight fraction of ionomer with no percolation threshold [1,2] and good durability (i.e. low in-plane swelling upon hydration) [1]. In a series of papers, Pintauro and co-workers have highlighted the flexibility of the dual fiber electrospinning technique, including the utilization of various polymers [1,3–8] and the creation of novel anion-exchange, cation-exchange, and bipolar membrane structures for fuel cell, redox flow battery and electrodialysis applications.

For H_2/air fuel cell membranes, achieving high power densities over a long operational period is desirable. In general, high power densities are achieved through the

use of a proton-exchange membrane (PEM) with a low area-specific resistance (i.e. a thin and/or highly conductive membrane); this reduces the performance losses due to resistance to proton transport through the membrane. However, high proton conductivity is typically accompanied by large dimensional changes upon membrane hydration, which can compromise the long term durability. During on/off fuel cell operation, the membrane (which is confined between two electrodes) undergoes cyclic stresses as it expands and contracts in the areal (in-plane) direction when it goes from hot/wet to cold/dry. These stresses lead to the formation of cracks or pinholes in the membrane, which ultimately ruin the membrane. The importance of low in-plane swelling is represented by the Humidity Stability Factor (HSF) for a membrane, as shown in the following equation (reported by GM [9]).

$$HSF = \frac{Strain\ at\ Break\ at\ 25℃,50\%\ RH\ (\%)}{In-Plane\ Swelling\ after\ 100℃\ boil\ in\ H_2O\ (\%)} \quad (6.1)$$

A high HSF has been correlated with good membrane durability in an on/off humidity cycling experiment [9], so a ductile PEM with low in-plane swelling is desired. Proton-conducting ionomers, such as Nafion, 3M's perfluorosulfonic acid (PFSA), or a sulfonated hydrocarbon, typically exhibit good ductility [10,11] (strain at break > 100%), but exhibit high in-plane swelling values (for example, the in-plane swelling of Nafion is 16% [12]). Thus, the strategy for improving membrane durability often involves reducing membrane swelling.

The reinforcing uncharged polymer fiber network in a dual fiber membrane controls volumetric water swelling, leading to improved durability of PEMs in H_2/air fuel cells. In particular, numerous studies have shown that excessive areal dimension changes of PEMs in a fuel cell membrane-electrode-assembly during on/off fuel cell operational

cycling (where the membrane expands when hot/wet and contracts when cold/dry) leads to the formation of membrane cracks and pinholes [13–17]. It has been shown that an unwelded reinforcing uncharged polymer fiber network in a composite fuel cell membrane restricts in-plane swelling while allowing for water swelling in the membrane thickness direction. Non-isotropic swelling (where in-plane swelling is lower than through-plane/thickness swelling) is key to prolonged durability of fuel cell membranes, but is not seen in conventional blended polymer membranes (e.g., a solution cast blend of sulfonated poly(arylene ether sulfone) and sulfonated polyimide [18] or Nafion and poly(vinylidene fluoride) and in dual fiber membranes where Nafion fibers are embedded in a continuous polyphenylsulfone uncharged matrix [1]. It is generally thought that one should use a high strength polymer for the reinforcing fibers. Li *et al.* [19] report on a model for membrane swelling that incorporates the tensile modulus of the reinforcing component. The swelling of the membrane is modeled using the Flory-Rehner theory [20] that considers the free energy of water sorption into the ionomer, the free energy of the ionomer expansion, and the external energy of the constraining material. Based on this model, an increased tensile modulus of the reinforcing component leads to a reduced in-plane swelling of the composite membrane. Similarly, GM has reported a model for composite membrane swelling that is dependent on the stiffness of the components, as shown in the following equation.

$$S_c = \frac{(1-f)E_i S_i}{fE_f + (1-f)E_i} \tag{6.2}$$

In Eq. 6.2, S_c and S_i represent the in-plane swelling of the composite film and ionomer, f is the fiber volume fraction, E_i is the modulus of the ionomer in the wet state, and E_f is the modulus of the reinforcing fiber. Based on Eq. 6.2, a reduction in composite

membrane in-plane swelling can be achieved through an increase in the fiber volume fraction (which has been shown in references [1,4,5]) or an increase in the fiber modulus.

Recent work has suggested that reducing the diameter of an electrospun fiber can result in an increase in its strength [21–23] Research performed by Wong *et al.* has shown that a ~100 MPa increase in the tensile modulus of poly(capralactone) was observed when the fiber diameter was reduced from 2500 nm to 400 nm [22], where the increase in strength was attributed to better alignment of polymer chains. Similarly, Stachewicz *et al.* observed an increase in tensile modulus of electrospun poly(vinyl alcohol) as the fiber diameter was reduced from ~600 nm to ~50 nm [21].

The goal of the present study is to determine the relationship between uncharged fiber diameter on the membrane strength (ease of handling thin films) and durability (in-plane water swelling) of a dual fiber electrospun fuel cell PEM. First, electrospun poly(vinylidene fluoride) (PVDF) fiber mats were fabricated with an average diameter ranging from 150 nm up to 2200 nm, and the mechanical strength of the resultant mats was measured. Next, two types of dual fiber membranes were fabricated, where PVDF fibers were embedded into a perfluoroimide acid (PFIA) or perfluorosulfonic acid (PFSA) matrix and where the average diameter of the PVDF fibers was systematically varied. The first set of membranes was composed of 75 wt.% 700 EW PFIA ionomer with 25 wt.% PVDF. The second set of membranes contained 80 wt.% PFSA (825 EW) with 20 wt.% PVDF fibers. Membranes were characterized in terms of in-plane and through-plane proton conductivity, gravimetric water uptake, in-plane water swelling, and tensile strength. The effect of PVDF fiber diameter on membrane properties was

determined and the optimal PVDF fiber diameter that minimized in-plane swelling while maximizing proton conductivity was identified.

6.2 Experimental

6.2.1 Materials

Perfluoroimide acid (PFIA) and perfluorosulfonic acid (PFSA) ionomers with an equivalent weight of 700 and 825 g/mol, respectively, (as determined by ion-exchange capacity measurements) were obtained from 3M Company as dry solids. Poly(vinylidene fluoride) (PVDF, MW of 670-700 kDa) was obtained from Solvay Specialty Chemicals as dry powder. N,N-dimethylacetamide (DMAc), acetone, n-propanol, and poly(ethylene oxide) (PEO) with a molecular weight of 1 MDa were obtained from MilliporeSigma and used without further purification.

6.2.2 Electrospinning

Because PFSA and PFIA do not form a true polymer solution in alcohol/water solvents (instead, they form a micellar dispersion), a carrier polymer must be added in order to induce chain entanglements and enable electrospinning [24]. In the present study, the carrier polymer was PEO, which has been shown to enable electrospinning at a low loading. In addition, PEO can easily be removed after membrane fabrication by water soaking [1,25]. Separate solutions of ionomer and PEO were prepared using a 2:1 (wt:wt) n-propanol:H_2O or ethanol:water solvent. The PFIA used in this study was from a different batch than the material used in Chapter 5 of this dissertation. The new batch of PFIA required ethanol (as opposed to n-propanol) to obtain well-formed fibers. The 825 EW PFSA ionomer utilized n-propanol:water, as described in Chapter 3 and Chapter 4 of this dissertation. The PEO solution was added to the ionomer dispersion to form a 20

wt.% mixture with a 99:1 ionomer:PEO mass ratio. A PVDF electrospinning solution was prepared by dissolving the polymer into a 7:3 (wt:wt) DMAc:Acetone mixture to a concentration ranging from 10 wt.% to 17.5 wt.%.

Dual fiber electrospun mats were prepared using the procedure described in reference [1]. The ionomer/PEO mixture and PVDF solution were loaded into separate syringes that were fitted with 22-gauge needles. The flow rates of the ionomer solution (0.50 – 2.50 mL/hr) and PVDF solution (0.25 – 0.85 mL/hr) were controlled with an automatic pump. Electrospinning conditions used to fabricate a mixed fiber mat consisting of 75 wt.% 700 EW PFIA/25 wt.% PVDF or 80 wt.% 825 EW PFSA/20 wt.% PVDF are summarized in Table 6.1.

Table 6.1: Electrospinning conditions for 700 EW PFIA:PVDF and 825:PVDF dual fiber mats.

Parameter	99:1 PFIA:PEO Fibers	PVDF Fibers	99:1 PFSA:PEO Fibers	PVDF Fibers
Voltage [kV]	8	10	10	10
Flow Rate [mL/hr]	0.50	0.20	0.50	0.14
Spinner-to-Collector Distance [cm]	8	10.5	8	10.5
Relative Humidity [%]	25	25	25	25
Solvent	2:1 EtOH:H_2O	7:3 DMAc:Acetone	2:1 nPrOH:H_2O	7:3 DMAc:Acetone
Concentration [wt.%]	20	12.5	20	12.5

6.2.3 Membrane Fabrication

Mixed nanofiber mats were dried under vacuum for 24 hours prior to transformation into a dense membrane. The mats were pressed at 2500 psi and 143°C for 5 minutes to soften the ionomer fibers and allow them to fill the interfiber space between PVDF fibers. This temperature was chosen in order to selectively soften the ionomer (with an alpha-transition temperature less than 138°C [26]) without melting the PVDF fibers. The fully dense membrane was then thermally annealed at 200°C for 30 minutes. Previous studies have shown that the addition of PEO to PFSA leads to a substantial loss in proton conductivity [27], but membrane soaking at 80°C in 1.0 M H_2SO_4 and 80°C DI water for 1 hour removed the carrier polymer. Low equivalent weight PFIA is insoluble in hot water due to its unique chemical structure (high crystallinity), with two fixed charges per side chain that are separated by ~7 tetrafluoroethylene groups (as discussed in Chapter 5). Membranes with 825 EW PFSA were also soaked in acid and water to remove PEO prior to characterization experiments. All of the dual fiber membranes had the same basic morphology, namely a PVDF fiber network embedded in an 825 EW PFSA or 700 EW PFIA matrix. The PFIA-based membranes contained 75 wt.% PFIA, while the PFSA-based membranes contained 80 wt.% PFSA.

6.2.4 Conductivity

In-plane proton conductivity was determined in room temperature water and in water vapor at 80°C where the relative humidity varied from 20%-90%. An AC impedance method was used with a BekkTech 4-electrode conductivity cell, and conductivity was calculated using the following equation:

$$\sigma = {}^{L}/_{wtR} \tag{6.3}$$

where L [cm] is the distance between the electrodes, w [cm] is the width, t [cm] is the thickness, and R [Ω] is the real impedance of the sample. For conductivity in water, the wet dimensions of the membrane sample were used. Measurements in water vapor used the dry dimensions of the membrane. Membrane samples were allowed to equilibrate at ambient conditions prior to testing in vapor.

Through-plane conductivity was determined in room-temperature liquid water, as described in a previous publication [4]. Water-equilibrated membranes were loaded into a custom-built 2-electrode cell, and through-plane conductivity was determined using the following equation:

$$\sigma_{Through-Plane} = {}^{t}/_{A(R-R_n)} \quad (6.4)$$

where $\sigma_{\text{Through-Plane}}$ is the through-plane conductivity (S/cm), t (cm) is membrane thickness, A is the electrode area of 0.63794 cm^2, R (Ω) is the measured resistance of the membrane, and R_n is the extrapolated non-membrane resistance (which accounts for contributions of the cell). The measured cell resistance included non-membrane contributions [28]. In order to determine the membrane impedance, several membrane samples (2-8 membranes) were stacked and their resistance was measured as a function of the total membrane thickness. The measured cell resistances were plotted against the stack thickness, and the extrapolated y-axis intercept (*i.e.* membrane thickness of 0 μm) was used to determine the non-membrane resistance, R_n.

6.2.5 Gravimetric Water Uptake & In-Plane Swelling

Membrane gravimetric water uptake and in-plane water swelling were determined before and after equilibration in water at room temperature, using Eq. 6.5:

$$Swelling[\%] = 100\times\frac{X_w - X_d}{X_d} \quad (6.5)$$

where X represents the mass (for gravimetric water uptake) or length (for in-plane water swelling) of the sample in the wet (w) or dry (d) state. Gravimetric water uptake of vapor-equilibrated membranes at 80°C and 0% - 90% relative humidity was determined using Eq. 6.5, where the membrane wet and dry masses were measured using a TA Q5000 sorption apparatus, and where the dry membrane weight was found after sample equilibration in a dry nitrogen gas stream.

6.2.6 IEC Determination and Membrane Composition

The ion-exchange capacity (IEC) of neat ionomer and composite membranes was determined through a standard acid-exchange and base-titration method. After equilibration in water at room temperature, the protons in a membrane of known dry mass were exchanged for Na^+ ions by soaking in 2.0 M NaCl for 48 hours. The soak solution was titrated with 0.01 N NaOH, and the IEC of the membrane was determined using Eq. 6.6:

$$IEC\ \left[\frac{mmol}{g}\right] = \frac{V_{titr}N}{m_d} \tag{6.6}$$

where V_{titr} [L] is the volume of the titrating solution, N [mol/L] is the normality of the titrant, and m_d [g] is the dry mass of the membrane sample. The composition of a membrane was determined by the ratio between the IEC of a composite membrane compared to that of the pristine ionomer as described in Chapter 4.

6.2.7 Mechanical Properties

The mechanical properties of nanofiber mats and composite membranes were obtained with a TA Q800 Dynamic Mechanical Analyzer (DMA). Samples were dried at 70°C for 3 hours prior to testing. The DMA was operated in tension mode and the

samples were strained at ambient laboratory conditions (25°C and ~40% relative humidity). Samples were elongated at a constant rate of 5% per minute until fracture.

6.2.8 Scanning Electron Microscopy (SEM) Imaging

SEM images of nanofiber mats and dual fiber membranes were obtained using a Zeiss scanning electron microscope with an accelerating voltage of 5 kV and a working distance of 10 mm. Samples were sputter-coated with ~5 nm of gold prior to imaging. Cross-sectional images were prepared by fracturing the sample after 2 minutes of submersion in liquid nitrogen. The average fiber diameter in an electrospun mat was determined from top-down micrographs using ImageJ software.

6.3 Results and Discussion

6.3.1 Controlling the Average Diameter of Electrospun PVDF Fibers

PVDF fiber mats were prepared with an average fiber diameter between 150 and 2,200 nm. Figure 6.1 shows SEM images of three mats, with an average fiber diameter of 150 nm, 600 nm, and 2200 nm, and Table 6.2 lists the electrospinning conditions for all five PVDF mats fabricated in this study. The PVDF fiber diameter was increased by increasing the polymer concentration in solution and the polymer solution flow rate during electrospinning, where the other electrospinning parameters (applied voltage, spinneret-to-collector distance, and air relative humidity) were held constant. These fiber diameter results are consistent with prior literature studies [24,27,29,30] which found that an increase in polymer solution viscosity resulted in large diameter electrospun fibers. With increased solution viscosity, the fiber jet undergoes less bending when acted upon by the electric field, resulting in a shorter travel distance between the spinneret tip and collector surface and a reduced "necking down" effect [23,30]. Similarly, the fiber

diameter increases with solution flow rate due to the higher volume of material ejected from the spinneret [29].

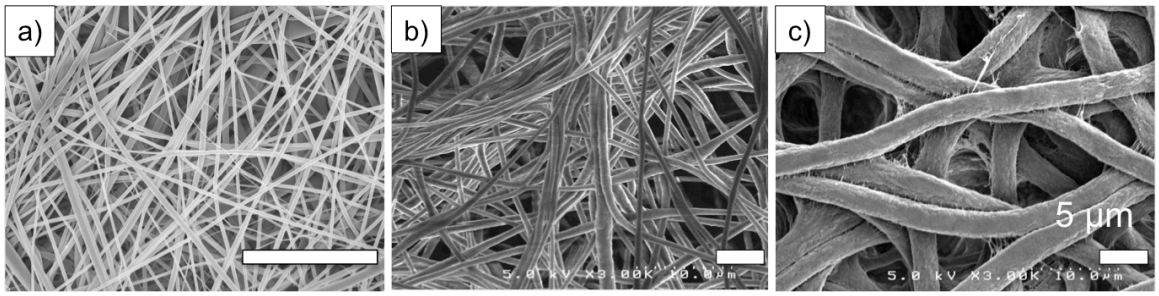

Figure 6.1: SEM Images of electrospun PVDF with diameter of 150 nm (a), 600 nm (b), 2200 nm (c) with 5 µm scale bar.

Table 6.2: Electrospinning conditions, average fiber diameters with standard deviations, and mechanical properties of PVDF nanofibers (at an applied voltage of 10 kV, a spinneret-to-collector distance of 10.5 cm, and an air relative humidity of 25%).

Fiber Diameter [nm]	Concentration [%]	Flow Rate [mL/hr]	Tensile Modulus [GPa]	Elongation at Break [%]	Mat Porosity [%]
PVDF					
150 ± 60	10	0.10	0.30	25	57.5
600 ± 180	12.5	0.25	1.17	70	67.2
840 ±320	15	0.25	1.24	120	59.5
1000 ± 400	17.5	0.50	1.35	25	58.4
2200 ± 500	17.5	0.85	1.52	70	56.3
Pristine PVDF film	12.5	---	1.80	150	0

6.3.2 Mechanical Properties of Electrospun Fibers

The tensile strength of electrospun PVDF mats were corrected for mat porosity, which was ~60% and are summarized in Table 6.2. Increases in the average PVDF fiber diameter were accompanied by an increase in tensile modulus. These results differ significantly from the work of Wong *et al.*, where a decrease in tensile modulus (from 350 to 250 MPa) of an electrospun poly(ε-caprolactone) fiber was observed as its diameter increased from 250 to 2600 nm [22]. The increase in tensile modulus of electrospun PVDF (which is not observed for poly(ε-caprolactone), PEO, or PVA) would suggest molecular chain alignment during electrospinning is not the dominant factor affecting the mechanical properties of the resultant mat. The mechanical properties reported here were evaluated for the electrospun mat (rather than a single fiber), so contributions of fiber entanglement and interwoven fibers (which would be present and potentially beneficial in a dual fiber membrane) are included. Reference [19] reports on a model for composite membrane swelling which considers swelling as a combination of the mixing of the solvent (water) with the network (ionomer), an elastic contribution from the network, and an elastic energy exerted onto the ionomer by the confining material (PVDF fibers in this study). As the stiffness of the reinforcing (confining) fiber increased, the swelling of the composite material decreased. This suggests that an increase in the tensile modulus of the PVDF reinforcing component of a dual fiber membrane would lead to a decrease in its in-plane swelling. Thus, the utilization of large-diameter PVDF fibers is expected to lead to the lowest in-plane swelling.

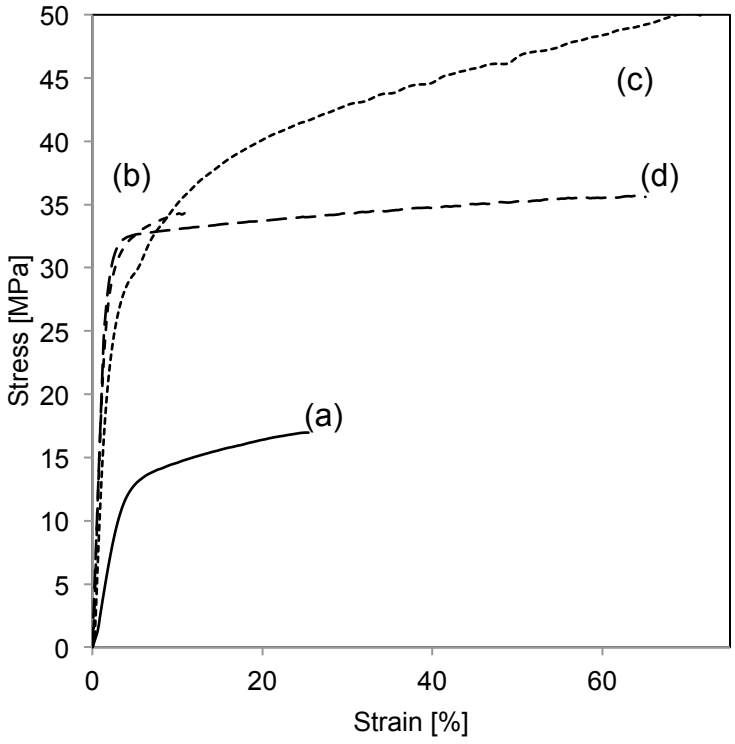

Figure 6.2: Stress-strain curves of electrospun PVDF fiber mats with average diameters of 150 nm (a), 600 nm (b), 1000 nm (c), and 2200 nm (d). Stress-strain curves were corrected for mat porosity.

6.3.3 Composite Membrane Morphology

A series of dual fiber membranes, each with a thickness of approximately 20 μm, was fabricated utilizing either 700 EW PFIA or 825 EW PFSA ionomer and an embedded PVDF reinforcing fiber mat, where the average diameter of the PVDF fibers ranged from 150 nm to 2200 nm. It was found that the conditions in Table 6.2 for varying the diameter of PVDF fibers were applicable when PVDF is co-electrospun with an ionomer. After electrospinning a dual fiber mat, the ionomer fibers were selectively softened and allowed to flow (by hot pressing the mats above the α-transition temperature of the ionomer), leading to a dense and defect-free composite membrane where PVDF fibers

were embedded in an ionomer matrix. SEM freeze-fractured cross-section images of two PFIA/PVDF membranes with different average PVDF fiber diameters are shown in Figure 6.3. A continuous ionomer network is observed in both cross-sections, despite the differences in size of the reinforcing fibers. As the diameter of the reinforcing fiber is increased, fewer fibers are present in the membrane because the PVDF content was held constant (*e.g.* for a given volume fraction of uncharged polymer fibers, by doubling the average diameter of a PVDF fiber, 4x fewer fibers are present in the film). A summary of the dual fiber membranes and their corresponding thicknesses is shown in Table 6.3.

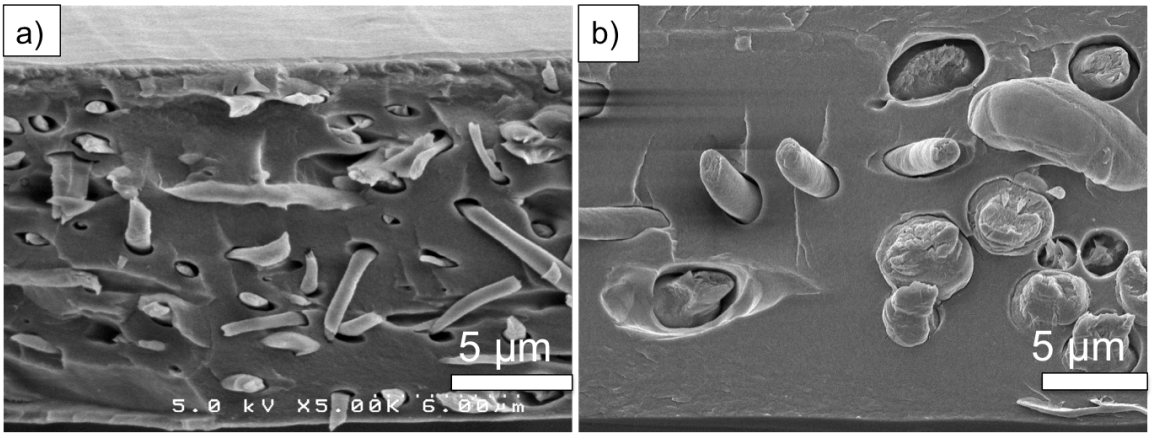

Figure 6.3: SEM cross-section images of dual fiber membranes where the matrix polymer is 700 EW PFIA and the reinforcing fibers are PVDF, with 75 wt.% PFIA and 25 wt.% PVDF. The average diameter of PVDF fibers is a) 600 nm and b) 1000 nm PVDF.

Table 6.3: Summary of dual fiber membrane thickness and reinforcing fiber diameters.

PVDF Fiber Diameter [nm]	Dry Thickness [μm]
PFIA-based membranes (75 wt.% PFIA*)*	
150	20
600	24
1000	25
2200	18
825 EW PFSA-based membranes (80 wt.% PFSA*)*	
150	21
600	23
1000	21
2200	19

6.3.4 Proton Conductivity of Composite Membranes

The in-plane and through plane conductivities of the dual fiber membranes in room temperature water are shown in Figure 6.4a and Figure 6.4b as a function of reinforcing fiber diameter. The conductivity of the 700 EW PFIA-based dual fiber membranes was greater than that of the 825 EW PFSA-based samples, which was expected based on the greater effective IEC of the PFIA samples (the IECs of the 825 EW PFSA/PVDF dual fiber membranes are ~0.95 mmol/g, compared to ~1.1 mmol/g for the 700 EW PFIA/PVDF dual fiber membranes). As has been shown [1,4,27], a continuous network of ionomer is obtained in the dual fiber membranes, allowing the proton conductivity to be dictated by ionomer content through a simple ionomer weight fraction mixing rule. An 80 wt.% 825 EW PFSA dual fiber membrane with 600 nm PVDF fibers exhibited approximately 80% of the pure ionomer's conductivity (0.0897 S/cm for the dual fiber membrane vs. 0.115 S/cm for the pristine PFSA), as shown in Table 6.4. Similar results were observed for the PFIA-based dual fiber and solution cast blended membranes. The variations in PVDF fiber diameter had negligible impact on the

overall membrane conductivity; the conductivity of all electrospun films followed a simple ionomer weight fraction mixing rule. Despite the increase in fiber diameter, ionomer penetration between the reinforcing polymer fibers was achieved (as shown Figure 6.3) due to the high PFSA or PFIA content, leading to the formation of continuous proton-conducting pathways. The through-plane conductivity (shown in Figure 6.4b) of the membranes was slightly lower and showed more experimental scatter, as compare to the in-plane values, but there was no obvious trend with increasing PVDF fiber diameter. Through-plane conductivity measurements are difficult to perform accurately. Non-membrane contributions to impedance measurements are substantial compared to the impedance of the membrane samples, and errors in the determination of the non-membrane resistance can have significant effects on conductivity measurements. Thus, larger errors in through-plane conductivity measurements are to be expected. Solution cast blended membranes also exhibited high proton conductivities. This was unexpected, as conventional polymer blends typically exhibit proton conductivities less than expected based on a linear rule of mixtures [4,31–33]. However, the conductivities of the composite films reported in Table 6.4 were similar to that of the dual fiber membranes, which suggests that the high ionomer content allows for the formation of continuous proton-conducting pathways in both membrane structures.

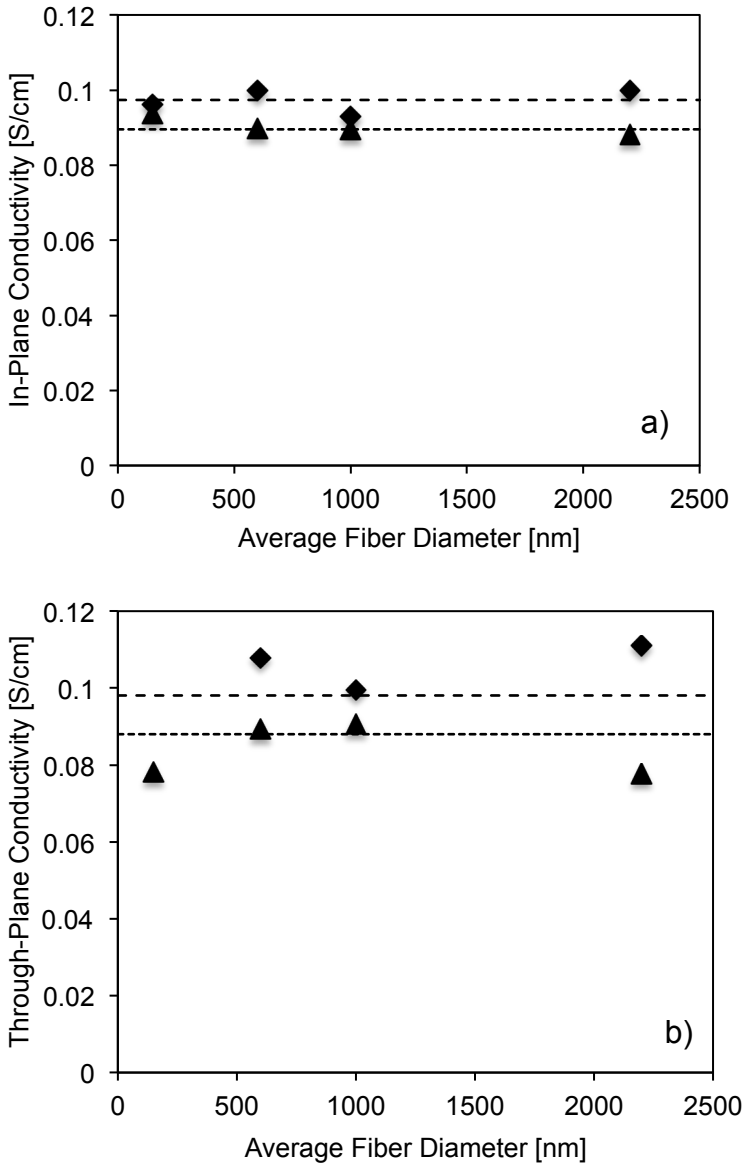

Figure 6.4: Proton conductivity of 75 wt.% 700 EW PFIA/25 wt.% PVDF (◆) and 80 wt.% 825 EW PFSA/20 wt.% PVDF (▲) dual fiber membranes as a function of reinforcing fiber diameter in 25°C liquid water. (a) In-plane conductivity and (b) through-plane proton conductivity. Dashed lines represent expected conductivity based on ionomer weight fraction mixing rule.

Table 6.4: Proton conductivity (in-plane and through-plane) and water swelling (in-plane & gravimetric) in 25 °C water of solution-cast 700 EW PFIA, 825 EW PFSA, 75 wt.% PFIA (25 wt.% PVDF) solution cast blended membrane, and 80 wt.% PFSA (20 wt.% PVDF) solution cast blended membrane.

	In-Plane/Through-Plane Conductivity[c] [S/cm]	Gravimetric Water Uptake[c] [%]	In-Plane Swelling [c] [%]	IEC [mmol/g]
Neat Ionomer				
700 EW PFIA[a]	0.131/0.126	120	34	1.44
825 EW PFSA[b]	0.115/0.110	60	30	1.21
Solution-Cast Blends				
75 wt.% PFIA (25 wt.% PVDF)[a]	0.093/0.075	62	20	1.05
80 wt.% PFSA (20 wt.% PVDF)[b]	0.089/0.077	34	18	0.98

[a] Treated in 1.0 M H_2SO_4 and H_2O at room temperature
[b] Treated in 1.0 M H_2SO_4 and H_2O at 80°C
[c] Measured in room temperature water

Similar to the behavior in liquid water, the conductivities of the 700 EW PFIA/PVDF and 825 EW PFSA/PVDF dual fiber membranes in 80°C water vapor showed a negligible dependence on fiber diameter, as shown in Figure 6.5a and Figure 6.5b. The mixing of the ionomer with uncharged polymer diluted the concentration of fixed charges, reducing the effective membrane conductivity across all levels of humidity. Maintaining high proton conductivity at low levels of humidification is beneficial for fuel cell operation because it helps reduce ohmic resistance, leading to greater power densities. Substantial losses in conductivity were observed under low humidification conditions (this behavior is typical for proton-conducting ionomers). The decrease in conductivity with RH was not affected by the diameter of PVDF fibers; there was no statistical trend of conductivity vs. PVDF fiber diameter at a given RH. PFIA-

based composite membranes exhibited a somewhat higher conductivity at 40-50% RH, as compared to the PFSA-based membranes. These results are similar to the findings of Choi *et al.*, which found that the diameter of the ionomer fiber has no bearing on the conductivity of the overall membrane [27]. Because continuous proton conducting pathways were maintained through the membrane in the thickness and in-plane directions, the variations in ionomer tortuosity did not significantly affect proton conductivity (*i.e.* a tortuosity factor of 1 is maintained).

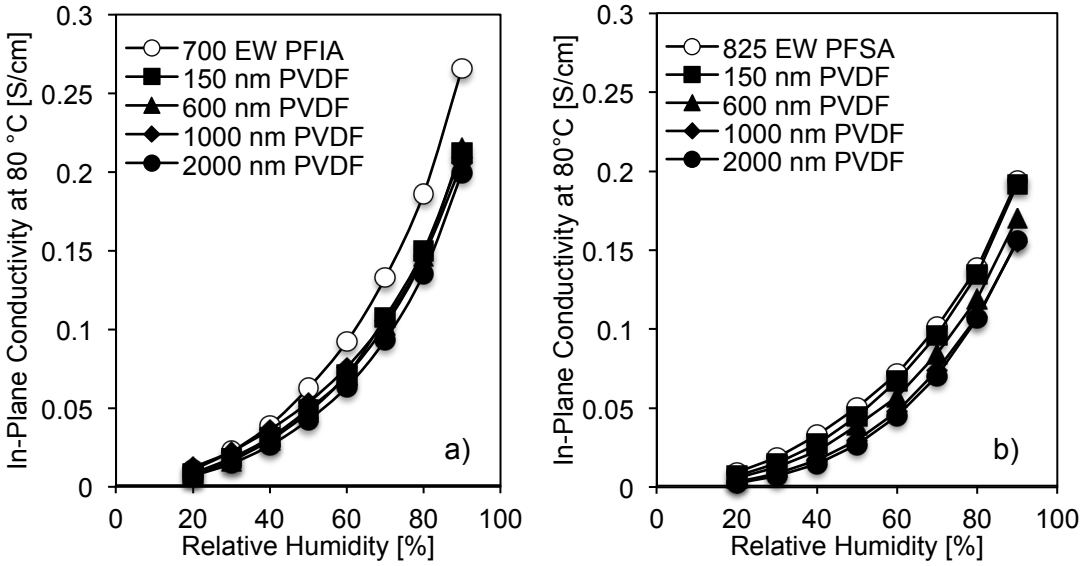

Figure 6.5: In-plane conductivity in water vapor at 80 °C of a) a solution-cast 700 EW PFIA film (O) and 75 wt.% PFIA (25 wt.% PVDF) dual fiber membranes, and b) a solution-cast 825 EW PFSA film (O) and 80 wt.% 825 EW PFSA (20 wt.% PVDF) dual fiber membranes using 150 nm (■), 600 nm (▲), 1000 nm (◆), and 2200 nm (●) PVDF fibers.

6.3.5 Swelling of Dual Fiber Membranes in Water Vapor

Equilibrium gravimetric water vapor uptake as a function of relative humidity (RH) at 80°C is shown in Figure 6.6 for pure solution-cast ionomer films (700 EW PFIA

and 825 EW PFSA) and dual fiber membranes with PFIA/PVDF and PFSA/PVDF, where the average PVDF fiber diameter is 600 nm or 2200 nm. The results for 700 EW PFIA-based composites and 825 EW PFSA-based composites are presented in Figure 6.6a and Figure 6.6b, respectively, as the hydration number λ (number of water molecules per fixed charge site) vs. RH. Minor differences in the hydration number of the composite membranes were observed compared to that of the neat ionomer due to the simultaneous reduction of water uptake and IEC (λ accounts for the IEC of the membrane). The hydration numbers of the 825 EW PFSA-based composite membranes were lower than those of the 700 EW PFIA-based membranes. The lower IEC of the 825 EW PFSA-based films led to lower gravimetric water uptake. The 700 EW PFIA-based samples sorb more water molecules than the 825 EW PFSA-based samples, which is a result of the increased hydrophilicity of the PFIA (due to the higher IEC). Finally, the increased conductivity of the 700 EW PFIA dual fiber membranes (shown in Figure 6.4) is consistent with their greater λ-values compared to 825 EW PFSA-based membranes.

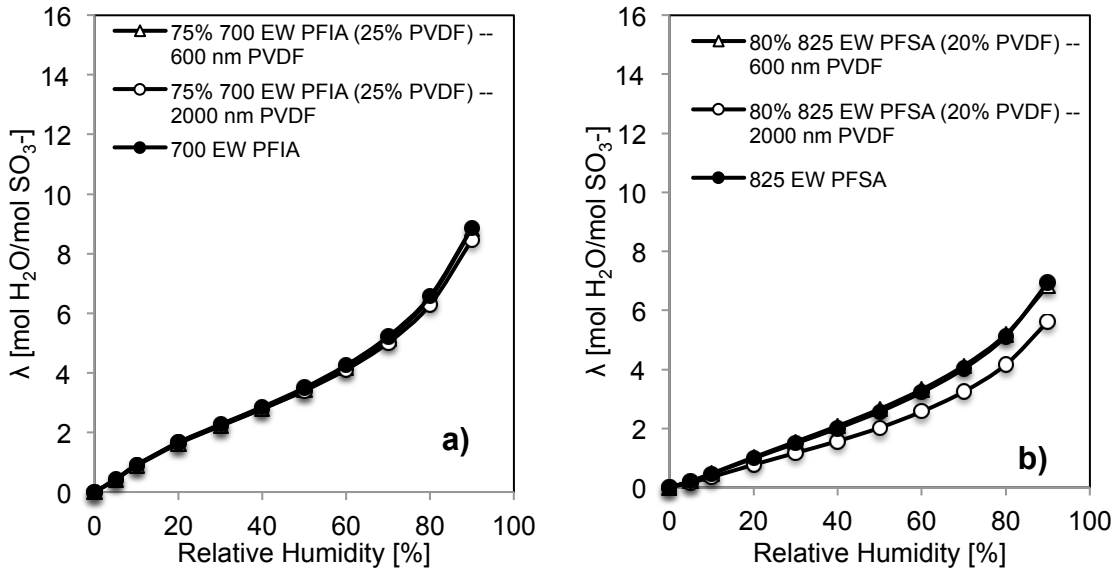

Figure 6.6: Hydration number λ (mol H_2O/mol SO_3H) of a) 700 EW PFIA (●), 75 wt.% 700 EW PFIA (25 wt.% PVDF) with 600 nm (△) and 2200 nm (○) PVDF fibers; b) 825 EW PFSA (●), 80 wt.% PFSA (20 wt.% PVDF) nanofiber membranes with 600 nm (△) and 2200 nm (○) PVDF fibers.

6.3.6 Swelling of Dual Fiber Membranes in Liquid Water

The in-plane swelling and gravimetric water uptake in room-temperature water were also evaluated for dual fiber membranes using 80 wt.% 825 EW PFSA and 75 wt.% 700 EW PFIA dual fiber membranes. The results are shown in Figure 6.7a and Figure 6.7b. The gravimetric water uptake of the PFSA composite membrane in liquid water is practically independent of PVDF fiber diameter. For the PFIA membrane, constant swelling was seen when the fiber diameter was 600 nm or greater. The low-diameter PVDF fiber (150 nm) was not strong enough to control the swelling of PFIA (the modulus of the 150 nm-PVDF fiber mat was low). The in-plane conductivity, gravimetric water uptake, in-plane water swelling, and IEC of the pure solution-cast ionomers, as

well as 80 wt.% PFSA (20 wt.% PVDF) and 75 wt.% PFIA (25 wt.% PVDF) solution cast blended membranes, are listed in Table 6.4. Pristine PFIA exhibits an in-plane swelling of 34%, which was reduced to 20% when it was blended with 25 wt.% PVDF. The incorporation of PVDF fibers allowed the in-plane swelling of a PFIA-based dual fiber membrane to be reduced to 8% when utilizing 600 nm PVDF. With 2200 nm PVDF fibers, the in-plane swelling was further reduced to 4%. These high diameter fibers (strong fibers) are better in reducing in-plane swelling with no adverse effect on proton conductivity.

Similar reductions in swelling are observed in 825 EW PFSA/PVDF dual fiber membranes. The gravimetric water uptake of the water-equilibrated PFSA/PVDF dual fiber membranes ranged from 25 - 30% for all PVDF fiber diameters tested. The constant gravimetric water uptake with increasing PVDF fiber diameter for 825 EW PFSA-based samples (compared to the PFIA-based samples) is due to the reduced uptake of the base polymer, as shown in Table 6.4 (825 EW PFSA wells less than 700 EW PFIA due to the lower IEC). As shown in Figure 6.7b, the in-plane swelling of an 825 EW PFSA/PVDF dual fiber membrane decreased as the PVDF fiber diameter is increased, going from 15% with 150 nm PVDF fibers to 4% with 2200 nm fibers. The 825 EW PFSA/PVDF and 700 EW PFIA/PVDF dual fiber membranes exhibited a similar reduction in the in-plane swelling with PVDF fiber diameter. This would suggest that fiber strength controls in-plane swelling. The 4% in-plane swelling and conductivity of 0.1 S/cm in water of the 700 EW PFIA/PVDF dual fiber membrane with 2200 nm PVDF fibers is comparable to similar electrospun membranes (such as Ballengee's 3M660/polyphenylsulfone (PPSU)

dual fiber membrane with an average fiber diameter of 335 nm [3], which had a conductivity of 0.107 and an in-plane swelling of 5%).

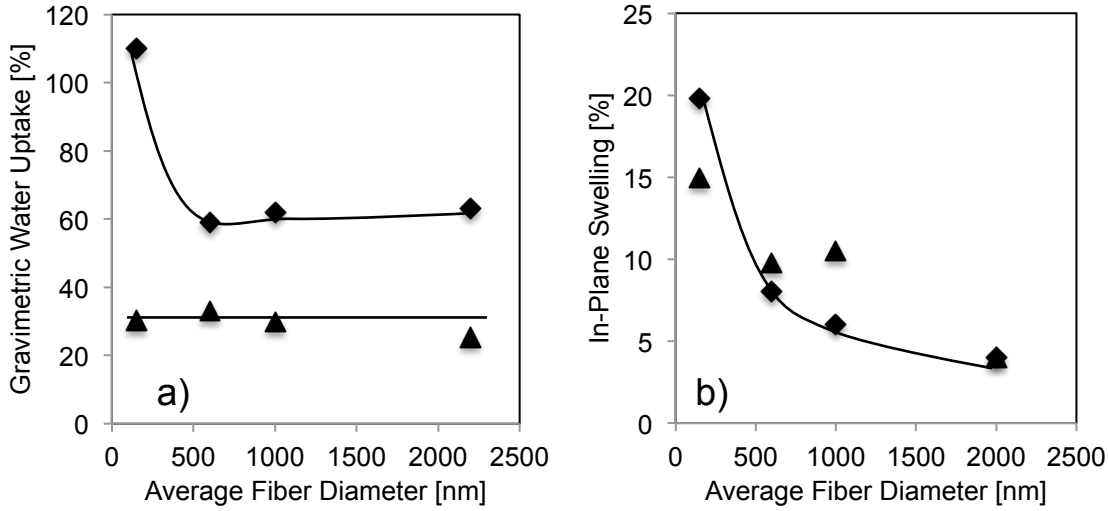

Figure 6.7: Dependence of composite membrane swelling as a function of reinforcing PVDF fiber diameter. (a) Gravimetric water uptake and (b) in-plane water swelling. (◆) 75 wt.% 700 EW PFIA (25 wt.% PVDF) and (▲) 80 wt.% 825 EW PFSA (20 wt.% PVDF) dual fiber membranes. Solid lines included as a guide.

6.3.7 Mechanical Properties of Dual Fiber Membranes with Various Reinforcing Fiber Diameters

Strain-strain curves for several 700 EW PFIA-based and 825 EW PFSA-based dual fiber membranes are shown in Figure 6.8. As expected, the presence of PVDF in the membrane improved the modulus and proportional limit stress of the membranes. This is in contrast with the dual fiber membrane reported by Ballengee *et al.* [3] where the presence of PPSU nanofibers in a 3M 660 EW PFSA matrix did not improve the dry mechanical strength of a dual fiber membrane compared to a solution-cast PFSA film. The membranes reported here utilized a greater uncharged polymer content (25 wt.%,

compared to 19 wt.% PPSU in reference [3]), presumably leading to the improved mechanical strength. Increasing the diameter of the PVDF reinforcing fibers also resulted in an improvement to the mechanical strength of the PFIA-based dual fiber membrane. Transitioning from 600 nm PVDF fibers to 1000 nm PVDF fibers resulted in a 35% increase in the modulus of the membrane. Surprisingly, the presence of 2200 nm PVDF fibers did not result in a further improvement in the modulus of the membrane; instead, there was a loss in strength. This is due to the reduced number of PVDF reinforcing fibers in this particular membrane. The mechanical properties of the dual fiber membranes are summarized in Table 6.5.

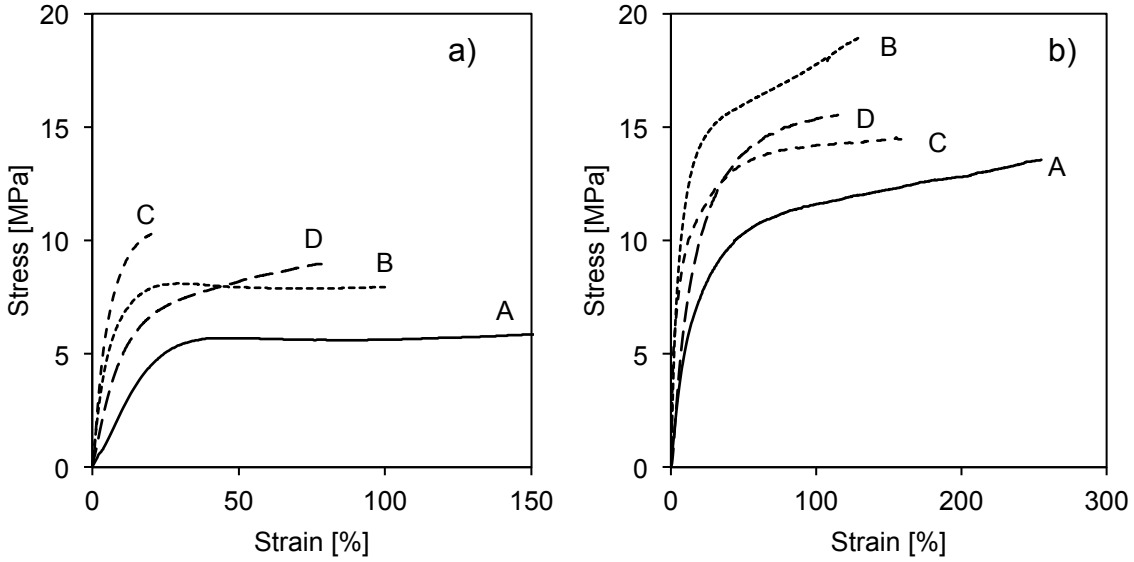

Figure 6.8: Stress-strain curves of air-dried membranes. (a) Solution cast 700 EW PFIA (A) and 75 wt.% 700 EW PFIA (25 wt.% PVDF) dual fiber membranes utilizing 600 nm (B), 1000 nm (C), and 2200 nm (D) PVDF fibers. (b) Solution cast 825 EW PFSA (A) and 80 wt.% 825 EW PFSA (20 wt.% PVDF) dual fiber membranes utilizing 600 nm (B), 1000 nm (C), and 2200 nm (D) PVDF fibers.

While the incorporation of PVDF fibers into the 825 EW PFSA matrix resulted in a stronger membrane, there was a negligible effect as the average diameter of the reinforcing component was increased. The modulus showed essentially no change as the fiber diameter is increased from 150 nm to 2200 nm. As 825 EW PFSA is mechanically stronger than 700 EW PFIA, the increased strength of the embedded PVDF fibers likely has a lesser impact on the strength of the composite membrane.

Table 6.5: Young's Modulus and Strain at Break (SAB) of dual fiber membranes with varied reinforcing fiber diameters and solution-cast films of the pure polymers evaluated at ambient conditions.

Fiber Diameter	**75 wt.% 700 EW PFIA (25 wt.% PVDF)**		**80 wt.% 825 EW PFSA (20 wt.% PVDF)**	
	Young's Modulus [MPa]	Strain at Break [%]	Young's Modulus [MPa]	Strain at Break [%]
150 nm	100.8	10	93.3	138
600 nm	114.4	100	89.5	130
1000 nm	153.7	30	95.3	164
2200 nm	90.5	78	85.1	120
Neat Membrane	Young's Modulus [MPa]		Strain at Break [%]	
700 EW PFIA	24.9		170	
825 EW PFSA	43.5		250	
PVDF	1799		5	

Using the strain at break data in Table 6.5, the humidity stability factor (HSF in Eq. 6.1) of the composite films was calculated. The HSF of several composite membranes reported from this work, along with those for composite films in the literature, are given in Table 6.6. Good fuel cell performance of a membrane has been correlated with HSFs that are greater than 10 [9]. The mixing of PVDF with PFSA or PFIA (to make a solution cast blended membrane) led to a reduction in the membrane's

in-plane swelling, thus increasing its HSF as compared to the pristine ionomer. However, the electrospun membranes achieved greater HSFs as compared to the solution cast blended films due to the significant reduction in their in-plane swelling values. The HSF highlights two important points regarding the composite membranes with variable PVDF fiber diameter. First, increasing the average PVDF fiber diameter reduces the in-plane water swelling of the composite film at the cost of ductility (elongation at break). This effect was most pronounced in PFIA-based composite films, and suggests that improving strength alone may not be enough to achieve good membrane swelling/shrinking durability. Second, the HSF observed for the membranes reported in this work are similar to the values estimated for electrospun composite membranes found in the literature [1,3,5]. The composite membrane with the greatest HSF fabricated in this work utilized 825 EW PFSA with 2200 nm PVDF reinforcing fibers; by comparison the Nafion/PPSU dual fiber membrane reported by Ballengee and Pintauro [1] had a similar HSF but a greater area-specific resistance (the membrane was thicker with a lower proton conductivity). The greater conductivity potentially makes these membranes advantageous for fuel cell usage.

Table 6.6: Humidity Stability Factor (HSF) for select dual fiber membranes.

Ionomer	Uncharged Polymer Fiber	Uncharged Polymer Fiber Diameter [nm]	Membrane Structure	HSF
700 EW PFIA	None	---	Neat film	5
	PVDF	600	Dual Fiber	12.5
	PVDF	2200	Dual Fiber	19.5
	PVDF	---	Blend	9.4
825 EW PFSA	None	---	Neat film	8.3
	PVDF	150	Dual Fiber	7.0
	PVDF	600	Dual Fiber	13.3
	PVDF	2200	Dual Fiber	30
	PVDF	---	Blend	11.8
Literature Data				
sPEK [5]	PEK	170	Dual Fiber	8.2
Nafion [1]	PPSU	340	Dual Fiber	30
660 EW [3]	PPSU	335	Dual Fiber	14

6.4 Conclusion

A series of dual fiber membranes, in which the average diameter of the reinforcing component was varied, were fabricated and tested. Electrospun PVDF fibers were fabricated with average diameters ranging from 150 nm to 2200 nm. Electrospun PVDF exhibited an increase in tensile modulus as the fiber diameter was increased, and was used to reinforce a dual fiber membrane containing 80 wt.% 3M 825 EW PFSA (effective IEC of 0.95 mmol/g) or 75 wt.% 700 EW PFIA (effective IEC of 1.1 mmol/g). The increase in modulus of PVDF led to membranes with greater strength and lower in-plane swelling.

Water uptake and proton conductivity in liquid water and water vapor at 80°C were measured for the composite membranes. There was no difference in gravimetric water uptake (liquid water or water vapor) for membranes using 825 EW PFSA or 700 EW PFIA as the PVDF fiber diameter increased. Similarly, the in-plane and through-

plane conductivity of the membranes were both dictated by the ionomer content (i.e. isotropic conductivities were observed), and were unaffected by the average diameter of the reinforcing component. The single most important finding of this study was that in-plane swelling was strongly affected by the average diameter of the PVDF fibers, reaching 4% when 2200 nm PVDF fibers were used. Thus, an 80 wt.% 825 EW PFSA dual fiber membrane using 2200 nm PVDF fibers exhibited a HSF of 30, which is among the highest for the composite films reported in this work, making it acceptable for fuel cell usage. For comparison, blending PVDF with an ionomer led to an in-plane swelling of ~20% and an HSF of ~10. These results suggest that increasing the fiber diameter of a semicrystalline reinforcing polymer in a dual fiber membrane can lead to an improvement in overall membrane strength and durability in a fuel cell.

6.5 Acknowledgements

The authors would like to thank the US DOE (EERE Cooperative Agreement No. DE-EE0006362) for funding this work, as well as Dr. Michael Yandrasits at 3M for providing the low equivalent weight ionomers used in this study.

6.6 References

[1] J.B. Ballengee, P.N. Pintauro, Composite fuel cell membranes from dual-nanofiber electrospun mats, Macromolecules. 44 (2011) 7307–7314. doi:10.1021/ma201684j.

[2] J. Choi, K.M. Lee, R. Wycisk, P.N. Pintauro, P.T. Mather, Nanofiber network ion-exchange membranes, Macromolecules. 41 (2008) 4569–4572. doi:10.1021/ma800551w.

[3] J.B. Ballengee, G.M. Haugen, S.J. Hamrock, P.N. Pintauro, Properties and Fuel Cell Performance of a Nanofiber Composite Membrane with 660 Equivalent Weight Perfluorosulfonic Acid, J. Electrochem. Soc. 160 (2013) F429–F435. doi:10.1149/2.088304jes.

[4] J.W. Park, R. Wycisk, P.N. Pintauro, Nafion/PVDF nanofiber composite membranes for regenerative hydrogen/bromine fuel cells, J. Memb. Sci. 490 (2015) 103–112. doi:10.1016/j.memsci.2015.04.044.

[5] M. Oroujzadeh, S. Mehdipour-Ataei, M. Esfandeh, Proton exchange membranes with microphase separated structure from dual electrospun poly(ether ketone) mats: Producing ionic paths in a hydrophobic matrix, Chem. Eng. J. 269 (2015) 212–220. doi:10.1016/j.cej.2015.01.088.

[6] A.M. Park, P.N. Pintauro, Alkaline Fuel Cell Membranes from Electrospun Fiber Mats, Electrochem. Solid-State Lett. 15 (2012) B27. doi:10.1149/2.010203esl.

[7] C. Shen, R.J. Wycisk, P.N. Pintauro, High performance electrospun bipolar membrane with a 3D junction, Energy Environ. Sci. 10 (2017) 1435–1442. doi:10.1039/C7EE00345E.

[8] A.M. Park, F.E. Turley, R.J. Wycisk, P.N. Pintauro, Electrospun and Cross-Linked Nano fiber Composite Anion Exchange Membranes, Macromolecules. 47 (2014) 227–235. doi:10.1021/ma401932h.

[9] C. Gittleman, Automotive Perspective on PEM Evaluation, 2009. doi:10.1172/JCI46043.rons.

[10] R. Borup, J. Meyers, B. Pivovar, Y.S. Kim, R. Mukundan, N. Garland, D. Myers, M. Wilson, F. Garzon, D. Wood, P. Zelenay, K. More, K. Stroh, T. Zawodzinski, X.J. Boncella, J.E. Mcgrath, O.M. Inaba, K. Miyatake, M. Hori, K. Ota, Z. Ogumi, S. Miyata, A. Nishikata, Z. Siroma, Y. Uchimoto, K. Yasuda, K. Kimijima, N. Iwashita, Scientific Aspects of Polymer Electrolyte Fuel Cell Durability and Degradation, (2007) 3904–3951.

[11] M. Javad, S. Rowshanzamir, F. Gashoul, Comprehensive investigation of physicochemical and electrochemical properties of sulfonated poly (ether ether ketone) membranes with different degrees of sulfonation for proton exchange membrane fuel cell applications, Energy. 125 (2017) 614–628. doi:10.1016/j.energy.2017.02.143.

[12] K.S. Lee, M.H. Jeong, Y.J. Kim, S. Bin Lee, J.S. Lee, Fluorinated aromatic polyether ionomers containing perfluorocyclobutyl as cross-link groups for fuel cell applications, Chem. Mater. 24 (2012) 1443–1453. doi:10.1021/cm203539m.

[13] A. Kusoglu, A.M. Karlsson, M.H. Santare, S. Cleghorn, W.B. Johnson, Mechanical behavior of fuel cell membranes under humidity cycles and effect of swelling

anisotropy on the fatigue stresses, J. Power Sources. 170 (2007) 345–358. doi:10.1016/j.jpowsour.2007.03.063.

[14] F.A. De Bruijn, V.A.T. Dam, G.J.M. Janssen, Review : Durability and Degradation Issues of PEM Fuel Cell Components, (2008) 3–22. doi:10.1002/fuce.200700053.

[15] J. Wu, X.Z. Yuan, J.J. Martin, H. Wang, J. Zhang, J. Shen, S. Wu, W. Merida, A review of PEM fuel cell durability: Degradation mechanisms and mitigation strategies, J. Power Sources. 184 (2008) 104–119. doi:10.1016/j.jpowsour.2008.06.006.

[16] T.T. Aindow, J. O'Neill, Use of mechanical tests to predict durability of polymer fuel cell membranes under humidity cycling, J. Power Sources. 196 (2011) 3851–3854. doi:10.1016/j.jpowsour.2010.12.031.

[17] M.P. Rodgers, L.J. Bonville, H.R. Kunz, D.K. Slattery, J.M. Fenton, Fuel Cell Perfluorinated Sulfonic Acid Membrane Degradation Correlating Accelerated Stress Testing and Lifetime, (2012).

[18] S. Chen, X. Zhang, K. Chen, N. Endo, M. Higa, K.I. Okamoto, L. Wang, Cross-linked miscible blend membranes of sulfonated poly(arylene ether sulfone) and sulfonated polyimide for polymer electrolyte fuel cell applications, J. Power Sources. 196 (2011) 9946–9954. doi:10.1016/j.jpowsour.2011.08.091.

[19] X. Li, Z. Shen, T.A.O. He, M. Wessling, Modeling on Swelling Behavior of a Confined Polymer Network, J. Polym. Sci. Part B Polym. Phys. 46 (2008) 1589–1593. doi:10.1002/polb.

[20] P.J. Flory, J. Rehner, Statistical mechanics of cross-linked polymer networks II. Swelling, J. Chem. Phys. 11 (1943) 521–526. doi:10.1063/1.1723792.

[21] U. Stachewicz, R.J. Bailey, W. Wang, A.H. Barber, Size dependent mechanical properties of electrospun polymer fibers from a composite structure, Polymer (Guildf). 53 (2012) 5132–5137. doi:10.1016/j.polymer.2012.08.064.

[22] S.C. Wong, A. Baji, S. Leng, Effect of fiber diameter on tensile properties of electrospun poly(ε-caprolactone), Polymer (Guildf). 49 (2008) 4713–4722. doi:10.1016/j.polymer.2008.08.022.

[23] J. Pelipenko, J. Kristl, B. Jankovi, P. Kocbek, The impact of relative humidity during electrospinning on the morphology and mechanical properties of nanofibers, Int. J. Pharm. 456 (2013) 125–134. doi:10.1016/j.ijpharm.2013.07.078.

[24] K.M. Lee, J. Choi, R. Wycisk, P.N. Pintauro, P. Mather, Nafion Nanofiber Membranes, ECS Trans. 25 (2009) 1451–1458. doi:10.1149/1.3210701.

[25] J. Choi, R. Wycisk, W. Zhang, P.N. Pintauro, K.M. Lee, P.T. Mather, High conductivity perfluorosulfonic acid nanofiber composite fuel-cell membranes, ChemSusChem. 3 (2010) 1245–1248. doi:10.1002/cssc.201000220.

[26] W. Zhang, R. Wycisk, D.L. Kish, P.N. Pintauro, Pre-Stretched Low Equivalent Weight PFSA Membranes with Improved Fuel Cell Performance, J. Electrochem. Soc. 161 (2014) F770–F777. doi:10.1149/2.085406jes.

[27] J. Choi, K.M. Lee, R. Wycisk, P.N. Pintauro, P.T. Mather, Nanofiber composite membranes with low equivalent weight perfluorosulfonic acid polymers, J. Mater. Chem. 20 (2010) 6282–6290. doi:10.1039/c0jm00441c.

[28] C.H. Lee, H.B. Park, Y.M. Lee, R.D. Lee, Importance of Proton Conductivity Measurement in Polymer Electrolyte Membrane for Fuel Cell Application, (2005) 7617–7626.

[29] J.B. Ballengee, P.N. Pintauro, Morphological Control of Electrospun Nafion Nanofiber Mats, J. Electrochem. Soc. 158 (2011) B568–B572. doi:10.1149/1.3561645.

[30] C. Mit-uppatham, M. Nithitanakul, P. Supaphol, Ultrafine Electrospun Polyamide-6 Fibers : Effect of Solution Conditions on Morphology and Average Fiber Diameter, 6 (2004) 2327–2338. doi:10.1002/macp.200400225.

[31] C. Zhao, Z. Wang, D. Bi, H. Lin, K. Shao, T. Fu, S. Zhong, H. Na, Blend membranes based on disulfonated poly(aryl ether ether ketone)s (SPEEK) and poly(amide imide) (PAI) for direct methanol fuel cell usages, Polymer (Guildf). 48 (2007) 3090–3097. doi:10.1016/j.polymer.2007.03.064.

[32] S. Swier, M.T. Shaw, R.A. Weiss, Morphology control of sulfonated poly(ether ketone ketone) poly(ether imide) blends and their use in proton-exchange membranes, J. Memb. Sci. 270 (2006) 22–31. doi:10.1016/j.memsci.2005.06.037.

[33] J. Lin, J.K. Lee, M. Kellner, R. Wycisk, P.N. Pintauro, Nafion-Flourinated Ethylene-Propylene Resin Membrane Blends for Direct Methanol Fuel Cells, J. Electrochem. Soc. 153 (2006) A1325. doi:10.1149/1.2196687.

Chapter 7

Conclusions

(1) Dual fiber electrospinning of a low equivalent weight (EW) 3M ionomer with an uncharged polymer was employed to fabricate composite proton-exchange membranes (PEM) for fuel cells. After electrospinning, the perfluorosulfonic acid (PFSA) or perfluoroimide acid (PFIA) ionomer was selectively softened, leading to a dense and defect-free membrane in which uncharged fibers were embedded in the ionomer matrix. A summary of the composite membranes fabricated in the course of this work is provided in Table 7.1.

Table 7.1: Summary of composite membranes for H_2/air fuel cells fabricated in this dissertation.

Ionomer	Reinforcing Polymer		Structure
825 EW PFSA	PAI	*i.*	Ionomer matrix with embedded reinforcing fibers
		ii.	Tri-layer membrane with embedded reinforcing fibers
		iii.	Ionomer matrix with embedded reinforcing fibers of variable diameter
		iv.	Solution cast blended membrane
825 EW PFSA	PVDF	*i.*	Ionomer matrix with embedded reinforcing fibers
		ii.	Ionomer matrix with embedded reinforcing fibers of variable diameter
		iii.	Single fiber membrane
		iv.	Solution cast blended membrane
725 EW, 660 EW PFSA	PVDF	*i.*	Ionomer matrix with embedded reinforcing fibers
		ii.	Single fiber membrane
		iii.	Solution cast blended membrane
700 EW PFIA	PVDF	*i.*	Ionomer matrix with embedded reinforcing fibers
		ii.	Ionomer matrix with embedded reinforcing fibers of variable diameter
		iii.	Single fiber membrane
		iv.	Solution cast blended membrane

(2) Dual fiber electrospun membranes were fabricated using poly(amide imide) (PAI) or poly(vinylidene fluoride) (PVDF) as the uncharged reinforcing fiber. All electrospun membranes exhibited proton conductivities that could be described by a simple ionomer weight fraction mixing rule. The following membranes were fabricated in this work:

a. Single layer membranes, which utilized a homogeneous distribution of PFSA or PFIA through thickness of the membrane.
b. Multi-layer membranes, where the PFSA composition was varied through the thickness of the membrane. These membranes exclusively utilized PAI as the reinforcing fiber. The first set of multi-layer membranes had alternating high-PFSA content layers and low-PFSA content layers designed to reduce the effective in-plane swelling of the composite film. A second set of tri-layer membranes was also fabricated, which used surface layers with a high PFSA content and an inner layer with either: (i) a homogeneous distribution of PFSA and PAI in the inner layer or (ii) a gradient distribution of PFSA and PAI in the inner layer.
c. Single layer membranes with variable uncharged reinforcing polymer fiber diameter. These membranes utilized electrospun PVDF (with an average diameter ranging from 150 nm – 2200 nm) to reinforce a matrix of 825 EW PFSA or 700 EW PFIA ionomer.
d. Single layer membranes, which were fabricated using 3M ionomers of varying EW. Each membrane had the same effective ion-exchange capacity (IEC) of ~0.95 mmol/g, and the effect of ionomer EW (825, 725,

and 660 EW PFSA were used) on the composite membrane performance was determined.

(3) The effect of the number of layers and the thickness/composition of the reinforcing layer of multi-layer membranes was evaluated in dual fiber membranes containing 825 EW PFSA and PAI. The films had the following properties:

a. The in-plane and through-plane conductivity was not affected by the number of layers or the composition of the layers. Thus, membrane conductivity was independent of structure, and only dependent on the ionomer content via a simple weight fraction mixing rule. All tri-layer membranes (which contained ~80 wt.% 825 EW PFSA) exhibited proton conductivities of ~0.09 S/cm, as compared to 0.115 S/cm for the pristine ionomer.

b. Gravimetric water uptake was not dependent on the membrane structure, but in-plane water swelling was strongly affected by membrane structure. The addition of PAI fibers (as a single layer membrane) led to a reduction in the in-plane swelling (from 30% for the pristine ionomer to 12% for the single layer membrane). The utilization of a tri-layer structure allowed for an in-plane swelling of ~5%, which meets the DOE target. The addition of more layers did not provide any further reductions to membrane swelling.

c. The mechanical properties were improved by the multi-layering technique. The strongest membrane utilized a tri-layer structure with an inner layer that contained 75 wt.% PFSA.

d. The tri-layer membranes were dense (low feed gas crossover was measured in an operational fuel cell) and thin. The best membrane was 17 μm, leading to an area-specific resistance (ASR, membrane thickness divided by conductivity) of 0.019 Ωcm^2.

e. Partial curing of the PAI fibers was performed during the annealing process, where the PFSA/PAI dual fiber membranes were annealed at 200°C for 1 hour. More extensive annealing steps were performed, and the results of those steps are provided in Appendix A.

(4) Single fiber electrospinning was employed to fabricate blended fiber mats containing 3M's low EW PFSA or PFIA. PVDF acted as both the carrier and reinforcing polymer for these electrospun mats. Well-formed nanofibers were obtained with ionomer contents ranging up to 80 wt.% PFSA or PFIA. The resultant fibers had diameters ranging from 300 – 1000 nm, which were dependent on the PFSA:PVDF mass ratio, as well as the overall polymer content in the electrospinning solution. After electrospinning, the mats were hot pressed and annealed, leading to nano-dispersed films that were free of voids or defects. Membrane thicknesses were typically 20-30 microns.

(5) A series of solution cast blended films utilizing a 3M's low EW PFSA or PFIA and PVDF or PAI were fabricated via a solution casting technique. An ionomer was dispersed into an organic solvent, and subsequently mixed with an uncharged polymer. Such a mixture contained a high ionomer:uncharged polymer mass ratio (for example, 80:20 PFSA:PVDF) with a solids content of 15-20 wt.%. After casting, the blends were annealed, and free-standing composite films were removed from the substrates.

(6) Single fiber and dual fiber membranes utilizing 825 EW PFSA and PVDF were compared in terms of their proton conductivities, water swelling, and mechanical properties. The following observations were made:

a. Dual fiber membranes had the greatest proton conductivities. At high PFSA contents, the single fiber membranes exhibited proton conductivities that were slightly lower than expected based on a simple ionomer weight fraction mixing rule, but as mid-range compositions (below ~70 wt.% PFSA), larger deviations in conductivity were observed.
b. Dual fiber membranes exhibited lower in-plane swelling and greater gravimetric water uptake values. The un-welded reinforcing fiber structure of a dual fiber membrane allowed for selective expansion in the thickness direction upon hydration, while the single fiber membranes exhibited a lower degree of swelling anisotropy. The presence of PVDF in the single fiber membranes reduced the hydrophilic forces that cause water sorption into the ionomer, leading to reduced gravimetric water uptake compared to the dual fiber membranes.
c. Single fiber membranes generally exhibited weaker mechanical properties than the dual fiber membranes.

(7) Dual fiber, single fiber, and solution cast blended membranes were fabricated with the same effective IEC using PFSA ionomers of varying EWs (825, 725, and 660 EW PFSA were used). The effect of ionomer EW on the resultant membrane properties was determined, and the following observations were made:

a. Solution cast blended membranes exhibited the worst combination of properties. Such films exhibited losses in conductivity at mid-range compositions, along with excessive in-plane water swelling values. Thus, a solution cast blended film containing 80 wt.% 825 EW PFSA exhibited an in-plane conductivity of 0.085 S/cm, but an in-plane swelling of 20%. A blend with 66 wt.% 660 EW PFSA exhibited a proton conductivity of 0.067 S/cm and an in-plane swelling of 14%.

b. Single fiber and dual fiber membranes exhibited similar trends as discussed in point 6 above. The single fiber membrane that utilized 66 wt.% 660 EW PFSA exhibited a low conductivity (0.07 S/cm) compared to 0.09 S/cm for the dual fiber membrane.

c. The dual fiber membranes exhibited lower in-plane swelling than single fiber or solution cast blended membranes regardless of ionomer EW. An unusual minimum in the in-plane water swelling was observed for the dual fiber membrane when 725 EW PFSA was used. This membrane contained a sufficiently high PVDF loading to restrict swelling and sufficient PFSA crystallinity to prevent excessive ionomer swelling.

(8) The crystallinity of PVDF and PFIA were evaluated in a single fiber, a dual fiber, and a solution cast blended membrane via small-angle X-ray scattering and X-ray diffraction. The crystallinity of PFIA and PVDF in a composite membrane was controlled by the fabrication process, with dual fiber electrospinning leading to a higher degree of crystallinity as compared to the single fiber electrospinning and solution casting techniques. Membrane crystallinity was correlated with the resultant membrane

properties, with greater PFIA crystallinity leading to high conductivity in water and high PVDF crystallinity leading to good control of in-plane water swelling. Temperature dependence of a PFIA/PVDF dual fiber membrane is compared with that of Nafion 211 in Appendix B.

(9) Composite membranes containing 700 EW PFIA and 660 EW PFSA were fabricated using dual fiber and single fiber electrospinning. The change in ionomer structure did not affect the fabrication technique for the films, and at equivalent IECs, led to similar membrane properties. Thus, a multi-acid side chain ionomer such as PFIA is a potential alternative ionomer structure to achieve high IEC while maintaining ionomer crystallinity.

(10) Electrospun PVDF nanofibers were fabricated with average diameters ranging from 150 nm – 2200 nm. The range of fiber diameters was achieved by adjusting the solution concentration and flow rate. The mechanical properties of the resultant fiber mats were determined after compaction to correlate fiber diameter to mat strength.

(11) PFSA and PFIA were incorporated into dual fiber membranes with reinforcing PVDF fibers of variable average diameter. The following observations were made:

a. All membranes exhibited proton conductivities that were dictated by the ionomer content. The PFIA-based membranes exhibited greater conductivities than the PFSA-based films due to the greater effective IEC of the composite films (0.95 mmol/g for the 825 EW PFSA/PVDF membranes, 1.1 mmol/g for the 700 EW PFIA/PVDF membranes).
b. Water uptake was reduced in the composite membranes due to the presence of hydrophobic PVDF. Thus, the PFSA/PVDF membranes

exhibited water uptake values of ~30%, and no dependence on PVDF fiber diameter was observed. PFIA-based membranes exhibited a greater degree of gravimetric water uptake as compared to 825 EW PFSA-based membranes due to the greater effective membrane IEC.

(12) The in-plane swelling of the dual fiber membranes was strongly affected by the average diameter of the reinforcing PVDF fibers. For both PFIA/PVDF and PFSA/PVDF composite films, in-plane swelling decreased to ~4% when 2200 nm PVDF fibers were used. These films also exhibited high conductivities (0.09 S/cm or greater) in liquid water. This low in-plane swelling meets the DOE target. This effect was also demonstrated using 725 EW PFSA and 2200 nm PVDF fibers; those results are provided in Appendix C.

(13) Humidity stability factors (HSF, the ratio between the strain at break of a membrane and its in-plane water swelling) were determined for electrospun membranes. High HSFs have been correlated with good membrane durability during an on/off humidity cycling accelerated stress test. Dual fiber membranes containing PVDF were generally found to be more ductile than ones containing PAI. For example, the dual fiber membrane containing 80 wt.% 825 EW PFSA (20 wt.% PVDF) had a strain at break of ~130%. A dual fiber membrane with 80 wt.% 825 EW PFSA (20 wt.% PAI) fractured at ~30%. The two films exhibited similar proton conductivities (~0.09 S/cm in 25 °C water) and in-plane water swelling (9.8% for the PVDF-reinforced films vs. 11.5% for the PAI-reinforced film). The increased stiffness of the PAI-based membrane may negatively affect its long-term durability in a fuel cell (a HSF of 2.6 is obtained using PAI in a single-layer film, compared to 13.3 using PVDF).

(14) Select electrospun membranes with low thickness and high conductivity were made into membrane-electrode assemblies (MEAs) for testing in a H_2/air fuel cell. Gas diffusion electrodes utilizing 825 EW PFSA as the binder and Pt/C (Johnson Matthey HiSPEC 4000) were pressed onto a dual fiber membrane, a single fiber membrane, a solution cast blended membrane, or a neat ionomer film with thicknesses less than 50 μm. The MEAs were tested at 80°C at high and low relative humidity at ambient pressure and a H_2/air flow rate of 0.125/0.5 L/min. The membranes performed well; for example, a dual fiber membrane containing 70 wt.% 700 EW PFIA (30 wt.% PVDF) achieved a power density at 0.65 V of 364 mW/cm^2 at 80°C, 100% relative humidity, which was greater than that of a single fiber membrane of the same composition (302 mW/cm^2) or Nafion 211. The higher power density achieved by the dual fiber membrane is due to the reduced ASR of the composite membrane.

Chapter 8

Suggestions for Future Work

1) During fuel cell operation, the cathode encounters mass transport limitations that complicate oxygen penetration and water rejection [1–3]. Increasing the hydrophobicity of the cathode can mitigate these issues [4]. However, water is necessary in the cathode, as it is: a) critical for ionic conductivity and b) a product of the oxygen reduction reaction. A multi-layer electrospun cathode is envisioned in which layers utilizing poly(vinylidene fluoride) (PVDF) as the catalyst binder and layers utilizing perfluorosulfonic acid (PFSA) (with a carrier polymer) as the catalyst binder are stacked together to form the electrode. This is expected to facilitate water rejection and oxygen penetration while still maintaining sufficient hydration for proton transport and the oxygen reduction reaction.

2) Lithium-ion batteries are attractive due to their high specific energy and power, as well as their high round-trip efficiency. A critical part of these devices is the separator. Similar to the membrane in an membrane-electrode assembly (MEA), the separator prevents contact between the anode and cathode, as well as facilitating ionic transport via a liquid electrolyte [5]. Dual fiber electrospinning has the potential to lead to separators for Li-ion batteries that utilize a variety of polymers to impart the mechanical strength and the necessary electrolyte affinity for such materials [6]. A mixed fiber mat containing PFSA and poly (amide imide) (PAI) is envisioned as a separator, due to PAI's beneficial mechanical properties and chemical stability [7], as well as the affinity of fluorocarbons toward the electrolyte used in Li-ion batteries [5].

3) The tri-layer composite membranes fabricated in Chapter 3 utilized 3M's 825 EW PFSA, and exhibited in-plane conductivities, water swelling values, and mechanical properties that were attractive for H_2/air fuel cells. The tri-layer technique could be extended to fabricate alternative ion-exchange membranes, such as anion-exchange membranes for fuel cells, membranes for direction methanol or H_2/Br_2 fuel cells, or membranes for ion-selective separation processes. Similarly, single fiber membranes can be fabricated using a tri-layer structure. The variation in composition through the membrane's thickness may also result in reduced fuel crossover, which would be valuable for fuel cell performance.

4) Proper water management in a H_2/air fuel cell is critical for achieving high power densities due to the tendency of the anode to dry out during operation. Typically, water generation at the cathode and drying of the anode creates a concentration gradient that leads to back-diffusion of water. Using dual fiber electrospinning, a proton-exchange membrane (PEM) with a gradient in ionomer content can be fabricated which goes from a low ion-exchange capacity (IEC) at the anode to high-IEC at the cathode (or vice-versa). Such a membrane could further encourage back-diffusion of water during fuel cell operation, allowing for lower levels of humidification to be tolerated.

5) High membrane selectivity (ratio of proton conductivity to gas permeability) is an important parameter in direct methanol fuel cells (DMFC) or regenerative H_2/Br_2 fuel cells. The single fiber membrane utilizing 700 EW perfluoroimide acid (PFIA)/PVDF exhibited lower H_2-crossover in an operational fuel cell than a dual fiber membrane at the same composition. Thus, the single fiber membranes fabricated in this dissertation should

be tested in a DMFC or regenerative H_2/Br_2 fuel cell to determine if they are advantageous compared to dual fiber membranes.

6) Inorganic particles, such as cerium or manganese [8,9], have been shown to improve the chemical resistance of a PEM to highly reactive peroxides that are generated during the operation of a fuel cell [10,11]. While blending such materials with ionomer at a low content may not affect conductivity, losses in fuel cell performance have been observed [8,9]. Using dual fiber electrospinning, these peroxide radical scavenging agents can be selectively incorporated into the ionomer or uncharged polymer fiber (which would keep them away from the ionomer). These materials can also be incorporated into a separate phase utilizing triple fiber electrospinning, which would allow for varied distribution of the particles through the membrane's thickness. Alternatively, platinum nanoparticles can be incorporated into the membrane to scavenge H_2 or O_2 that penetrates the film [12]. These would serve as catalytic sites to convert the feed gases to water, thus hydrating the membrane even at low levels of humidity.

7) Recent work by Shen *et al.* has reported the properties of a bipolar membrane (BPM), which consisted of a dual fiber bipolar junction (cation-exchange polymer fibers co-electrospun with anion-exchange polymer fibers and embedded $Al(OH)_3$ water-dissociation catalyst) with dense cation and anion-exchange membrane surface layers [13]. The 3D junction provided increased interfacial area, leading to reduced water splitting voltages as compared to a 2D junction. Bipolar membranes also have the potential to be utilized in a fuel cell. Ünlu *et al.* [14] have reported bipolar membranes that were fabricated by lamination of an anion-exchange membrane and a cation-exchange membrane at room temperature. The resultant BPMs achieved very low current

densities [14] under dry conditions. These modest results could be due to a lack of interpenetration of the cation-exchange and anion-exchange polymers. The implementation of a 3D junction has the potential to lead to a self-humidifying fuel cell membrane with greater current and power densities, especially under low levels of humidity (due to the generation of water within the membrane) compared to the 2D junction.

8) The majority of the work performed in this dissertation utilized ex-situ measurements – conductivity in liquid water, conductivity in vapor at 80 °C, tensile measurements, gravimetric and dimensional swelling – to select PEMs with the potential to achieve high power densities and long lifetimes in a fuel cell. Accelerated stress tests – specifically humidity cycling to determine mechanical lifetime and open-circuit voltage holds to determine chemical stability – of the best performing membranes should be performed, as they will lend an additional degree of certainty to the potential of these techniques for fabricating high-performance PEMs.

9) Despite the importance of membrane durability during on/off cycling of a fuel cell, the effect of the various limiting factors of a PEM's lifetime – dimensional swelling, mechanical strength, creep, etc. – lacks an exhaustive model. A model for durability that details the role of swelling, fuel crossover, and mechanical properties (modulus and tensile strength) of the components (ionomer and reinforcing polymer) should be developed, as it will be a beneficial tool in the development of PEMs with long lifetimes. In addition, the behavior of a tri-layer membrane should be modeled in order to fully understand how the structure controls in-plane swelling.

10) The low EW multi-acid side chain (MASC) ionomer utilized in this study had an imide acid along the side chain to increase IEC while maintaining backbone crystallinity. Recent work from 3M Company has found that the imide acid linkage in the PFIA ionomer is unstable in oxidative environments [15]. Losses in the performance of MEAs utilizing PFIA have suggested that part of the side chain is cleaved during fuel cell operation, leading to the less conductive sulfonamide polymer. It is therefore of interest to investigate alternative linkages for these MASC ionomers that will provide improved chemical and mechanical stability without sacrificing IEC.

11) One of the limitations in using PAI in this work was the thermal processing necessary to achieve its expected strength. In order to get high strength and stiffness from the polymer, it should be melt-processed at temperatures approaching 300°C [7]; however, these conditions would damage the PFSA or PFIA used in these studies. Therefore, it could be beneficial to electrospin the PAI from a melt instead of a solution. Doing so would allow for improved strength from the polymer while potentially protecting the ionomer from thermal degradation. Such fibers will likely exhibit much greater average diameters than fibers electrospun from a solution [6,16]. Successful melt-electrospinning of PAI would imply potential for other highly stable polymers – such as PEEK or PTFE – to be incorporated into a dual fiber membrane in a similar fashion.

12) PEM durability is typically estimated through its swelling (gravimetric and/or in-plane) and its mechanical strength under tensile strain. However, membrane failure typically occurs due to compressive stresses applied to the membrane during on/off cycling [17,18]. Characterization of the shear, compressive, or tear strength of various membranes has the potential to serve as a more meaningful metric for membrane

durability. The strength (shear, compressive, tear, and tensile) of a series of membranes should be tested and compared to their lifetimes to determine whether these alternative techniques are beneficial in predicting durability.

13) The tri-layer technique allowed for controlled distribution of PFSA and PAI through the thickness of the composite membrane. In theory, this technique could be applied to any structure that requires variation in properties (permeability, catalytic activity, hydrophilicity, etc.) through the thickness of the film. For example, a fully electrospun MEA is envisioned, where a gradient electrospinning technique can allow for an interpenetrating network of electrode fibers and the PEM. Doing so can reduce interfacial resistances that arise during MEA fabrication or reduce the chance of delamination between the membrane and electrodes.

14) The electrospun membranes reported in this dissertation were approximately 20 μm in thickness. The thickness of composite membranes with the best combination of low in-plane water swelling, high proton conductivity, and good mechanical properties should be reduced in order to be competitive with commercial fuel cell membranes (such as the GORE-Select, which is as thin as 5 μm [19–21], or Nafion XL [22], which is 27.5 μm in thickness).

15) The fabrication of ultra-thin membranes (below 10 μm) can lead to a number of benefits for a PEM, including back-diffusion of water and significant reductions in area-specific resistance. The fabrication of a thin tri-layer membrane in particular can be challenging, as the thickness of a fiber can constitute a significant portion of the membrane or layer thickness. Thus, techniques to fabricate well-formed PFSA and PAI

fibers of low average diameter will be critical to reduce the thickness of a tri-layer membrane.

16) Perfluorosulfonic acid (PFSA) ionomers with equivalent weights (EW) of 825, 725, or 660 g/mol were available in this work. Blends of high- and low-EW PFSAs should be prepared in order to determine (a) if such a blend mimics the properties of an as-received PFSA of similar EW and (b) if improvements to the properties of a dual fiber membrane using a low EW PFSA can be improved due to optimization of ionomer crystallinity and PVDF content.

8.1 References

[1] F. Liu, G. Lu, C.Y. Wang, Water transport coefficient distribution through the membrane in a polymer electrolyte fuel cell, J. Memb. Sci. 287 (2007) 126–131. doi:10.1016/j.memsci.2006.10.030.

[2] T. Ous, C. Arcoumanis, Degradation aspects of water formation and transport in Proton Exchange Membrane Fuel Cell : A review, J. Power Sources. 240 (2013) 558–582. doi:10.1016/j.jpowsour.2013.04.044.

[3] I.H. Hristov, S.J. Paddison, R. Paul, Molecular modeling of proton transport in the short-side-chain perfluorosulfonic acid ionomer, J. Phys. Chem. B. 112 (2008) 2937–2949. doi:10.1021/jp7108434.

[4] M. Brodt, R. Wycisk, N. Dale, P. Pintauro, Power Output and Durability of Electrospun Fuel Cell Fiber Cathodes with PVDF and Nafion / PVDF Binders, J. Electrochem. Soc. 163 (2016) 401–410. doi:10.1149/2.0711605jes.

[5] S.S. Zhang, A review on the separators of liquid electrolyte Li-ion batteries, J. Power Sources. 164 (2007) 351–364. doi:10.1016/j.jpowsour.2006.10.065.

[6] B. Yu, X.-M. Zhao, X.-N. Jiao, D.-Y. Qi, Composite Nanofiber Membrane for Lithium-Ion Batteries Prepared by Electrostatic Spun / Spray Deposition, J. Electrochem. Energy Convers. Storage. 13 (2017) 1–6. doi:10.1115/1.4034030.

[7] S.H. Lee, S.Y. Kim, J.R. Youn, D.G. Seong, S.Y. Jee, J. Il Choi, J.R. Lee, Processing of continuous poly(amide-imide) nanofibers by electrospinning, Polym. Int. 59 (2010) 212–217. doi:10.1002/pi.2710.

[8] M. Zaton, J. Roziere, D.J. Jones, Mitigation of PFSA membrane chemical degradation using composite cerium oxide – PFSA nano fibres, (2017) 5390–5401.

doi:10.1039/C6TA10977B.

[9] C.D. Urso, C. Oldani, V. Baglio, L. Merlo, Towards fuel cell membranes with improved lifetime : Aquivion ® Per fl uorosulfonic Acid membranes containing immobilized radical scavengers, 272 (2014) 753–758. doi:10.1016/j.jpowsour.2014.09.045.

[10] B.P. Pearman, N. Mohajeri, R.P. Brooker, M.P. Rodgers, D.K. Slattery, M.D. Hampton, D.A. Cullen, S. Seal, The degradation mitigation effect of cerium oxide in polymer electrolyte membranes in extended fuel cell durability tests, J. Power Sources. 225 (2013) 75–83. doi:10.1016/j.jpowsour.2012.10.015.

[11] M.P. Rodgers, L.J. Bonville, H.R. Kunz, D.K. Slattery, J.M. Fenton, Fuel Cell Perfluorinated Sulfonic Acid Membrane Degradation Correlating Accelerated Stress Testing and Lifetime, (2012).

[12] R. Wang, W. Zhang, G. He, P. Gao, Controlling fuel crossover and hydration in ultra-thin proton exchange membrane-based fuel cells using Pt-nanosheet catalysts, J. Mater. Chem. A. 2 (2014) 16416–16423. doi:10.1039/C4TA03799E.

[13] C. Shen, R.J. Wycisk, P.N. Pintauro, High performance electrospun bipolar membrane with a 3D junction, Energy Environ. Sci. 10 (2017) 1435–1442. doi:10.1039/C7EE00345E.

[14] M. Ünlü, J. Zhou, P.A. Kohl, Hybrid Anion and Proton Exchange Membrane Fuel Cells, J. Phys. Chem. C. (2009) 11416–11423.

[15] M. Yandrasits, New Fuel Cell Membranes with Improved Durability and Performance, in: DOE Annu. Merit Rev., 2017.

[16] S. Megelski, J.S. Stephens, D.B. Chase, J.F. Rabolt, Micro- and Nanostructured

Surface Morphology on Electrospun Polymer Fibers, Macromolecules. 35 (2002) 8456–8466.

[17] A. Kusoglu, A.M. Karlsson, M.H. Santare, S. Cleghorn, W.B. Johnson, Mechanical behavior of fuel cell membranes under humidity cycles and effect of swelling anisotropy on the fatigue stresses, J. Power Sources. 170 (2007) 345–358. doi:10.1016/j.jpowsour.2007.03.063.

[18] J. Wu, X.Z. Yuan, J.J. Martin, H. Wang, J. Zhang, J. Shen, S. Wu, W. Merida, A review of PEM fuel cell durability: Degradation mechanisms and mitigation strategies, J. Power Sources. 184 (2008) 104–119. doi:10.1016/j.jpowsour.2008.06.006.

[19] R. Wycisk, P.N. Pintauro, J.W. Park, New developments in proton conducting membranes for fuel cells, Curr. Opin. Chem. Eng. 4 (2014) 71–78. doi:10.1016/j.coche.2014.01.012.

[20] B.B. Jeffrey A. Kolde, W.L. Gore, Advanced Composite Polymer Electrolyte Fuel Cell Membranes, Proc. First Int. Symp. Prot. Conduct. Membr. Fuel Cells , Electrochem. Soc. Inc. 95–23 (1995) 193–201.

[21] B.L. Kienitz, J.A. Kolde, S. Priester, C. Baczowski, M. Crum, Ultra-Thin Reinforced Ionomer Membranes to Meet Next Generation Fuel Cell Targets, ECS Trans. 41 (2011) 1521–1530.

[22] S. Shi, A.Z. Weber, A. Kusoglu, Structure/property relationship of Nafion XL composite membranes, J. Memb. Sci. 516 (2016) 123–134. doi:10.1016/j.memsci.2016.06.004.

Appendix A

Curing of PAI

The focus of Chapter 3 was to fabricate dual fiber membranes utilizing 3M's 825 EW perfluorosulfonic acid (PFSA) with poly (amide imide) (PAI) reinforcing fibers. PAI is a partially-imidized thermoplastic, which requires treatment at temperatures in excess of 330°C to achieve its expected mechanical strength [1]. However, the use of such an extreme treatment is risky in a dual fiber membrane. One of the limitations of PFSA is that it undergoes thermal degradation when exposed to temperatures exceeding 300°C [2]. Partial curing of solution-cast PAI was performed to increase its mechanical strength, which may lead to a reduction in the in-plane swelling when the polymer is used to reinforce a PFSA matrix. Solution-cast PAI membranes were prepared by dissolving the polymer into a 98:2 (wt:wt) DMF:THF mixture, then casting a film onto a glass substrate and allowing the solvent to evaporate for up to 16 hours at 70°C. The resultant films were then thermally cured by exposure to temperatures ranging from 170°C to 290°C (the glass transition temperature of PAI is 285°C [1]) for times ranging from 15 minutes to 7 hours. Several stress-strain curves of the resultant films are shown in Figure A.1, and are compared to the uncured solution-cast PAI film.

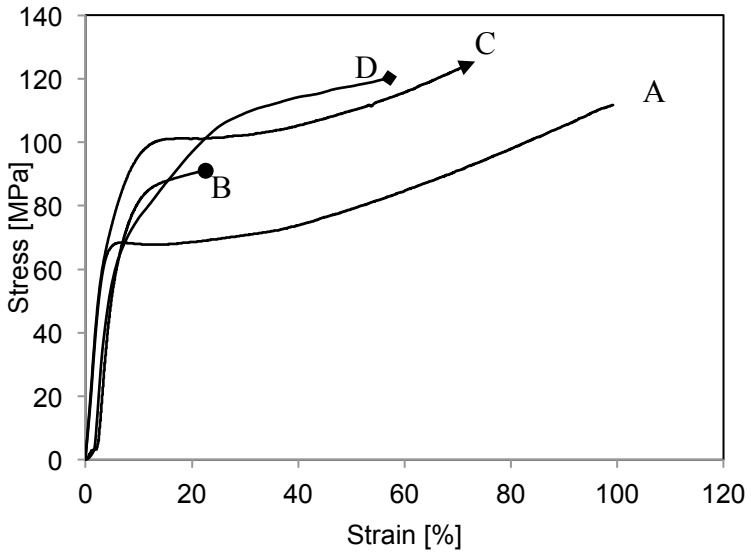

Figure A.1: Stress-strain curves of solution-cast PAI films after curing at: a) no curing (–), b) 170°C for 5 hours (●), c) 270°C for 4 hours (▶), or d) 290°C for 4 hours (◆).

The thermal curing step increases the yield strength of the solution-cast PAI film. The mechanical properties of the films were observed to increase with both temperature and time. Of the solution-cast films that were cured at 170°C, the ones that received the longest exposure (7 hours) exhibited the greatest strength. However, the abbreviated curing of PAI at 170°C does not bring it to the expected stress at break of 120 MPa [3], indicating that a more extreme thermal treatment is necessary to further improve its mechanical properties. While the stress at break is variable among the films, the samples that underwent the most extreme thermal conditions – 270°C and 290°C for 4 hours – exhibit the greatest strength.

These results were implemented into several of the 825 EW PFSA/PAI dual fiber membranes that were described in Chapter 3. After boiling in acid and water, the 825 EW PFSA/PAI dual fiber membranes underwent ion-exchange in 2.0 M NaCl, which converted the ionomer from the proton-form into the sodium-form. The sodium-form of

PFSA is known to exhibit greater thermal stability [4], which allowed the resultant membranes to undergo elevated thermal curing steps.

The sodium-form 825 EW PFSA/PAI dual fiber membranes were pressed at 260°C for 5 minutes. The membranes were subsequently treated in 1.0 M H_2SO_4 and water to convert the sodium-form ionomer back to the proton-form. The proton conductivity and in-plane water swelling of the membranes before and after the thermal treatment are shown in Table A.1. Minor differences in proton conductivity were observed after the thermal treatment. The in-plane swelling of the membranes generally decreased by ~2%. This reduction, though small, allows several membranes to meet the 5% in-plane swelling target. This treatment is a somewhat tedious step and was not applied to all PAI-based dual fiber membranes. However, it represents a potential avenue to further reduce the in-plane swelling of an electrospun membrane, thus making it more suitable for fuel cell usage.

Table A.1: In-plane swelling and proton conductivity in 25°C water of 825 EW PFSA/PAI dual fiber membranes after high-temperature curing at 260°C.

Membrane	**In-Plane Conductivity [S/cm]**		**In-Plane Swelling [%]**	
	Standard Cure	Elevated Cure	Standard Cure	Elevated Cure
80 Single-Layer	0.091	0.090	11.5	9.9
95/75/95 Tri-Layer	0.089	0.089	6.6	5.6
95-75-95 Gradient	0.082	0.087	5.2	3.7
95/60/95 Tri-Layer	0.088	0.091	7.9	9.9
95-60-95 Gradient	0.089	0.087	6.2	4.2

A.1 References:

[1] S.H. Lee, S.Y. Kim, J.R. Youn, D.G. Seong, S.Y. Jee, J. Il Choi, J.R. Lee, Processing of continuous poly(amide-imide) nanofibers by electrospinning, Polym. Int. 59 (2010) 212–217. doi:10.1002/pi.2710.

[2] Z. Shao, P. Joghee, I. Hsing, Preparation and characterization of hybrid Nafion – silica membrane doped with phosphotungstic acid for high temperature operation of proton exchange membrane fuel cells, J. Memb. Sci. 229 (2004) 43–51. doi:10.1016/j.memsci.2003.09.014.

[3] T.J. Murray, Poly (amide-imides): Wire Enamels with Excellent Thermal and Chemical Properties, Macromol. Mater. Eng. 293 (2008) 350–360. doi:10.1002/mame.200700365.

[4] S.H. De Almeida, Y. Kawano, Thermal Behavior of Nafion Membranes, 58 (1999) 569–577.

Appendix B

Conductivity of PFIA/PVDF Dual Fiber Membranes as a Function of Temperature

Chapter 5 and Chapter 6 introduced the utilization of 3M's novel perfluoroimide acid (PFIA) ionomer in single fiber and dual fiber membranes. Proton conductivity of a 25 μm dual fiber membrane which utilized 70 wt.% 700 EW PFIA (30 wt.% PVDF) was evaluated in water vapor as a function of temperature using an ESPEC temperature- and humidity-controlled oven. Figure B.1 shows an Arrhenius plot of the conductivity of both the PFIA/PVDF dual fiber membrane and Nafion 212 at 100% and 40% relative humidity. The activation energy for each sample, which describes the relationship between proton conductivity and temperature, is calculated by linearly fitting the Arrhenius equation (Eq. B.1) to the data. The activation energies for proton conduction for the two membranes at 100%, 60%, and 40% relative humidity are shown in Table B.1.

$$\sigma = Ae^{-E_a/RT} \tag{B.1}$$

Table B.1: Activation energy for proton conduction of Nafion and a PFIA/PVDF dual fiber membrane.

Membrane	**Activation Energy of Proton Conduction (kJ/mol)**		
	100% rH	60% rH	40% rH
Nafion 211	10.86	10.27	9.64
75 wt.% PFIA (25 wt.% PVDF) dual fiber membrane	13.08	11.52	13.37

In Eq. B.1, σ is the proton conductivity (S/cm), A (S/cm) is a temperature-independent factor that can be obtained from the linear fit, R is the universal gas constant of 8.314 J/mol-K, T (K) is temperature, and E_a (kJ/mol) is the activation energy.

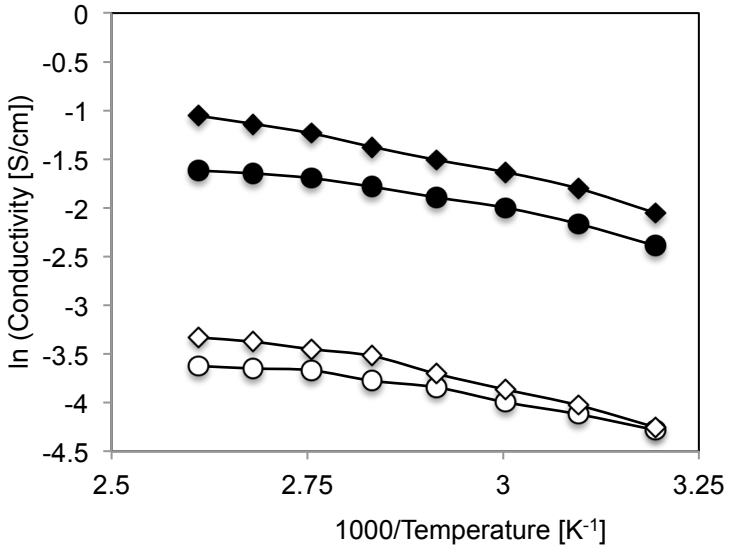

Figure B.1: In-plane conductivity of a PFIA/PVDF dual fiber membrane (◆) and Nafion 211(●) as a function of temperature at 100% (filled symbols) and 40% (open symbols) humidity.

Several aspects of the membrane behavior can be observed from Figure B.1 and Table B.1. The PFIA-based dual fiber membrane exhibited greater proton conductivity at both high and low levels of humidification as compared to 1100 EW Nafion. This is to be expected, as the composite membrane has a greater IEC than Nafion, which results in greater water content and conductivity as discussed previously. The membranes have a similar activation energy, which is somewhat unaffected by relative humidity. The value of E_a ranges from 9.6 – 10.9 kJ/mol for Nafion 211, and from 11.5 – 13.4 kJ/mol for the PFIA-based dual fiber membrane, which corresponds well with data reported for various

other PEM materials [1–4], and is corroborated by the sorption isotherms, shown in Figure B.2a. The gravimetric uptake of the PFIA/PVDF dual fiber membrane at 25°C and 80°C are similar for levels of humidity below 90%, and are quite close for levels of humidity ranging from 90-98%. Similarly, the sorption isotherms of the single fiber and solution cast blended membranes (Figure B.2b and Figure B.2c) are essentially unaffected by temperature.

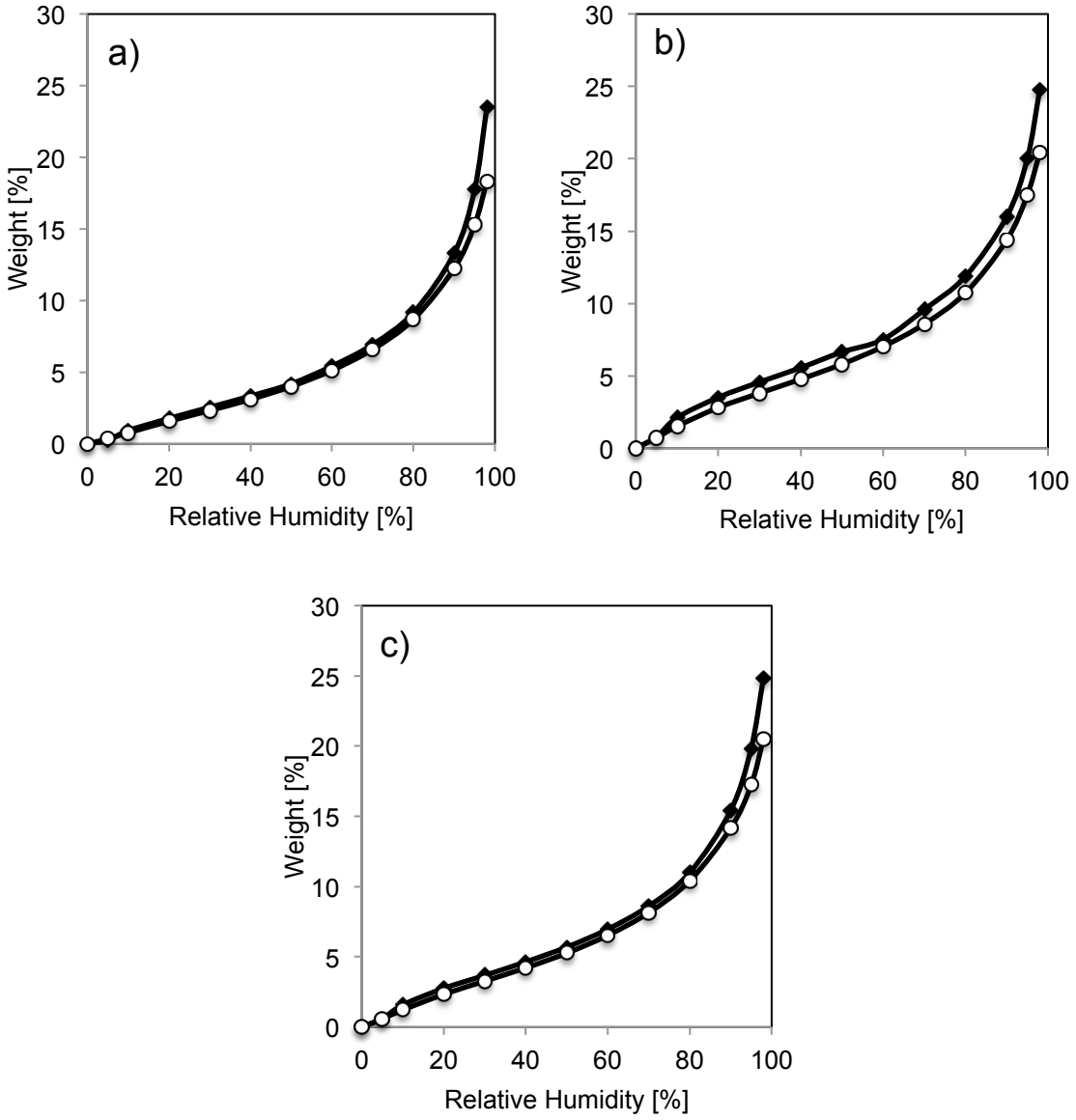

Figure B.2: Sorption isotherm of 70 wt.% PFIA (30 wt.% PVDF) a) dual fiber membrane, b) single fiber membrane, and c) solution cast blended membrane in water vapor at 25°C (◆) and 80°C (○).

B.1 References

[1] C.H. Lee, H.B. Park, Y.M. Lee, R.D. Lee, Importance of Proton Conductivity Measurement in Polymer Electrolyte Membrane for Fuel Cell Application, (2005) 7617–7626.

[2] H.-Y. Li, Y.-L. Liu, Nafion-functionalized electrospun poly(vinylidene fluoride) (PVDF) nanofibers for high performance proton exchange membranes in fuel cells, J. Mater. Chem. A. 2 (2014) 3783–3793. doi:10.1039/C3TA14264G.

[3] H. Xie, D. Tao, J. Ni, X. Xiang, C. Gao, L. Wang, Synthesis and properties of highly branched star-shaped sulfonated block polymers with sulfoalkyl pendant groups for use as proton exchange membranes, J. Memb. Sci. 497 (2016) 55–66. doi:10.1016/j.memsci.2015.09.035.

[4] A. Kusoglu, A.Z. Weber, New Insights into Perfluorinated Sulfonic-Acid Ionomers, Chem. Rev. 117 (2017) 987–1104. doi:10.1021/acs.chemrev.6b00159.

Appendix C

Dual Fiber Membranes Utilizing 725 EW PFSA And PVDF

In Chapter 4, the 725 EW perfluorosulfonic acid (PFSA) was found to produce dual fiber membranes with a high conductivity, low in-plane swelling, and ionomer stability in hot water due to the preservation of ionomer crystallinity and the sufficient amount of poly(vinylidene fluoride) (PVDF) to restrict water swelling. Further, the utilization of large-diameter PVDF fibers was found to result in composite membranes with attractively low in-plane swelling and high proton conductivity in Chapter 6. Thus, a series of dual fiber membranes, utilizing 725 EW PFSA and PVDF were prepared in order to achieve higher conductivity and lower in-plane swelling in liquid water. Similar to the membranes reported in Chapter 4, these utilized PEO (MW = 600 kDa) as a carrier to enable electrospinning of PFSA. The presence of PVDF fibers with diameters of ~600 nm or greater was found to restrict the in-plane water swelling of a dual fiber membrane without adversely affecting proton conductivity. The electrospinning conditions used to fabricate the 725 EW PFSA/PVDF dual fiber mats are summarized in Table C.1.

Table C.1: Electrospinning conditions for 725 EW PFSA/PVDF mixed fiber mats

Parameter	99:1 725 EW PFSA:PEO (600 kDa) Fibers	PVDF Fibers
Voltage [kV]	10	10
Flow Rate [mL/hr]	0.50	0.20
STC [cm]	8.5	10.5
Concentration [wt.%]	20	12.5
Solvent	2:1 EtOH:H_2O	7:3 DMAc:Acetone

[a] STC: Spinner-to-Collector Distance

After electrospinning of 725 EW PFSA and PVDF, the mat was compacted at elevated temperature (143°C for 5 minutes) to selectively soften the ionomer, allowing it to fill the void spaces between PVDF fibers. After annealing at 200 °C for 30 minutes, the composite membrane was soaked at 80°C in 1.0 M H_2SO_4 for 1 hour, followed by soaking at 80°C in H_2O for 1 hour. The neat 725 EW PFSA ionomer exhibited a negligible loss (2%) in mass after this same treatment, which highlights its stability (according to reference [1] 660 EW PFSA loses 40% of its dry mass after boiling in acid and water). The conductivity and swelling of the resultant membranes, along with Nafion 211 that was treated at the same conditions, are shown in Table C.2. The high IEC of the 725 EW PFSA allows for the fabrication of dual fiber membranes with high proton conductivities and low in-plane swelling values. Furthermore, the utilization of large-diameter PVDF reinforcing fibers allows for a further reduction in the in-plane water swelling (from ~9% to 6.5%) with no change in proton conductivity.

These membranes were not converted into a membrane-electrode assembly and tested in an operational fuel cell. A series of long-term humidity cycling experiments on these membranes would make a valuable addition to this work.

Table C.2: Proton conductivity, in-plane swelling, and gravimetric water uptake in 25°C water of 725 EW PFSA/PVDF dual fiber membranes.

Membrane	In-Plane Conductivity [S/cm]	In-Plane Swelling [%]	Gravimetric Water Uptake [%]
725 EW PFSA	0.12	25	42
80 wt.% PFSA	0.099	8.9	34
80 wt.% PFSA with 2200 nm PVDF fibers	0.097	6.5	35
Nafion 211	0.087	15.6	27.2

C.1 References

[1] J.B. Ballengee, G.M. Haugen, S.J. Hamrock, P.N. Pintauro, Properties and Fuel Cell Performance of a Nanofiber Composite Membrane with 660 Equivalent Weight Perfluorosulfonic Acid, J. Electrochem. Soc. 160 (2013) F429–F435. doi:10.1149/2.088304jes.